UNIVERSITY OF OKLAHOMA

GRADUATE COLLEGE

SYNTHESIS, ISOLATION, AND REACTIVITY OF KINETICALLY STABILIZED AROMATIC NITROSAMIDES AND NEW LOW DIMENSIONAL ORGANIC INORGANIC HYBRID MATERIALS

A DISSERTATION

SUBMITTED TO THE GRADUATE FACULTY

in partial fulfillment of the requirements for the

Degree of

DOCTOR OF PHILOSOPHY

By

MATTHEW B. HOUCK
Norman, Oklahoma
2019

SYNTHESIS, ISOLATION, AND REACTIVITY OF KINETICALLY STABILIZED AROMATIC NITROSAMIDES AND NEW LOW DIMENSIONAL ORGANIC INORGANIC HYBRID MATERIALS

A DISSERTATION APPROVED FOR THE
DEPARTMENT OF CHEMISTRY AND BIOCHEMISTRY

BY

Dr. Daniel T. Glatzhofer, Chair

Dr. George Richter-Addo

Dr. Ronald L. Halterman

Dr. Wai Tak Yip

Dr. Steven P. Crossley

Dedicated to my loving parents Jan Brenner and Bill Houck. I couldn't have done this without you.

Acknowledgements

The pursuit of my academic goals as well as my research goals these past 5 years has been more of an experience in failure rather than in success. I found myself questioning if I was really cut out for life as a scientist or if it was a life I even wanted. I have to thank Dr. Glatzhofer for always being there to help me keep going, especially towards the end. I wouldn't have completed this dissertation if it wasn't for him. Beyond just helping me to the finish line Dr. Glatzhofer has provided me with the intellectual freedom to pursue my own ideas no matter how crazy, and he gave me the room I needed to both succeeded and fail. I couldn't imagine having a better advisor. I need to thank Dr. George Richter-Addo for all of the support and kind words he has given me over the years. He is one of the few people who will always take time out of his busy day just to talk about life, I hope that never changes. I have to thank both Dr. Bayrammurad Saparov and Rachel Roccanova for introducing me to the world of perovskites and for being wonderful people to work with. The Glatzhofer group, both past and present members, have been a huge help to me. I would like to especially thank both Nick Godman and Dan Bamper for always being there for me and guiding me in my development as a scientist. I also need to thank my friend and colleague Nate Lavey who has been the best friend a person could ask for these past few years. Having you around made things a lot more bearable, and I can't wait to see where your career takes you. Finally, I need to thank my Mom and Dad who have been nothing but supportive of me and my educational pursuits. I think that this is now more for you two than it is for me. I couldn't have embarked on this journey without your help and I can't wait to celebrate the end of it with the both of you.

Table of Contents

List of Tables

List of Figures

Abstract

The conversion of aromatic amines to esters and phenols is a useful transformation typically carried out using diazonium salt intermediates, but the yields can vary wildly. It has been demonstrated that the reaction of aromatic amides with nitrite in a solution of acetic anhydride and acetic acid can give access to a number of functional groups including the corresponding esters. It is presumed that these transformations go through the initial formation of an intermediate N-aromatic nitrosamide which can than decompose either homolytically or heterolytically. While this reactive intermediate is potentially synthetically useful and has demonstrated to give more consistent reactivity than its related diazonium salt, much is still not known about the mechanistic behavior of these compounds with various postulated mechanisms suggesting these N-aromatic nitrosamides decompose into radicals through a variety of complex intermediates. The elucidation of this mechanistic behavior is made more difficult by the fact that N-aromatic nitrosamides are fairly reactive making their isolation and purification difficult. This makes the study of these systems in pure solvent systems difficult and in some cases impossible. In order to harness the synthetic potential of these species their mechanistic behavior must be further elucidated. In this work N-aromatic nitrosamides stabilized by the presence of steric bulk have been synthesized, isolated and characterized by NMR as well as X-ray crystallography. The reactions of these N-aromatic nitrosamides have been studied in a wide variety of solvents. These studies demonstrated that the dielectric constant of the solvent has a large degree of influence over the reaction mechanism of N-aromatic nitrosamide decomposition with higher dielectric constant solvents favoring addition of the solvent to the aromatic ring while lower dielectric constant solvents favored the formation of indazole formation in cases where cyclization was possible. These results indicate that stabilized N-aromatic nitrosamides decompose through carbocationic like

intermediates in high dielectric constant solvents while neutral pathways dominate in low dielectric constant solvents suggesting that, for the stabilized nitrosamide systems presented in this work, radical reaction pathways are not present or minimal in the decomposition of these systems. Beyond the mechanistic implications established in this work the potential synthetic utility of these systems has also been established. In general, the decomposition of these stabilized N-aromatic nitrosamide systems in straight solvent environments resulted in the corresponding addition products in over 90% yield. In another of examples these N-aromatic nitrosamide systems were able to be competitive or outperform other established synthetic methods. In the case of 2,6 methyl substituted and 2,5 methyl substituted nitrosamide systems decomposition in methanol and ethanol gave the corresponding aryl ethers in over 80% yield, while decompositions of 2 methyl substituted diazonium salt in methanol and ethanol gave less than 30% of the corresponding aryl ether. The methods developed in this work also led to the synthesis of sterically hindered aryl tert-butyl ethers in over 80% yield which is directly competitive with the yields obtained from using the more difficult to prepare diaryliodonium salts (75-95% yields). The chemistry developed in this work has been applied to the post functionalization of two new cyclophane amide systems, with the goal that this chemistry could be used as a key transformation in the synthesis of redox active quinone cyclophanes. Nitrosolation and rearrangement of the *anti*-5,8,13,16-tetramethyl-4,7,12,15-tetraamido[2.2]paracyclophane to the *anti*-5,8,13,16-tetramethyl-4,7,12,15-tetraacetoxy[2.2]paracyclophane was successful but low yielding giving yields below 20% limiting the utility of this method as a route to the quinone cyclophane. The nitrosolation and rearrangement of the *anti*-5,8,13,16,21,24,29,32-octamethyl-4,7,12,15,20,23,28,31-octaamido[2.2.2.2]paracyclophane was found to be unsuccessful, yielding none of the desired *anti*-5,8,13,16,21,24,29,32-octamethyl-4,7,12,15,20,23,28,31-octaacetoxy[2.2.2.2]paracyclophane,

but instead gave large complex mixtures of products that could not be resolved. NMR studies of the parent amide demonstrated that two pairs of the aryl methyl groups and two pairs of the amides were in fact pointed into the center of the macrocycle, making the nitrosolation and rearrangement of this system difficult or impossible due to the steric influence of the surrounding structure. This work has also focused on the development of low dimensional organic-inorganic hybrid structures for the development of light emitting materials. The synthesis of a series of methylated benzyl ammonium salts have been synthesized and used to fabricate low dimensional organic inorganic hybrid structures. These materials demonstrated light emission behavior with the majority of the structures behaving as broadband white light emitters. Importantly, for many of the fabricated compounds improvements in the light emitting behavior of the organic compounds were observed in the hybrid structures when compared to the light emitting properties of the free organic salts.

Chapter 1: Introduction

N-aromatic nitrosamides have been known since 1876. Since then N-aromatic nitrosamides have largely remained a chemical curiosity until a recent resurgence of N-aromatic nitrosamide research has demonstrated that they can be used to accomplish a number of transformations in a synthetically useful manner, making these compounds of interest to the wider synthetic organic community.[1]

While interest in these compounds has increased, research and use of these class of compounds has been limited by their general instability. Most nitrosamides readily decompose at or near room temperature making their isolation and purification difficult to achieve. As such, nitrosamides are either typically generated and used *in situ* or generated on a large scale in high concentration and rapidly precipitated out of solution in order to obtain the nitrosamides as solids, which generally show better stability. Both of these methods have their own issues. The conditions needed to generate of N-aromatic nitrosamides typically require the use of excess mineral acid, which can lead to unwanted side reactions during the *in situ* generation. Large scale precipitation procedures can fail due to the fact that many N-aromatic nitrosamides do not form solids but instead are liquids or oils, which limits the utility of this process.[1,2]

1.1 Historical Overview of Nitrosamides and their Chemical Reactivity

The synthesis of aromatic nitrosamides was first carried out by Emil Fischer in 1876 as key intermediates in the synthesis of aromatic hydrazine compounds.[1] Bamberger followed up on this work in 1897 by demonstrating that N-nitroso-N-phenylacetamide could be isolated by precipitation from ice water, then decomposed smoothly at room temperature in benzene to yield biphenyl and acetic acid (Figure 1).[1,2] In 1930 Grieve and Hey expanded on the work done by

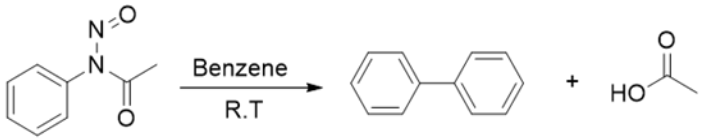

Figure 1: Decomposition of N-nitroso-N-phenylacetamide in benzene to yield biphenyl.[1,2]

Bamberger by demonstrating that substituted biaryls could be made using nitrosamides.[3,4] Decomposition of N-aromatic nitrosamides in substituted benzenes gave biphenyls substituted at the 2- and 4- position regardless of the substituent (Figure 2). The results obtained by Grieve and

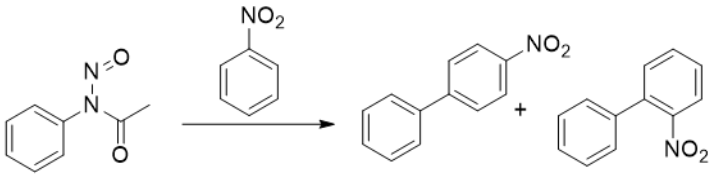

Figure 2: Decomposition of N-nitroso-N-phenylacetamide in nitrobenzene to yield nitro-biphenyls.[3]

Hey suggested that electrophilic and nucleophilic substitution mechanisms were not responsible for the biaryl formation, the results appearing more consistent with phenyl radicals as key intermediates in the reactions.[3] Hey and coworkers conducted a kinetic investigation of the reaction and demonstrated that in a wide range of solvents the first-order evolution of nitrogen was unchanged, which led them to suggest that the rate determining step for the decomposition was the homolysis of the benzenediazoacetate intermediate (A) subsequent to a rearrangement (Figure 3).[5]

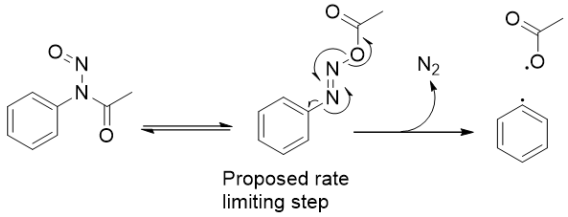

Figure 3: Mechanism of decomposition proposed by Grieve and Hey in which the homolysis of the phenyldiazoacetate species is rate limiting.[5]

This proposal was dismissed by Huisgen, who showed that N-aromatic nitrosamides reacted with 2-naphthol in a variety of solvents at the same rate as nitrogen had been evolved in the absence of 2-naphthol.[4,6,7] This led Huisgen and co-workers to propose that a rearrangement of the N-aromatic nitrosamide to the phenyldiazoacetate was the rate determining step in the reaction (Figure 4).[4,6,7]

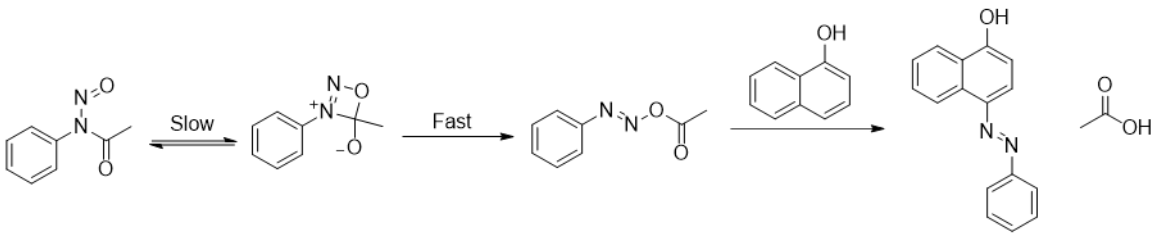

Figure 4: Trapping studies by Huisgen suggesting that the rearrangement to the phenyldiazoacetate species is the rate limiting step.[6,7]

Huisgen and co-workers demonstrated that the rearrangement was indeed occurring by converting N-nitrosobenzolactams to phenylacetic acids, consistent with the reaction proceeding through a cyclic phenyldiazoacetate intermediate (Figure 5).[4,7] In this case the nitrosamide was

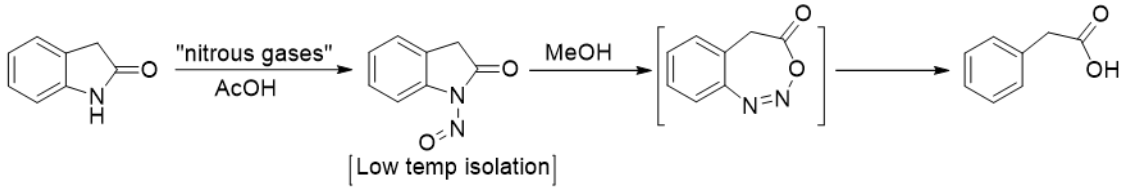

Figure 5: Rearrangement and trapping of indolin-2-one by Huisgen and co-workers suggesting that rearrangement to the phenyldiazoacetate species is occurring.[7]

crashed out of solution over ice and recrystallized from petroleum ether to give a yellow solid. Failure to keep the solid cold resulted in rapid decomposition of the material with a large amount of gas evolution.[4,7] Work by De Tar using isolated N-nitroso-N-phenylacetamide suggested that under acidic conditions a diazonium cation was the primary species responsible for the observed reactivity of nitrosamides, rather than the phenyldiazoacetate intermediate.[8] This suggestion arose from the fact that N-nitroso-N-phenylacetamide, when decomposed in methanol under neutral conditions, gave benzene and formaldehyde, which was due to the formation of phenyl radicals that oxidized the corresponding alcohol. Under acidic conditions, addition of methanol was observed to yield anisole, which De Tar proposed was due to the formation of aryl cations which would be favored under acidic conditions (Figure 6).[8] De Tar postulated that solvent conditions most likely played a large role in regard to the mechanism of nitrosamide decomposition, and

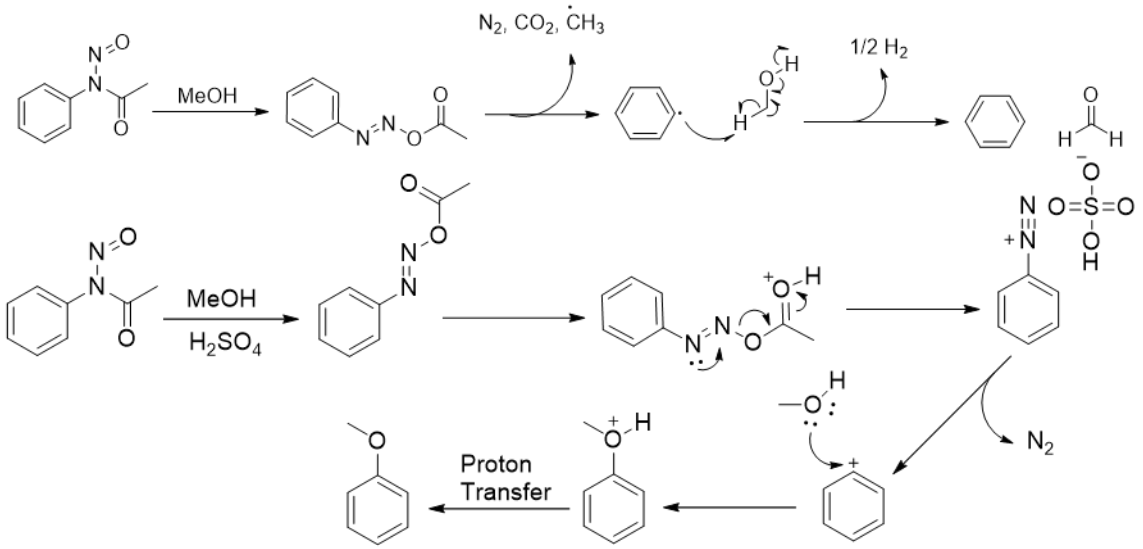

Figure 6: De Tars proposed mechanisms for the decomposition of N-nitroso-N-phenylacetamide under neutral and acidic conditions.[8]

proposed that in neutral solvents radical decomposition would be the dominate mechanism while solvents with acidic protons would result in the formation of the aryl carbocation being the dominant pathway of decomposition.[8] The proposition that solvent conditions could alter the mechanism of nitrosamide decomposition was further supported by Huisgen and Nakaten, who demonstrated that the decomposition of *ortho*-methyl-N-aromatic nitrosoamides in a reaction mixture of acetic acid diluted with chloroform yielded the corresponding indazole in a quantitative fashion.[9] Performing the decomposition in a reaction mixture of acetic acid diluted with alcohols resulted in the formation of toluene and acetaldehyde, which was isolated as the hydrazone derivative (Figure 7).[9]

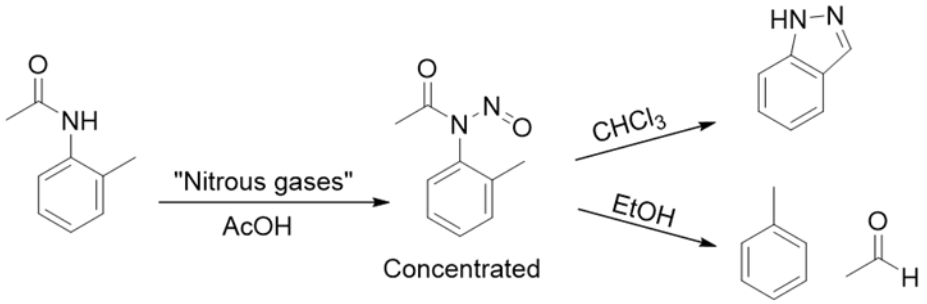

Figure 7: Decomposition of N-nitroso-N-(o-tolyl)acetamide in chloroform and ethanol by Huisgen and Nakaten. It is important to note that the N-nitroso-N-(o-tolyl)acetamide was not isolated but was concentrated from the initial acetic acid solvent due to the fact that the resulting nitrosamide did not crystallize and could not be readily isolated without decomposition.[9]

Based on the formation of the indazole in chloroform, and the lack of observed CO_2 gas, Huisgen and Nakaten postulated that it was, in fact, the phenyldiazonium species that was responsible for the oxidation reactions taking place and not the phenyl radical as postulated by De Tar. In reactions with alcohols, it is the formation of the phenyldiazonium acetate ion pair that allows for the alcohol to attack the diazonium species. This complex then decomposes homolytically to yield the corresponding benzene and aldehyde (Figure 8).[9] In the case of the

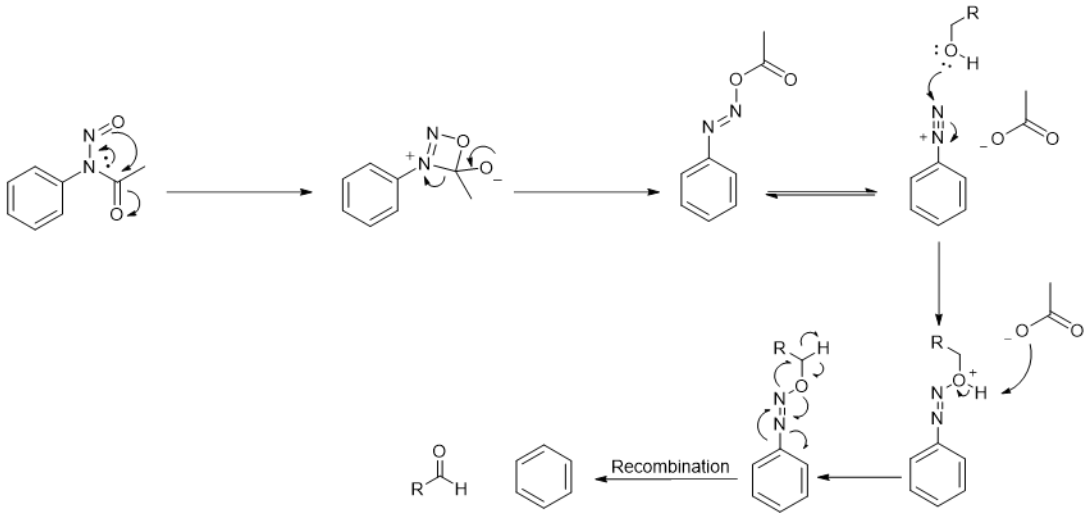

Figure 8: Mechanism of decomposition in ethanol postulated by Huisgen and Nakaten.[9]

formation of the indazole the phenyldiazonium acetate ion pair is sufficiently long lived enough

to allow for deprotonation of the benzylic position, resulting in the formation of a carbon nucleophile which can then attack the nitrogen of the diazonium yielding the indazole (Figure 9).[9]

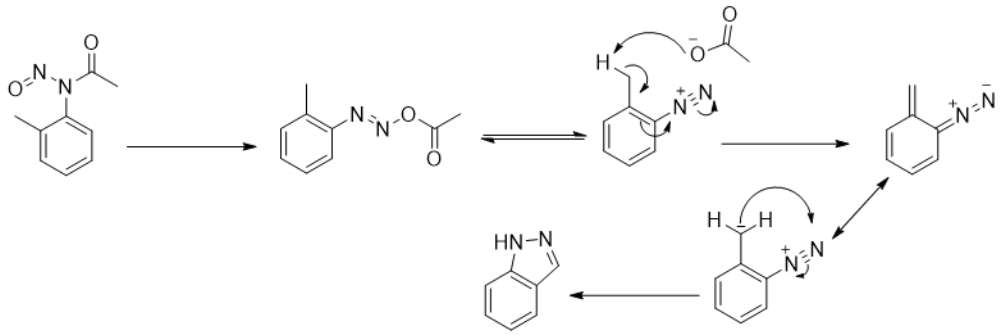

Figure 9: Mechanism of decomposition in chloroform postulated by Huisgen and Nakaten.[9]

Fluorine labeling experiments by Suschitzky and colleagues provided further evidence that the postulated phenyldiazonium acetate ion pairs were indeed present in benzene solutions of substituted N-aryl nitrosamides, further cementing that the formation of the phenyldiazonium acetate ion pair does in fact occur, and that the acetate species is labile.[10] This was demonstrated by analyzing the products of the decomposition of isolated N-(4-fluorophenyl)-N-nitrosobenzene, which yielded the expected 4-fluoro-1,1'-biphenyl as well as [1,1'-biphenyl]-4-yl benzoate in nearly equal amounts.[10] This led Suschitzky and colleagues to propose an ionic mechanism of decomposition in which the phenyldiazonium acetate ion pair plays a key role (Figure 10).[10] The

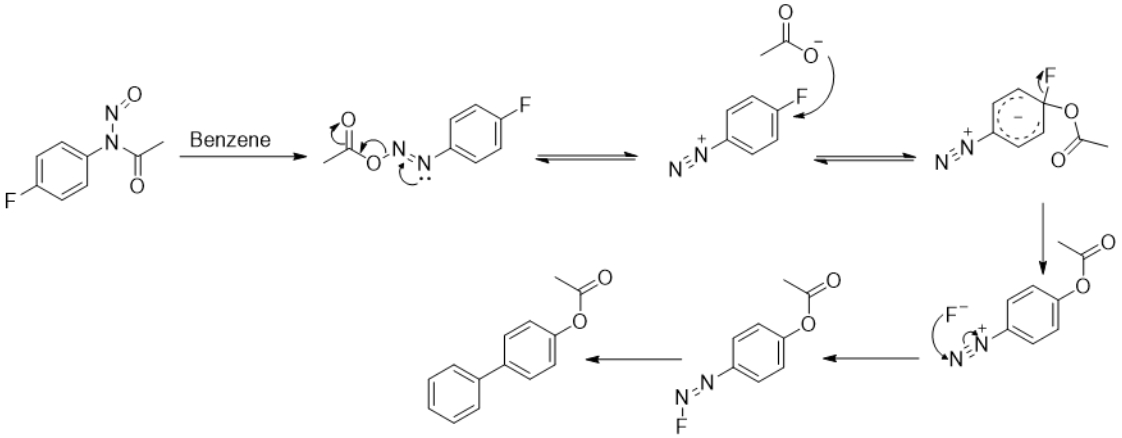

Figure 10: Mechanism proposed by Suschitzky and colleagues to explain the results of their fluorine experiments.[10]

experimentally verified formation of the phenyldiazonium acetate ion pair and helped Richard and Freudenberg propose a mechanism for a radical decomposition pathway, in which a

phenyldiazotate radical, along with a phenyl radical, is formed through an oxidation, rather than an acetate radical (Figure 11).[4,11,12] This postulated mechanism was supported by electron spin

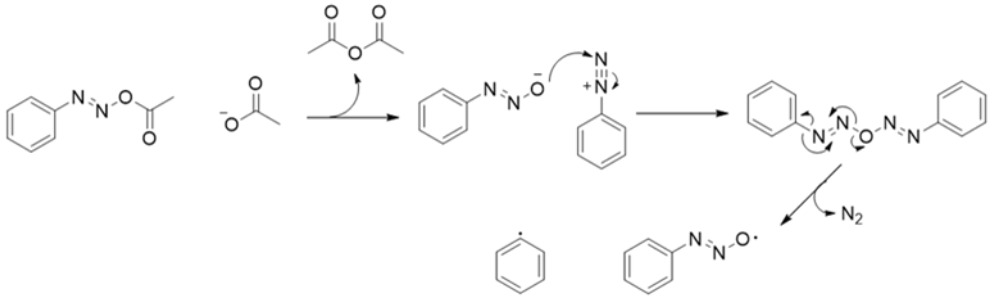

Figure 11: Mechanism postulated by Richard and Freudenberg which results in a phenyldiazotate radical and a phenyl radical rather than an acetoxy radical.[4,11,12]

resonance (E.S.R) experiments, in which Richard and Freudenberg probed their reaction for the presence of unpaired electrons. Richard and Freudenberg observed a long-lived E.S.R signal which they attributed to the phenyldiazoate radical.[12]

This mechanism was seemingly confirmed by Suschitzky and co-workers who used further fluorine labeling studies to bolster the evidence provided by Richard and Freudenberg.[13] Decomposition of the N-(4-fluorophenyl)-N-nitrosobenzamide in benzene by Suschitzky and co-workers yielded benzoyl fluoride as a side product, which also demonstrated that dissociation of an acyl ion was occurring spontaneously (Figure 12).[13] This work was further expanded by Hey and Perkins, who suggested that the E.S.R signal observed by Richard and Freudenberg was in fact due to the formation of a (N-phenyl-acetamido)phenyl nitroxide radical species, which was

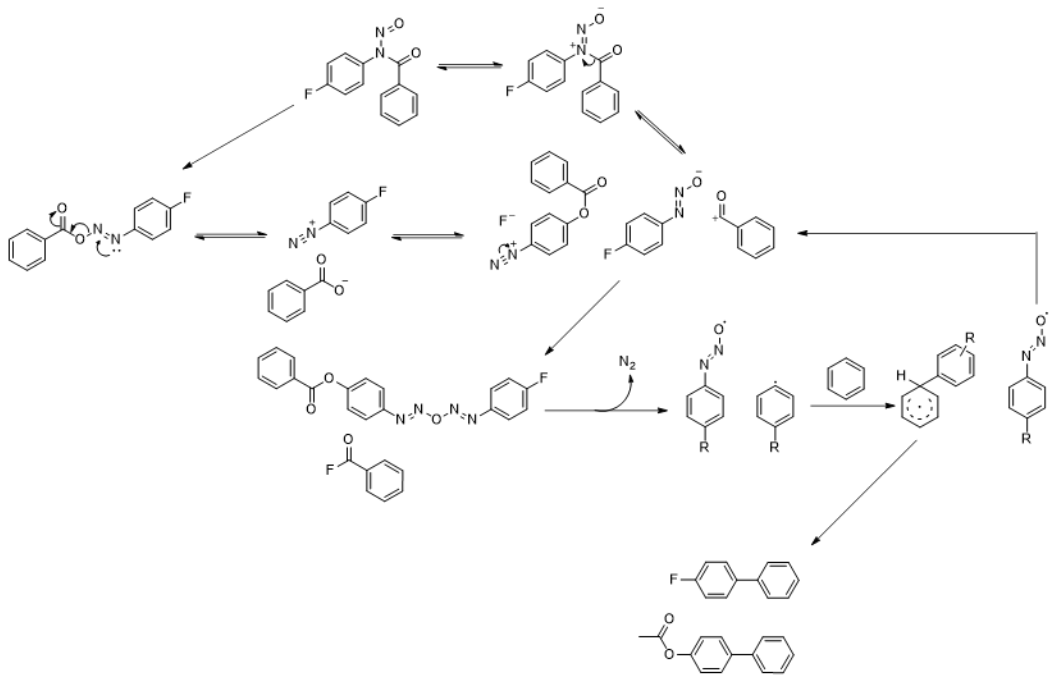

Figure 12: Proposed mechanism by Suschitzky and co-workers that bolsters the mechanism originally proposed by Richard and Freudenberg.[13]

confirmed by the independent synthesis and study of the (N-phenyl-acetamido)phenyl nitroxide (Figure 13).[14] The conformation of the a (N-phenyl-acetamido) phenyl nitroxide radical suggested

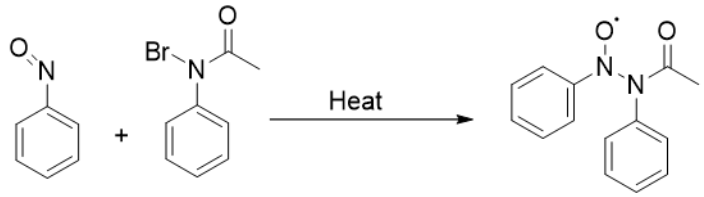

Figure 13: Synthesis of the (N-phenyl-acetamido)phenyl nitroxide radical.[14]

that the phenyldiazotate radical was not forming, resulting in the need for a new mechanism that could explain the formation of the (N-phenyl-acetamido)phenyl nitroxide radical.[14] Chalfont and Perkins were able to propose a new mechanism (Figure 14) for the N-aromatic nitrosamide

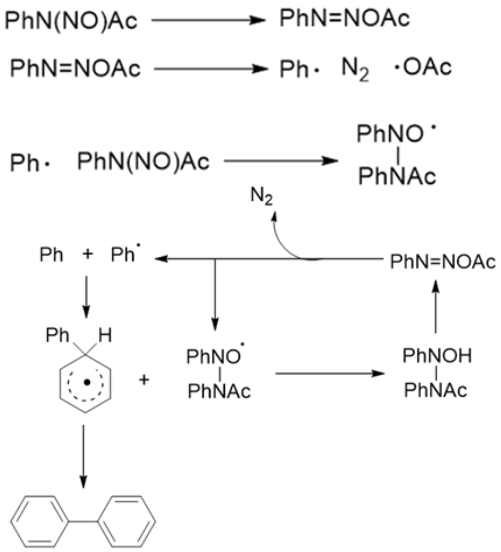

Figure 14: Mechanism proposed by Chalfont and Perkins in which (N-phenyl-acetamido)phenyl nitroxide acts as the primary radical carrier.[14]

decomposition in which the (N-phenyl-acetamido)phenyl nitroxide played a key role.[14] With the results of the mechanistic studies performed by Chalfont and Perkins, it seemed that the question of how N-aromatic nitrosamide decomposition occurs was finally answered, yet this was demonstrated to not be the case, as 2 years later Cadogen and co-workers would call into question the mechanistic behavior of N-aromatic nitrosamides. E.S.R studies by Cadogen and co-workers demonstrated that the (N-phenyl-acetamido)phenyl nitroxide species did not form in all solvents.[15] Cadogen and co-workers also observed a second signal in all solvent systems which indicated that another radical existed besides the (N-phenyl-acetamido)phenyl nitroxide. This second radical was determined to be the phenyldiazotate radical originally proposed by Richard and Freudenberg (Figure 11).[15,16] Further work by Cadogan and co-workers demonstrated that another radical species was at play, explicitly a diazonium radical, which was formed by electron transfer to the

diazonium species. This led Cadogan and co-workers to propose a new mechanism, which once again invoked the formation of an acetate radical species (Figure 15).[17] The work performed by Cadogen and co-workers seemingly has provided the most comprehensive mechanistic picture of

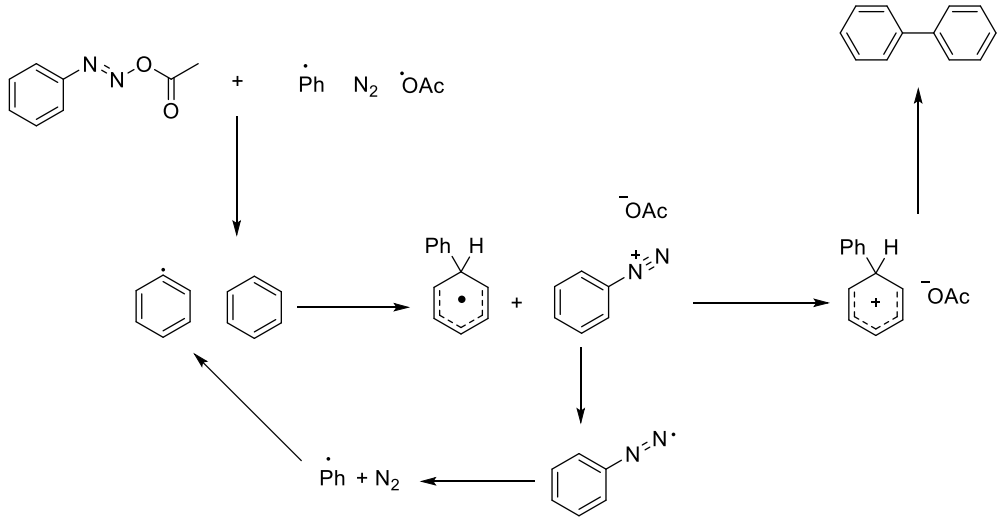

Figure 15: Latest mechanism proposed by Cadogan and co-workers based on E.S.R studies.[17]

general N-aromatic nitrosamide decomposition, with the proposed intermediates being able to explain how N-aromatic nitrosamides can give different products depending on what reaction solvent they are decomposed in. Yet, as the study of N-aromatic nitrosamide chemistry is limited by the instability of the nitrosamides themselves, much remains unknown in regard to how the structure of N-aromatic nitrosamides affects their reactivity.

Since Cadogen and coworkers had postulated their mechanism for nitrosamide decomposition, little work has been done in regard to advancing the understanding and applicability of N-aromatic nitrosamide chemistry due to the difficulty in isolating and purifying N-aromatic nitrosamides before they can decompose. What work has been done has demonstrated that N-aromatic nitrosamides show good synthetic promise as a way of preparing functionalized aromatic molecules in a controlled and facile manner. In 1999 Glatzhofer and Roy demonstrated that decomposition of aromatic nitrosamides in acetic acid/acetic anhydride could give aromatic esters in excellent yields, with high functional group and steric tolerance (Figure 16).[18] Solvent

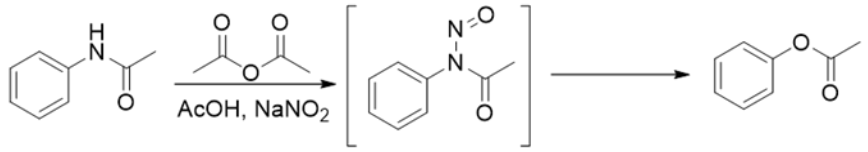

Figure 16: The synthesis of aromatic esters through nitrosamide decomposition by Glatzhofer and Roy.[18]

studies conducted by Glatzhofer and co-workers were consistent with the decomposition of N-aromatic nitrosamides through a radical pathway. When decompositions were performed in methyl methacrylate (MMA), the resulting polymethymethacrylate (PMMA) polymer was obtained. MMA can only be initiated anionically with strong nucleophiles, and radically with radical initiators, but not cationically.[18] This provided strong evidence for a radical pathway. Further evidence was provided by decomposition studies performed in toluene, which resulted in the formation of bibenzyl instead of the formation of biphenyl. (Figure 17) .[18]

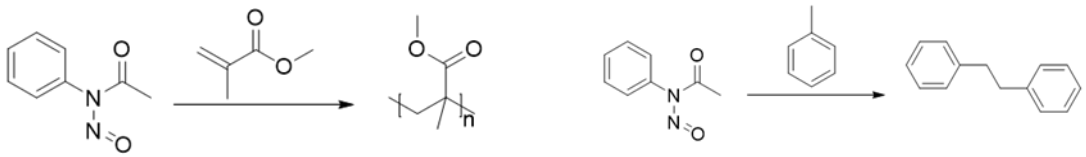

Figure 17: Nitrosamide decompositions carried out by Glatzhofer and Roy demonstrating the radical behavior involved in the nitrosamide decomposition.[18]

In 2006 Bartberger and co-workers showed that fluorinated aromatic nitrosamides exhibit aryne behavior, resulting in excellent Diels-alder reactivity upon decomposition of the nitrosamide. These results suggested that an ionic mechanism was at play, as the increased aryne behavior was attributed to the lowered pKa of the proton adjacent to the N-aromatic nitrosamide.[19,20] The N-aromatic nitrosamide could undergo normal rearrangement to the phenyldiazoacetate, which could then dissociate into the resulting diazonium acetate ion pair.[20] The acetate ion is then capable of deprotonating the proton adjacent to the diazonium moiety, resulting in a push-pull system in which the aryne could be formed as the diazonium moiety is eliminated as N_2 gas (Figure 18).[20]

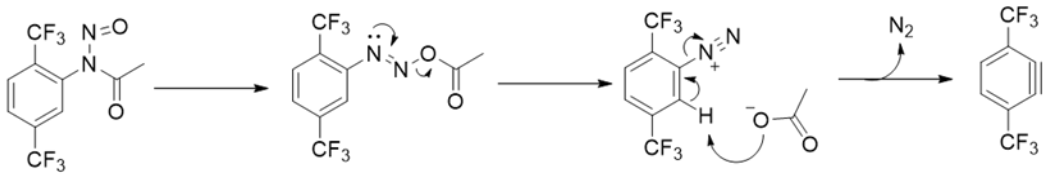

Figure 18: Postulated mechanism for the formation of benzynes through nitrosamide decomposition.[20]

While this was not the first reported case of benzyne behavior being observed in the decomposition of N-aromatic nitrosoamides, Bartbergers work does represent a unique example of how the electronics of aryl nitrosamides can be used to tune and control their reactivity.[20] Based on the work carried out in the literature, it seems reasonable that the decomposition of N-aromatic nitrosamides can be used to access a number of different functional group transformations in a controlled and high yielding manner under the right conditions.[1] As a number of issues are currently associated with the functionalization of aromatic rings, the use of N-aromatic nitrosamide chemistry may prove to be a powerful tool for overcoming these issues if the chemistry continues to develop.[1]

1.2 Synthesis of Aromatic Nitrosamides and Their Utility in The Functionalization of Aromatic Rings

The functionalization of aromatic rings has proven to be an important synthetic transformation in organic synthesis as aromatic rings play a key role in the function of many different molecules, whether they are small molecule drugs or molecules with desirable material properties. The functionalization of aromatic rings is still primarily accomplished through electrophilic aromatic substitution reactions where a strong electrophile is introduced to the aromatic ring, allowing the aromatic ring to act as a nucleophile. This has led to the ability to access a diverse array of functionalized aromatics (Figure 19).[21,22] Once installed, many of these functional groups can be readily transformed to access other molecular structures.

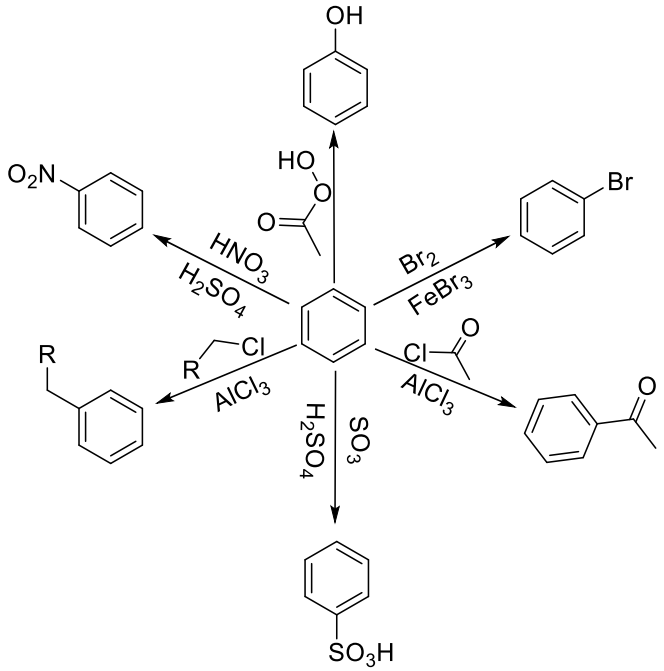

Figure 19: Various examples of electrophilic aromatic substitution reactions yielding functionalized aromatics.

While this approach has proven to be a diverse and powerful tool it has its drawbacks. Aromatic rings functionalized with electron withdrawing groups are poor substrates for such reactions as they are poor nucleophiles. These reactions are also highly susceptible to steric and

electronic directing effects, which can make functionalization at a specific position difficult to achieve.[1,22] These problems become further exacerbated for specific targeted functional groups. Aromatic alcohols, also known as phenols, are a key functional group in nearly all areas of chemistry. Not only are phenols important in their own right but they also serve as precursors to other important functional groups, such as quinones and aryl ethers. Yet only a handful of methods exist for making phenols and their related functionalities, and most of these methods suffer from the problems stated earlier.[1,22]

Phenols can be synthesized directly through the use of peroxyacids which act as a source of electrophilic "$^{+}$OH," in which the $^{+}$OH is added to the aromatic ring by using an electrophilic aromatic substitution, which can go through either an intermediate epoxide or an intermediate carbocation (Figure 20).[1,22] This method in particular suffers from a number of problems, the first

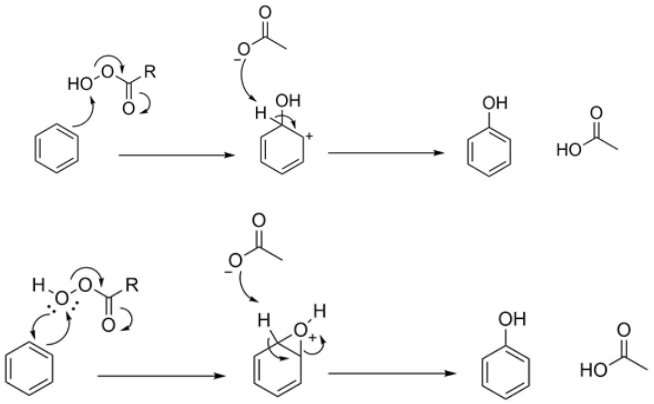

Figure 20: Possible mechanistic pathways for the hydroxylation of aromatic rings by peroxyacids.[22]

being that OH groups are strongly electron donating, and once installed on the aromatic ring can result in undesired over-addition, even when stoichiometric amounts of the peroxyacid are used.[1] As previously stated, this reaction employs peroxyacids, which are strong oxidizers and can react

with other substituents that are already installed on the aromatic ring leading to undesired side reactions (Figure 21).[22] Due to these issues, indirect methods have been developed in order to

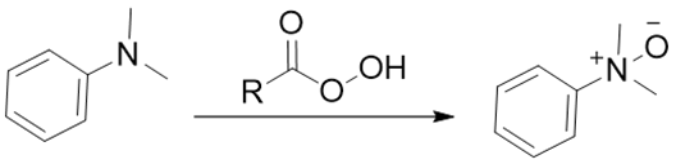

Figure 21: Oxidation of aryl amides by peroxyacids.

synthesize phenols. One of these indirect strategies is the Baeyer-Villiger Oxidation, which yields an ester from a ketone through a concerted oxidative rearrangement (Figure 22).[1,21,22] After

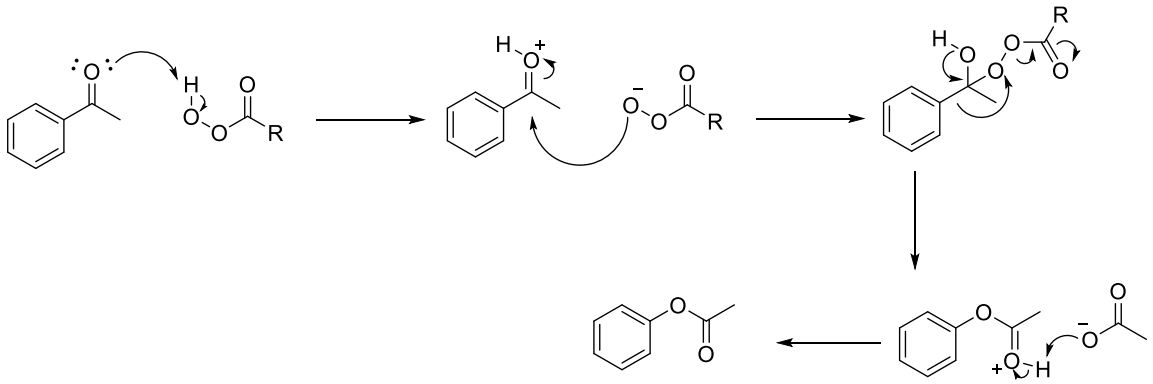

Figure 22: Mechanism of the Baeyer-Villiger Oxidation to synthesize aromatic esters.

successful installation, the ester can be readily hydrolyzed under mild conditions to yield the corresponding phenol. While this methodology does solve the regiospecificity and over-addition issues that can accompany the use of direct phenol synthesis with peroxyacids, this method still uses peroxyacids to carry out the key transformation, which can result in the same functional group tolerance issues discussed earlier.[1]

A strategy for making phenols and aryl ethers that circumvents many of the issues present in the peroxyacid methodology is the solvolysis of diazonium salts which can be readily prepared from anilines (Figure 23).[1,21,22] Diazaonium salt chemistry is well established and its ability to give access to a wide variety of functionalized aromatics under Sandmeyer reaction conditions is well proven.[21,22] In the Sandmeyer reaction a copper (I) reagent is used to reductively eliminate N_2 gas from the aromatic ring allowing for the radical addition of one of the copper ligands (Figure 24).[21]

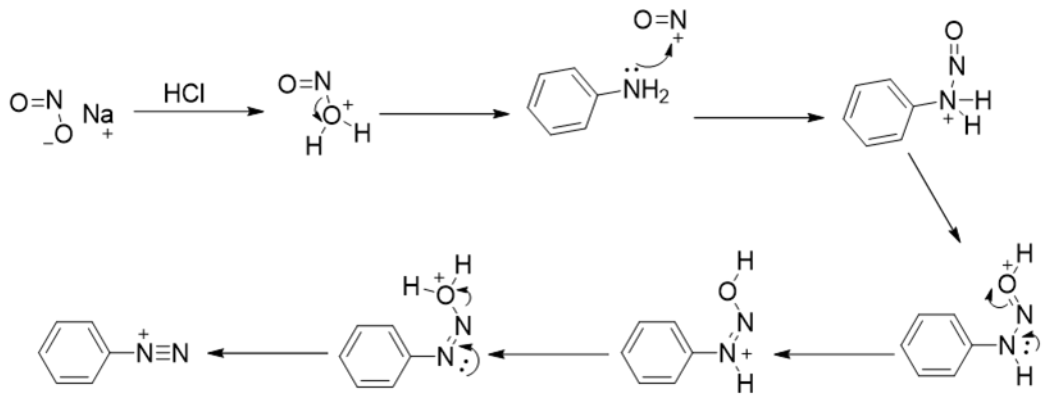

Figure 23: Synthesis if diazonium salts from aromatic amines.

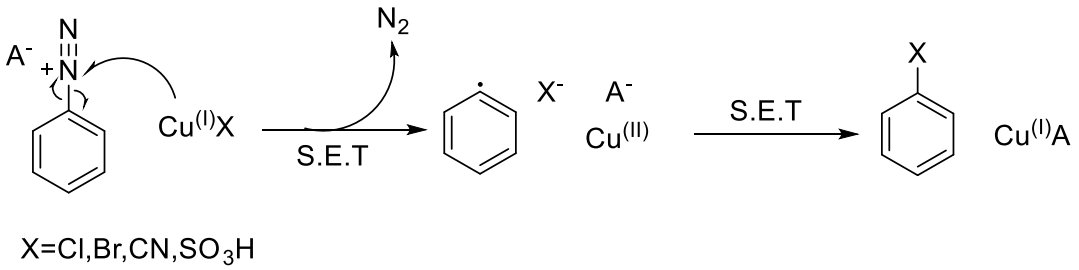

Figure 24: Example of the Sandmayer reaction allowing for the formation of cyanobenzenes, aryl halides and aryl sulfonates.

This method is highly selective due to the election deficient nature of the diazonium cation, making it the primary sight for electron transfer to occur. This method also has the advantage that isolation of the diazonium salt is generally not necessary.[21,22] The synthetic utility of this reaction was readily demonstrated by Evans and co-workers during their total synthesis of teicoplanin aglycon in which they used the Sandmayer reaction to affect the late stage transformation of an aryl amine to an aryl chloride in 58% yield (Figure 25).[23] Considering the number of other reactive

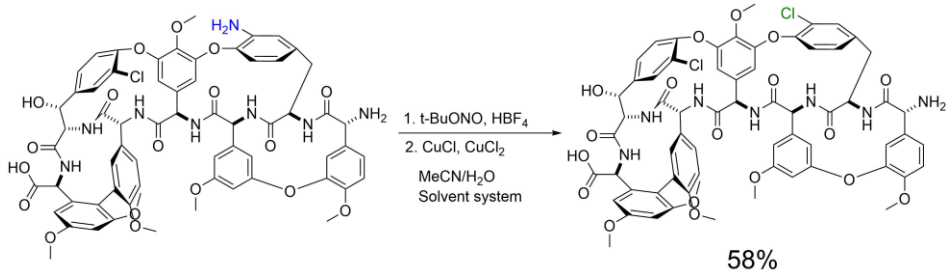

Figure 25: Use of the Sandmayer reaction to affect the late stage installation of a chloride in the total synthesis of teicoplanin aglycon.[23]

functionalities present in the compound, it is impressive that such a significant yield can be obtained under these conditions, demonstrating how powerful of a tool diazonium displacements can be at accomplishing desired aromatic transformations.[23]

The utility of diazonium salts can be easily extended beyond the limited range of the Sandmeyer reaction through solvolysis reactions. By simply heating the diazonium salt substrate in a desired solvent, a number of different functional groups can be obtained. In the synthesis of phenols the diazonium salt is typically heated in water.[24] In the case of aryl ethers the diazonium salt is heated in the desired alcohol solvent.[25] Aryl esters can also be obtained by heating the diazonium salt in a mixture of acetic acid and acetic anhydride (Figure 26).[24] In most cases these

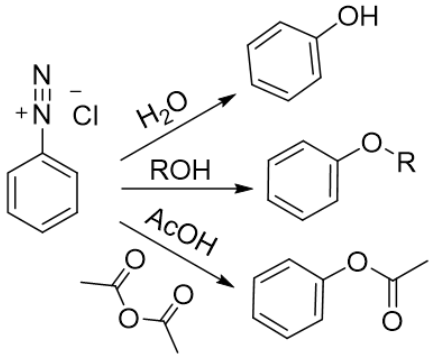

Figure 26: Examples of diazonium solvolysis reactions allowing for the formation of phenols, aryl ethers, and O-aromatic esters.

reactions are thought to go through a concerted S_NAr like mechanism, or through an S_N1 like mechanism where a formal carbocation is formed (Figure 27). In both cases the liberation of N_2

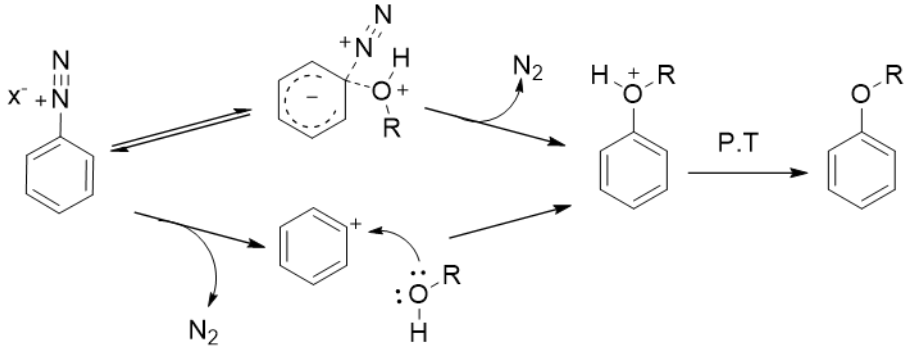

Figure 27: Postulated mechanisms of diazonium solvolysis.

gas acts as a strong thermodynamic driving force for the reaction.[21,22,24] There are a number of unique features that make this reaction methodology an effective way of synthesizing phenols and related functional groups. The first of these is that, unlike the previous methodologies which go through electrophilic aromatic substitution, these reactions operate under nucleophilic addition conditions and, as a result, milder reagents, such as water, can be used to form the phenol, eliminating the issues that are typically encountered when strong electrophilic reagents are used.[1] Diazonium solvolysis also presents a major advantage over other methods due to the carbocation-like species that is formed during these solvolysis reactions. The importance of this reactive species comes down to the fact that the empty p orbital left behind by the elimination of N_2 gas is orthogonal to the π system of the aromatic ring, which inhibits any strong resonance effects from impacting the reaction.[1,22] As a result, diazonium solvolysis reactions typically give good regioselectivity regardless of steric or electronic effects, overcoming many of the issues present in the methodologies discussed earlier (Figure 28).[1,22] Despite these large number of attractive

Figure 28: Decomposition of diazonium salts to yield non-resonance stabilized aryl cations.

features, diazonium reactions are not without their own problems. Generally, the diazonium salt must be isolated if the desired solvolysis reaction is to be performed in a high yielding manner, otherwise competition will occur between the components of the solvent system, resulting in complex mixtures.[24] Isolation can be problematic as many diazonium salts are shock sensitive and are prone to undergoing high energy decompositions in the solid state.[1] Diazonium salt reactions have also been demonstrated to have highly variable behavior between substrates leading to inconsistent reaction behavior (Figure 29).[25] While all of these methodologies have their strengths

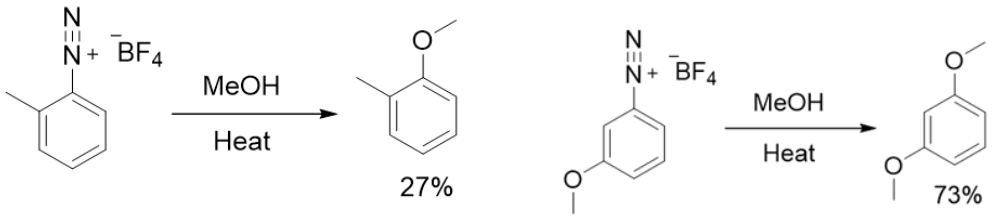

Figure 29: Literature examples of the solvolysis of diazonium salts in methanol, demonstrating the wide variability in diazonium reaction yield.[25]

and weaknesses, it is clear that in regard to the synthesis of phenols and related functional groups, a better methodology is needed that can readily allow for the synthesis of the desired phenol or related functionality in a consistent and nearly universal manner.

N-Aromatic nitrosamides are a potential solution to the problems found with the methodologies discussed earlier. N-Aromatic nitrosamides are prepared, in a fashion similar to that of diazonium salts, by treating the corresponding N-aromatic amide with $NaNO_2$ in a mixture of acetic acid and acetic anhydride.[1] The resulting nitrosamide can undergo rearrangement to form an acetoxyazoaromatic intermediate (Figure 30 (A)) which can cleave heterolytically or

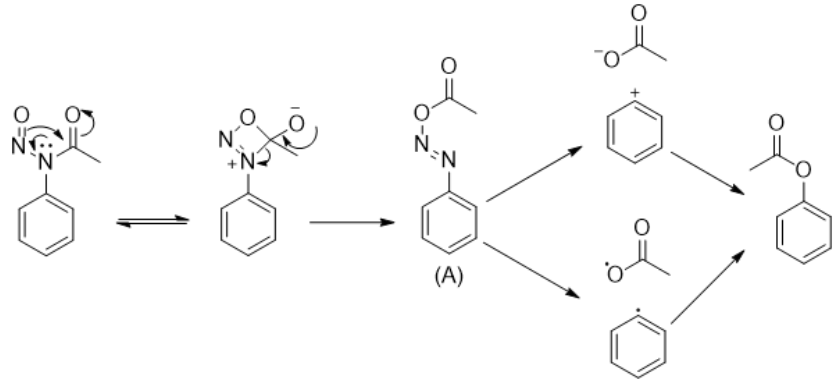

Figure 30: Proposed modes of nitrosamide decomposition leading to the formation aryl esters.

homolytically, giving either an aryl cation or an aryl radical (Figure 30).[1] Work in the literature has already demonstrated that these nitrosamide reactions are a highly effective, functional group tolerant way of preparing O-aromatic esters, which can then be readily transformed into phenols by hydrolysis (Figure 31).[1,18] Despite the promise of this methodology, it is currently hindered by the same isolation problems as diazonium salts. While O-aromatic esters can be readily obtained

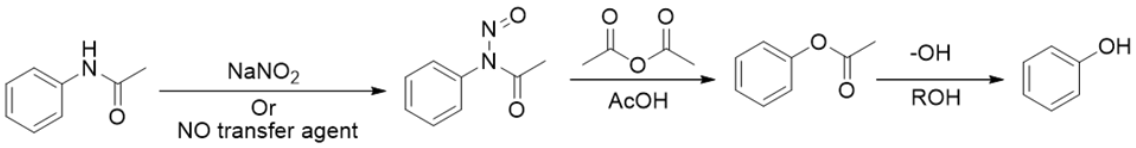

Figure 31: The synthesis of aromatic esters and phenols from aromatic nitrosamides.[1,18]

from nitrosamides, attempting to access other substrates through solvent mixture solvolysis typically leads to complex product mixtures and poor yields. Isolation and storage of nitrosamides suffers from the same instability problems as diazonium salts due to the rapid formation of the acetoxyazoaromatic intermediate which quickly decomposes.[2,4] In the decomposition of N-nitroso-N-(2,4,6-tri-*tert*-butylphenyl)acetamide it was shown that stable N-aromatic nitrosamides can be made by introducing a sterically hindered environment around the nitrosamide functionality.[26] In the case of N-nitroso-N-(2,4,6-tri-*tert*-butylphenyl)acetamide the excessive steric bulk makes decomposition almost impossible requiring 9 days in refluxing benzene to achieve the desired N-aromatic nitrosamide decomposition (Figure 32).[26] Similar behavior was

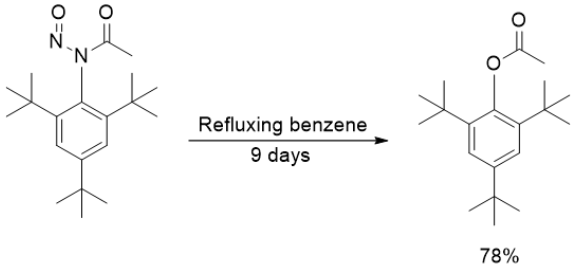

Figure 32: The decomposition of N-nitroso-N-(2,4,6-tri-*tert*-butylphenyl)acetamide to form 2,4,6-tri-*tert*-butylphenyl acetate.[26]

demonstrated in the synthesis of N-(2,6-dimethylphenyl)-N-nitrosoacetamide, which was demonstrated to be stable enough for spectroscopic analysis at room temperature.[27] Unfortunately, nothing further was reported regarding its long term or thermal stability.

Beyond N-nitroso-N-(2,4,6-tri-*tert*-butylphenyl)acetamide, steric induced stability in other nitrosamides has yet to be evaluated. In this work it is hypothesized that a sterically congested environment of the right proportions can inhibit the formation of the unstable phenyldiazoacetate intermediate, allowing for the isolation, purification, and long-term storage of these nitrosamides,

while still being able to allow these species to readily undergo rearrangement, then solvolysis, in a reasonable timeframe, when heated, allowing for the synthesis of phenols, as well as a diverse array of other functionalized aromatics.[1,4,18,26] It is proposed in this work that phenyldiazoacetate formation will be inhibited due to the increased steric bulk, hindering the nucleophilic attack of the nitroso oxygen on the carbon of the amide carbonyl, and preventing the formation of the proposed four membered ring transition state (Figure 33).[1,18,26] These stable nitrosamides will also

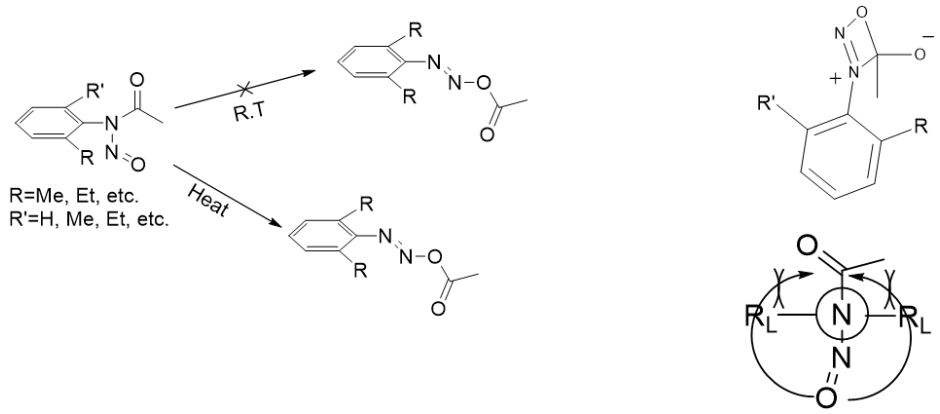

Figure 33: Induced kinetic stability of N-aromatic nitrosamides by steric hindrance. Steric clashing of the NO group with bulky alkyl groups prevents nucleophilic attack of the carbonyl from occurring at room temperature.

allow for the probing of the nitrosamide decomposition mechanism. It has long been debated as to whether nitrosamides form aryl cations or aryl radicals upon decomposition.[1,18] The understanding of this reaction behavior is key if the synthetic utility of nitrosamides is to be realized. It is hypothesized in this work that the formation of the aryl cation versus the formation of the aryl radical is highly dependent upon solvent and substrate conditions, and that aryl cation intermediates will dominate in high dielectric solvents, while radical intermediates or other possible reaction pathways will dominate in low dielectric solvents.[25] Based on the hypothesized cationic and radical intermediates it is proposed that a number of other functional groups can be accessed beyond phenols, esters, and ethers. It is proposed that solvolysis of the kinetically stable nitrosamides in any nucleophilic solvent with a high dielectric constant will lead to addition of the solvent molecule to the aromatic ring (Figure 34).

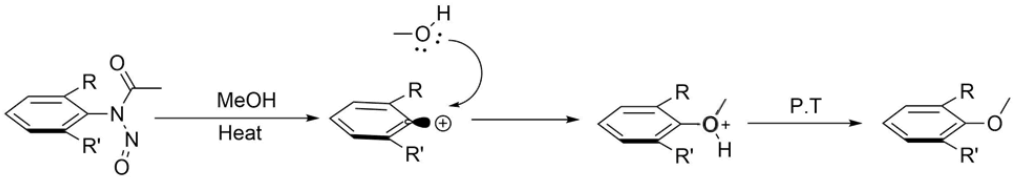

Figure 34: Formation of aryl cations from N-aromatic nitrosamides in solvents with high dielectric constants.

It is proposed that the methodology developed in this work can be readily applied to a wide range of aromatic systems containing steric bulk at positions adjacent to the nitrosamide functionality, allowing for a threshold of steric stability to be established for the N-aromatic nitrosamide systems. Once a threshold for the amount of steric bulk needed to stabilize N-aromatic nitrosamides is established, stable N-aromatic nitrosamides can be readily prepared and isolated allowing for their decomposition in a wide variety of solvents to be studied. These solvent decomposition studies can help establish the variety of products that can be quickly accessed through solvolysis reactions and establish how solvent conditions favor the formation of these products. In the case of phenol or aryl ether formation, as well as other selected product formations, direct comparisons can be made between the yields of the nitrosamide reactions and the yields of reported diazonium reactions, establishing the relative synthetic efficiency of these N-aromatic nitrosamide reactions. The results of these studies will allow for the continued improvement of these N-aromatic nitrosamide reactions. The results of these studies will be discussed in Chapters 2 & 3.

The methodology developed in this work can be applied to polyaromatic systems as well to gain access to poly(aryl) ethers that can act as precursors to electroactive polyquinones or polyphenols, which can be used directly as electroactive materials for energy storage and transport.[28] Polyquinones are of interest to the scientific community due to their biological

relevance, as well as their redox behavior, making them prime targets for material applications.[28,29] In particular, cyclophane quinones are an interesting subset of polyquinones that display a number of unique redox properties due to the close proximity of the quinone moieties, but they are difficult to access due to the unique chemical challenges that are associated with cyclophane structures.[29] A more in-depth analysis of cyclophanes demonstrates why these synthetic difficulties arise and also demonstrates how N-aromatic nitrosamide chemistry may be useful in solving these synthetic problems.

1.3. Brief Overview of Cyclophanes

Cyclophanes are hydrocarbons consisting of an aromatic unit and an aliphatic chain that forms a bridge between two positions of the aromatic ring. Many different cyclophane motifs are known and can be synthesized in a variety of ways.[29] The confined geometries of the often-distorted aromatic rings in these classes of molecules have allowed many studies of the fundamental properties of aromaticity.[29] The well-defined structure and high strain of cyclophanes has found utility in several applications including asymmetric catalysis, organic electronics, molecular machines, and in the Parylene process in industry (Figure 35).[29,30] The first man-made

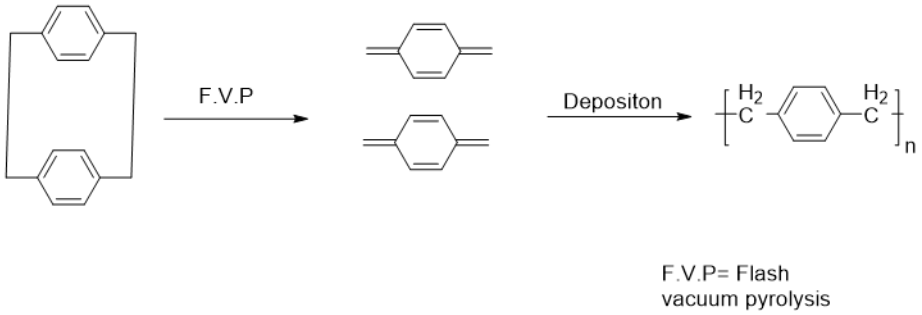

Figure 35: Process of making polyparylene form [2.2] paracyclophanes.[29,30]

cyclophane was [2.2]metacyclophane which was synthesized by Pellerin in 1899 using Wurtz coupling methodology.[31] Some years later Cram reported the synthesis of [2.2]paracyclophane, which was also accomplished using Wurtz coupling methodology (Figure 36).[32] Since these initial

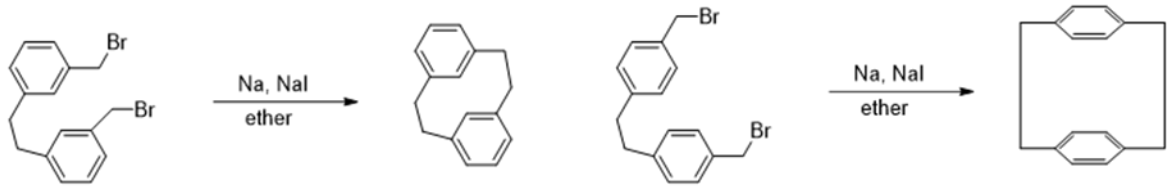

Figure 36: Original syntheses of [2.2] meta and paracyclophanes using Wurtz couplings.[31,32]

developments, cyclophane chemistry has advanced significantly and many different cyclophane structures are now known bearing various functionalities (Figure 37).[33,34,35] Yet despite the large

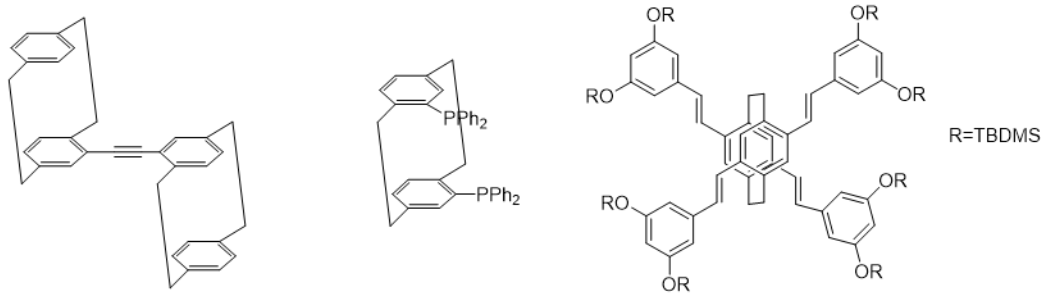

Figure 37: Synthesized [2.2] Paracyclophanes bearing various functional groups.[35]

amount of work that has been accomplished in the field, the synthetic manipulation of cyclophanes remains a challenge due to the generally low yielding nature of their synthesis, as well as the difficulty in performing post-modifications of the cyclophane system due to steric and electronic effects.[29] This is especially apparent for [2.2]paracyclophane systems, where excessive steric bulk on the precursor compounds can completely inhibit cyclophane formation, and instead result in uncontrolled polymerization. A classic example of where these issues appeared was in the synthesis of octamethyl[2.2]paracyclophane (Figure 38) which results in less than 10% yields of

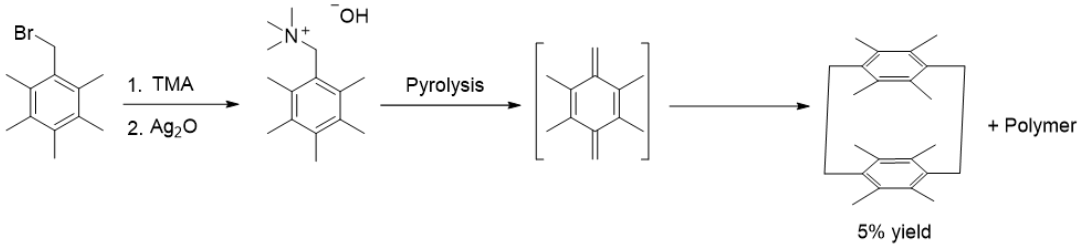

Figure 38: Synthesis of octamethyl[2.2]paracyclophane using Hofmann elimination methodology. The low yield of the desired cyclophane is due to the high steric demand of the dimerization.[36]

the final cyclophane product.[36] Such issues result in the need to post-functionalize the cyclophane system, which generally calls for highly reactive reagents and results in poor yields and poor regioselectivity for the desired transformation.[35] These issues are particularly evident in the synthesis of amido-[2.2]paracyclophanes, which are sought after as novel ligands for new metal catalysts.[37] Typically, the corresponding cyclophane is nitrated to yield the desired nitrocyclophanes, which are then reduced to the corresponding amines in acetic anhydride, which yields the desired amide. The nitration of these cyclophanes is typically low yielding and results in a mixture of various nitrocyclophanes, which must then be separated, further lowering the yield of the reaction (Figure 39).[38] These nitrocyclophanes can also be obtained by preparing the

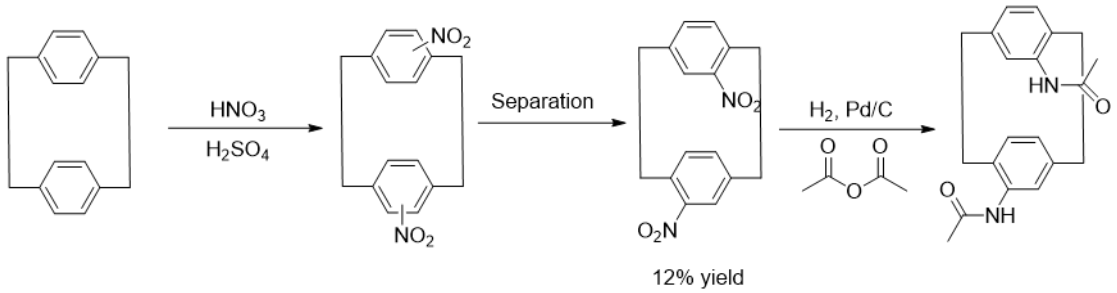

Figure 39: Synthesis of diamido [2.2]paracyclophane (A) from the nitration of [2.2]paracyclophane.

Hofmann salt of the nitro monomer and carrying out the subsequent elimination (Figure 40).[38] The

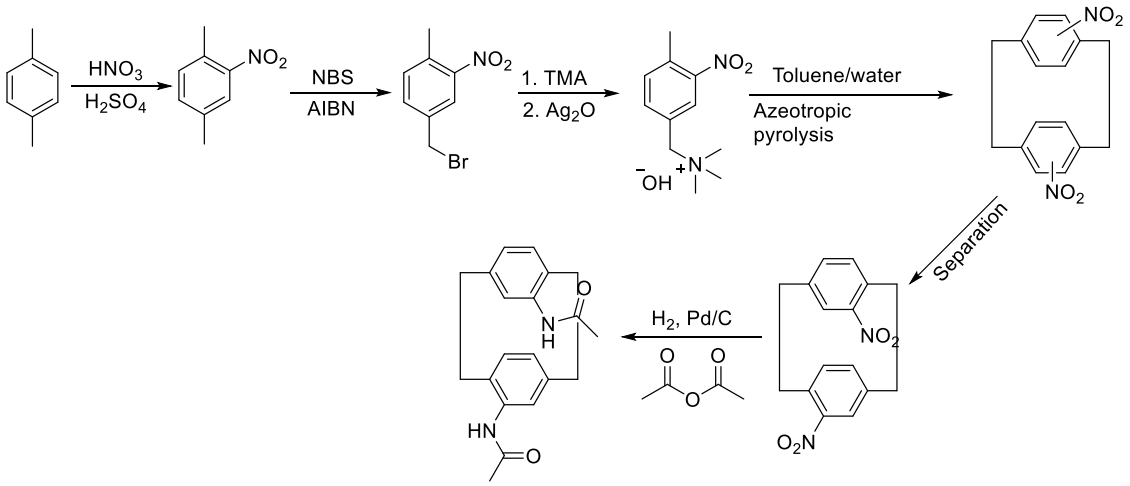

Figure 40: Synthesis of diamido [2.2]paracyclophane (A) from Hofmann elimination.

elimination method yields cyclophane mixtures with fewer components. As a result, this route gives higher yields of the desired nitrocyclophane which was obtained in 38% yield, a marked improvement over the 12% obtained when trying to install the nitro groups on the cyclophane scaffold.[37] While cyclophanes containing diverse functionalities are sought after due to their potential applications in the development of new materials, the barrier to their synthesis has made this a difficult goal to achieve without better synthetic methods for their late stage functionalization.

1.4 Ester and Phenol Cyclophanes

Cyclophanes bearing ester or hydroxy groups are a unique subset of cyclophane systems due to the highly electron rich nature of the molecules in conjunction with the close proximity of the ring systems. These molecules are also of interest from the standpoint that they are precursors to quinone cyclophanes, which are of interest due to their strong charge transfer interactions and unique redox behavior, making them promising materials for molecular electronics and energy storage applications. This can be seen in the case macrocyclic quinone cyclophanes, such as [5] pillarquinone, where the large number of redox active moieties in close proximity to one another result in larger redox potentials and higher capacities, making these promising molecules for organic battery applications.[40] The charging and discharging of these macrocyclic quinone cyclophanes also results in the increase and decrease of their cavity size, making these molecules promising candidates for molecular machines (Figure 41).[40] While several [2.2]cyclophane ester and phenol derivatives are known, the difficulty involved in synthesizing these chemical species has limited their study and development into potentially useful electrochemical materials. In order

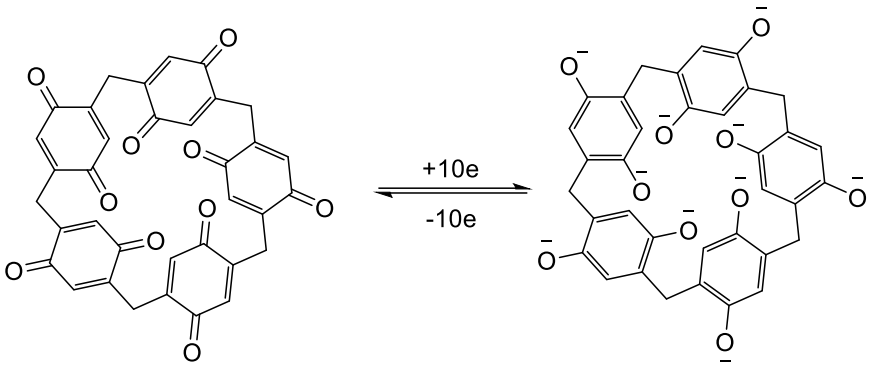

Figure 41: Pillar[5]quinone and its reversible 10 electron redox behavior.[40]

for these compounds to become promising precursors to electrochemical materials, better synthetic methods are needed in order to access these cyclophane derivatives.

Inspired by the initial attempts made by Donald Cram, Staab and co-workers synthesized the first quinone cyclophane in 1973 (Figure 42).[42] Staab and co-workers put together

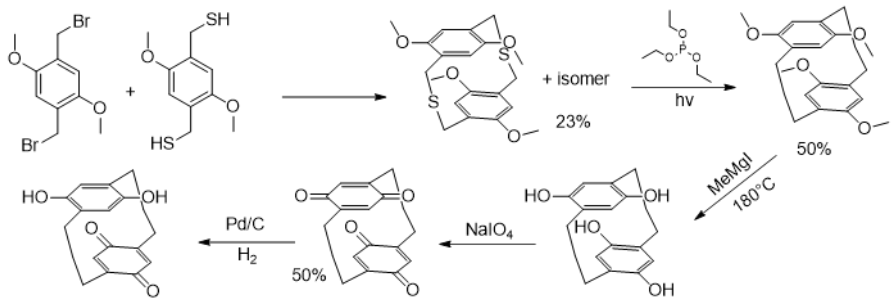

Figure 42: Synthesis of [2.2]paracyclophane bis-quinone and its quinhydrone.[42]

their cyclophane structure using a sulfur dimerization of 1,4-bis(bromomethyl)-2,5-dimethoxybenzene, followed by a sulfur extrusion to give 4,7,12,15-tetramethoxy[2.2]paracyclophane.[42] The resulting cyclophane was demethylated using methyl magnesium iodide to give the hydroquinone, the key intermediate species, which was oxidized with sodium periodate to give the desired [2.2]paracyclophane bis-quinone.[42] The bis-quinone was hydrogenated to give the quinhydrone, which exhibited strong charge transfer characteristics.[42] Staab and co-workers expanded on this work in 1977 with the synthesis of [2.2](1,4)naphthalenophane-4,7,14,17-tetrone using a Hofmann elimination route, followed by demethylation and oxidation (Figure 43).[43] Reduction of the synthesized quinones gave the

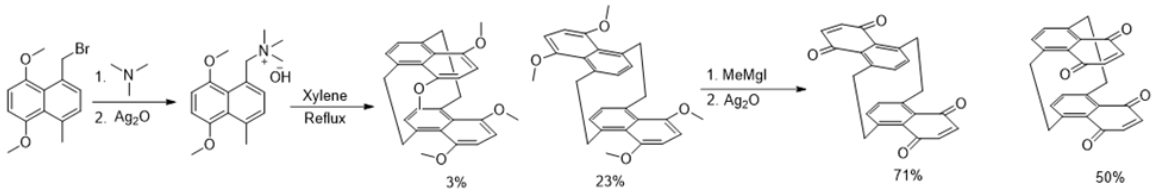

Figure 43: Synthesis of [2.2](1,4)Naphthalenophane-4,7,14,17-tetrone.[43]

corresponding quinhydrones which were then studied using Uv-vis spectroscopy.[43] Interestingly, the charge-transfer behavior of the two quinhydrone isomers was found to be almost identical, indicating that the charge transfer process was mediated through the overlapping aromatic rings in both systems, thus demonstrating clear delocalization of the charge transfer process in the π system of the two quinhydrones.[43] In 1978 Volker synthesized [2.2.2.2](1,2,4,5)-cyclophane quinhydrone, as well as the quinone, using the same methodology used by Staab and co-workers.[44] The synthesis was performed over several steps, with many of the key reaction steps giving yields less than 30% (Figure 44).[44] Uv-vis studies of the [2.2.2.2](1,2,4,5) Cyclophane quinhydrone showed broad charge transfer bands with an extinction coefficient of 1600 and a lambda max of 492 nm.[44]

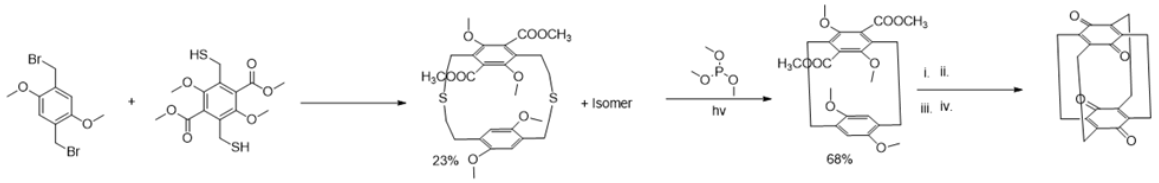

Figure 44: Synthesis of [2.2.2.2](1,2,4,5) Cyclophane bis quinone, carried out by sulfur dimerization, followed by sulfur extrusion. Chloromethylation (i) followed by reduction with dibahl (ii) give dimethyl-bis aldehyde species. Treatment with tosylhydrazene and heating resulted in carbene insertion and the formation on the last two cyclophane bridges (iii). Treatment with methyl magnesium iodide with heat followed by oxidation with silver oxide gave the desired quinone (iv).[44]

In 1992 Taniguchi and co-workers were able to develop a stepwise synthesis of Calix[4]quinone from 25.26.27.28- tetrahydroxycalix[4]arene (Figure 45).[45] The strategy employed by Taniguchi and co-workers relied on the pre-installed hydroxy groups of the 25.26.27.28- tetrahydroxycalix[4]arene which could be used to install hydroxy groups *para* to the initial hydroxy group through a Fries rearrangement followed directly by a Beyer-Villager

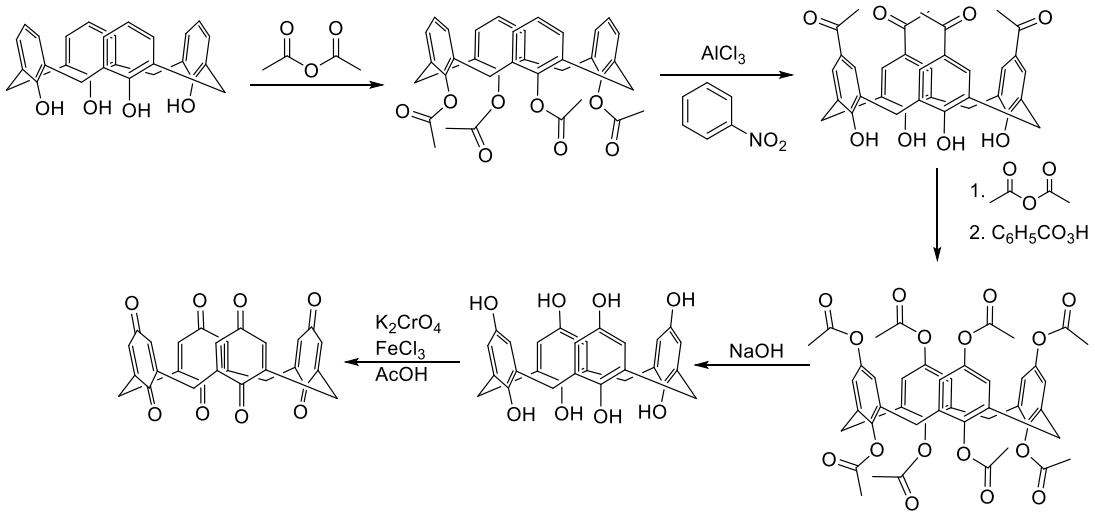

Figure 45: Synthesis of Calix[4]quinone with a total yield of 41%.[45]

oxidation.[45] The resulting 25.26.27.28- octaacetoxycalix[4]arene could then be saponified to give the 25.26.27.28- octahydroxycalix[4]arene which could then be oxidized to the calix[4]quinone.[45] In 2011 Ogoshi and co-workers were able to synthesize a macrocyclic hydroquinone cyclophane, dubbed pillar[5]arene, in an unprecedented 71% yield using a Lewis acid catalyzed cyclization, followed by demethylation (Figure 46).[47] While impressive, the synthesis of pillar[5]arene remains the exception to hydroquinone/quinone cyclophane synthesis, and not the rule with most cyclophane systems requiring many low yielding synthetic steps.

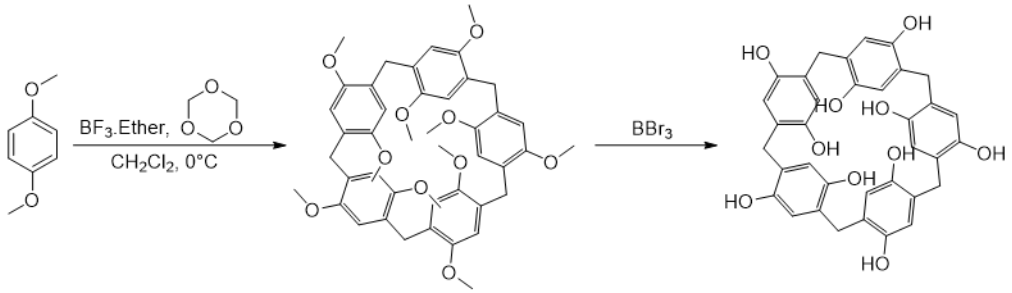

Figure 46: Synthesis of pillar[5]arene by Ogoshi and co-workers.[47]

While the work accomplished in these reported syntheses is impressive, the majority of these reported syntheses rely on preinstalled oxygen bearing groups in the form of aryl ethers or aryl hydroxyl groups limiting the diversity of the starting materials that can be used. Alternative routes to ester and hydroxy bearing cyclophanes have been able to circumvent these limitations

through the use diazonium and nitrosamide chemistry. Schultz and co-workers were able selectively synthesize 4-hydroxy[2.2]paracyclophane from [2.2]paracyclophane by mono-nitration of the cyclophane followed by reduction with palladium on carbon and then treatment with $NaNO_2$ under acidic conditions to give the diazonium tetrafluoroborate salt which was then allowed to decompose in a mixture of acetic acid and acetic anhydride to give the 4-acetoxy [2.2]paracyclophane which was then readily hydrolyzed to give the desired 4-hydroxy [2.2]paracyclophane (Figure 47).[48] This methodology was advanced by Glatzhofer and co-workers

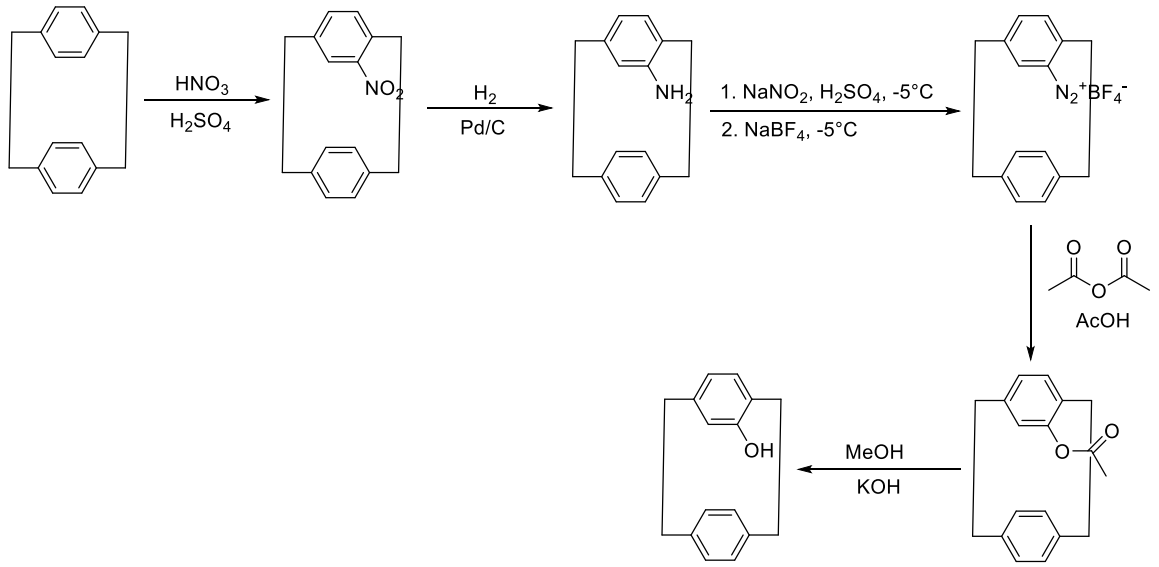

Figure 47: Synthesis of 4-hydroxy [2.2]paracyclophane by Schultz and co-workers using a cyclophane diazonium salt as a key intermediate.[48]

who demonstrated the same transformation could be readily accomplished using N-aromatic nitrosamide chemistry without requiring the isolation of the formed amide (Figure 48).[18] This work

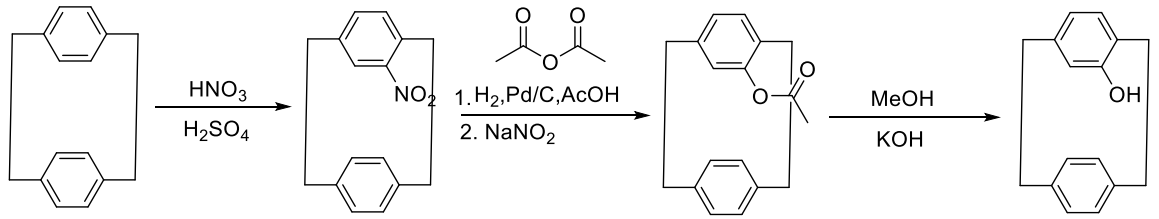

Figure 48: Simplified synthesis of 4-hydroxy [2.2]paracyclophane by Glatzhofer and co-workers using nitrosamide chemistry.[18]

was further expanded on by Ma and co-workers who used the nitrosamide methodology reported by Glatzhofer to synthesize chiral cyclophanes as ligands for developing catalysts for asymmetric Henry reactions (Figure 49).[49]

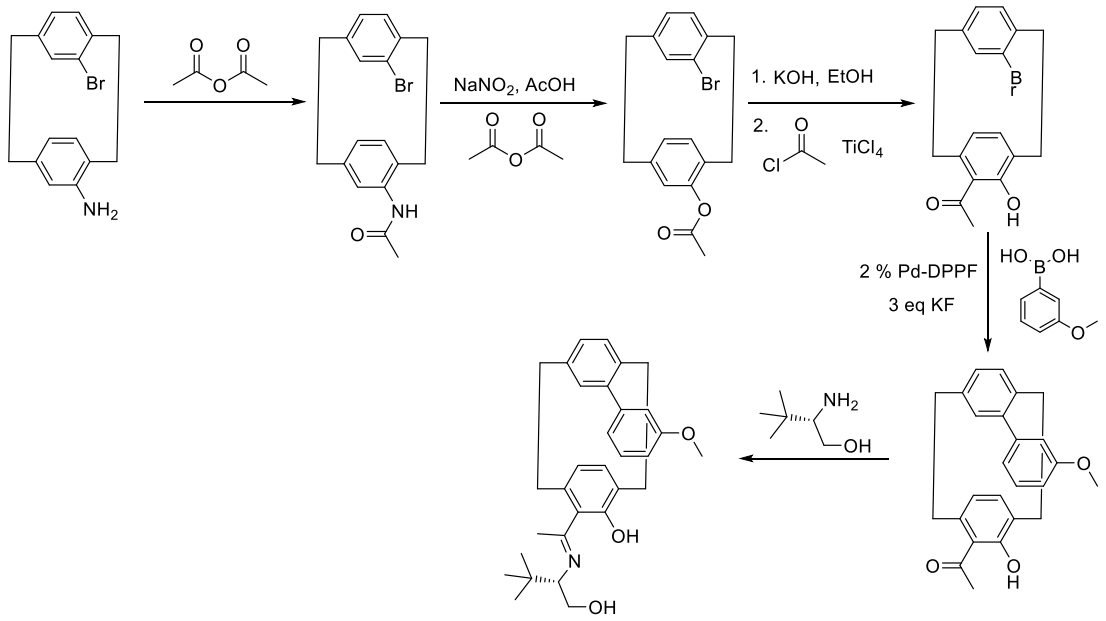

Figure 49: Synthesis of cyclophane ligands by Ma and co-workers, using the nitrosamide methodology established by Glatzhofer as a key intermediate in the installation of an aryl hydroxy group.[49]

The controlled and selective installation of ester functional groups using nitrosamide chemistry makes this method attractive for the synthesis of other ester or phenol bearing cyclophanes. Relative to the other synthetic strategies discussed for the synthesis of functionalized cyclophanes, nitrosamides are also useful in regard to the synthesis of more complex cyclophane architectures, as was demonstrated by Bartburg and co-workers who were able to build cyclophane

hydrocarbon derivatives though benzyne intermediates accessed using N-aromatic nitrosamides (Figure 50).[20]

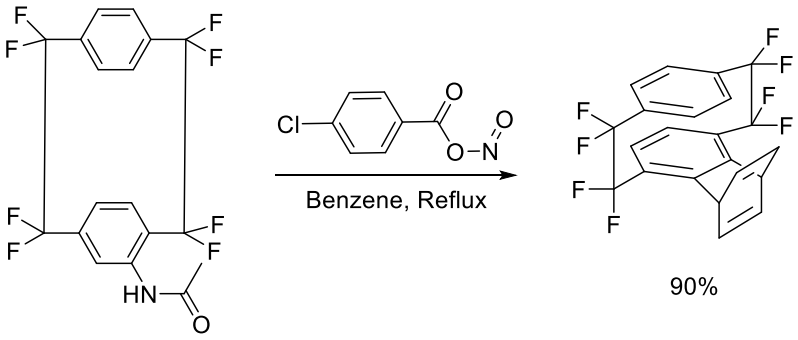

Figure 50: Use of Nitrosamide chemistry by Bartburg and co-wokers to generate cyclophane benzynes.[20]

As evidenced by the literature, only a handful of ways exist to install ester and phenol functionalities in complex polyaromatic architectures. N-aromatic nitrosamides provide a potential route by which esters can be directly installed from amides in a facile manner on these complex polyaromatic architectures which can then be readily transformed into their corresponding esters. Work by Morvant and co-workers demonstrated that sterically hindered polynitroaromatic systems could be readily prepared from the Hofmann elimination of dinitrodurene ammonium salts.[38] This elimination yielded nitrocyclophanes (A) and (B) .[38] It is proposed in this work that these sterically hindered nitropolyaromatics can be readily converted to their corresponding amides, which can then be converted into their corresponding nitrosamides (Figure 51).[38] These polyamide systems provide a testing ground for demonstrating the synthetic utility of N-aromatic nitrosamides in the synthesis of polyaromatic phenols and quinones, especially in regard to the cyclophane systems

presented in (Figure 51), which both present a high steric demand with regard to the rearrangement and elimination of the nitrosamide functionality.

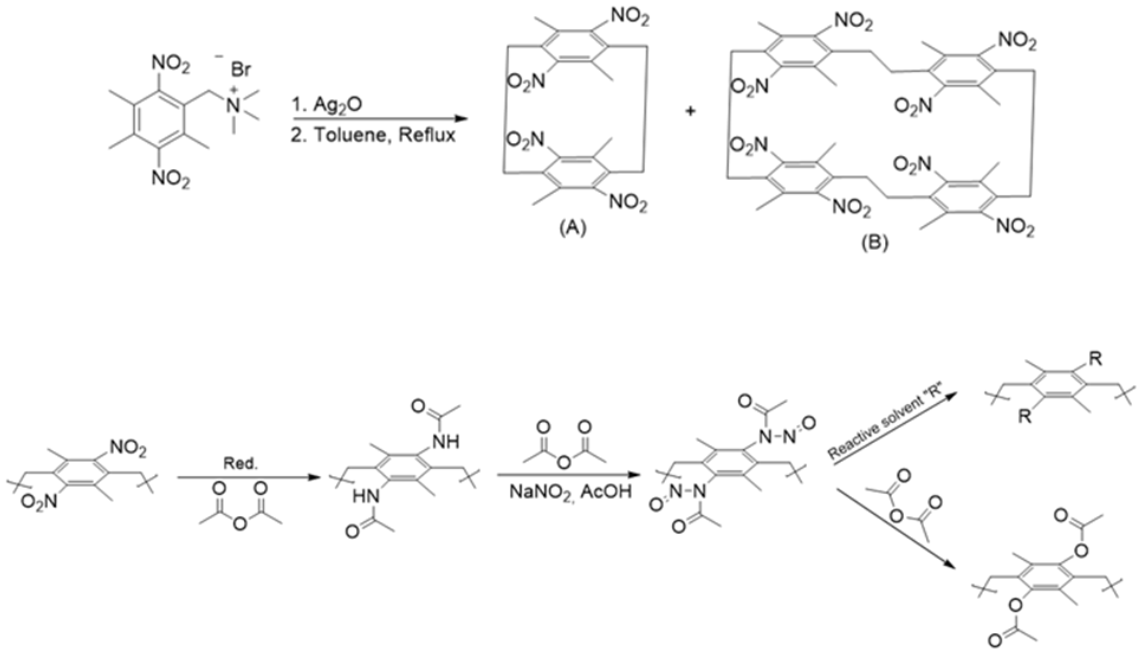

Figure 51: Synthesis of Nitrocyclophanes (A) and (B) using Hoffman elimination methodology, followed by the proposed general synthetic approach to the synthesis of functionalized cyclophanes using nitrosamide decomposition. Reduction of the nitrogroups in the presence of acetic anhydride will yield the amide which can then be transformed into the desired nitrosamide under standard conditions.[38]

Work from the literature has already demonstrated that the rates of nitrosamide decomposition reactions increased when performed on [2.2]paracyclophane scaffolds, which is possibly due to the high ring strain that is induced by the presence of nitroso functionality.[18] The release of this strain provides an extra driving force for the decomposition of the nitrosamide functionality. In the case of cyclophanes (A) and (B) it is proposed that the presence of the methyl groups on the aromatic ring will provide enough steric hindrance to induce kinetic stability that will be similar in nature to what is observed for the simple nitrosamide systems previously discussed. Decomposition of these nitrosamides in reactive solvents will be performed in order to evaluate the extent to which nitrosamide cyclophanes can be used to synthesize cyclophanes with

various functionalities. Nitrosamide decomposition will also be carried out in order to produce the desired phenols, which can then be oxidized to their corresponding quinones. It is proposed in this work that nitrosamide decomposition can be used to access cyclophane quinones/polyquinones by decomposing the nitrosamides in acetic anhydride to yield the corresponding esters, which can then be saponified to the desired phenols (Figure 52). Phenol oxidation can then be carried out

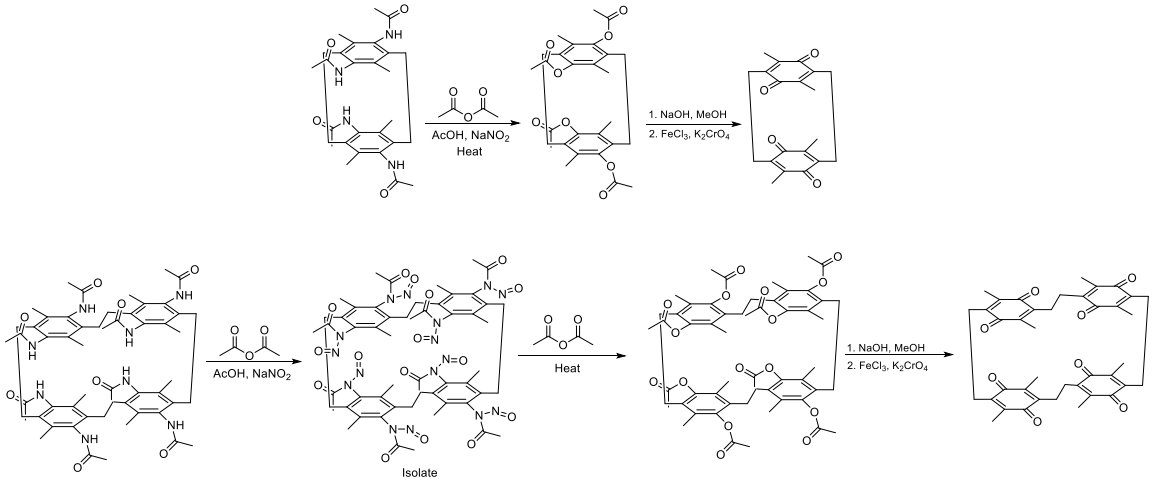

Figure 52: Proposed synthetic routes to quinone cyclophanes (A) and (B).[38,50]

with a wide variety of potential oxidizing agents such as $FeCl_3$ or K_2CrO_4. These studies will also help probe the fundamental relationship between cyclophane structure and rearrangement behavior. While N-aromatic nitrosamide rearrangements have been performed on cyclophanes and other complex systems, such rearrangement reactions have consisted the rearrangement of a single nitrosamide group. Regarding cyclophane nitrosamide reactions, only [2.2]paracyclophane scaffolds have been explored, while larger cyclophane systems have remained completely unexamined. The nitrosamide reactivity of these cyclophane systems must be explored in order to understand the extent to which N-aromatic nitrosamide chemistry can be used to effectively functionalize cyclophanes or other complex aromatic systems. The results of these N-aromatic nitrosamide studies, as well as the properties of the resulting cyclophanes, will be discussed in Chapter 4.

1.5 General Overview of Inorganic Organic Hybrid Materials

Organic–inorganic hybrids are promising materials by virtue of their strong performance characteristics, such as high mechanical strength, thermal stability, gas permeability, light emission/adsorption and electron mobility. Perovskite solar cells in particular are of great interest due to the fact that they hold an advantage over traditional silicon solar cells in the simplicity of their synthesis and processing. Traditional silicon cells require expensive, multistep processes, conducted at high temperatures (>1000 °C) in a high vacuum in special clean room facilities.[51] Organic-inorganic perovskite/hybrid materials can be manufactured with simple wet chemistry techniques.[51] While organic-inorganic perovskite/hybrid compounds have shown a great deal of promise as next generation optoelectrical and photovoltaic materials, there are issues that must be addressed in order to establish these compounds as working materials. Many organic-inorganic hybrids are plagued by instability issues and or require the use of toxic lead in their structure to achieve high efficiencies/desirable properties. As such, new inorganic organic hybrids are needed in order to overcome these issues.[51]

The first perovskite was calcium titanate ($CaTiO_3$), which was discovered by German mineralogist Gustav Rose in 1839. He gave them the name "perovskites" in honor of a Russian mineralogist Lev Alekseevich von Perovski. In 1892, the first series of lead halide perovskite structures were prepared from cesium and lead salts by H.L Well and co-workers, using aqueous solutions of the salts in order to produce the desired perovskite structures, demonstrating that perovskites could be synthesized at ambient conditions.[52,53] In 1957 C.K. Moller proved that the compounds made by Well and co-workers were determined to have a perovskite structure.[52] From 1959-1975, the applications of perovskite materials became more evident as many resistors and piezoelectric transducers made from perovskites became commercially available.[52] In 1978 Weber

and co-workers synthesized the first inorganic-organic hybrid perovskites by replacing cesium with methylammonium cations in the synthesis of the lead halides first made by Well and co-workers.[53] This work demonstrated that organic cations of the right size could be used to fabricate perovskite structures from solution. In 1994 Mitzi and co-workers developed a layered organic-inorganic halide perovskite using tin iodide, methylammonium iodide, and n-butylammonium iodide.[51,52,54] The resulting layered structure was synthesized using simple solution-based chemistry, in which a solution of the ammonium salts and tin iodide was slowly cooled to give large crystals of the layered structure. Resistivity studies of the synthesized material demonstrated that it had intrinsic semiconducting properties.[54]

In 2009 Shirai and co-workers reported that a lead halide dye-sensitized solar cell, in which methylammonium lead bromide acting as the photoactive sensitizer in a TiO_2 electrode system gave an overall device efficiency of 3.8 %, demonstrating for the first-time photovoltaic behavior in perovskite materials.[55] Upon the revelation that perovskite materials themselves had photovoltaic properties, a great deal of progress was made very quickly in regard to perovskite synthesis and device fabrication. It was quickly realized that liquid electrolyte/mediator design of dye sensitized perovskite solar cell systems led to degradation of the perovskite dye and, as such, a shift to solid state devices containing no liquid electrolyte/mediator was first realized in 2012 by Snaith and co-workers who developed a solid-state perovskite solar cell using thin films of methylammonium lead iodide chloride as the photoactive layer and thin films of spiro-OMeTAD as the hole conducting layer.[56] Using this solid state design, a power conversion efficiency of 10.9% was achieved.[56] Since 2012 a number of high efficiency perovskite solar cells have been made, with the most recent efficiency increase being reported in 2018 by Jeangros and co-workers, who synthesized a layered lead iodide cesium bromide formamidinium bromide perovskite which,

when fabricated into a solid-state device, gave an unprecedented efficiency of 25.2%, competitive with commercial silicon based solar cells.[57]

The applications of perovskite materials go far beyond the development of high efficiency solar cells. Recent work has demonstrated that perovskite materials can also be used to make efficient light emitting diodes, as was demonstrated in 2018 by Friend and co-workers who showed that a lead halide perovskite polymer composite internal quantum efficiencies of 100% which is directly competitive with a number of existing LED technologies such as organic light emitting diodes (OLED's).[58] The recent work of Friend and co-workers, shows that the development of light emitting perovskite materials is a potentially rich area of research and furthermore demonstrates that the potential applications of perovskite materials are just beginning to be developed, making perovskites an exciting area of research.[58] As the properties of perovskite materials results heavily from their continuous solid state structure, the key to developing better and more efficient perovskite materials lies in understanding how the structure of perovskites result in their observed properties.

1.6 Organic-Inorganic Perovskites and Organic-Inorganic Hybrids: Structure and Properties

The basic structure of the organic-inorganic perovskites family is AMX_3. It consists of corner-sharing MX_4^- 6 octahedra, where X is typically an anion and the M atom is generally a divalent metal that can adopt an octahedral coordination geometry, such as $Ge^{(II)}$, $Sn^{(II)}$, $Pb^{(II)}$, $Co^{(II)}$, $Fe^{(II)}$, $Cu^{(II)}$, $Ni^{(II)}$, $Mn^{(II)}$, $Cr^{(II)}$, $Pd^{(II)}$, $Cd^{(II)}$, or $Eu^{(II)}$.[59] A is an organic cation that fills the large coordinated holes between the octahedra (Figure 53).[59] Based on the geometric constraints

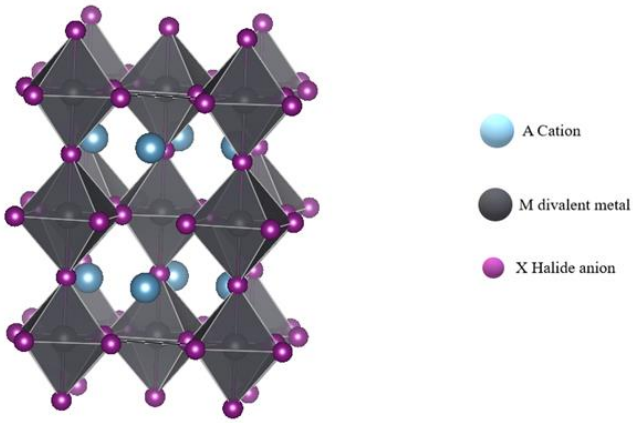

Figure 53: Generic 3-dimensional perovskite structure adhering to the AMX_3 structure motif.

imposed by a rigid sphere model, the size of the cation influences how the perovskite structure forms. Here t is defined as the tolerance factor which satisfies the relation: $(RA + RX) = t \sqrt{2}(RM + RX)$, where RA, RM, and RX are the corresponding ionic radii of A, M and X ions. Values of (RA + RX) and (RM + RX) are approximately the distances for A-X and M-X bonds respectively. For a perfectly packed cubic perovskite structure, t is equal to 1.[59] If the tolerance factor $t > 1$, the structure tends to distort towards a tetragonal structure; if the tolerance factor $t < 1$, there is a tendency to distort towards buckling of the octahedral 3-dimensional networks: Although the t value is theoretically regarded to be 1 for perfect 3-D perovskite networks, it is empirically found that for most cubic perovskite structures: $0.8 < t < 0.9$. Besides the 3D networks mentioned above, 2-dimensional networks are also common for organic-inorganic hybrids.[59] 2-D structures occur when the group A is too large to fit into the space provided by the nearest-neighbors X within the inorganic sheet. The organic group A then causes distortion of the structure and in this situation the tolerance factor t is much larger than 1. In such cases, the organic group needs to be held away from the inorganic sheets by a spacer, such as an alkyl chain, in order to grow 2-D perovskites layered structures. The 2-D layered perovskites systems include two typical groups of compounds: $(RNH_3)_2MX_4$ and $(NH_3\text{-}R\text{-}NH_3)MX_4$, where R is an aliphatic or aromatic ammonium cation, M is a divalent metal that can adopt an octahedral coordination, and X is a usually a halogen: Cl, Br or

I.[59] In $(R\text{-}NH_3)_2MX_4$ systems the perovskites consist of single layers of oriented inorganic sheets separated by bilayers of organic ammonium cations.[59] Contrary to the 3-D perovskite structure AMX_3, where the organic cation A must fit into a rigidly defined hole, in the 2-D layered systems the distance between the inorganic sheets can vary with the length of the organic cation. Consequently, larger and more complex organic cations can be incorporated (Figure 54).[59] Beyond

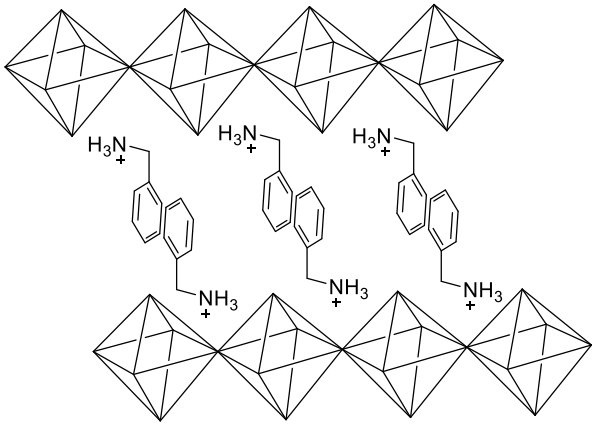

Figure 54: Example of a 2-Dimensional perovskite structure containing benzyl ammonium cations.[56]

2-D perovskites systems are 1-D perovskites which consist of single chains rather than layered structures. These 1-D structures allow for the use of much larger and more exotic cations, but typically have a much more confined electronic structure relative to the 2-D and 3-D perovskite materials.[59]

The structure of a perovskite material directly determines its electronic structure and material properties, with 3-D and 2-D perovskite materials typically having impressive semiconducting behavior.[59] While the organic cation plays a central role in determining the physical structure of the perovskite material, certain organic cations can also directly influence the electronic structure of the perovskite material as well by interacting with band structure of the metal halides of the perovskite. As such, the right combination of metal halides and organic cations is key in regard to developing robust perovskite materials with desirable structures.[59] The useful properties of both the organic and inorganic perovskite material can be taken advantage of by

taking some simple design principles into account. By using highly conjugated organic compounds a lower HOMO-LUMO gap can be achieved, which effectively translates into a lower band gap of the organic material.[59] More importantly, these HOMO-LUMO gaps can be further tuned, through functionalization, to match the bandgap of the metal ions in the perovskite structure, making these hybrid materials tunable for a number of different material applications. An example of this can be seen in thiophene perovskite hybrids, where the bandgap of the thiophene units can be tuned to the bandgap of the metal ions by changing the length of the thiophene unit (Figure 55).[59] When

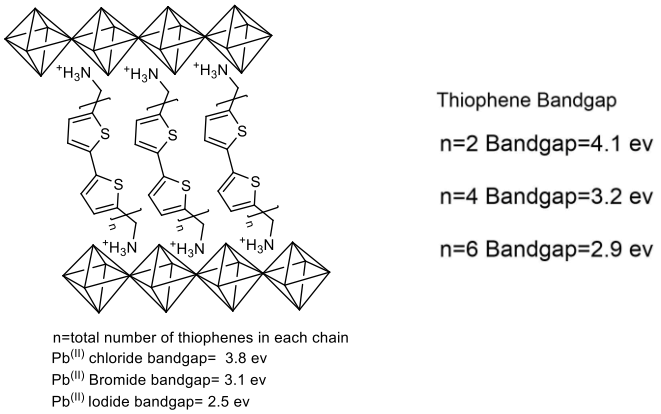

Figure 55: Demonstrated bandgap matching in perovskite materials as a result of lowering the homo lumo gap of the organic cation by extending its π conjugation.[59]

thiophene chains are used consisting of 4 or 6 thiophene units excellent bandgap overlap can be achieved with the lead bromide or lead iodide units in the perovskite system. This overlap allows for energy transfer between the inorganic and organic layers, making the material a more effective energy carrier which is important for applications that require efficient conductive or semi-conductive materials.[59] Bandgap matching is also desirable for the development of high-performance solar cell devices. As stated before, the general consensus is that for many hybrid perovskite structures the organic cation only plays a role in determining the physical structure of the perovskite. In such cases the ability of the perovskite to become photoconductive is dependent upon the electronic structure of the metals. By having organic cations that match the energy level

of the photoconductive metal both the organic and inorganic components can become photoconductive, theoretically increasing the efficiency of the perovskite material.[59]

Electronic properties are not the only factors that are considered when designing hybrid perovskites as the stability of the hybrid material is also critical to its performance in both the short and long term. The stability of perovskite hybrid materials is due to the culmination of a number of factors, with the individual properties of the organic cation and the metal halide playing a major role. Generally, metal halides consisting of chlorine or bromine have greater stability than their iodide derivatives. As such, most inorganic-organic hybrids containing metal halides show greater instability towards water and air than their metal chloride and bromide counterparts.[59] Organic cations can also induce instability in inorganic-organic hybrids as a result of their hygroscopic nature. Many organic cations will readily adsorb water from the atmosphere, a process that results in the gradually degradation of an inorganic organic hybrid as the majority of the sought-after metal halides are soluble or reactive with water. All of these factors must be considered in order to design perovskite materials for long term applications.[59]

While a great deal of work has gone into improving the electronic properties and stabilities of complex 3-D and 2-D hybrid structures less attention has been paid to 1-D and especially 0-D inorganic organic hybrids due to the fact that the large organic cations used in the fabrication of these systems result in isolated sheets of organic cations and metal halides, which results in a very electronically isolated system.[56] While the inability for charge to move freely in these systems makes them unsuitable for certain applications, such as the development of solar cells, these very same properties make these systems potentially useful for the development of light emitting materials. In light emitting materials an initial input of energy can promote an electron from a low energy state to a high energy state forming electron hole pairs or so-called excitons. In these low

dimensional organic-inorganic hybrids, the confined electronic states of the material can result in these electron hole pairs recombining and upon doing so giving off energy in the form of light.[59] Light emission behavior was demonstrated by Ma and co-workers, who showed that 0-D tin halide hybrid structures possessed significant luminescent properties with measured photoluminescence quantum efficiencies over 95%.[60] In the work reported by Ma and co-workers light emission was derived exclusively from the metal halides, as is generally the case with most of the organic inorganic hybrid materials reported in the literature.[60] Despite the wealth of conjugated organic molecules that have the potential to emit light, few low dimensional inorganic organic hybrids with conjugated molecules are known.[61] As light emission from both the organic and metal halide portions of low dimensional materials could result in far more efficient light emitting materials, a better understanding of how metal halides and conjugated organic cations in low dimensional materials should be developed.[61]

In this work, organic cations based on methylated benzenes with varying degrees of steric bulk have been used to prepare low dimensional organic inorganic hybrids (Figure 56). It is

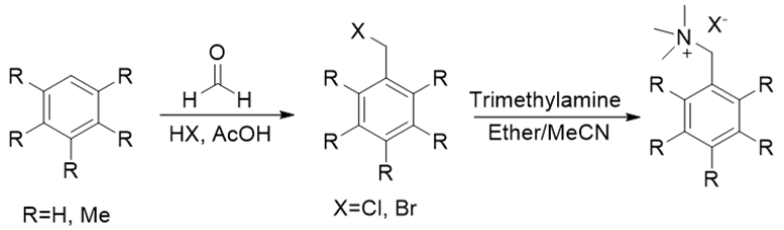

Figure 56: Standard synthetic method for synthesizing methylated benzene ammonium salts.

proposed that by varying the steric bulk of the conjugated organic cations a relationship can be established between the low dimensional hybrid structures that are induced that by the degree of steric bulk on the organic cation and the observed optical and electronic properties of the organic molecule. It is further proposed that, by varying the degree of methylation a relationship between the ionization potential of the organic cation and the optical and electronic properties of the hybrid material can be established. As the degree of methylation of the organic cation is increased, the

ionization potential of the molecule should become lower making the organic cation a stronger electron donor and lowering the energy required to excite an electron from the organic cation.[61] This is supported by the measured ionization potentials of various methylated benzenes, which show that the ionization potential decreases from benzene to hexamethyl benzene.[62] It is hypothesized in this work that larger degrees of electron donating steric bulk around the organic cation will result in a larger degree of charge localization within the hybrid material allowing both the metal halide and organic cation to luminesce efficiently. It is also hypothesized that increasing the degree of electron donating steric bulk around the organic cation will result in lower energy transitions, making the light emission behavior of these hybrids tunable through variation of steric bulk. By establishing the effects that ionization potential and steric bulk have on the optical and electronic properties of low dimensional inorganic-organic hybrids, guidelines for the development of low dimensional inorganic-organic hybrids with desired light emission behavior can be developed. The results of these studies will be discussed in Chapter 5. It should be noted that the majority of this work regarding these inorganic-organic hybrids has already been published in the journal ACS Omega.[61]

Chapter 2: Synthesis and Reactions of Stable N-Aromatic Nitrosamides

Work by Ruchardt, Glatzhofer, and Bartberger demonstrated that clean, high yielding reactions could be performed on nitrosamides generated *in situ*.[11,18,20] It is more often the case that yields for reactions involving *in situ* generated nitrosamides suffer from poor yields due to the fact that the solvent conditions required for the generation of the nitrosamide result in competing side reactions.[1] Use of excess nitrosating agent could also play a role in facilitating undesired side reactions, which in turn makes elucidating the mechanistic behavior of nitrosamide decomposition difficult.

2.1 Synthetic Approach to Stable N-aromatic nitrosamides

In order to develop synthetic methodologies that lead to higher yielding reactions, as well as better understanding of the mechanism behind nitrosamide decomposition, stable N-aromatic nitrosamides must be developed that can be fully isolated and purified before use in order to ensure optimal reactivity. To design a stable nitrosamide, the pathway by which nitrosamides most generally decompose was examined (Figure 30). The formation of the highly unstable phenyldiazoacetate intermediate is a key step in the decomposition of these nitrosamide species.[1] It is proposed in this work, as well as in other works, that excess steric bulk surrounding the nitrosamide functionality would inhibit the formation of the unstable phenyldiazoacetate by hindering nucleophilic attack on the carbonyl by the oxygen of the NO, preventing the formation of the required 4 membered ring transition state (Figure 32).[1,26]

This proposal was tested by converting 2,6-dimethylaniline into N-(2,6-dimethylphenyl)acetamide using acetic anhydride. The resulting amide was treated with 3 equivalents of $NaNO_2$ in a mixture of acetic acid and acetic anhydride at 10 °C and the reaction

vessel was sealed. The reaction mixture evolved a brown gas which slowly dissipated, resulting in a deep blue solution that gradually transitioned to green, and then to yellow. The reaction mixture was allowed to stir for 2 hours at 10 °C and then for 16 hours at room temperature. Workup by evaporation of the reaction solvent gave a mixture of sodium acetate and the desired nitrosamide. Purification of the nitrosamide was carried out by extracting the product from the mixture with diethyl ether. The resulting bright yellow solution was run through a neutral alumina plug. The solution was then concentrated under vacuum to give a bright yellow oil, and ^{1}H-NMR showed this to be the desired nitrosamide (Figure 57).[27,63] The ^{1}H-NMR spectrum of N-(2,6-

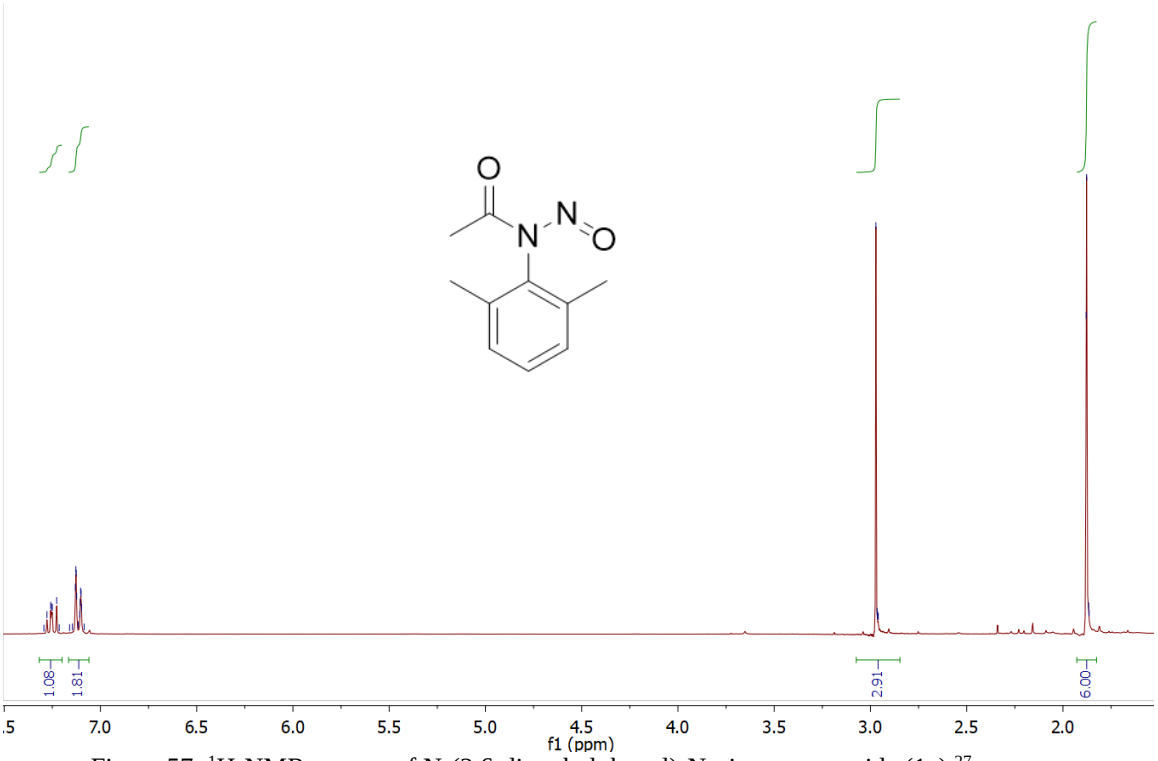

Figure 57: ^{1}H-NMR spectra of N-(2,6-dimethylphenyl)-N-nitrosoacetamide (1a).[27]

diethylphenyl)N-nitrosoacetamide showed 2 singlets and 2 multiplets with the proper integration values (^{1}H-NMR (300 MHz, Chloroform-d) δ 7.29-7.19 (m, 1H), 7.11 (d, J=7.6 Hz, 2H), 2.97 (s, 3H), 1.88 (s, 6H). The singlet at 2.97 ppm was assigned to the CH_3 of the acetyl group, which is shifted away from its value of 2.3 ppm, for the parent amide, toward almost 3 ppm is likely due to a deshielding effect of the NO group. The peak at 1.88 was assigned to the methyl groups of the

aromatic ring due to its integration value of 6 protons. The shift of 1.88 ppm from 2.2 ppm is postulated to be due to the methyl groups being in the shielding zone of the carbonyl. Room temperature solvent studies in acetic anhydride, methanol, and chloroform were monitored using NMR spectroscopy and showed that the nitrosamide exhibited long term stability at room temperature, as no changes in the NMR spectrum were observed over a period of 72 hours. Heating the isolated nitrosamide to 80 °C in pure acetic anhydride yielded the N-aromatic ester in over 90% yield (purity was determined by NMR, yield was determined by weight relative to the amount of starting amide) (Figure 58).[27] Encouraged by these results, the extent to which steric bulk was

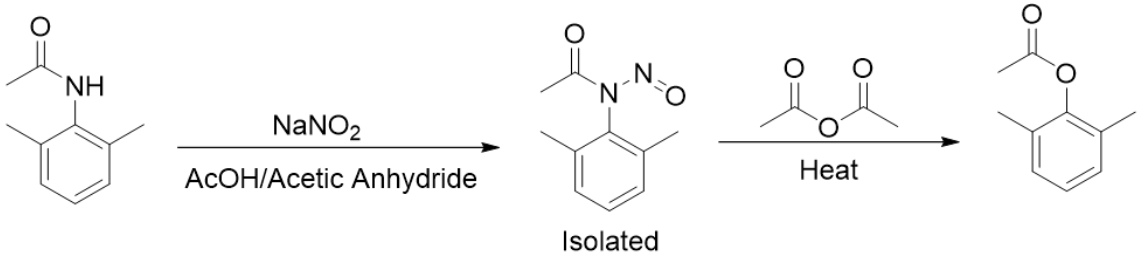

Figure 58: Preparation of 2,6-dimethylphenyl acetate from N-(2,6-dimethylphenyl)acetamide.

stabilizing the nitrosamide functionality was explored by synthesizing a series of nitrosamides with alkyl groups in the same manner as N-(2,6-dimethylphenyl)-N-nitrosoacetamide. N,N'-(2,3,5,6-tetramethyl-1,4-phenylene)bis(N-nitrosoacetamide) was synthesized from the starting durene as shown in Figure (59).[64] Isolation of nitrosamides (1a) and (2a) always gave viscous yellow oils. In

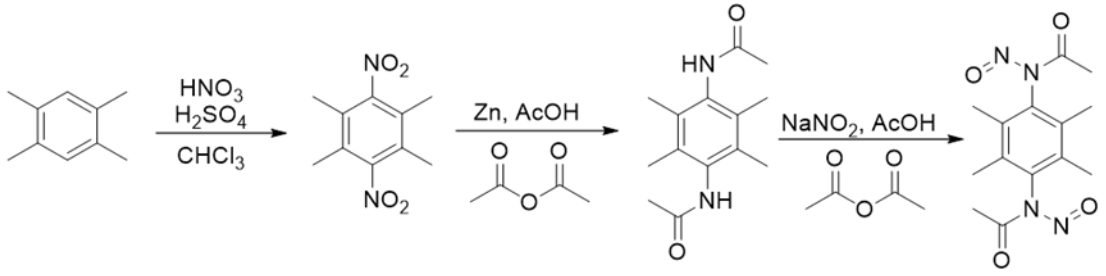

Figure 59: Synthesis of N,N'-(2,3,5,6-tetramethyl-1,4-phenylene)bis(N-nitrosoacetamide) from durene.[64]

the case of nitrosamide (3a) the nitrosamide was isolated as a polycrystalline solid. Stability studies were performed for nitrosamides (2a) and (3a) in the same manner as nitrosamide (1a).

Nitrosamide (2a) demonstrated the same stability seen for nitrosamide (1a), while nitrosamide (3a) slowly decomposed over a period of 48 hrs to give new products (Table 1). Recrystallizing

Table 1: 2,6-substituted nitrosamides and their stability behavior.

Amide	N-Aromatic Nitrosamide	Stability
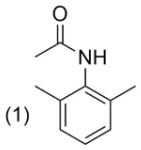 (1)	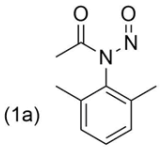 (1a)	Stable in solution for over 72 hours at room temperature, decomposes at 70 °C
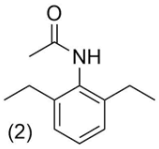 (2)	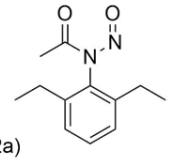 (2a)	Stable in solution for over 72 hours at room temperature, decomposes at 70 °C
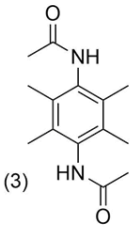 (3)	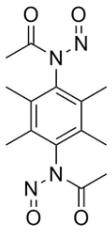 (3a)	Stable for over a month at room temperture as a dry solid. Slowly decomposes in all solvents over a period of 48 hours. Rapidly decomposes at 70 °C.

nitrosamide (3a) from acetonitrile at 0 °C gave large single crystals that were suitable for x-ray diffraction which gave proof of the proposed nitrosamide structure (Figure 60) (Appendix A,

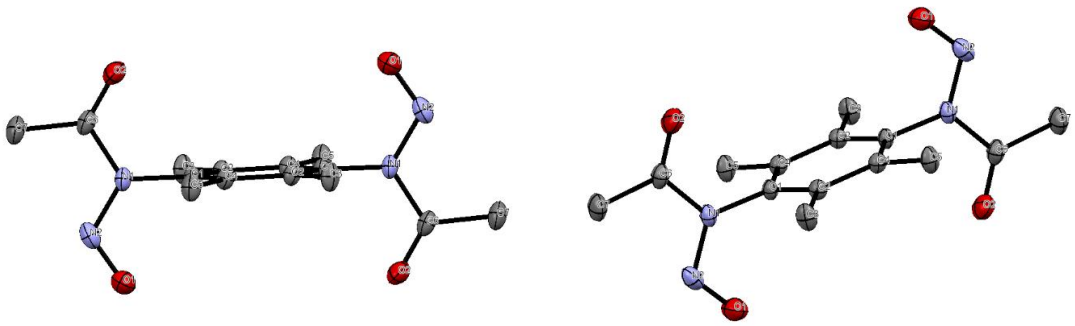

Figure 60: Two perspectives of the crystal structure of N,N'-(2,3,5,6-tetramethyl-1,4-phenylene)bis(N-nitrosoacetamide).

220). The crystal structure of nitrosamide (3) shows that the nitrosamide functionalities are orthogonal to the ring system, placing the methyl groups of the ring between the two reactive functionalities. This prevents the oxygen of the NO from readily attacking the carbonyl carbon,

and results in a higher energy barrier to the rearrangement to the phenyldiazoacetate. Seemingly, this crystal structure represents the first crystal structure of an N-aromatic nitrosamide, but crystal structures of N-aromatic nitrosoureas are known.[65] Comparison of the obtained bond lengths to the bond lengths of nitrosoureas shows that the measured bond lengths for nitrosamide (3a) are fairly unremarkable and show no evidence of elongation due to steric repulsion or any evidence of bond shortening due to hyper-conjugation effects.[65] The observed bond lengths are surprising given the significant stability that is observed relative to the nitrosourea, which is unstable at room temperature and readily undergoes decomposition, lending further credence to the idea that the observed stability is due to steric factors inhibiting the rearrangement (Table 2).[65] The proposed

Table 2: Comparison of selected bond lengths from the crystal structures of nitrosamide (3a) and a nitrosourea reported in the literature.[65]

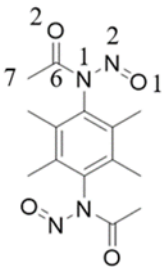

Bond lengths	
A1 A2 Length	A1 A2 Length
O1 N2 1.209 (2)	N5 O6 1.219 (5)
O2 C6 1.198 (2)	O3 C2 1.224 (6)
N1 N2 1.373 (2)	N1 N5 1.357 (6)

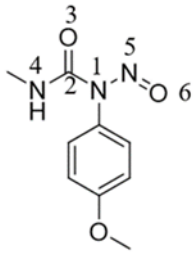

steric bulk induced stabilization of N-aromatic nitrosamides was further supported by NMR studies done by Sueyoshi and co-workers who showed that *ortho*-substituted N-aromatic nitrosoureas would not decompose in solution at room temperature, while *para*-substituted N-aromatic nitrosoureas would.[66] Sueyoshi and co-workers also used ^{13}C NMR studies to show that the nitrosourea functionality was orthogonal to the aromatic ring at room temperature due to the steric repulsion caused by the methyl group in the *ortho* position (Figure 61).[66] The reported carbon

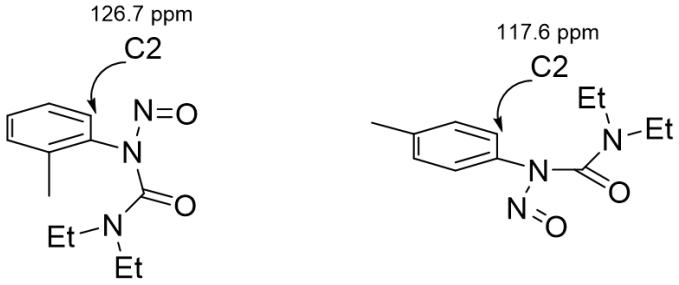

Figure 61: NMR studies on nitrosoureas demonstrating the conformationally changes induced by steric bulk at the *ortho* position relative to the nitrosourea.[66]

chemical shifts refer to the carbon at the C2 position which experiences a deshielding effect when the nitroso group is orthogonal to the ring system relative to the planar nitrosamide.

In order to further probe the extent to which steric influence is capable of stabilizing the nitrosamide functionality, the effect of mono-substitution on nitrosamide stability was explored. N-(2,5-Dimethylphenyl)acetamide, N-(2-(*tert*-butyl)phenyl)acetamide, 2-acetamidobenzoic acid and N-(2-nitrophenyl)acetamide were prepared from their corresponding anilines and were reacted with 3 equivalents of $NaNO_2$ in a mixture of acetic acid and acetic anhydride. In the case of 2-acetamidobenzoic acid, 6 equivalents of $NaNO_2$ was required to achieve nitrosation. Reaction times to form the corresponding nitrosamides were much shorter, taking only 30 minutes to an hour to form, and unsurprisingly the formed nitrosamides were less stable. However, all were easily isolatable at room temperature, with the exception of N-(2-nitrophenyl)-N-nitrosoacetamide which decomposed rapidly to form the corresponding aryl ester. The results of these reactions are summarized in (Table 3). By having only one functional group present at the *ortho* position rather

Table 3: 2,5 and 2-substituted nitrosamides and their stability behavior.

Starting Amide		Nitrosamide	Stability
(4) 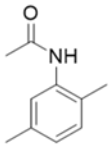	(4a)	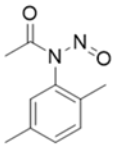	Formed in 30 minutes, slowly decomposes in solution over a period of 24 hrs, decomposes rapidly when heated.
(5) 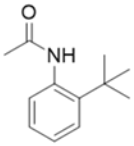	(5a)	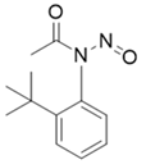	Formed in 1 hr, stable in solution over a period of 24 hrs, decomposes rapidly when heated.
(6) 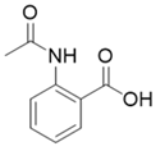	(6a)	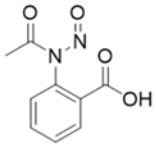	Formed in 30 minutes, stable in solution for up to 2 hours in acetic acid at room temperature. Stable as a solid for over 2 days at room temperature. Rapidly decomposes upon heating.
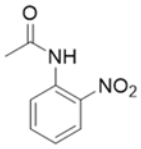	Not detected		Full decomposition to the ester at room temperature.

than two, the energy barrier to forming the phenyldiazoacetate decreased, although there is possibly still enough of an energy barrier present to grant the majority of the nitrosamides some stability at room temperature. In the case of N-(2-(*tert*-butyl)phenyl)-N-nitrosoacetamide the steric hindrance induced by the *tert*-butyl group provides a sufficiently large energy barrier to the formation of the phenyldiazoacetate species, such that its stability is similar to that of the bis-substituted nitrosamides in (Table 1). observed instability in N-(2-Nitrophenyl)-N-nitrosoacetamides is most likely due to a combination of electronic effects and lack of steric bulk from the nitro group.

2.2 Decomposition of Stable N-aromatic Nitrosamides to form Aryl Esters

The established stability of the prepared nitrosamides and the ease with which they were isolated presented an opportunity to examine their reaction behavior under experimental conditions free of residual acetic acid or nitrous acids. In the work performed by Glatzhofer and Roy, N-aromatic nitrosamides were used to readily prepare aryl esters. Glatzhofer and Roy proposed that the ester formation was due to recombination between either an acetoxy anion and an aryl cation or an acetoxy radical and an aryl radical, with recombination being favored due to the fact that the acetic anhydride solvent system was unlikely to readily react with the formed intermediates and allowing the acetic anhydride to act as an inert solvent cage. While this proposal is reasonable, the role of acetic acid or acetate anions possibly acting as the source of the acetoxy group for the formation of these aryl esters could not be ruled out as Glatzhofer and Roy generated their N-aromatic nitrosamides *in-situ* in a 2:1 mixture of acetic anhydride to acetic acid.

In order to evaluate the proposed idea that recombination was the pathway by which aryl ester formation occurred, stable N-aromatic nitrosamides were prepared, isolated and purified, in the same manner as nitrosamide (1a), before being decomposed in 100% acetic anhydride. Initial experiments were performed with N-(2,6-dimethylphenyl)-N-nitrosoacetamide (1a), which was dissolved in acetic anhydride and slowly heated. Upon reaching 80 °C, the strongly yellow solution gradually transitioned to transparent over the period of approximately 2 hours. The reaction was worked up by evaporation to give a white solid, which was recrystallized from diethyl ether. ^{1}H-NMR analysis showed that all of nitrosamide (1a) had been converted into the desired 2,6-

dimethylphenyl acetate (Figure 62). [67,68] Subjecting nitrosamides (2) and (3) to the

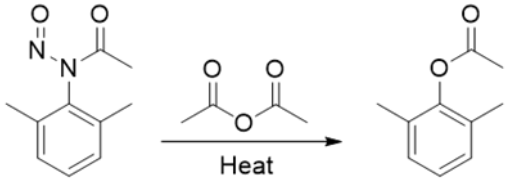

Figure 62: Conversion of nitrosamide (1) to 2,6-dimethylphenyl acetate.

same reaction procedures yielded their corresponding esters in high yields (Table 4).[67,68,69] No

Table 4: Solvolysis of 2,6 substituted nitrosamides in acetic anhydride.

Nitrosamide		Product		Yield
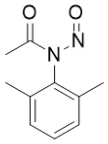	(1a)	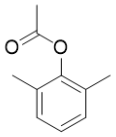	(7)	98%
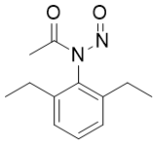	(2a)	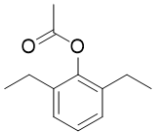	(8)	98%
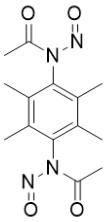	(3a)	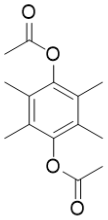	(9)	87%

significant difference was observed between the bis-*ortho*-substituted substrates with regard to reaction time. All reactions were complete within 2 hours and gave yields near or in excess of 90%. Product yields were determined by weight relative to the amount of starting amide while purity was determined by ^{1}H-NMR, which in the case of all three N-aromatic nitrosamides showed that the corresponding esters were the only product. Decompositions of the mono-*ortho*-substituted nitrosamides were performed in the same manner as the decompositions of the bis-*ortho*-substituted nitrosamides. Except for the decomposition of the N-(2-(*tert*-

butyl)phenyl)nitrosoacetamide, which required a full two hours to reach full conversion, the mono-*ortho*-substituted systems had faster reaction times (Table 5) .[68,69,70] The

Table 5: Decomposition reactions of 2,5 and 2-substituted nitrosamides.

Nitrosamide		Product		Yield
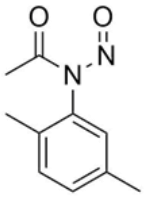	(4a)	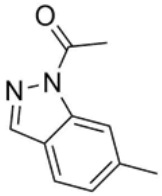	(10)	Complex mixture no ester was detected.
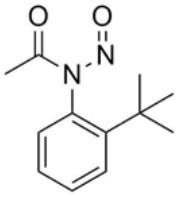	(5a)	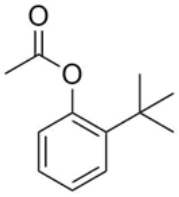	(11)	93%
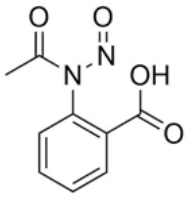	(6a)	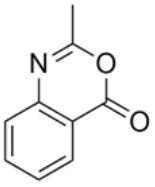	(12)	86%

results obtained for these systems were much different than what was observed for the 2,6-systems. In the case of N-(2,5-dimethylphenyl)-N-nitrosoacetamide, the major product was 1-(6-methyl-1H-indazol-1-yl)ethan-1-one (Figure 63). This was a surprising result, considering that excellent

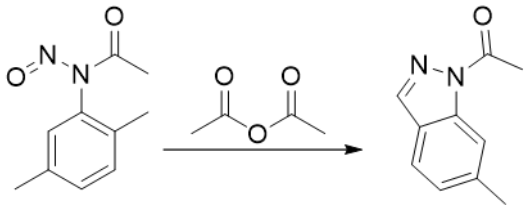

Figure 63: Cyclization of N-(2,5-dimethylphenyl)-N-nitrosoacetamide under ester forming conditions.

conversion and no cyclization was observed in the bis-*ortho*-substituted systems. Comparison of N-aromatic nitrosamide (4) to N-aromatic nitroamides (1) and (3) does not yield any obvious reasons as to why N-aromatic nitrosamide (4) should deviate in reactivity from the other nitrosamide systems. Possible explanations for this observed reaction behavior will be discussed later in Chapter 3. In the case of nitrosamide (6) heating in acetic anhydride gave 2-methyl-4H-benzo[d][1,3]oxazin-4-one in over 80% yield. This is most likely due do the fact that treatment with $NaNO_2$ results in the formation of the 2-(N-nitrosoacetamido)benzoate, upon heating the oxygen of the acetate can readily attack the carbonyl carbon of the amide, followed by elimination of water. This cyclization is known and will occur on its own when 2-acetamidobenzoic acid is heated in acetic anhydride for several hours at temperatures exceeding 80 °C. Seemingly, the nitrosation reaction accelerates this process, allowing for the cyclization to occur readily within one to two hours of heating (Figure 64).[71]

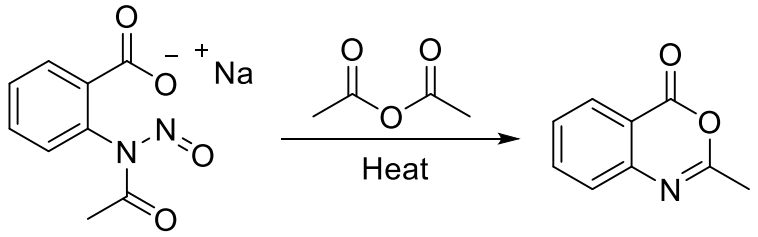

Figure 64: Cyclization 2-(N-nitrosoacetamido)benzoate under ester forming conditions.[71]

The decomposition of the prepared 2,6-substituted N-aromatic nitrosamides gave their corresponding esters in good yields, which is in line with the observations reported by Glatzhofer and Roy. Glatzhofer and Roy previously reported that the treatment of N-([1,1'-biphenyl]-4-yl)-2,2,2-trifluoroacetamide with $NaNO_2$ in a mixture of acetic acid and acetic anhydride resulted in the formation of [1,1'-biphenyl]-4-yl 2,2,2-trifluoroacetate (Figure 65).[1] This reaction strongly

Figure 65: Ester formation by recombination, demonstrated by Roy and Glatzhofer.[1]

supported the proposal that in acetic anhydride recombination, possibly through a radical mechanism, was occurring with no solvent exchange. In order to confirm that solvent exchange was not occurring for these stable nitrosamide systems N-(2,6-dimethylphenyl)-2,2,2-trifluoro-N-nitrosoacetamide was prepared from 2,6-dimethylaniline by treatment with trifluoroacetic anhydride, followed by treatment with $NaNO_2$ in a mixture of acetic acid and acetic anhydride (Figure 66).[72] The resulting nitrosamide was isolated and purified in the usual manner, then

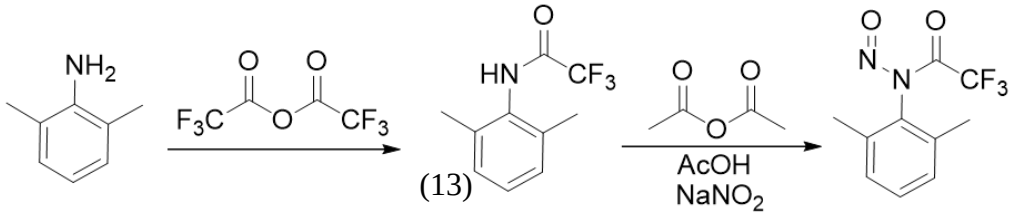

Figure 66: Synthesis of N-(2,6-dimethylphenyl)-2,2,2-trifluoro-N-nitrosoacetamide.[72]

dissolved in acetic anhydride and heated to 80 °C for 2 hours. Work-up of the reaction by evaporation gave a white solid. ^{1}H-NMR analysis showed the material to be the 2,6-dimethylphenyl acetate in (Figure 67). ^{19}F-NMR experiments showed no fluorine signal was

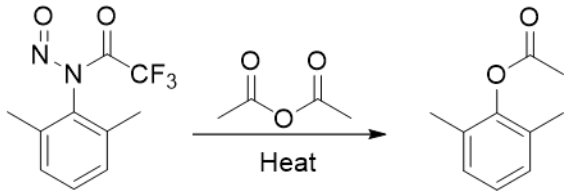

Figure 67: Formation of 2,6-dimethylphenyl acetate from N-(2,6-dimethylphenyl)-2,2,2-trifluoro-N-nitrosoacetamide, demonstrating solvent exchange.

present. To determine that solvent exchange was due to the nature of the nitrosamide decomposition and not behavior that was exclusive to the trifluoro system, the decomposition of nitrosamide (1) in trifluoracetic anhydride was carried out. The solvolysis was carried out in a sealed Schlenk bomb in order to achieve the necessary decomposition temperature. ^{1}H and ^{19}F NMR analysis of the reaction mixture suggested 2,6-dimethylphenyl 2,2,2-trifluoroacetate was the major product (Figure 68). The observed solvent exchange suggests that the decomposition of

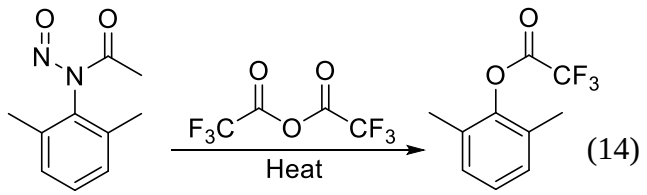

(14)

Figure 68: Formation of 2,6-dimethylphenyl 2,2,2-trifluoroacetate from N-(2,6-dimethylphenyl)-N-nitrosoacetamide, demonstrating solvent exchange.

these sterically hindered nitrosamide systems is more likely going through an ionic pathway than a radical pathway. Based on the observed reaction behavior, a possible mechanism for decomposition of these hindered nitrosamides in acetic anhydride is presented (Figure 69). In this proposed solvolysis mechanism the formation of the diazonium acetate ion pair results in the

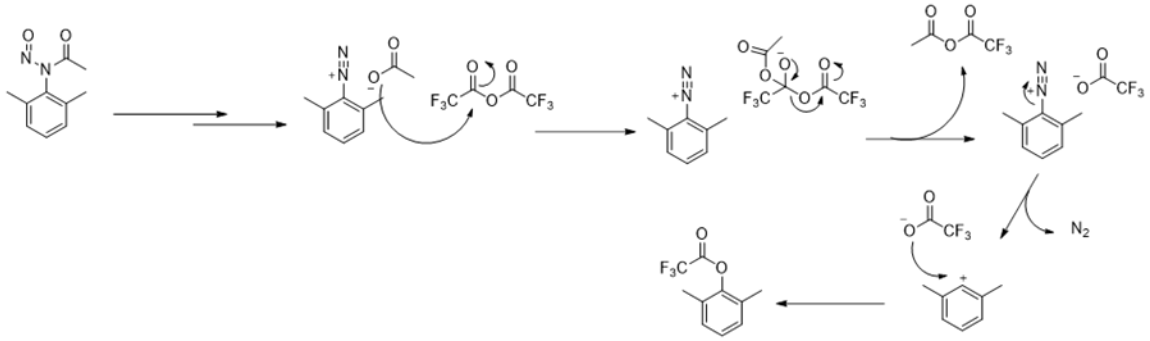

Figure 69: Proposed mechanism of ester formation based on solvent exchange experiments.

acetate ion attacking the trifluoracetic anhydride, the resulting tetrahedral intermediate collapses to give the trifluoroacetate ion and acetic 2,2,2-trifluoroacetic anhydride. Dissociation of the diazonium as nitrogen gas forms the carbocation, which is then readily attacked by the trifluoroacetate ion. The results of this reaction suggest a different mechanism from what has been previously proposed in the literature.[1,18] If formed, the presence of a carbocationic intermediate in acetic anhydride suggests that solvent dielectric constant is playing a significant role in determining the mechanistic pathway. Solvents with a higher dielectric constant will be able to better support the formation of charged species. In the case of acetic anhydride, the dielectric constant is relatively high with acetic anhydride having a dielectric constant of 21. In the case of mixtures of acetic acid and acetic anhydride the dielectric behavior of the medium is clear. Acetic

acid has a measured dielectric constant of 6.15 which is surprisingly weak. Acetic acid acetic anhydride mixtures presumably will exhibit lower dielectric properties, thus disfavoring the formation of charged species. In these situations, it is possible that solvent exchange is postulated to be disfavored with neutral radical or neutral concerted pathways becoming more favorable (Figure 70). This behavior could readily explain why solvent exchange was observed in reactions

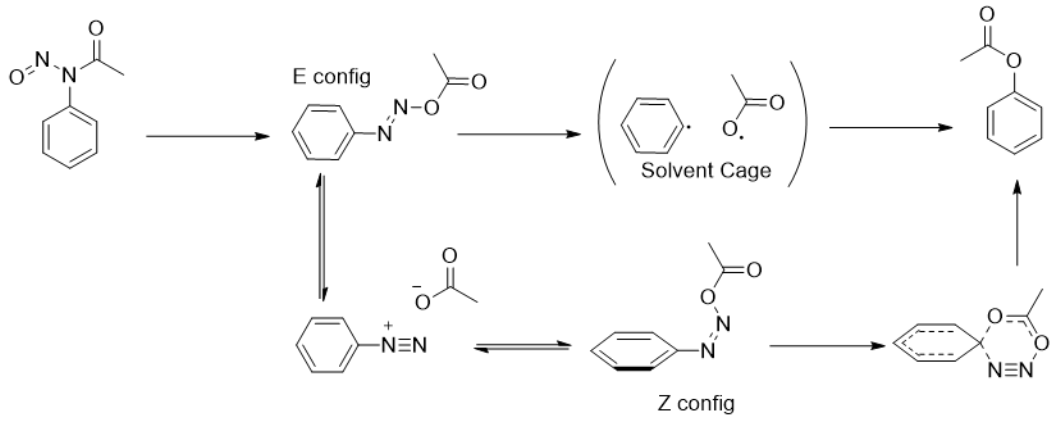

Figure 70: Possible mechanisms of ester formation in low dielectric constant solvents.[18]

performed in straight acetic anhydride while recombination was observed in acetic acid acetic anhydride mixtures as reported by Glatzhofer and Roy. The results of the studies here suggest that evaluating the relationship between N-aromatic nitrosamide reactivity and solvent dielectric constant was key to further understanding and predicting N-aromatic nitrosamide behavior.

2.3 Decomposition of Stable N-aromatic Nitrosamides in Solvents with Various Dielectric Constants: Mechanistic Implications

In order to probe the effect, if any, that dielectric constant has on the nitrosamide reaction mechanism, the solvolysis of N-(2,6-dimethylphenyl)-N-nitrosoacetamide was carried out in both high and low dielectric constant solvents. Water with a dielectric constant of 80.4 and methanol with a dielectric constant of 32.7 were chosen for initial experiments due to their high dielectric constants and good nucleophilic behavior.[73] It was proposed that carbocation formation will be

favored in high dielectric constant solvents and a solvent with good to moderate nucleophilicity should be able to trap it readily.[73]

Solvolysis of the nitrosamide in water was carried out by dissolving the isolated nitrosamide in 5 mL of acetone and the solution was mixed with 30 mL of water. The yellow mixture was stirred while being heated. Heating at 70 °C for 2 hours gave a pale-yellow solution which, when extracted and dried, gave the expected 2,6-dimethylphenol with no other observable products as determined by ^{1}H-NMR. Solvolysis in methanol was carried out by dissolving the nitrosamide in methanol and heating the reaction mixture for 2 hours. Workup gave the expected 2,6-dimethylanisole with no other observable products (Figure 71).[74] In both cases nucleophilic

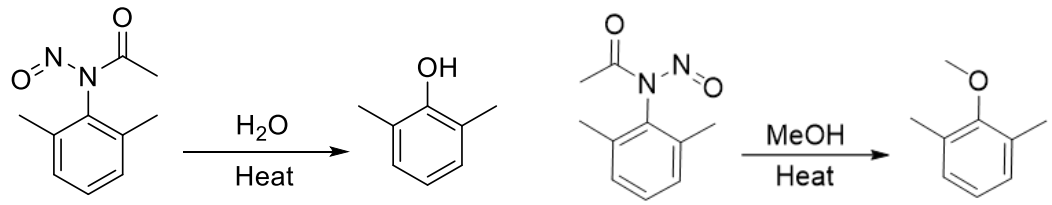

Figure 71: Solvolysis of N-(2,6-dimethylphenyl)-N-nitrosoacetamide in methanol to give dimethyl anisole.[72]

addition of the solvent occurred at the former position of the nitrosamide, consistent with addition occurring through the formation of the aryl cation or by a concerted S_NAr mechanism. Given the steric bulk that surrounds the nitrosamide position and the lack of electron withdrawing groups *ortho* or *para* to the nitrosamide a concerted S_NAr mechanism should be unfavorable making the cation the most reasonable mechanistic pathway to explain this behavior (Figure 72). The lack of radical products such as 2,6-dimethylbenzene also suggests that competing radical reaction mechanisms are minimal, thus lending support to the hypothesis that aryl carbocation formation will be favored in high dielectric solvents. Changing from high dielectric constant solvents to low dielectric constant solvents gave significantly different mechanistic behavior. Solvolysis of nitrosamide (1) in benzene, carbon tetrachloride, and toluene gave the same product which was

determined to be the 7-methyl-1H-indazole as the exclusive product (Figure 73).[75] This result in itself is not surprising as work by Huigsen had shown that 1H-indazole was formed in excess of

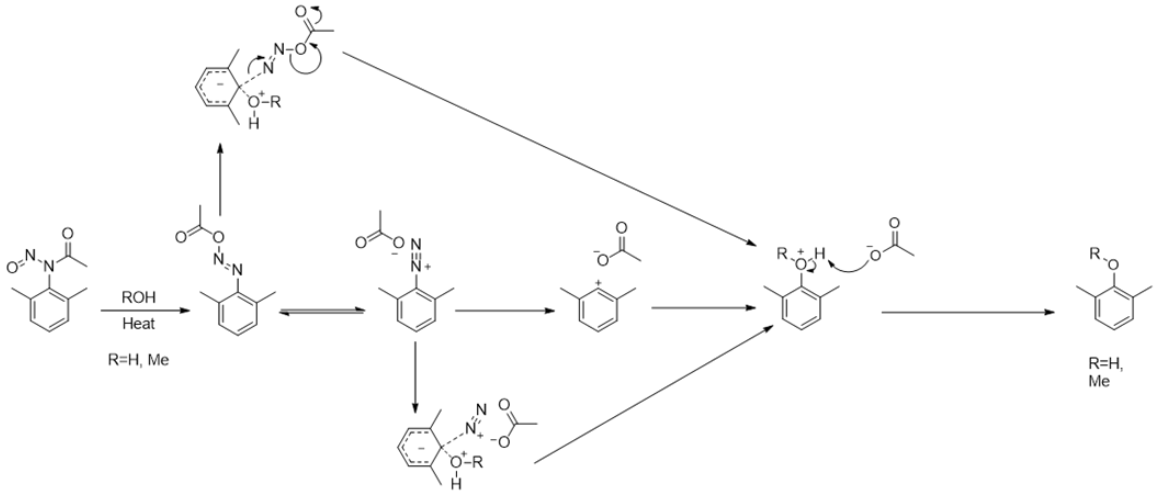

Figure 72: Possible mechanistic pathways for the solvolysis of *ortho*-substituted nitrosamides in water and methanol.

80% yield when N-nitroso-N-(o-tolyl)acetamide was heated in chloroform (Figure 7).[9] Huigsen and others have proposed that formation of the indazole goes through a concerted or zwitterionic mechanism in which deprotonation at the benzylic position by an acetate species gives a carbon nucleophile, which can readily attack the diazonium species, leading to the observed heterocycle product (Figure 9).[4,9] Examination of the proposed intermediates of this reaction helps explain why the formation of the indazole occurs so readily.

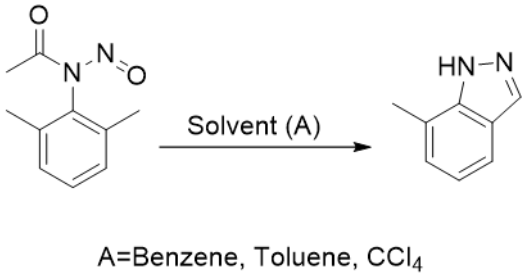

Figure 73 : Formation of the 7-methyl-1H-indazole in benzene, toluene, and carbon tetrachloride.[9]

Comparison of the proposed *ortho*-quinodiazomethane and the aryl radical suggests that the *ortho*-quinoadiazomethane should be a lower energy intermediate when compared to the unstablized aryl radical (Figure 74). It is also most likely the case that in non-polar, low dielectric

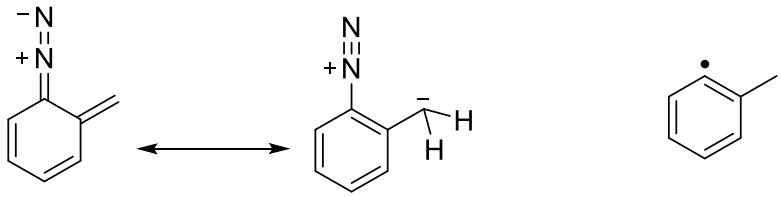

Figure 74: Comparison of the postulated *ortho*-quinodiazomethane and non-resonance stabilized aryl radical. While both species are charge neutral the ability the of *ortho*-quinodiazomethane to engage in resonance delocalization suggests that energetically it should be favored over the unstablized aryl radical.

constant solvents, the diazonium acetate species will exist as a closely bound ion pair, maintaining the close proximity of the acetate to the benzylic position. As such, it seems likely that the deprotonation step required to form the *ortho*-quinoazomethane is fast relative to the homolytic dissociation of the diazonium, making the radical kinetically and thermodynamically unfavorable in situations where benzylic protons at the *ortho* position are available (Figure 75). This proposal

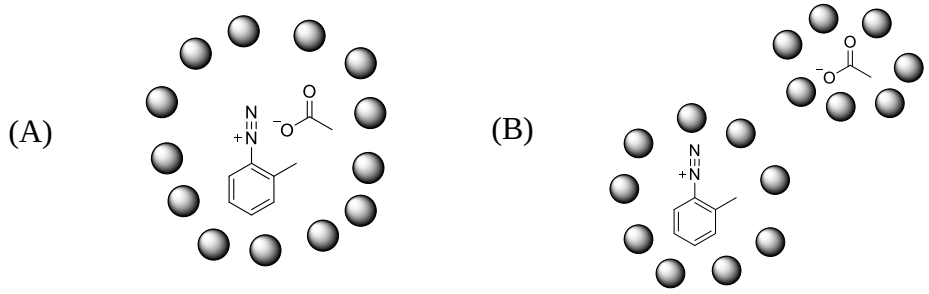

Figure 75: Generalized models for the solvation processes occurring in low dielectric constant solvents (A) and high dielectric constant solvents (B). In model (A) the low dielectric constant solvent is unable to stabilize the ions resulting in a tight ion pair which will favor the deprotonation of the benzylic protons. In model (B) the high dielectric solvent is able to stabilize and solvate the independent ions resulting in charge separation making the heterolysis of the diazonium more favorable.

is supported by the work of Glatzhofer and Roy, who demonstrated that the decomposition of N-(2-(*tert*-butyl)phenyl)-N-nitrosoacetamide in benzene gave the expected biphenyl in 53% yield (Figure 76).[1] The ability for N-(2-(*tert*-butyl)phenyl)-N-nitrosoacetamide to undergo aryl coupling

with benzene is due to the fact that no labile proton is available at the benzylic position, leaving radical formation or carbocation formation as the only productive pathway of decomposition.[1]

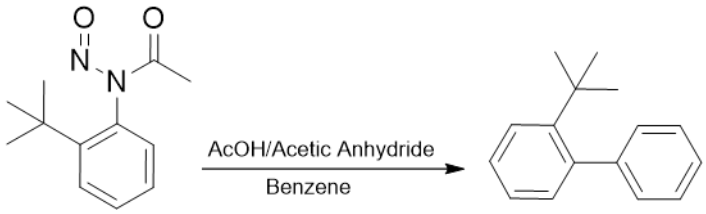

Figure 76: Synthesis of 2-(*tert*-butyl)-1,1'-biphenyl from N-(2-(*tert*-butyl)phenyl)-N-nitrosoacetamide by Roy.[1]

Further analysis of work related to indazole formation from diazo species showed that indazoles could be formed from diazonium tetrafluoroborate salts by adding a large excess of sodium or potassium acetate.[74] It was noted that, without the acetate additive indazole formation was greatly hindered, providing strong evidence that the acetate species acts as the proton sink for the benzylic proton. This realization led to the question of how the pKa of the acetate species impacts the reaction, and if cyclization should be able to be inhibited by using a starting amide that will produce an acetate species with a sufficiently low enough pKa that deprotonation will be inhibited. N-(2,6-dimethylphenyl)-2,2,2-trifluoro-N-nitrosoacetamide was chosen as a promising candidate to probe this reaction mechanism as the pKa of trifluoroacetic acid is 0.23, while the pKa of acetic acid is 4.76, making trifluoroacetate several orders of magnitude less basic than acetate, which may result in slower rates of deprotonation, thus hindering cyclization. Solvolysis of N-(2,6-dimethylphenyl)-2,2,2-trifluoro-N-nitrosoacetamide in toluene was carried out by heating the solution at 80 °C for 2 hours. Reaction workup failed to yield any biphenyl, bibenzyl, or benzhydryl, and instead gave 7-methyl-1H-indazole as the only detectable product (Figure 77). The observed results suggest that the dissociation of the diazonium in low dielectric constant solvents must be slow enough that the deprotonation step is still faster, even when trifluoroacetate is used as the base/proton sink.

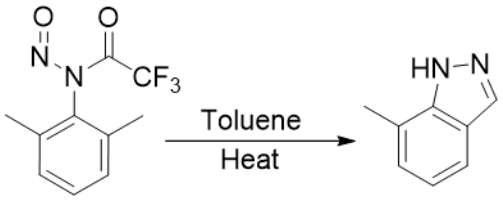

Figure 77: Formation of 7-methyl-1H-indazole in toluene from N-(2,6-dimethylphenyl)-2,2,2-trifluoro-N-nitrosoacetamide.

2.4 Decomposition of Stable N-Aromatic Nitrosamides in the Presence of Alkenes

The observed reaction behavior of N-aromatic nitrosamides in low dielectric constant solvents suggests that *ortho* substitution results in radical behavior being kinetically disfavored with regard to reactions with hard to activate solvents such as benzene and carbon tetrachloride. Work demonstrated by Glatzhofer and Roy showed that N-aromatic nitrosamides were also capable of reacting with methyl methacrylate (MMA) to form polymethyl methacrylate (PMMA).[18] As MMA can readily be initiated by anions and radicals, but not by cations due to the electron poor nature of the alkene, Glatzhofer and Roy speculated that the observed polymerization must be radical initiated, with the phenyl radical being the primary initiator.[18] As MMA serves as an excellent radical trap, it was proposed that MMA could be used to determine if radical formation with *ortho* substituted N-aromatic nitrosamides was possible. As MMA has a dielectric constant of 6.32, which is relatively low, it was speculated that polymerization would be impeded or would not occur as cyclization to the indazole would be the favored reaction pathway.

Solvolysis of nitrosamide (1a) in inhibitor free MMA was carried out by heating the solution at 70 °C, with the yellow solution transitioning to clear over the course of 2 hours. The solution was allowed to cool to room temperature, at which time methanol was added to the

solution. Upon the addition of methanol, a large amount of PMMA immediately precipitated out of the reaction solution (Figure 78). This procedure was repeated again with 35 mg of nitrosamide

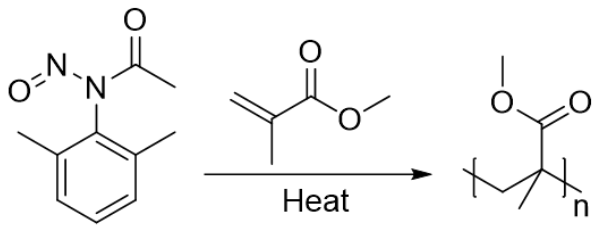

Figure 78: Polymerization of MMA initiated by nitrosamide (1a).

(3a) in 15 ml of MMA which gave 415 mg of PMMA (Figure 79). Heating the MMA by itself or

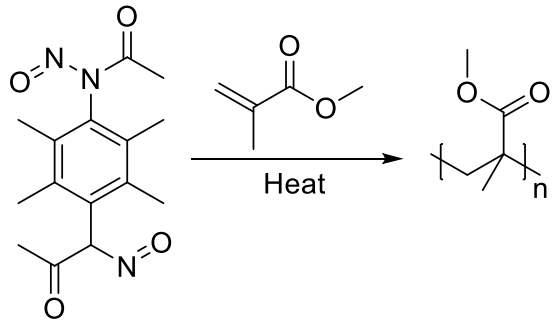

Figure 79: Polymerization of MMA initiated by nitrosamide (3a).

in the presence of excess sodium acetate failed to give any polymer upon the addition of methanol, demonstrating that the nitrosamide is required in order for polymerization to occur. Considering the low dielectric constant of MMA, and the fact that its polymerization cannot be effectively initiated cationically, it is highly unlikely that dissociation of the diazonium to form the cation is occurring in this reaction and most likely some radical process is responsible for the observed polymerization.

In an attempt to observe these reaction dynamics directly, the reaction between nitrosamide (1a) and MMA was carried out in neat MMA with the hope that a chemically induced dynamic nuclear polarization (CIDNP) effect would be observed in one or both of the reactions, which would readily confirm the existence of a biradical mechanism. The mixture was heated in the NMR spectrometer while spectra acquisition was performed. Unfortunately, all that was observed was the appearance of PMMA with the disappearance of the nitrosamide. In the case of the neat MMA

reaction, isolation and characterization of the resulting PMMA was readily achievable by precipitation with methanol yielding 0.146 g (1.46 mmol) of polymer from the reaction which had contained approximately 0.01 g (0.05 mmol) of nitrosamide and 1 mL of MMA (0.943 g) (9.42 mmol) giving a concentration of 0.05 M of the nitrosamide. NMR of the polymer as well as the residue left behind in the methanol mixture showed that, in fact, a significant amount of the indazole had formed during the course of the reaction along with the PMMA. It is also noted that no other aromatic peaks were observed other than those relating to the free indazole, which suggests that the amount aromatic incorporation into the polymer is either very small or that incorporation of the aromatic ring is not occurring at all.

It was also noted that, based on the obtained weights of polymer from the reactions, the polymerization process that is occurring is fairly inefficient with the yield of polymer not exceeding 20%, based on the weight of the dry polymer relative to the weight of the solvent used. If the formed indazole were somehow responsible for the observed polymerization one would expect yields to be higher. The innocence of the indazole was confirmed by simply heating 0.03 g (0.23 mmol) of the indazole in 15 mL of MMA (14 g) (140 mmol) for 2 hours. Addition of methanol yielded no polymer precipitate. An attempt to hinder the reaction with MMA was made by diluting the reaction mixture with benzene before heating. The reaction was performed with MMA (100 μL) and N-(2,6-dimethylphenyl)-N-nitrosoacetamide (1a) (0.01 g)(0.05 mmol) dissolved in deuterated benzene (1 mL). In this case the consumption of MMA was non-existent while indazole formation occurred readily, no PMMA was observed to form in this reaction. This result is significant as it shows that the concentration of the nitrosamide relative to the MMA impacts the polymerization process, suggesting that the nitrosamide is in some way initiating the polymerization.

In considering that the reaction in MMA results in both indazole formation, as well as polymerization, and demonstrates a degree of concentration dependence relative to the MMA, it seems likely that a radical process which is initiated by electron transfer between the alkene and the diazonium is responsible for the observed reaction behavior. In this proposed process rearrangement to the phenyl diazoacetate occurs normally, followed by heterolysis to the diazonium acetate ion pair, which in MMA will be an intimate ion pair. At this point competition between the cyclization reaction and the reaction with MMA becomes significant. Examination of this proposed process through pi complex formation between the alkene and the diazonium resulting in a reaction occurring which then gives way to the radical chain process seems to show that such a process is unlikely to occur due to the fact an electron deficient species such as MMA would be a poor electron donor and that a positively charged MMA intermediate would need to be formed (Figure 80).

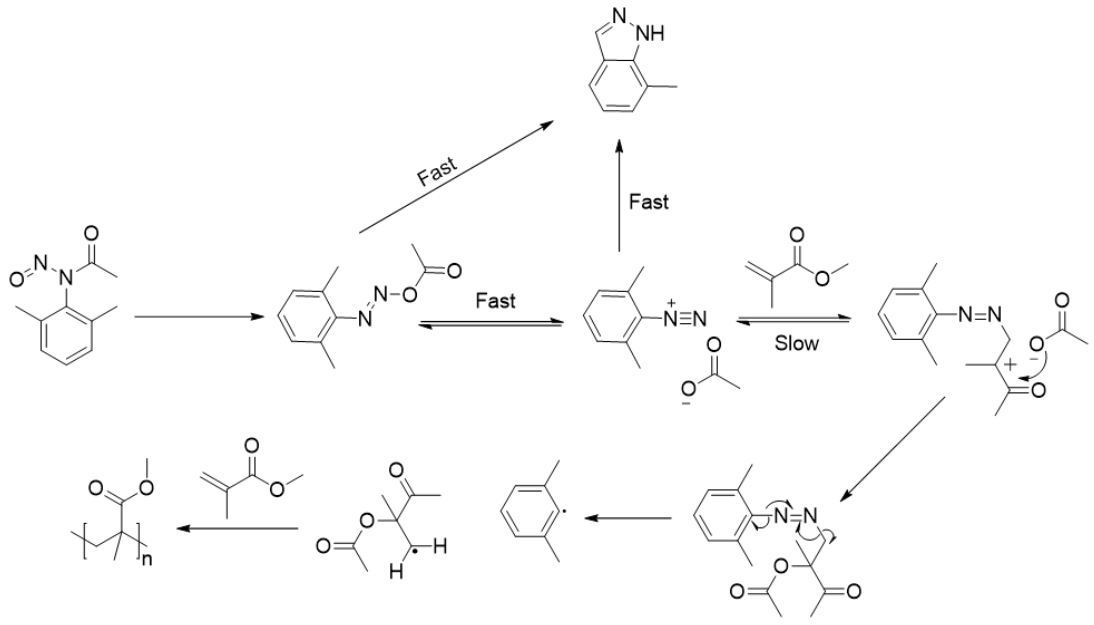

Figure 80: Postulated mechanism for the polymerization of MMA in which a reaction between the diazonium species and MMA results in the eventual formation of a phenyl radical.

In considering possible radical or electron transfer pathways that could explain the formation of PMMA, the *ortho*-quinoazomethane was considered as a possible initiator for the polymerization (Figure 81). As it was established that significant indazole formation occurred during N-aromatic nitrosamide decomposition in MMA, it follows that the *ortho*-quinoazomethane intermediate could be present during the reaction. The *ortho*-quinoazomethane would be formed through its normal pathway but, rather than cyclizing with the azo group, the

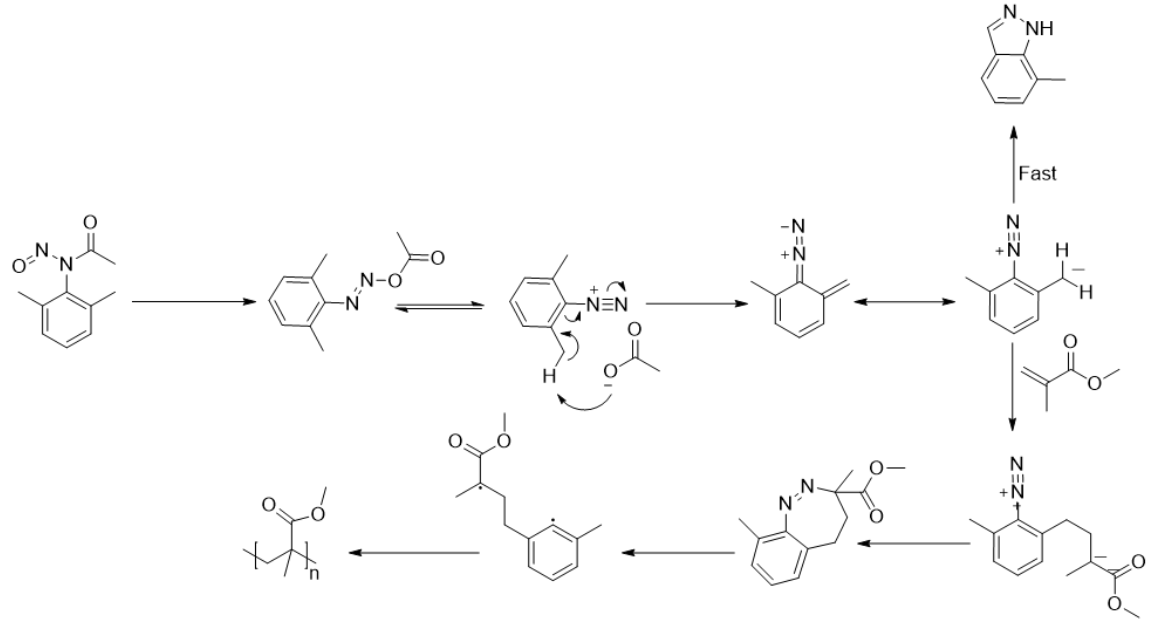

Figure 81: Postulated mechanism for the polymerization of MMA in which an *ortho*-quinoazomethane anionically initiates MMA. The resulting anion cation pair can then undergo a redox reaction to give a phenyl radical and a MMA radical.

carbon nucleophile would attack the alkene in a Michael type reaction. In this situation polymerization would be initiated anionically, which is far more favorable from the standpoint of reacting with MMA. From this point the diazonium could then go on to still decompose through a homolytic or heterolytic pathway. Considering the low dielectric constant of MMA and the charge balance issues that would be presented by cation formation, it seems feasible that an electron

transfer process from the anion of the initiated MMA to the diazonium would result in the liberation of nitrogen gas leading to a biradical species which could go on to rapidly polymerize. Finally, it is also possible that this process simply proceeds by the production of aryl radicals from the homolysis of the phenyldiazoacetate. Given that the aryl radical is seemingly a higher energy species than the *ortho*-quinoazomethane, it would only be formed in relatively small amounts, and as such, would most likely not be an effective radical initiator resulting in the observed low yielding polymerization (Figure 82).

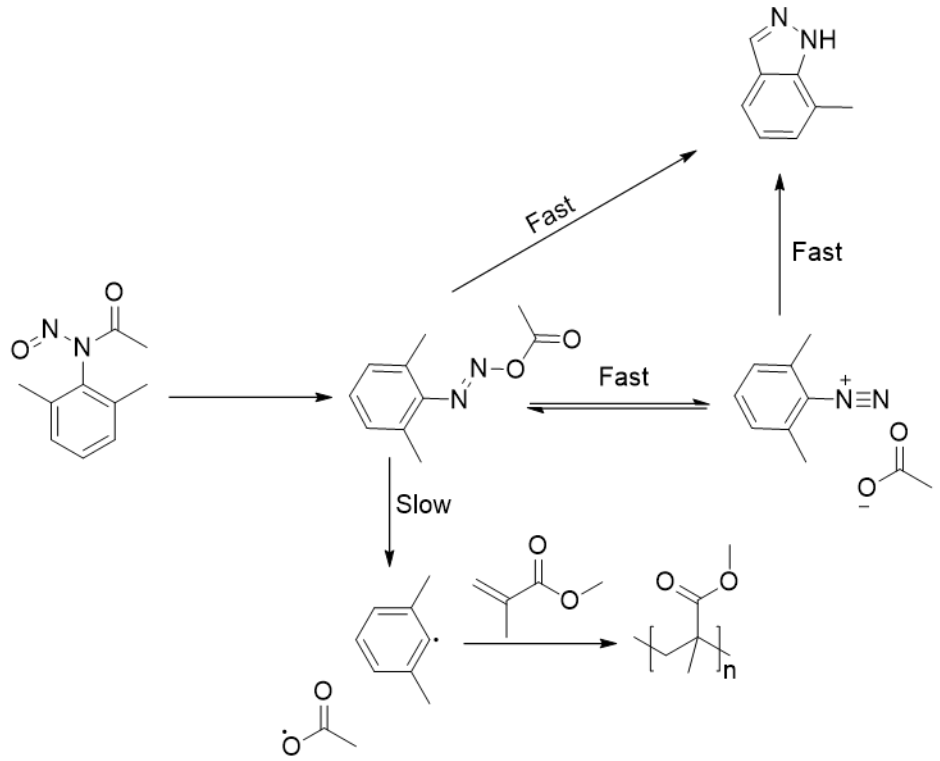

Figure 82: Postulated mechanism for the polymerization of MMA in which homolysis of the phenyl diazo acetate results in a phenyl radical which can then initiate the radical process.

The reaction of kinetically stable nitrosamides with alkenes was probed further by performing the solvolysis of nitrosamide (1a) in cyclohexene. Cyclohexene has a reported dielectric constant of 18.3. As such, it was proposed that aryl cation formation would be able to occur allowing for cyclohexene addition to the aromatic ring. The resulting positive charge formed

on the cyclohexene could then be quenched by the acetate or could react further giving oligomer or polymer. Carrying out the reaction at 70 °C for 2 hours gave a deep red solution. Concentrating the deep red solution under vacuum gave a deep red liquid with a boiling point well above 100 °C. ^{1}H-NMR analysis of the red oil showed it to be a complex mixture of cyclohexene addition products/oligomers with no observed indazole side products (Figure 83). Based on the observed solvent effects, it seems most likely cyclohexene addition/oligomerization is due to a cationic process rather than a radical process (Figure 84).

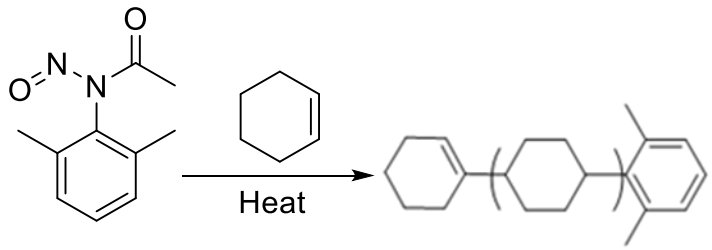

Figure 83: Solvolysis of N-(2,6-dimethylphenyl)-N-nitrosoacetamide in cyclohexene giving a mixture of cyclohexene oligomers.

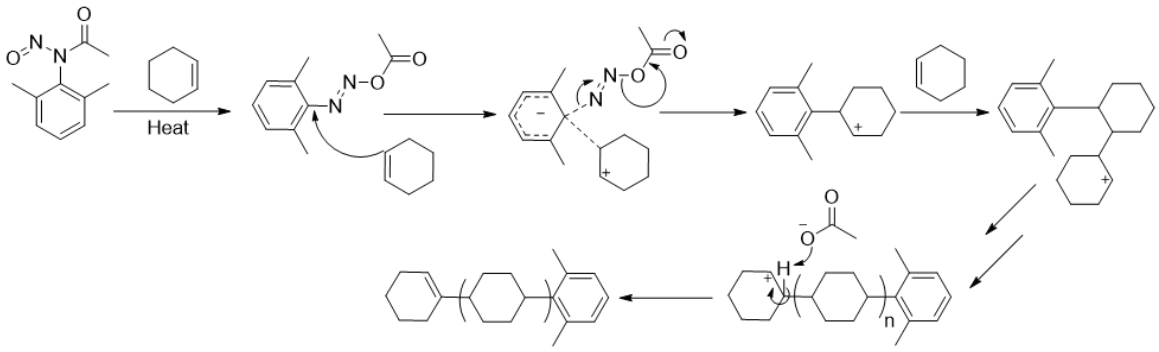

Figure 84: Postulated cationic initiation process for the formation of cyclohexene oligomers.

2.5 Conclusions and Future Work

The synthesis and isolation of kinetically stable nitrosamides has been probed. X-ray diffraction data, along with data from the literature supports the claim that the kinetic stability of these nitrosamides is due to the steric bulk surrounding the nitrosamide group, hindering

rearrangement to the unstable phenyldiazoacetate. Carrying out the reactions of these kinetically stable nitrosamides in pure solvent systems suggested a relationship between the mechanism of nitrosamide decomposition and the dielectric constant of the solvent. High dielectric constant solvents likely favor the formation of an aryl cation, which then undergoes nucleophilic addition by the solvent. Low dielectric constant solvents resulted in the formation of indazoles through a cyclization pathway.

This observed reactivity presents a stark contrast to the reactivity of other N-aromatic nitrosamides in which the reaction mechanism is generally unaffected by solvent conditions, as in the case with N-nitroso-N-phenylacetamide, which readily decomposes to form phenyl radicals regardless of solvent dielectric constant. It is clear that radical pathways are greatly hindered for *ortho* substituted nitrosamides with labile benzylic protons. It is also evident that strong enough electron donors can react directly with the diazoester/diazonium moieties through an ionic or redox process.

What remains unclear is why certain substrates, such as N-nitroso-N-phenylacetamide so readily undergo radical decomposition in all solvents while other substrates favor ionic intermediates depending on the solvent conditions. Future studies of these systems should focus on the kinetics of these reactions and characterization of reaction by-products, as these studies can further elucidate the reaction mechanisms of these nitrosamides in different solvents and can potentially shed light on the observed dielectric dependence that develops in *ortho*-substituted nitrosamide systems. In line with this area of investigation the role of the resulting acetate species should be subject to further investigation.

This work, as well as work from the literature, makes it apparent the acetate species that results from the nitrosamide decomposition plays a significant role in determining the reaction

pathway. Exploring the nitroso chemistry of acetate derivatives, such as thioamides and acetamidine derivatives could open up entirely new areas of nitrosamide chemistry (Figure 85). To date these systems remain poorly studied and seemingly are readily synthesizable, as such, new work in the field should be focused in these areas.

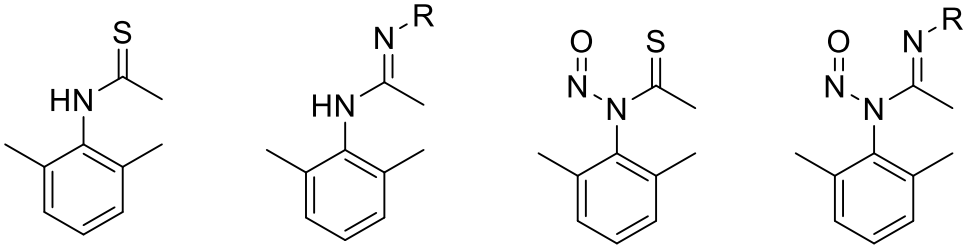

Figure 85: Examples of thioamides, acetamidines and their hypothetical nitroso derivatives.

It is clear that these kinetically stable nitrosamides have potential as highly efficient reagents for regiospecific aromatic functionalization. The conditions under which these nitrosamides can be efficiently decomposed to give single products in high yields should be explored in order to determine the extent of their synthetic utility. These studies will also shed light on how these conditions can be improved to optimize reactions that give low yields or undesired products, which in turn would help increase the synthetic utility of these substrates. Based on the results reported in this work, it seems reasonable that high dielectric constant solvents will result in the formation of a cationic species during N-aromatic nitrosamide decomposition which can be trapped by strong or moderate nucleophiles. Many high dielectric constant solvents are known that contain a wide variety of functionalities. N-Aromatic nitrosamide decomposition in these solvents should result in a diverse array of functionalized aromatics, while further elucidating the effect that dielectric constant has on the decomposition pathways of N-aromatic nitrosamides. Other factors may also impact N-aromatic nitrosamide decomposition as well, as the work performed by De Tar demonstrated that the presence of strong acids was capable of altering the decomposition pathway of N-aromatic nitrosamides, presumably by inducing the

formation of a cationic species.[8] Such as result suggests that strong acids could be used to overcome the indazole cyclization that so readily occurs for N-aromatic nitrosamides that contain benzylic protons *ortho* to the nitrosamide functionality by protonating the hypothesized acetate ion that is formed during decomposition. The results from this work have already been carried out and will be presented in Chapter 3 and will act as a guide for the development of further experiments.

2.6 Experimental Section

General Methods:

Unless otherwise noted, all starting materials and reagents were obtained from commercial suppliers and used without further purification. All solvents were used as obtained unless noted. All reactions were performed in dried glassware under open atmosphere with magnetic stirring unless otherwise noted. Chromatography: TLC was performed on silicagel 60 F_{254} sheets from Merck and visualized under UV light. Alumina chromatography was performed on 150 mesh neutral aluminum oxide from Sigma Aldrich. Analytical Instrumentation: IR spectra were recorded on a Thermo Scientific Nicolet 6700 FTIR spectrometer with peaks reported in cm^1. NMR spectra were recorded on a Varian VNMRS 300, 400, and 500 MHz NMR spectrometers. Chemical shifts are expressed in ppm relative to solvent signals. NMR spectra were processed using Mnova (www.mestrelab.com/software/mnova-nmr). X-ray crystallography analysis was carried out at the University of Oklahoma using a Bruker APEX ccd area detector (1) and graphite-monochromated Mo Ka radiation (l = 0.71073 Å) source. Crystal structures were visualized using CCDC Mercury software (http://www.ccdc.cam.ac.uk/products/mercury/). Nomenclature: IUPAC nomenclature was used to name each compound. Compounds reported in the literature that lack spectral data are marked with an (*). Compounds not reported in the literature are marked with an (**). Coupling constants are reported for compounds not reported in the literature.

General Procedure for the Synthesis of N-Aromatic Acetamides:

All of the N-aromatic acetamides reported in this work were prepared from their corresponding aryl amines and acetic anhydride using the procedure outlined by Behbahani and co-workers (Mojtahedi, M., Saeed Abaee, M., Heravi, M.; Behbahani, F. K. Additive-Free

Chemoselective Acylation of Amines and Thiols. *Monatsh. Chem.* **2007,** *95*, 138.) unless otherwise noted (in the preparation of amide (13) trifluoroacetic anhydride was used as the reactive solvent). The ^{1}H-NMR spectra of the prepared aryl amides were a match to their reported literature spectra.

N-(2,6-dimethylphenyl)acetamide (1)

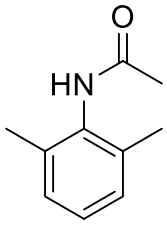

^{1}H-NMR (300 MHz, Chloroform-*d*) δ 7.10 (m, 3H, ArH), 2.24 (s, 6H, ArMe), 2.21 (s, 3H, O=CCH_3).

Powell, E.; P.; Lee, Y. H.; Partch, R.; Dennis, D.; Morey, T.; Varshney, M. Pi-Pi complexation of bupivacaine and analogues with aromatic receptors: implications for overdose remediation. *International Journal of Nanomedicine*. **2007**, *2*, 449-459.[78]

N-(2,6-diethylphenyl)acetamide (2)

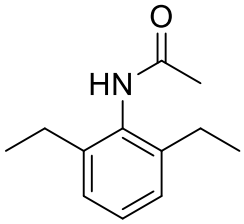

^{1}H-NMR (300 MHz, Chloroform-*d*) δ 7.34 – 7.04 (m, 3H, ArH), 2.59 (q, *J* = 7.5, 4H, ArCH_2), 2.19 (s, 3H, O=CCH_3), 1.19 (t, *J* = 7.6, 6H, CH_3).

Mohan, R.; Kalla, N.; Lim, J.; Bae, J.; Kim, I. Sulfated choline ionic liquid catalyzed acetamide synthesis by grindstone method. *Tetrahedron Letters*. **2017**, *58*, 1595-1599.[79]

N,N'-(2,3,5,6-tetramethyl-1,4-phenylene)diacetamide (3)*

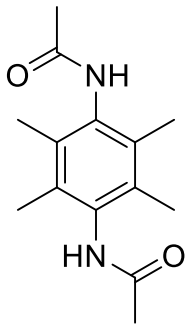

^{1}H-NMR (300 MHz, DMSO-d_6) δ 2.02 (s, 6H, O=CCH_3), 1.99 (s, 12H, ArMe).

IR: 3250 cm^{-1}, 1648 cm^{-1}

Nef, J. U. XXXVI.-Carboxyl-derivatives of benzoquinone. *J. Chem. Soc., Trans*. **1888**, *53*, 428-459.[64]

N-(2,5-dimethylphenyl)acetamide (4)

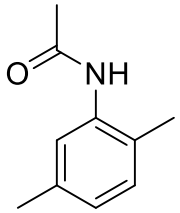

^{1}H-NMR (300 MHz, Chloroform-*d*) δ 7.58 (s, 1H, ArH), 7.08 (d, 1H, ArH), 6.88 (d, 1H, ArH), 2.31 (s, 3H, O=CCH_3), 2.21-219 (s, 6H, ArMe).
Shilpa, G.; Basavalinganadoddy, T. ^{1}H and ^{13}C NMR spectral studies on N-(j,k-dichlorophenyl)- and N-(j,k-dimethylphenyl)acetamides and substituted acetamides. *Zeitschrift fuer Naturforschung, A: Physical Sciences*. **2007**, *62*, 84-90.[80]

N-(2-(*tert*-butyl)phenyl)acetamide (5)

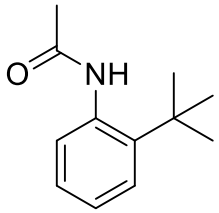

^{1}H-NMR (400 MHz, Chloroform-*d*) 1.41 (s, 9H, C(CH_3)$_3$), 2.21 (s, 3H, ArMe), 7.17 (t, 1H, ArH), 7.23 (t, 1H, ArH), 7.40 (d, 1H, ArH), 7.51 (d, 1H, ArH).

(It should be noted that in $CDCl_3$ a minor conformer as observed, this has been reported in the literature as well (see the below reference).

Neumann, J. J.; Rakshit, S.; Droege, T.; Glorius, F. Palladium-Catalyzed Amidation of Unactivated C(sp3)-H Bonds: from Anilines to Indolines. *Angew. Chem. Int. Ed*. **2009**, *48*, 6892 –6895.[81]

2**-acetamidobenzoic acid (6)**

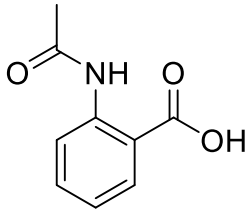

^{1}H-NMR (400 MHz, Methanol-*d4*) 2.19 (s, 3H, O=CCH_3), 7.13 (t, 1H, ArH), 7.54 (t, 1H, ArH), 8.07 (d, 1H, ArH), 8.53 (d, 1H, ArH).

Giri, R.; Lam, J. K.; Yu, J. Q. Synthetic Applications of Pd(II)-Catalyzed C-H Carboxylation and Mechanistic Insights: Expedient Routes to Anthranilic Acids, Oxazolinones, and Quinazolinones. *J. Am. Chem. Soc*. **2010**, *132*, 686-693.[82]

N-(2,6-dimethylphenyl)-2,2,2-trifluoroacetamide (13)*

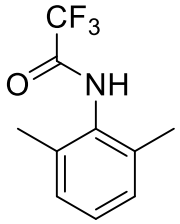

^{1}H-NMR (400 MHz, Chloroform-*d*) δ 7.02 (d, *J* = 7.5 Hz, 2H), 6.87 (t, *J* = 7.5 Hz, 1H), 2.28 (s, 6H).

^{19}F NMR (400 MHz, Chloroform-*d*) δ -75.92 (s).

(No literature spectra have been reported for this compound, but the melting point was found to be a match to what has been reported in the literature).

Melting point: 91°C

Ohtaka, J.; Sakamoto, T.; Kikugawa, Y. A one-pot procedure for trifluoroacetylation of arylamines using trifluoroacetic acid as a trifluoroacetylating reagent. *Tetrahedron Letters*, **2009**, *50*, 1681-1683.[72]

General Procedure for the Synthesis of N-Aromatic Nitrosamides:

The desired acetamide (0.2-0.3 mmol) was placed in a round bottom flask and dissolved in 8 mL of a 2:1 mixture of acetic anhydride and acetic acid. The flask was cooled to 10 °C in an ice bath. Solid sodium nitrite (3 equiv, 6 equiv if the molecule has a carboxylic acid or is a trifluoro acetamide) was added to the mixture, and the vessel is sealed. Evolution of a brown gas occurred, followed by the solution changing color to blue then yellow. The flask is kept in the ice bath for 30 minutes and allowed to warm to room temperature, where it was typically kept overnight, although the reaction may be complete much sooner. The solution sometimes darkened on standing, but this did not impact the results. The mixture was poured into a vacuum flask and dried under reduced pressure to give a solid mixture of the desired nitrosamide and what was assumed to be sodium acetate. The crude product was purified by extracting the product from the mixture with diethyl ether. The yellow solution was then passed through an alumina plug to remove trace

impurities. The yellow solution was then dried under reduced pressure to give a bright yellow oil (in the case of compound (3a) a solid was obtained) ^{1}H NMR analysis showed that the nitrosamide was sufficiently pure, as no residual starting material, acetic acid, acetic anhydride, or other impurities were detected.

N-(2,6-dimethylphenyl)-N-nitrosoacetamide (1a)

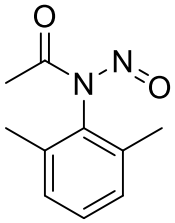

^{1}H-NMR (300 MHz, Chloroform-*d*) δ 7.25 (t, 1H, ArH), 7.11 (d, 2H, ArH), 2.97 (s, 3H, O=CCH$_3$), 1.88 (s, 6H, ArMe).

Joergensen, K. A.; Ghattas, A. B.; Lawesson, S. O. Studies on organophosphorus compounds. XLV. Thiation of some sterically hindered N-nitrosamides. *Bulletin de la Societe Chimique de France*. **1984**, *204*, 5-6.[27]

N-(2,6-diethylphenyl)-N-nitrosoacetamide (2a)**

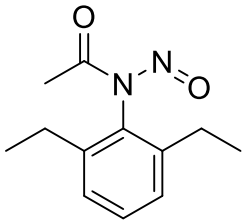

^{1}H-NMR (300 MHz, Chloroform-*d*) δ 7.37 (t, J=7.1 Hz, 1H, ArH), 7.18 (d, J=7.5 Hz, 2H, ArH), 2.98 (s, 3H, O=CCH$_3$), 2.13 (q, J= 7.8 Hz, 4H, ArCH$_2$), 1.04 (t, *J*=7.5 Hz, 6H, CH$_3$).

N,N'-(2,3,5,6-tetramethyl-1,4-phenylene)bis(N-nitrosoacetamide)(3a)**

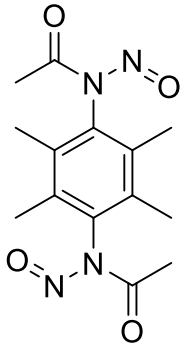

^{1}H-NMR (300 MHz, DMSO-d6) δ 2.98 (s, 6H, O=CCH$_3$), 1.70 (s, 12H).

N-(2,5-dimethylphenyl)-N-nitrosoacetamide (4a)**

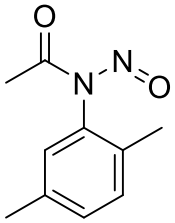

^{1}H-NMR (300 MHz, Chloroform-*d*) δ 7.17 (d, 2H, ArH), 6.59 (s, 1H, ArH), 2.95 (s, 3H, O=CCH$_3$), 2.30 (s, 3H, ArMe) 1.85 (s, 3H, ArMe).

N-(2-(*tert*-butyl)phenyl)-N-nitrosoacetamide (5a)*

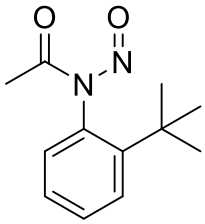

^{1}H-NMR (300 MHz, Chloroform-*d*) δ 7.56 (d, *J*=8 Hz, 1H, ArH), 7.45 (t, *J*=7.8Hz, 1H, ArH), 7.25 (t, *J*=7.6Hz, 1H, ArH), 6.51 (d, *J*=7.7Hz, 1H, ArH), 2.95 (s, 3H, O=CCH$_3$), 1.15 (s, 9H, (CH$_3$)$_3$C).

Glatzhofer, D. T.; Roy, R. R.; Cossey, K. N. Conversion of N-aromatic amides to O-aromatic esters. *Org. Lett.* **2002**, *4*, 2349–2352.[18]

2-(N-nitrosoacetamido)benzoic acid (6a)*

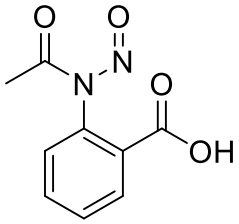

^{1}H-NMR (300 MHz, MeOH-d4) δ 2.87 (s, 3H, O=CCH$_3$), 8.23 (t, *J*=7.8Hz, 1H, ArH), 8.37 (t, *J*=7.7Hz 1H, ArH), 8.66 (d, *J*=7.9Hz 1H, ArH), 8.92 (d, *J*=8.1Hz, 1H, ArH).

Abdelhamid, A. O.; Mohamed, G. S.; .Reaction with hydrazonoyl halides XXIII [1]: Synthesis and reactions of C-coumarinoyl-N-arylformohydrazonoyl bromides. *Heteroatom Chemistry*, **1999**, *10*, 355-362.[83]

General Procedure for the Solvolysis of N-Aromatic Nitrosamides in Acetic Anhydride

The desired nitrosamide (0.2-0.3 mmol) was dissolved in 5ml of acetic anhydride. The solution was then added to a flask containing 30 mL of acetic anhydride. The mixture was stirred magnetically while being heated to 80 °C. The temperature was maintained for 2 hrs. Over the

course of the reaction the reaction transitioned from bright yellow to clear, which indicated that the reaction was finished. In situations where the mixture turned red or orange during heating the desired product was obtained in low yields or was not obtained at all. The mixture was allowed to cool to room temperature, poured into a vacuum flask, and dried under reduced pressure to give the desired ester as a solid. The resulting crude products were then analyzed by ^{1}H-NMR. Further purification was carried out if needed by column chromatography using a neutral alumina solid phase. Dichloromethane was employed as the mobile phase. In cases where dichloromethane gave poor separation a 50/50 mixture of hexanes and ethyl acetate was used as the mobile phase. Percent yields were based on isolated yields of the reactions. In the case of reactions that required purification percent yield was based off the isolated yield after purification. Purity was gauged by the ^{1}H-NMR spectra of the products. Products were determined to be sufficiently pure if only the desired product and residual NMR solvent peaks were observed in the ^{1}H-NMR spectrum of the product.

2,6-dimethylphenyl acetate (7)

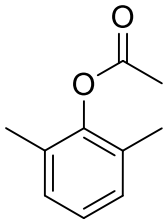

^{1}H-NMR (400 MHz, Chloroform-d) δ 7.06 (apt S, 3H, ArH), 2.35 (s, 3H, O=CCH3), 2.16 (s, 6H, $ArCH_3$).

Yield: >98%

Atsushi, A.; Tadashi, I.; and Satoru, M. Mechanism of the Double Aldol Reaction: The First Spectroscopic Characterization of a Carbon-Bound Boron Enolate Derived from Carboxylic Esters. *J. Am. Chem. Soc*. **2002**, *124*, 10759–10764.[68]

2,6-diethylphenyl acetate (8)

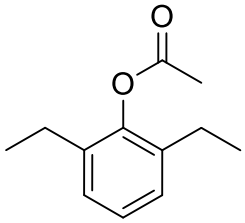

^{1}H-NMR (300 MHz, Chloroform-d) δ 7.12 (apt q, 3H, ArH), 2.50 (q, J = 7.7 Hz, 4H, $ArCH_2$), 2.34 (s, 3H, $O=CCH_3$), 1.19 (t, J = 7.6 Hz, 6H, CH_3).

Yield >98%

Atsushi, A.; Tadashi, I.; and Satoru, M. Mechanism of the Double Aldol Reaction: The First Spectroscopic Characterization of a Carbon-Bound Boron Enolate Derived from Carboxylic Esters. *J. Am. Chem. Soc*. **2002**, *124*, 10759–10764.[68]

2,3,5,6-tetramethyl-1,4-phenylene diacetate (9)

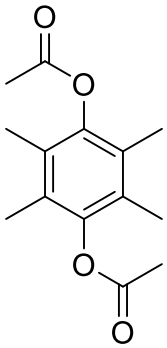

^{1}H-NMR (300 MHz, Chloroform-d) δ 2.34 (s, 6H, $O=CCH_3$), 2.04 (s, 12H, ArMe).

Yield: 87%

Pradal, A.; Toullec, P. Y.; Michelet, V. Gold-Catalyzed Oxidative Acyloxylation of Arenes. *Org. Lett*. **2011**, *13*, 6086-6089.[69]

2-(*tert*-butyl)phenyl acetate (11)

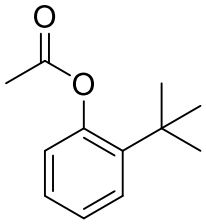

^{1}H-NMR (400 MHz, Chloroform-*d*): δ 7.41 (d, 1H, ArH), 7.25-7.15 (m, 2H, ArH), 7.01 (d, 1H, ArH), 2.34 (s, 3H, $O=CCH_3$), 1.35 (s, 9H, $(CH_3)_3C$).

Yield: 93%

Cook, A. K.; Emmert, M.H.; Sanford, M. S. Steric Control of Site Selectivity in the Pd-Catalyzed C–H Acetoxylation of Simple Arenes. *Org. Lett*. **2013**, *15*, 5428-5431.[84]

2-methyl-4H-benzo[d][1,3]oxazin-4-one (12)

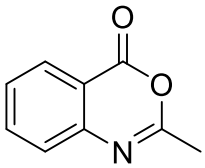

^{1}H-NMR (300 MHz, Chloroform-*d*): δ 2.35 (s, 3H, N=CCH$_3$), 7.14 (dd, J = 7.5, 2.0 Hz, 1H, ArH), 7.35 (td, J = 7.4, 2.0 Hz, 1H, ArH), 7.62 (td, J = 7.5, 2.0 Hz, 1H, ArH), 8.12 (dd, J = 7.5, 2.0 Hz, 1H, ArH).

Yield: 86%

Penhoat, M.; Bohn, P.; Dupas, G.; Papamicaël, C.; Marsais, F.; Levacher, V. New development of Meyers' methodology: stereoselective preparation of an axially chiral 5,7-fused bicyclic lactam related to circumdatins/benzomalvins and asperlicins. *Tetrahedron: Asymmetry*, **2006**, *17*, 281-286.[85]

2,6-dimethylphenyl 2,2,2-trifluoroacetate (14)**

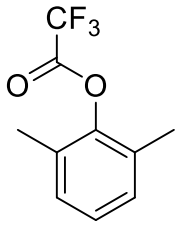

^{1}H-NMR (300 MHz, Chloroform-d) δ 7.16 (m, 3H, ArH), 2.25 (s, 6H, ArMe).

^{19}F NMR (300 MHz, Chloroform-*d*) δ -75.26 (s).

General Procedure for the Solvolysis of N-Aromatic Nitrosamides in MMA

40 mL of MMA was run through a column of activated alumina in order to remove any radical inhibitors. A flask was then charged with 30 mL of MMA followed by 0.0453 g of N-aromatic nitrosamide pre-dissolved in 5 mL of MMA. The solution was then heated to 80 °C. Upon reaching 80 °C the reaction was allowed to run for two hours. The reaction was then allowed to cool to room temperature. Methanol was then slowly added to the solution which resulted in the perception of PMMA as a white fluffy solid. The PMMA was dried over vacuum. The structure

of the PMMA was then analyzed using NMR. The yield of PMMA was calculated based off the measured weight of the dry PMMA relative to the weight of the MMA that was used in the reaction. The weight of MMA was calculated from its density and the volume used in the reaction.

Chapter 3: Application of N-Aromatic Nitrosamides to the Synthesis of Functionalized Aromatics

As discussed in Chapter 1 the synthesis of phenols and aryl ethers is typically achieved through the use of electrophilic sources of ^{+}OH which yields the corresponding phenol. The phenol can be used to access aryl ethers using the Willison ether synthesis, in which the corresponding phenol is treated with base to form the phenoxide that can readily attack the corresponding alkyl halide to form the desired ether.[1] These methods have a number of shortcomings that can be overcome using diazonium salts or related species to install the desired phenol or aryl ether through simple solvolysis reactions. While promising, the work reported on these solvolysis reactions shows that they are anything but straightforward.[1]

The main issue that arises when using diazonium salts to synthesize phenols are the rapid, undesired coupling reactions that occur between the initially formed phenol and the remaining diazonium salt. As the phenol is an electron rich species, it has the capability to add to the remaining diazonium salt yielding undesired azo coupling products, which then generally further which then generally further decompose into intractable tars (Figure 86).[86] Methods have been

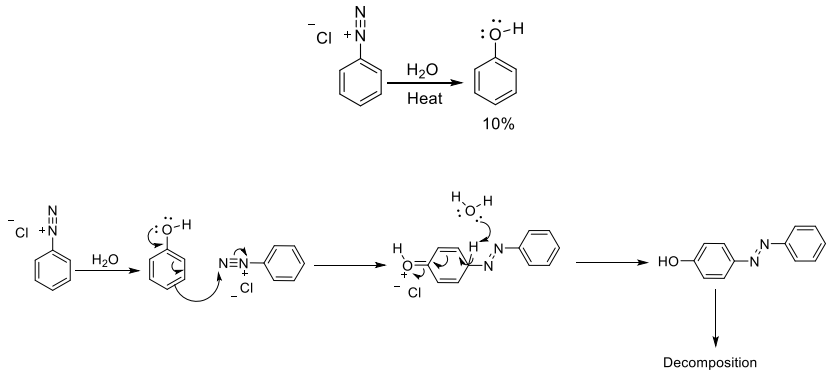

Figure 86: Production of unwanted azo phenol couplings during the synthesis of phenol from diazonium salts leading to low yields of the phenol.[86]

developed to work around these issues that generally involve removing the phenol from the reaction mixture as it is formed, either by some form of distillation, or through the use of biphasic solvent systems in which the phenol will partition into the organic solvent layer upon formation, thus preventing undesired side reactions with the diazonium species.[86,87] While these methods are capable of giving good to excellent yields, with reported yields exceeding 90%, they are not universal and substrates that lack the proper physical properties that are needed to be compatible with these methods will still suffer from poor yields under these conditions.[86,87]

The issues encountered in the synthesis of phenols using diazonium salts are also encountered in the synthesis of aryl ethers. While not as strongly electron donating as their related phenols, aryl ether moieties are strong electron donors and can also engage in undesired azo coupling reactions. The solvolysis of diazonium salts to form aryl ethers is also plagued by variable yields due to subtle substitution effects, making efficient synthesis difficult to achieve in these systems. This was demonstrated by Shriver and co-workers, who carried out the solvolysis of a number of diazonium salts bearing different functional groups at various positions (Table 6).[25] Selected reactions from their work demonstrate the variable yields that can be encountered when dealing with diazonium salts.[25] Shriver and co-workers also demonstrated that the dielectric constant of the solvent played a large role in the reaction effectiveness. Attempts to perform reactions with stoichiometric amounts of alcohol in solvents such as benzene or chloroform lead to complex mixtures with little to none of the desired aryl ether.[25] Reactions performed in ionic liquids with sight molar excess of alcohol typically only gave the desired aryl ethers in about 20-25 % yield, and were plagued by difficult workup procedures, but effectively demonstrated that aryl ethers could be formed without having to use the target alcohol as the solvent.[25] N-aromatic nitrosamides not only offer a potential solution to the issues encountered in phenol and aryl ether

synthesis, but also have the potential to open up new routes to other desirable functionalized aromatics. The decomposition of nitrosamides in water and alcohol solvents has been poorly explored, as most nitrosamide reactions are generally studied in benzene or related solvents, but the few examples that are known in the literature have shown that formation of the phenol or corresponding aryl ether was possible. Work carried out by De tar demonstrated that anisole could be preferentially formed under acidic conditions (Figure 6).[8]

Table 6: Solvolysis of diazonium salts in various alcohols performed by Shiver and co-workers.[25]

Diazonium salt	Aryl Ether	Yield
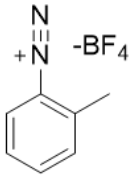	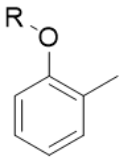	R= CH_3, 27% R= Et, 21% R= t-Bu, 16%
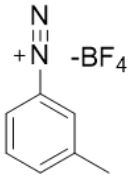	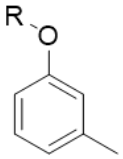	R= CH_3, 45% R= Et, 46% R= t-Bu, 38%
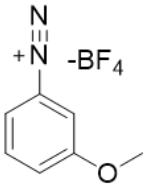	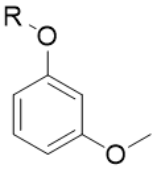	R= CH_3, 73% R= Et, 53% R= t-Bu, 0%

3.1 Reaction of Stable N-Aromatic Nitrosamides with Water and Alcohols

Initial investigations into the reactions of kinetically stabilized nitrosamides demonstrated efficient solvolysis with nucleophilic addition of the solvent could be achieved in solvents with relatively high dielectric constants, while low dielectric constant solvents resulted in the formation

of indazoles. While these results provided a clear relationship between solvent dielectric constant and the decomposition mechanism of the nitrosamide the exact range of dielectric constant values that allows for efficient solvolysis was not established. The dielectric constant dependence was elucidated by performing the solvolysis of nitrosamide (1) in a series of alcohols with progressively lowering dielectric constants. Decomposition of nitrosamide (1) was carried out in methanol, ethanol, propanol, iso-propanol, butanol, pentanol, and *tert*-butanol. Solvolysis of nitrosamide (1) worked well all the way up to butanol. Attempts to react nitrosamide (1) with pentanol or *tert*-butanol yielded the corresponding indazoles in well over 90% yield (Figure 87).

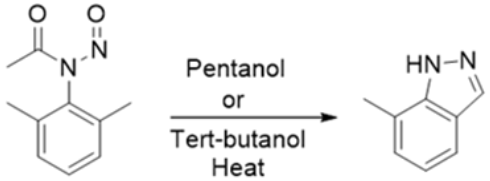

Figure 87: Solvolysis reaction of nitrosamide (1) in low dielectric constants alcohols.

These results gave a clear range of dielectric constant values that would allow for efficient solvolysis to occur, suggesting that any solvent with a dielectric constant of 17.6 or higher should be capable of affecting the solvolysis of these nitrosamide systems (Table 7).[88] The extent to which

Table 7: Dielectric constant values for selected solvents and the products from reactions with nitrosamide (1).[88]

Solvent	Dielectric constant	Result
Water	80	phenol
Methanol	30	ether
Ethanol	24.5	ether
Propanol	20.1	ether
Iso-propanol	17.9	ether
Butanol	17.6	ether (Major)+indazole (minor)
Acetic anhydride	21	ester
Pentanol	13.9	indazole
Tert-butanol	10.9	indazole

this hypothesis was valid was first tested by carrying out a comprehensive set of solvolysis reactions across the set of kinetically stabilized nitrosamides that had been isolated and characterized. Initial experiments were carried out using the 2,6-disubstituted nitrosamide systems, with solvolysis reactions being performed first in water, and then in alcohols in the order of decreasing dielectric constant. All reactions gave clear to yellow oils which were found to be the desired phenols/aryl ethers with the exception of nitrosamide (3a), which when hydrolyzed in water gave the corresponding quinone as a yellow solid, rather than the hydroquinone. This result is not totally surprising as the autoxidation of hydroduroquinone to duroquinone is a spontaneous process and is well documented in the literature (Figure 88).[89] The yields of these reactions were

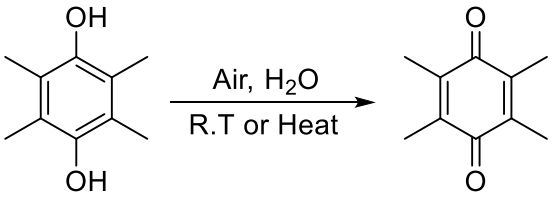

Figure 88: Oxidation of hydroduroquinone to duroquinone in open air.[89]

measured by the weight of the isolated final product compared to the weight of the starting amide that was used. The purity of the isolated products was determined by ^{1}H NMR spectroscopy. In situations where the isolated product needed to be purified, the reaction yield was based on the final weight of the purified product. It is worth noting that many of the aryl ethers derived from nitrosamide (1a) showed significant volatility, which is most likely the explanation for the slightly lowered yields relative to the other substrates. The results of these reactions are reported in (Table 8).

Within the 2,6-disubstituted series all attempted reactions with pentanol or *tert*-butanol gave the indazole along with a complex mixture of products, none of which were the desired aryl ethers. The results of the solvolysis reactions of the 2,6-disubstituted systems demonstrate that

Table 8: Solvolysis of 2,6 substituted nitrosamides in water or alcohols.

Nitrosamide	Product	Yield
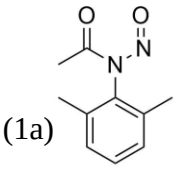 (1a)	(15) 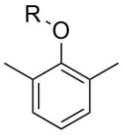	R=H (98%), R= CH3 (88%) R= Et (92%) R= i-Pr (85 %) R=Propyl (78%) R=Butyl (75%) 15a=H, 15b=CH3, 15c=Et, 15d=i-Pr 15e=propyl, 15f=butyl
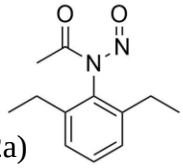 (2a)	(16) 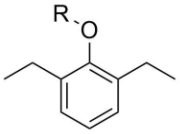	R=H (99%), R= CH3 (92%) R= Et (92%) R= i-Pr (90 %) R=Propyl (87%) R=Butyl (77%) 16a=H, 16b=CH3, 16c=Et, 16d=i-Pr 16e=propyl, 16f=butyl
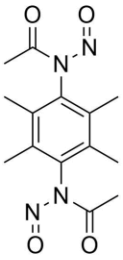 (3a)	(17) 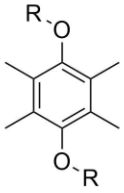	R=quinone (90%), R= CH3 (90%) R= Et (90%) R= i-Pr (78 %) R=Propyl (75%) R=Butyl (complex mixture, N.D) 17a=quinone, 17b=CH3, 17c=Et, 17d=i-Pr 17e=propyl

these nitrosamides all display the same dependence on solvent dielectric constant, as well as the same reaction behavior, with little variation in reaction yield. The results also demonstrate that the solvolysis of these nitrosamides in water and in alcohols is an efficient process with these reactions generally giving yields of 80% or higher with few exceptions. In cases where yields were low, the major observed side products were the indazoles, which could be separated from the aryl ether either by distillation of the aryl ether or by column chromatography of the crude mixture. No azo coupling products could be detected by ^{1}H NMR. To demonstrate that this reaction behavior was not simply confined to 2,6-disubstituted systems the 2-substituted nitrosamides were then subjected to the same reaction conditions. Examination of the 2-substituted nitrosamides demonstrated similar reaction behavior, with decreased yields as the dielectric constant of the solvent decreased, relative to the yields obtained for the 2,6-disubstituted nitrosamides. As with the 2,6-disubstituted systems, none of the desired aryl ether was formed in reactions with *tert*-butanol with the exception of nitrosamide (5a), demonstrating that the 2-substituted nitrosamides

are also subject to the effects of solvent dielectric constant, and in most cases were more sensitive to changing dielectric constant with large decreases in yield occurring at a dielectric constant of 18 (Table 9).

Table 9: Solvolysis of 2,5 and 2-substituted nitrosamides in water or alcohols.

Nitrosamide	Product	Yield
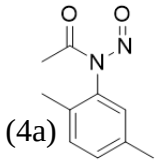 (4a)	(18) 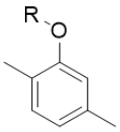	R=H (93%), R= CH3 (87%) R= Et (90%) R= i-Pr (48 %) R=Propyl (54 %) R=Butyl (Complex mixture, N.D) 18a=H, 18b=CH3, 18c=Et, 18d=i-Pr 18e=propyl
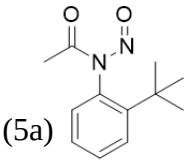 (5a)	(19) 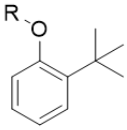	R=H (68%), R= CH3 (90%) R= Et (90%) R= i-Pr (0 %) R=Propyl (75%) R=*Tert*-butyl (complex mixture of isomers) 19a=H, 19b=CH3, 19c=Et, 19d=i-Pr 19e=propyl
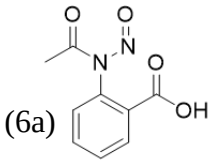 (6a)	(20) 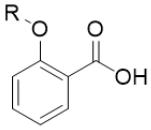	R= CH3 (93%) R= Et (95%) R= i-Pr (complex mixture, N.D) 20a=CH3, 20b=Et

In noting that the decomposition of nitrosamide (6a) in methanol and ethanol gave good yields of the desired aryl ethers (over 80%), it is also worth mentioning that when compared to the behavior of the corresponding diazonium salt, this is a significant achievement as solvolysis of 2-carboxybenzenediazonium in methanol gives only 17% of the desired ether and instead primarily results in the production of benzoic acid (Figure 89).[90] These sets of reactions highlight the

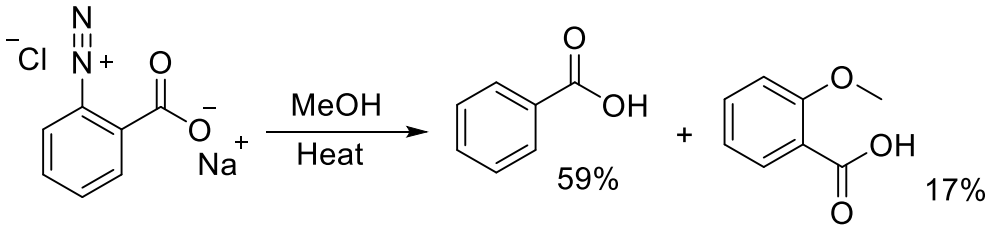

Figure 89: Behavior of 2-carboxybenzenediazonium chloride in methanol.[90]

chemical differences between nitrosamides and diazonium salts, and also help demonstrate the synthetic advantages that can be presented by N-aromatic nitrosamides.

The reaction of nitrosamide (5) in *tert*-butanol is important to note, as it sheds new light on the reaction behavior of nitrosamides. In the case of nitrosamide (1), decomposition in pentanol or *tert*-butanol led to the formation of 6-methyl-1H-indazole. Reactions of N-nitroso-N-phenylacetamide with alcohols under neutral or basic conditions were observed to oxidize alcohols to their corresponding aldehydes through a radical hydrogen abstraction. In the case of *tert*-butanol this oxidation is not possible and reactions between *tert*-butanol and N-nitroso-N-phenylacetamide resulted in complex mixtures. In the case of nitrosamide (5) one would expect a radical process to be a readily available mechanistic pathway due to the lack of benzylic protons. The reaction of nitrosamide (5) under the same conditions yielded a complex product mixture with the desired ether formation still being the major product of the reaction. Analysis of the reaction mixture using NMR spectroscopy showed 1-(*tert*-butoxy)-3-(*tert*-butyl)benzene (1.31 (s, 9H, *t*-bu), 1.34 (s, 9H, *Ot*-bu)), 1-(*tert*-butoxy)-2-(*tert*-butyl)benzene (1.35 (s, 9H, *t*-bu), 1.56 (s, 9H, *Ot*-bu)), and 2-(*tert*-butyl)phenyl acetate were significant reaction products, with 1-(*tert*-butoxy)-3-(*tert*-butyl)benzene being the major product in the mixture based on relative NMR integrations (Figure 90). Based on

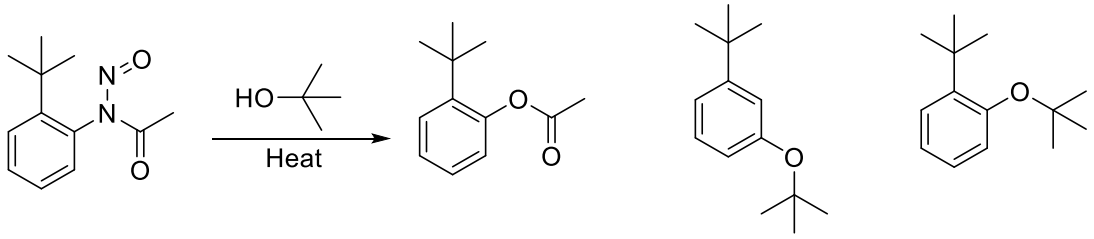

Figure 90: Reaction of nitrosamide (5) with *tert*-butanol.

the low dielectric constant of *tert*-butanol and the significant amount of other products that were formed along with the 1-(*tert*-butoxy)-2-(*tert*-butyl)benzene it maybe that a benzyne mechanism is the dominant reaction pathway for this process (Figure 91). In this process rearrangement and heterolysis gives the diazonium acetate ion pair. The acetate ion can then deprotonate the hydrogen

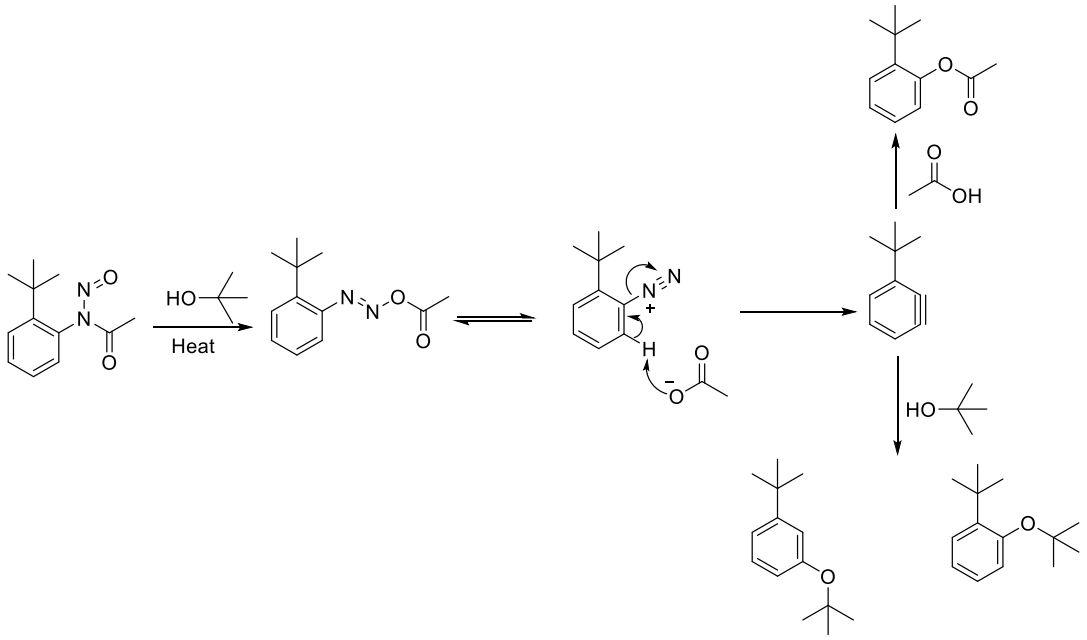

Figure 91: Mechanism of N-(2-(*tert*-butyl)phenyl)-N-nitrosoacetamide decomposition in *tert*-butanol.

ortho to the diazonium moiety, which can leave as N_2 gas in a concerted fashion, preventing the formation of any aryl anions or cations. The neutral benzyne can then readily combine with *tert*-butanol at the positions *ortho* and *meta* to the *tert*-butyl group.

While interesting, the observed reactivity is not unprecedented. Work by Cadogen and co-workers had suggested that nitrosamide (5) was capable of going through a benzyne pathway during its decomposition.[91] Cadogen and co-workers first demonstrated this upon observing that decomposition of nitrosamide (5) in benzene gave a mixture of 2-(*tert*-butyl)phenyl acetate and 3-(*tert*-butyl)phenyl acetate rather than the expected biphenyl (Figure 92).[91] Cadogan and co-workers

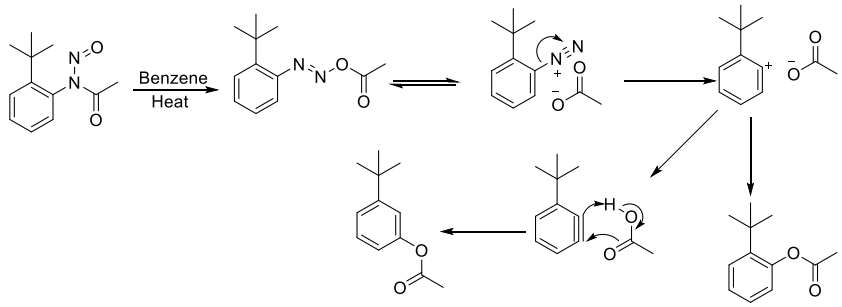

Figure 92: Mechanism of N-(2-(*tert*-butyl)phenyl)-N-nitrosoacetamide decomposition in benzene as proposed by Cadogan and co-workers.[91]

followed up on this observation by attempting to trap the benzyne with a series of arynophiles. These reactions were successful and gave the expected Diels-alder products (Figure 93).[91] It is

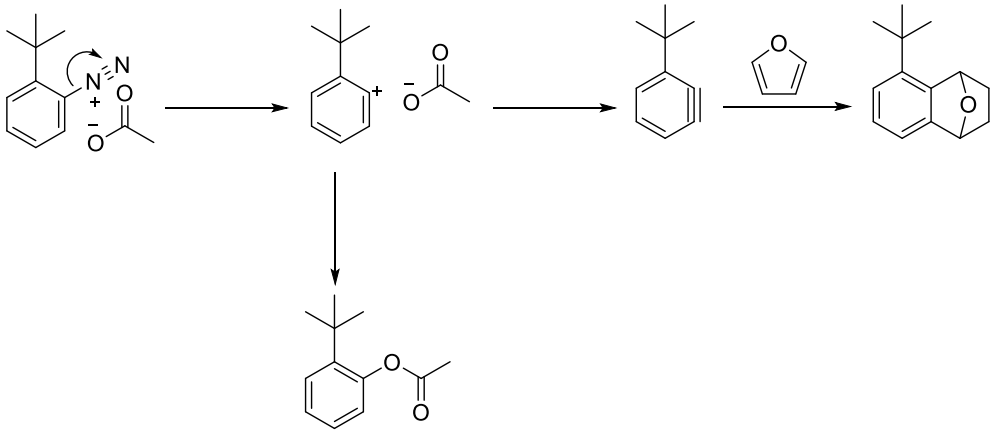

Figure 93: Benzyne formation and trapping as reported by Cadogan and co-workers.[91]

important to note that addition of arynophiles inhibited the formation of 3-(*tert*-butyl)phenyl acetate, but did not inhibit the formation of 2-(*tert*-butyl)phenyl acetate suggesting that diazonium heterolysis occurs first generating the aryl cation.[91] The acetate anion can then add leading to recombination, or deprotonation can occur giving the benzyne. These results support Cadogan's original postulation of a benzyne intermediate in the decomposition of nitrosamide (5), and also demonstrate that this reaction behavior is influenced by solvent dielectric constant as no benzyne products were observed in any of the high dielectric constant alcohols.

It should be noted that a radical mechanism is also capable of explaining the observed reaction behavior in which homolytic dissociation of phenyl diazoester yields N_2 gas and the corresponding phenyl and acetatoxy radicals (Figure 94). The acetate radical could rapidly recombine with the aryl radical, or radical hydrogen abstraction could occur directly on the aromatic ring giving the *ortho* bi-radical which is in resonance with the classical benzyne. Alternatively, the acetoxy radical could abstract a hydrogen from *tert*-butanol to form the *tert*-butoxy radical which is readily capable of either combining with the aryl radical or abstracting a hydrogen from the aromatic ring to form the benzyne.

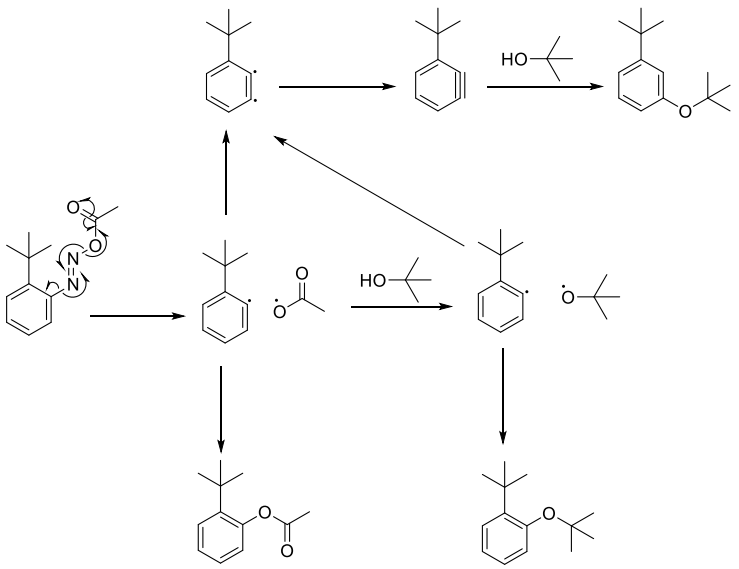

Figure 94: Postulated radical pathway for benzyne formation from the decomposition of N-(2-(*tert*-butyl)phenyl)-N-nitrosoacetamide.

From a mechanistic standpoint this finding further demonstrates the powerful effect that solvent dielectric constant has on these nitrosamide reaction mechanisms, as the benzyne formation from nitrosamide (5) is induced by low dielectric constant conditions, regardless of the mechanism it goes through, be it ionic or radical. This being said, the reaction yields from this reaction are poor, with the desired aryl ether being formed in less than 20% as part of a complex product mixture. In regard to the other kinetically stabilized nitrosamide systems, the situation is worse as indazole cyclization completely hinders aryl ether formation in low dielectric constant alcohols such as *tert*-butanol. From a synthetic methodology perspective, these nitrosamide systems will have limited utility unless a way to overcome this solvent dielectric issue is found.

3.2 Reactions of Stable N-Aromatic Nitrosamides in the Presence of Lithium Salts

The realization that one of the primary factors controlling reaction behavior was solvent dielectric constant led to the conclusion that the synthetic utility of these nitrosamide systems could be further improved by finding a way to increase the dielectric constant of the solvent media. The

drive behind this thought process being that the ability to control the dielectric constant of the medium would allow for the synthesis of other reaction products that normally would be inaccessible due to their inherently low dielectric constants.

Seemingly the best solution to the problem of developing a solvent with a high dielectric constant and chemical inertness was to use ionic liquids. These present their own problems as ionic liquids are expensive and can be difficult to use and, as a result of their high boiling points, can be extremely difficult to separate from the desired reaction products. Attempted reactions of diazonium salts with alcohols in ionic liquids from the literature show very minor improvements in yield with the best yields obtained being lower than 25%, demonstrating a need for methodology with a simple workup procedure that would allow for any reaction to be carried out with good efficiency and high yield.[25]

In order to determine if dielectric tuning was achievable without the use of ionic liquids, it was decided that the effect of salt additives should be explored. The effect of salts on reaction mechanisms and reaction rates have been well studied. Work by Hojo and co-workers showed that the rate of hydrolysis of organic halides is drastically increased in the presence of lithium perchlorate.[92] The rationale behind this process is twofold. The presence of excess salt stabilizes the formation of any charged species, while also displacing the chloride from the benzene, thus preventing recombination of the chloride (Figure 95).

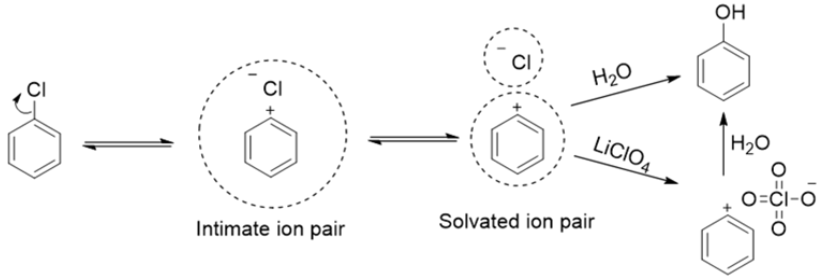

Figure 95: Salt assisted hydrolysis of chlorobenzene.[92]

Based on this behavior, it was postulated that similar salt effects could be used to overcome the dielectric constant problem in the reactions of N-aromatic nitrosamides that is presented by higher alcohols and other low dielectric constant solvents. Initial studies used 0.184 g (4.34 mmol) of lithium chloride in 35 mL of *tert*-butanol (0.124 M) with 0.041 g (0.21 mmol) of nitrosamide (1a). The reaction mixture was heated to 80 °C for 2 hours. Reaction workup yielded a light-yellow oil, which to was found to be a simple product mixture containing the starting amide and the desired *tert*-butyl ether in 50% yield (Figure 96).[93] The effect of the addition of lithium chloride presents a stark contrast in reactivity as all reactions attempted in *tert*-butanol alone yielded no

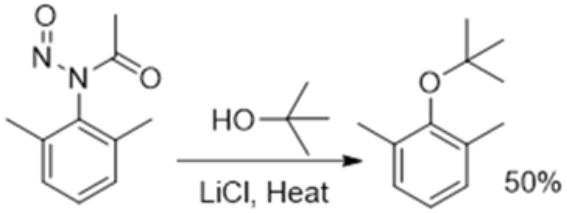

Figure 96: Salt assisted solvolysis of N-(2,6-dimethylphenyl)-N-nitrosoacetamide (1a).

detectable amount of the desired ether. Repeating the reaction several times gave varying yields with the highest observed yield being 93%.

The utility of this method was screened by carrying out the decompositions of nitrosamide (5a) and nitrosamide (2a) in *tert*-butanol saturated with lithium chloride using the procedure established for the decomposition of nitrosamide (1a). In the case of nitrosamide (2a) the desired *tert*-butyl aryl ether was readily obtained in 53 % yield with the other 47% being the aryl chloride. Performing the reaction with lithium perchlorate gave the desired aryl ether with no other observable products. In the case of nitrosamide (5a) ^{1}H NMR analysis showed that a complex product mixture formed yielding none of the expected ether, ester or chloride. The results of these reactions are reported in (Table 10). This generalized methodology demonstrates that through the use of salt additives, aryl ethers derived from low dielectric constant alcohols are readily obtainable making a number of aryl ethers potentially available. In the case of nitrosamide (5a) it is believed

that ether formation was inhibited by large steric demand of having two *tert*-butyl groups next to one another, while benzyne reactivity was inhibited by the

Table 10: Formation of *tert*-butyl aryl ethers through the use of lithium chloride in *tert*-butanol.

Nitrosamide		Product	Yield
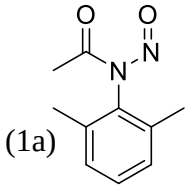 (1a)	(21)	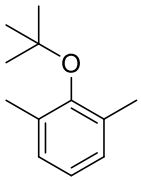	93%
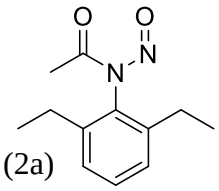 (2a)	(22)	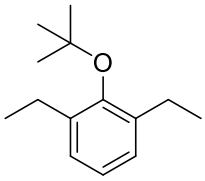	53% with lithium chloride 89% with lithium perchlorate
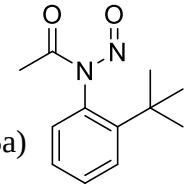 (5a)	(23)	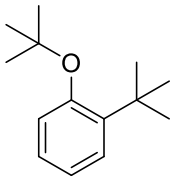	Complex mixture, aryl ether was not detected

displacement of the acetate by lithium chloride resulting in the change in reactivity.

While this method does present a simple and cheap solution to a difficult problem, it is not without its own issues. For this methodology to be effectively used in a wide variety of polar organic solvents the lithium perchlorate salts must be used, which have exceptional solubility in a number of organic solvents including diethyl ether. The main drawback to lithium perchlorates is their ability to potentially act as strong oxidizers and their known ability to form explosive organic compounds at elevated temperatures, making the use of these salts a potential hazard. What is needed is an additive that can improve the dielectric constant or ionic strength of a solution with a near universal solubility in all organic solvents and is safe to work with. Tetrabutylammonium

salts offer a potential solution to these issues, but suffer from their own issues, such as their low solubility in water, which makes removal of the salts from the reaction mixture problematic.

3.3 Reaction of Stable N-aromatic Nitrosamides with Sulfonic Acids

Sulfonic acids are a seemingly appealing route to realizing a way to optimize the decomposition of nitrosamides in low dielectric constant solvents. Sulfonic acids such as methanesulfonic acid and *para*-toluenesulfonic acid have good solubility in nearly all organic solvents, whereas many lithium salts have good solubility only in relatively polar solvents. More importantly a number of arenediazonium tosylates are known and demonstrate good stability as well as good synthetic utility (Figure 97).[94] Given the similarity between the chemical reactivity

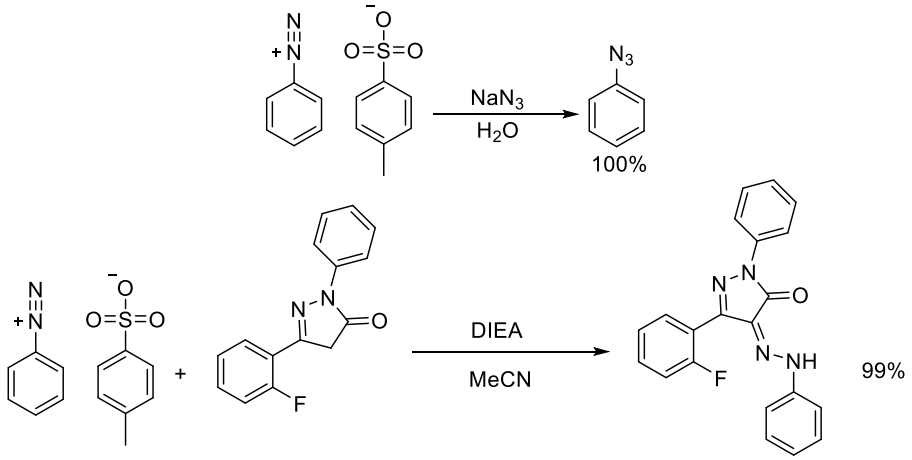

Figure 97: Examples of stable arenediazonium tosylates being used in controlled synthetic transformations.[94]

of diazonium salts with N-aromatic nitrosamides, sulfonic acids appear to be an ideal replacement for organic salts for use in the decomposition of N-aromatic nitrosamides in non-polar solvents. As one of the main objectives was to prevent the competitive formation of indazoles that occurs in non-polar solvents, which is likely to result from the intimate acetate ion acting as a base, sulfonic acids seemed an ideal choice due to their low pka's. It was speculated that the sulfonic acid would be able to protonate the resulting acetate anion, forming acetic acid, and effectively

forming the arenediazonium tosylate *in-situ*, preventing the formation of indazoles under all potential solvent conditions. In order to explore the potential of this chemistry, the decomposition of 45 mg of N-(2,6-dimethylphenyl)-N-nitrosoacetamide was carried out in 25 ml of *tert*-butanol containing 1 mL of methanesulfonic acid (Figure 98). The resulting solution was heated to 80 °C

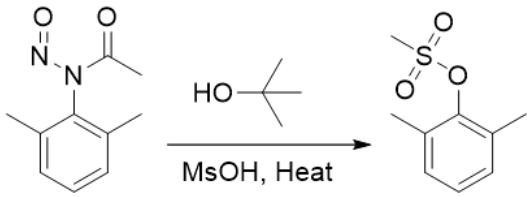

Figure 98: Conversion of N-(2,6-dimethylphenyl)-N-nitrosoacetamide to 2,6-dimethylphenyl methanesulfonate.[95]

for 2 hours with vigorous stirring, over the course of the reaction the solution transitioned from a strong yellow color to completely transparent. Workup of the resulting reaction solution, by drying under reduced pressure, followed by basic neutralization and extraction with 10% potassium bicarbonate and dichloromethane yielded a light-yellow organic layer. Concentrating the organic layer gave a white solid which was found to be 2,6-dimethylphenylmethanesulfonate in nearly 100% yield with no discernable side products based on its ^{1}H-NMR spectra.[95] A cursory search of the literature demonstrated that addition of trifluoromethanesulfonic acid to diazonium tetrafluoroborates has been reported.[85] Addition of methanesulfonic acid to diazonium like species has been reported as well but are sparse (Figure 99). [96,97,98]

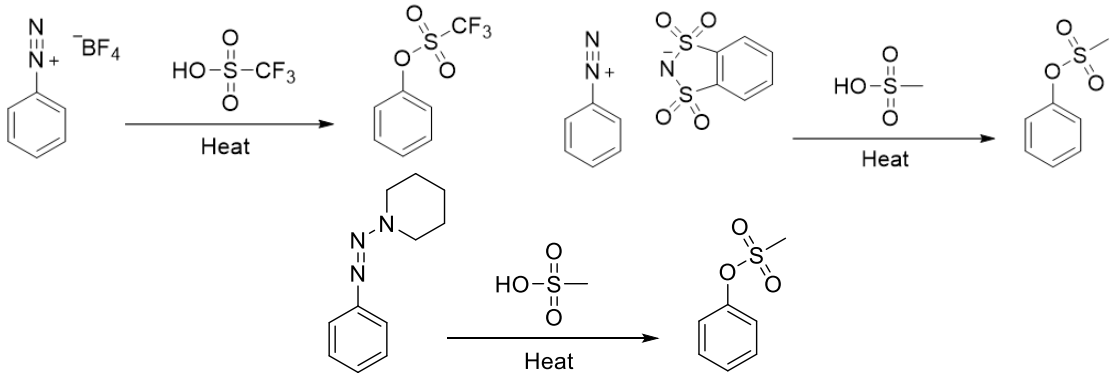

Figure 99: Known examples of the solvolysis of diazonium species in sulfonic acids.

Repeating the decomposition of nitrosamide (1) in benzene containing 1 mL of methanesulfonic acid yielded 2,6-dimethylphenyl methanesulfonate in 68% yield with the remaining 32% being the starting amide, indicating that denitrosation had occurred during the course of the reaction (Figure 100). This is not totally surprising as the denitrosation of

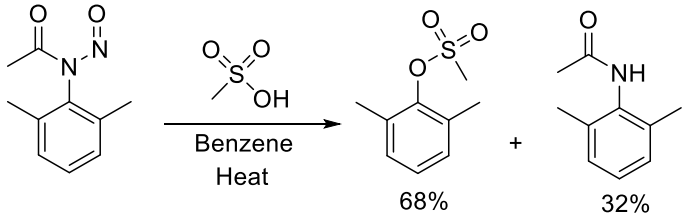

Figure 100: Reaction of nitrosamide (1a) with methanesulfonic acid in benzene.

nitrosamides when under acidic or basic conditions has been reported in the literature. In order to further probe the nature of this reaction, and its dependence of solvent dielectric constant as well as solvent nucleophilicity, the decomposition of N-(2,6-dimethylphenyl)-N-nitrosoacetamide in 25 mL of ethanol with 1.5 molar equivalents of methanesulfonic acid was carried out. NMR analysis showed that a 50/50 ratio of the aryl ether to the aryl mesylate was formed. These results indicate that formation of the aryl mesylate occurs regardless of solvent dielectric constant. In the case of decompositions in solvents with high dielectric constants and stoichiometric amounts of acid, competition between the reactive solvent and the conjugate base can occur. The decomposition of other stable nitrosamides in *tert*-butanol with excess acid yielded the corresponding methanesulfonates (Table 11).[95,99] Repeated decomposition of

Table 11: Solvolysis of kinetically stable nitrosamides in *tert*-butanol in the presence of excess methane sulfonic acid.

Nitrosamide		Product	Yield
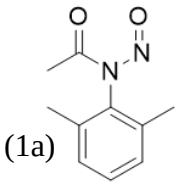 (1a)	(24)	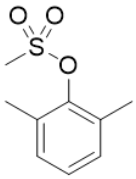	>98%
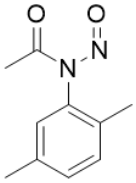 (4a)	(25)	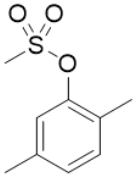	82%

N-(2,6-dimethylphenyl)-N-nitrosoacetamide in *tert*-butanol with 1.5 molar equivalents of *p*-toluenesulfonic acid yielded 2,6-dimethylphenyl 4-methylbenzenesulfonate as the major product, with no detectable amount of the aryl ether or indazole (Figure 101).[100] These findings led to a

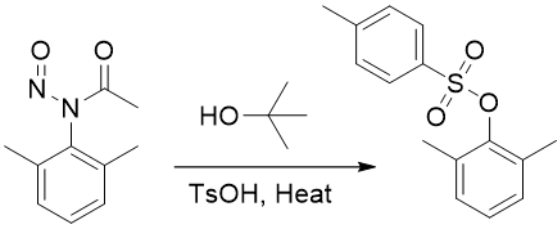

(26)

Figure 101: Conversion of N-(2,6-dimethylphenyl)-N-nitrosoacetamide to 2,6-dimethylphenyl 4-methylbenzenesulfonate.

proposed mechanism for the addition of sulfonic acids (Figure 102). Protonation of the nitrosamide leads to the formation of the protonated phenyl diazoester, which in its protonated state, results in the full heterolytic cleavage of the phenyl diazoester leading to the formation of the aryl cation rather than the diazonium mesylate salt. This hypothesized behavior helps to explain the differences observed between the nitrosamide systems and arenediazonium tosylates.

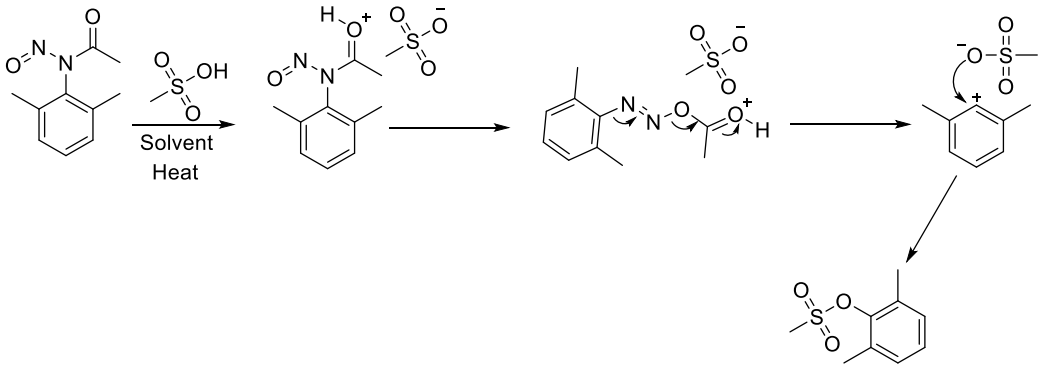

Figure 102: Proposed mechanism of solvolysis in the presence of sulfonic acids.

The success of this reaction demonstrates that sulfonate formation is not simply limited to methanesulfonic acid, and that potentially a wide variety of organic sulfonates can be accessed in this manner with relative ease and high yield. Given the demonstrated reaction efficiency and scope of these nitrosamide sulfonic acid reactions, this chemistry could prove to be very useful as aryl sulfonates have applications in both synthetic organic chemistry as reagents for palladium couplings, and in medicinal chemistry as potential anti-fungal chemicals.[100]

3.4 Reaction of Stable N-Aromatic Nitrosamides with Nitriles

The now evident relationship between nitrosamide reactivity and solvent dielectric constant led to the exploration of reacting nitrosamides with different nitriles, which possess high dielectric constants as well as moderate nucleophilicity. Examination of the literature showed that while reactions with N-aromatic nitrosamides were seemingly unknown, reactions of nitriles with diazonium salts in the presence of acetate salts could be used to produce both symmetric and asymmetric imides in good to excellent yields as was demonstrated by Kikukawa and co-workers (Figure 103).[101]

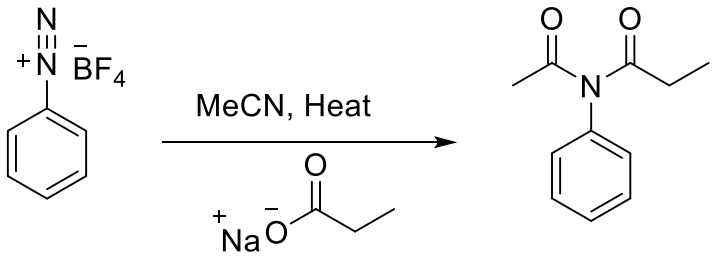

Figure 103: Synthesis of imides from diazonium salts.[101]

The degree to which this reaction was studied was limited to due to the small substrate scope that was used, as well as the limited selection of nitriles that was used.[101] Kikukawa and co-workers proposed a mechanism for this reaction, where the diazonium decomposed heterolytically to form the aryl carbocation, which can then be attacked by the surrounding solvent, resulting in the formation of a nitrilium species that can then be attacked by the excess acetate which leads to the observed imide (Figure 104) (Table 12). Initial investigations, based on the work by Kikukawa

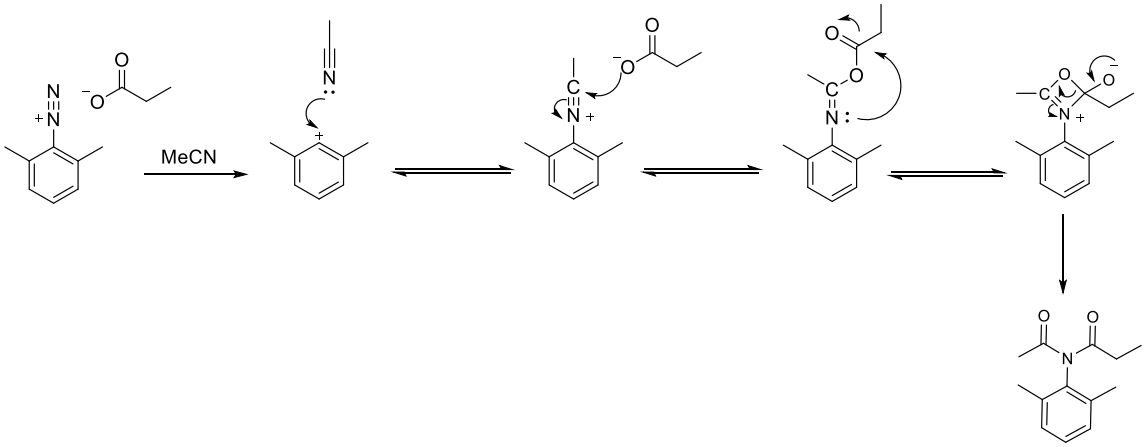

Figure 104: Mechanism of imide formation proposed by Kikukawa and co-workers.[101]

and co-workers, were carried out by decomposition of nitrosamide (1) in acetonitrile under standard reaction conditions. Reaction workup by evaporation, under reduced pressure, gave a white crystalline solid which was found to be N-acetyl-N-(2,6-dimethylphenyl)acetamide in 94% yield (Figure 105). A variety of different nitriles with the nitrosamide substrates were investigated, reactions with acetonitrile, benzonitrile and acrylonitrile all yielded the desired imides with moderate to excellent yields (Table 13). In the case of reactions with benzonitrile, reaction products

Table 12: Imides synthesized by Kikukawa and co-workers from the corresponding diazonium salts.[101]

Diazonium salt	Imide	Yield
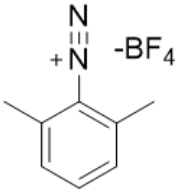	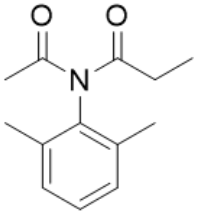	78%
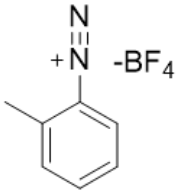	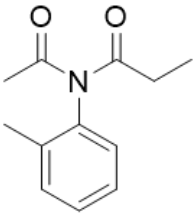	71%
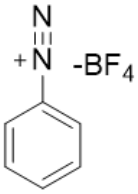	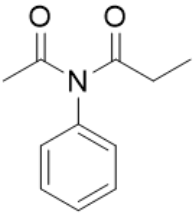	54%

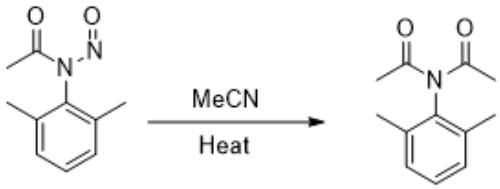

Figure 105: Formation of N-acetyl-N-(2,6-dimethylphenyl)acetamide by solvolysis of N-(2,6-dimethylphenyl)-N-nitrosoacetamide in acetonitrile.

were isolated and purified by column chromatography using dichloromethane as the mobile phase and products were characterized by NMR spectroscopy. In the case of reactions with acrylonitrile,

Table 13: Solvolysis of of 2,6 and 2,5-substituted nitrosamides in acetonitrile, benzonitrile and acrylonitrile.

Nitrosamide		Imide	Yield
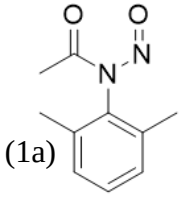 (1a)	(27)	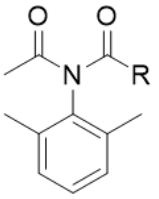	28 a R= CH3 (94%), 28 b R=Ph (68%), 28 c R=CHCH2 (89%)
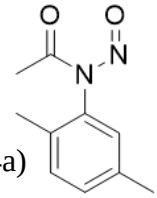 (4a)	(28)	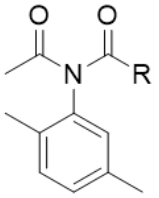	29 aR= CH3 (94%), 29 b R=Ph (64%), 29 c R=CHCH2 (86%)
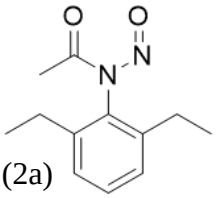 (2a)	(29)	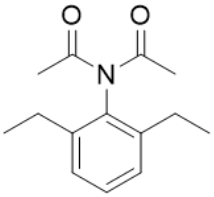	94%

polyacrylonitrile was produced as a byproduct of the reaction. Reaction work up and purification was carried out by first filtering the reaction mixture to remove the insoluble polymer. The resulting crude product mixture was dried and triturated with ether to give the corresponding imide (Figure 106). Seemingly the decomposition of nitrosamides in nitriles goes through the same

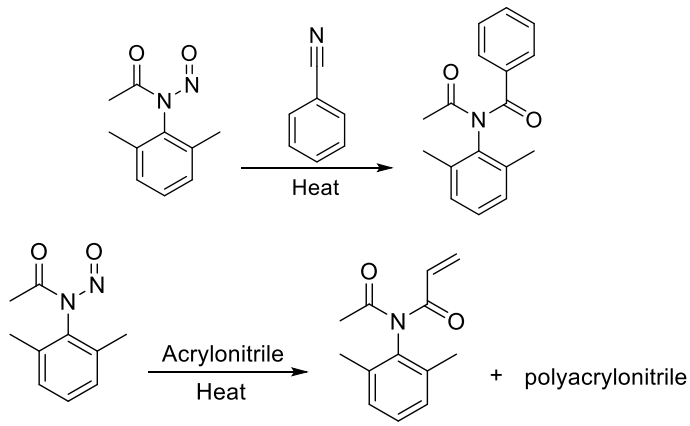

Figure 106: Products obtained from the reaction of nitrosamide (1) in benzonitrile and acrylonitrile. The same reaction byproducts are obtained from reactions with nitrosamide (4).

mechanistic process that is proposed for the decomposition of diazonium salts in nitriles (Figure 107) .[101]

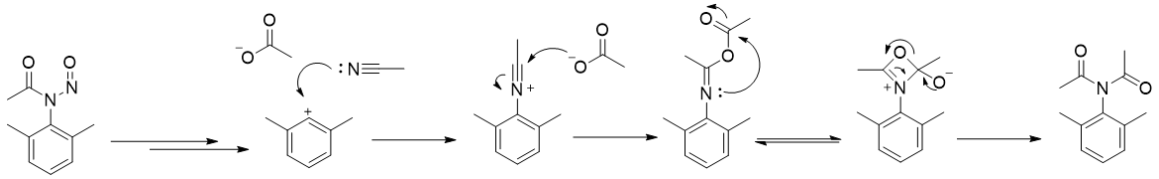

Figure 107: Mechanism of the solvolysis of nitrosamides in acetonitrile based on the mechanism proposed by Kikukawa and co-workers.[101]

Attempts to react butyronitrile, which has a dielectric constant above 30, with N-(2,6-dimethylphenyl)-N-nitrosoacetamide resulted in competitive cyclization resulting in a mixture of the corresponding indazole and imide, with the indazole being the major product. Attempts to perform the same reaction using propionitrile resulted in a complex mixture containing the indazole as the major product with none of the desired imide. In the case of nitrosamide (5), reactions with propionitrile yielded N-acetyl-N-(2-(*tert*-butyl)phenyl)propionamide (Figure 108). In the particular case of N-(2-(*tert*-butyl)phenyl)-N-nitrosoacetamide the formation of the imide is

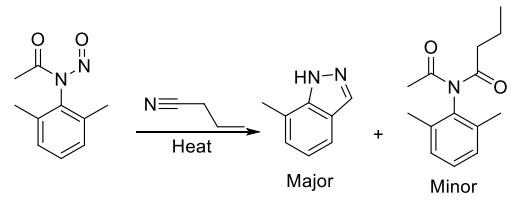

(30)

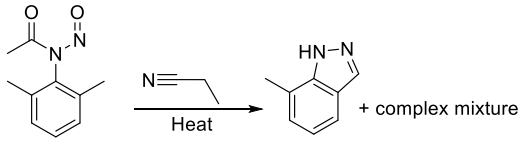

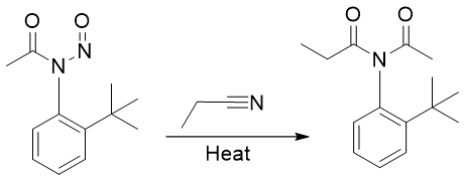

(31)

Figure 108: Formation of N-acetyl-N-(2-(*tert*-butyl)phenyl)propionamide due to the lack of a benzylic position.

able to occur due to the lack of a removable benzylic proton. Interestingly no *otho-meta* product distribution was observed for the reaction with nitrosamide (5) indicating that the nitrile simply adds to the ring. Attempts to perform similar reactions with nitrosamide (4) using butyronitrile and *iso*-butyronitrile resulted in a mixture of products with the indazole being the major product in each instance, with none of the desired imide being detected in either reaction (Figure 109). The

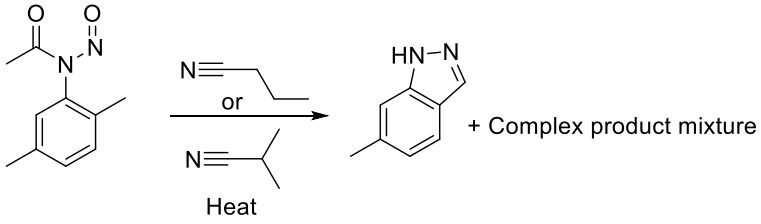

Figure 109: Decomposition of N-(2,5-dimethylphenyl)-N-nitrosoacetamide in alkyl nitriles, yielding the corresponding indazole and complex product mixtures. In all cases none of the expected imide was detected.

observed reaction behavior is not unprecedented. The work performed by Kikukawa and co-workers on the decomposition of diazonium salts in various higher nitriles demonstrated very similar behavior, in which reactions with benzonitrile, and acrylonitrile yielded the desired imides, but reactions with propiononitrile or other alkyl nitriles did not yield any of the desired imide, but

instead yielded complex product mixtures which Kikukawa and co-workers did not separate for further analysis (Figure 110).[101]

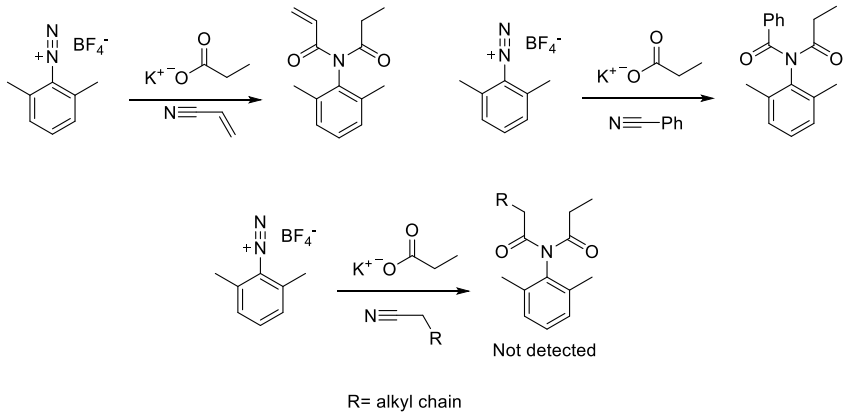

Figure 110: Results of the work performed by Kikukawa and co-workers, in which diazonium salts were decomposed in the presence of various nitriles and potassium acetates to yield aryl imides. In reactions with alkyl nitriles, Kikukawa and co-workers reported that the expected imide formation did not occur.[101]

The observed reaction behavior suggests that in the case of reactions with nitriles, the dielectric constant of the solvent is not the only factor determining N-aromatic nitrosamide reactivity. In the case of reactions with acetonitrile, which has a dielectric constant of 37.5, the fact that indazole formation is not observed in any of the methylated substrates suggests that the reaction goes through the proposed mechanism in Figure 107. In the case of the higher nitriles a possible mechanism that explains this reaction behavior is proposed in (Figure 111), which invokes

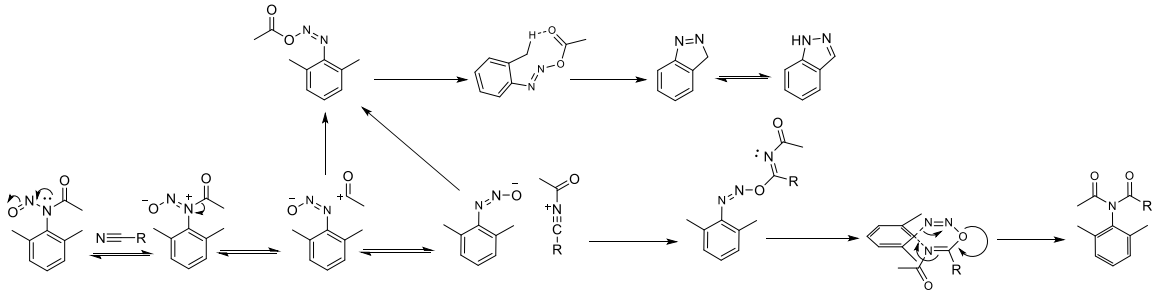

Figure 111: Proposed mechanism of N-aromatic nitrosamide decomposition in higher nitriles resulting in either imide formation or indazole formation.

the acyl migration behavior demonstrated by Suschitzky and co-workers (Figure 12).[13] In the proposed mechanism nitrosamide rearrangement occurs through an acyl migration rather than a four membered ring intermediate.[13] This process can result in the formation of the standard phenyldiazoacetate, or can instead result in the acylation of the nitrile solvent, activating the nitrile towards nucleophilic attack by the oxy diazo species which can either attack that acyl group, resulting in the formation of the phenyldiazoacetate, or the carbon of the nitrilium ion resulting in the formation of a diazo carboximidate which can then undergo a rearrangement in a manner similar to the known chapman rearrangement, resulting the elimination of N_2 gas the formation of the asymmetric imide product, while any formed phenyldiazoacetate can go on to from the corresponding indazole. As phenydiazoacetate formation can occur by two reaction pathways in the proposed mechanism, the formation of acyl nitrilium ion must be fairly favorable and addition to the carbon of the nitrilium must be fast in order to make imide formation the dominant reaction pathway. This proposed behavior is further supported by the reported donor number trends for nitrile solvents. In considering the donor number values of the used nitrile solvents, one would expect imide formation to improve when moving to larger alkyl chain nitriles, as their donor number is higher than that of acetonitrile. When moving to benzonitrile one would expect imide formation to suffer due to the lowering donor number when compared to acetonitrile. The fact that the opposite trend is what is observed suggests that in these reactions the nitrile solvent is not acting in a nucleophilic manner, but in an electrophilic manner.

In considering the nitriles used, benzonitrile and acrylonitrile both possess the ability to stabilize the positive charge of the nitrilium ion, making its formation more favorable. However, in the cases of the alkyl nitriles no resonance is available to assist in the stabilization of the formed nitrilium intermediate, making the formation of the phenyldiazoacetate, and thus indazole

formation, the dominant reaction pathway. The lack of nucleophilic displacement of the phenyldiazoacetate by the higher nitriles in this proposed mechanism can be rationalized by the lower dielectric constants of the examined higher nitriles, in conjunction with the fact that nitriles are weak nucleophiles making displacement a slow process relative to the formation of the indazole.

3.5 Reaction of Stable N-Aromatic Nitrosamides with Nitrobenzene

Reactions of the stable N-aromatic nitrosamides in high dielectric constant solvents suggested that a reactive cationic intermediate was being generated rather than a radical intermediate, which would then go on to rapidly react with the solvent environment. Based on these observed results it was determined that the behavior of stable N-aromatic nitrosamides in nitrobenzene should be probed, the reasoning behind this was three-fold. As nitrobenzene possesses a relatively large dielectric constant of 34.8, heating of stable N-aromatic nitrosamides in nitrobenzene should result in the formation of a carbocationic species. Given the electron poor nature of nitrobenzene, reactions between the nitrobenzene solvent and the carbocationic species should be disfavored. If radical intermediates are being formed during these reactions they would be able to react with nitrobenzene to make substituted biphenyls, as was reported by Grieve and Hey in the 1930's.[3] These experiments would allow for the direct testing of whether or not radical intermediates are being generated from the decomposition of these stable N-aromatic nitrosamides and in the case of a carbocationic intermediate being the dominate species formed would potentially demonstrate that nitrobenzene could serve as an inert solvent system for these reactions, allowing for better reaction control and potentially stoichiometric reactions to be performed with these stable N-aromatic nitrosamides.

Initial experiments were carried out by dissolving 35 mg of nitrosamide (1) in 15 mL of nitrobenzene. The reaction mixture was heated to 80 °C with stirring, the temperature and stirring were maintained over a two-hour period. During the course of the reaction the color of the reaction mixture transitioned from a bright yellow to a deep orange red color. After two hours the reaction mixture was allowed to cool. Workup by evaporation yielded a deep orange-red solid which was readily soluble in all common organic solvents. NMR analysis of the material showed that the product was in fact 2,6-dimethyl-4-(oxidophenylimino)-2,5-cyclohexadien-1-one (Figure 112).[102]

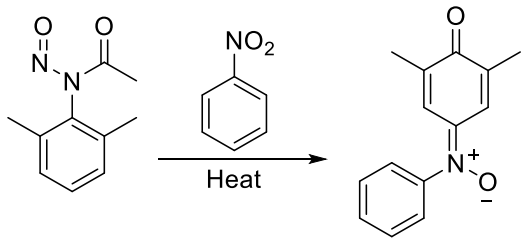

(32)

Figure 112: Formation of 2,6-dimethyl-4-(oxidophenylimino)-2,5-cyclohexadien-1-one from the decomposition of N-(2,6-dimethylphenyl)-N-nitrosoacetamide in nitrobenzene.

The results of this reaction were surprising, as the yield of the reaction was determined to be 85 % based on the weight of the recrystallized product relative to the weight of the starting amide. Analysis of the crude reaction product before recrystallization showed no other side products or byproducts, with the only observed impurity being residual nitrobenzene. Analysis of the literature showed that the 2,6-dimethyl-4-(oxidophenylimino)-2,5-cyclohexadien-1-one itself was a known compound. Examination of the reported syntheses for the compound showed that the compound was made by a condensation between the corresponding quinone and aniline followed by an oxidation to give the nitrone (Figure 113).[102] These findings indicate that the reaction reported in this work represents a new reaction in the area of N-aromatic nitrosamide chemistry.

A mechanism was proposed in order to explain how the observed product could form so efficiently under high dielectric constant conditions (Figure 114). In the proposed mechanism it

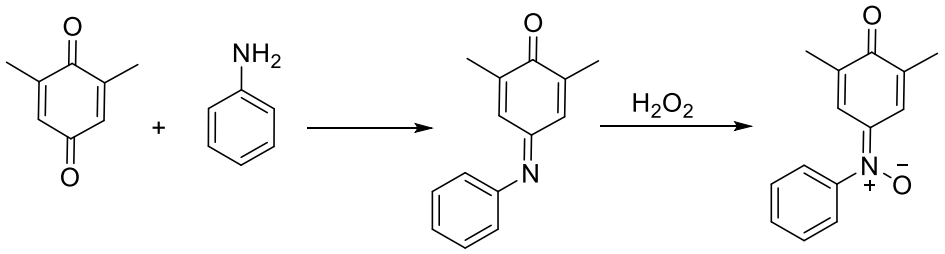

Figure 113: Reported synthesis for 2,6-dimethyl-4-(oxidophenylimino)-2,5-cyclohexadien-1-one.

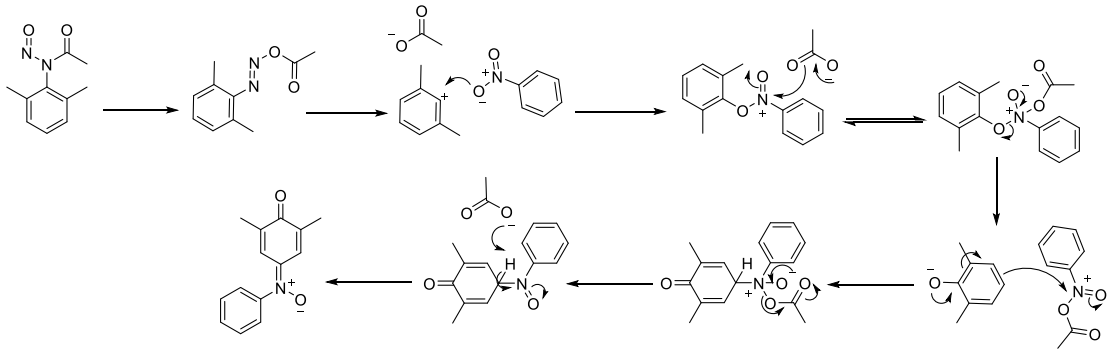

Figure 114: Proposed mechanism of the formation of 2,6-dimethyl-4-(oxidophenylimino)-2,5-cyclohexadien-1-one form the decomposition of N-(2,6-dimethylphenyl)-N-nitrosoacetamide in nitrobenzene.

was assumed that the rearrangement and decomposition of the N-aromatic nitrosamide would occur as normal to give the aryl carbocation. It is proposed that the generated aryl carbocation can undergo nucleophilic attack from one of the oxygens of the nitrobenzene, yielding a nitrobenzene complex which can undergo nucleophilic attack by the acetate anion generated from the nitrosamide decomposition. The resulting tetrahedral intermediate can collapse to give the 2,6-dimethylphenoxide and the N-acetoxy-nitrosobenzene cation. The electron density of the phenoxide makes the *para* position of the aromatic ring a sufficiently nucleophilic enough to attack the acetylated nitroso benzene at the nitrogen resulting in dearomatization of the ring. The resulting tetrahedral intermediate can then collapse, eliminating an acetate ion which then acts as a proton sink allowing for the formation of the observed product.

The results of this reaction strongly support the supposition that the stable nitrosamides reported in this work decompose through carbocationic intermediates when in high dielectric constant solvents with little to no radical activity being present during the course of the reaction.

3.6 Formation of Indazoles via N-aromatic Nitrosamides

One of the more well-known reactions that was observed under various conditions during these studies was the formation of indazoles.[9,103,104] While this reaction is well reported in the literature, the reaction conditions under which it can be performed typically are limited by the need to form and decompose the corresponding nitrosamide or diazonium salt *in-situ*.[4,9] As the reported nitrosamides here can be easily isolated, dried, and extensively purified optimal reaction conditions for the formation of indazoles from the 2,6 and 2,5 nitrosamide systems were investigated. Reactions in toluene, benzene, and CCl_4 all gave excellent yields of the corresponding indazoles, with benzene giving the best conversions for all of the examined nitrosamides. The results of the 2,6 and 2,5-indazole conversions are presented in (Table 14).[103]

Table 14: Dielectric constant controlled cyclization of 2,5 and 2,6 nitrosamides.[103]

Nitrosamide		Aryl Ether	Yield
(1a) 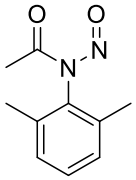	(33)	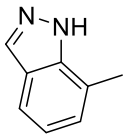	>98% Lit: 85%
(4a) 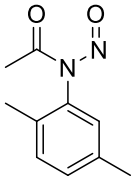	(34)	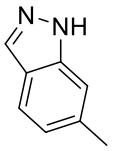	96% Lit: 85%
(2a) 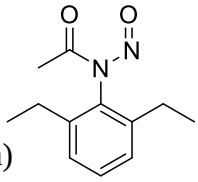	(35)	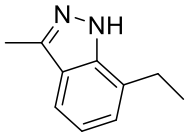	>98%

While the formation of indazoles using diazonium/nitroso chemistry is well documented, the mechanism by which this formation happens is still not fully understood.[93] Initial investigations sought to demonstrate that a radical process could be responsible for the formation of the indazole. Bartsch and co-workers reported the synthesis of a number of indazoles using diazonium salts in conjunction with potassium acetate and 18-crown-6 ether in chloroform. In an effort to demonstrate that radicals were present in the reaction, Bartsch and co-workers ran the corresponding reactions in the presence of 1,1-diphenylethylene which would act as a radical scavenger.[105] No change in the yield of the indazole product was observed, suggesting that radicals were not involved in the reaction, and that the process was most likely ionic in nature (Figure 115).[105] This claim is further supported by the work performed by Suschitzky who used fluorine labeling experiments to demonstrate that N-aromatic nitrosamide reactions which give rise to indazole formation most likely proceed through an ionic pathway as well (Figure 116).[13]

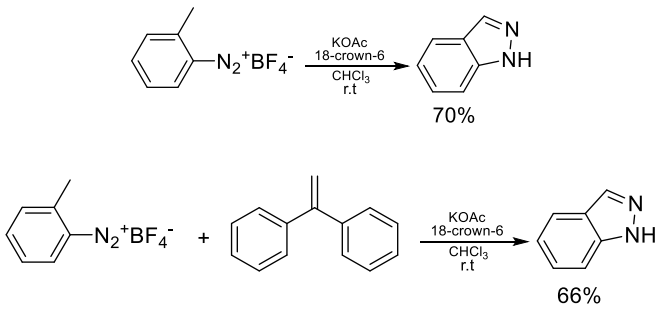

Figure 115 : Synthesis of indazoles from diazonium salts reported by Bartsch and co-workers, who found no significant change in reaction yield upon the addition of radical scavenges, suggesting that radical intermediates were not involved in indazole formation.[105]

Suschitzky showed that upon decomposing N-(4-fluoro-2-methylphenyl)-N-nitrosobenzamide in benzene, 5-fluoro-1H-indazole and 1H-indazol-5-yl benzoate were formed in approximately equal amounts.[13] The formation of 1H-indazol-5-yl benzoate can occur through the dissociation of the

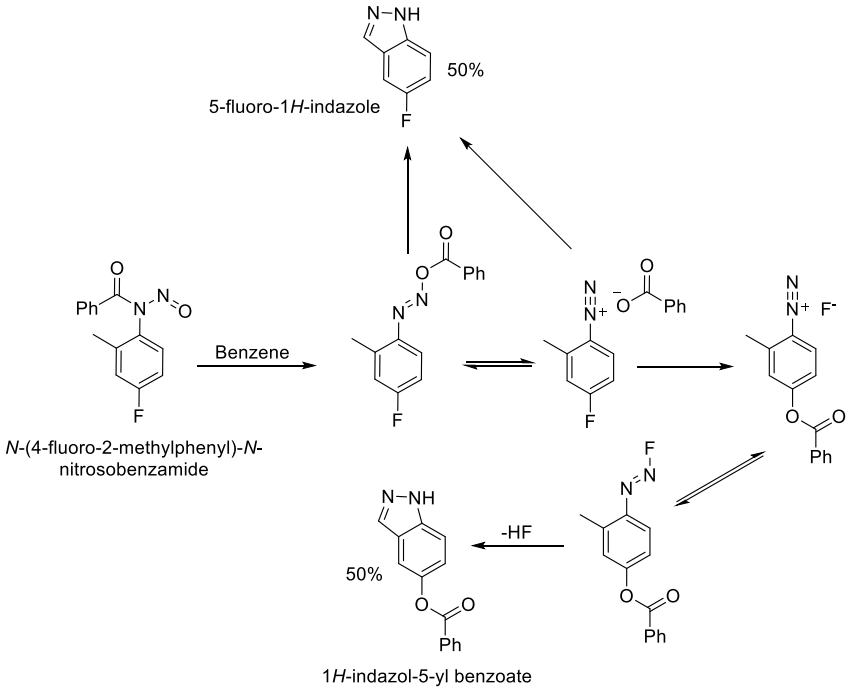

Figure 116: Fluorine labeling studies by Suschitzky suggesting that indazole formation occurs through either an ionic or concerted process.[13]

phenyldiazoacetate intermediate, resulting in the formation of the acetate anion, which can then readily displace the fluorine from the aromatic ring, resulting in the formation of the aryl ester. The resulting diazonium fluoride salt can then go on to form the observed 1H-indazol-5-yl

benzoate resulting in the formation of HF as a byproduct. These works strongly support the idea that indazole formation from N-aromatic nitrosamides does not go through a radical mechanism.[13,105] What remains unclear is whether or not these processes go through an ionic mechanism, a concerted mechanism or a mixture of both. In considering these possible pathways, all of which have been mentioned in the literature, it was noted that little to no discussion was given to the geometry of the transition state of the cyclization process. Examination of the two proposed mechanistic processes (Figure 117) shows that an ionic pathway seemingly leads to a

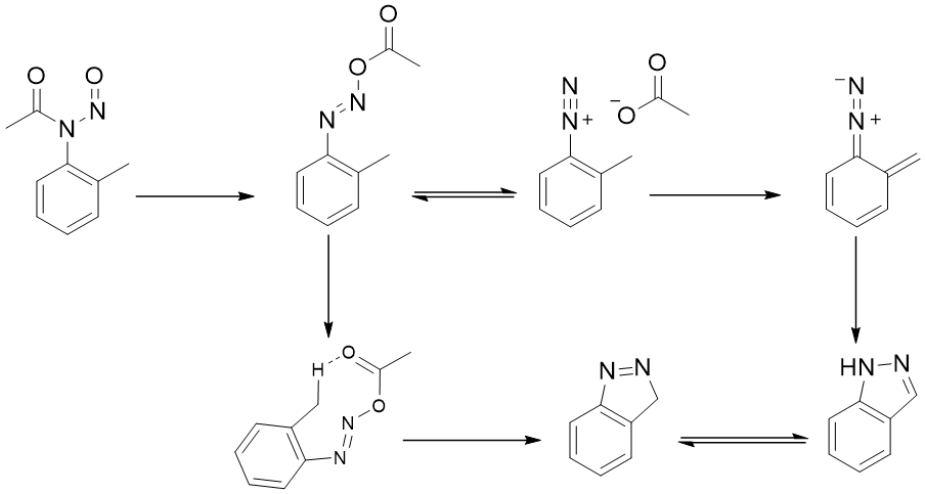

Figure 117: Proposed mechanistic pathways for the formation of indazoles, which can occur in either by an ionic or concerted pathway.

non-ideal geometry for the cyclization to occur, as the linear diazonium species lacks the proper angle to react with the methyl group of the aromatic ring, while the geometry of the phenyldiazoacetate intermediate in the E configuration could readily assume a nine membered ring transition state. This nine membered ring transition state would put the nitrogen and methyl group that must cyclize into a five membered ring geometry which can readily react during the concerted process, making this a more appealing pathway for the cyclization to the indazole. Based on these considerations, the concerted process first proposed by Huigsen appears to be the best explanation for the formation of these indazole species, although an ionic process is still not ruled out.[7]

While it is unlikely that a radical process is responsible for indazole formation in the 2,6-nitrosamide systems, radical behavior could help explain indazole formation from nitrosamide (4) under certain conditions, especially in regard to nitrosamide (4)'s preference to form its corresponding indazole in acetic anhydride, rather than the expected aryl ester (Figure 118). In the

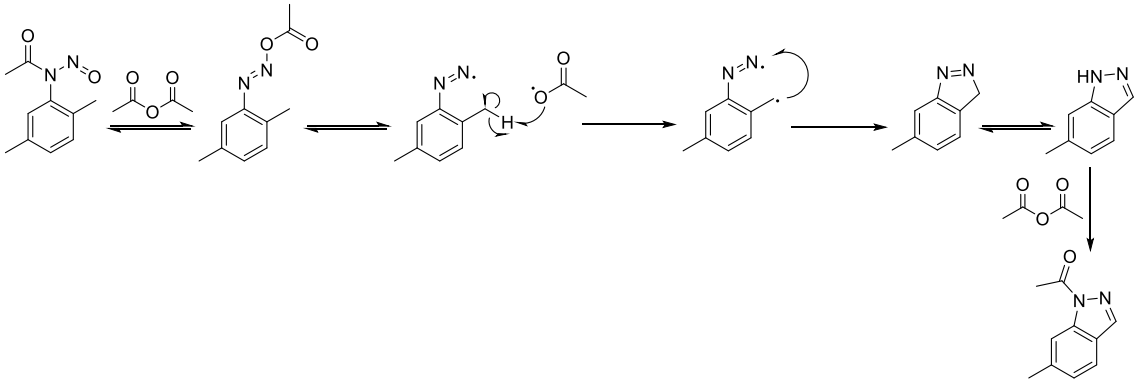

Figure 118: Proposed radical pathway for indazole formation in the case of nitrosamide (4) decomposition in acetic anhydride.

radical process proposed in this work, homolytic cleavage of the phenydiazoacetate can result in the formation of a diazo radical in a fashion, similar to what was proposed by Cadogan after their experimental detection of the diazo radical in benzene. In the case of the diazo radical, acetic anhydride can act as an inert solvent allowing for the formed acetoxy radical to carry out a radical hydrogen abstraction of the adjacent methyl group resulting in the formation of a benzyl radical which can than readily react with the radical diazo which is no longer confined to a liner geometry. The formed indazole can then react with the surrounding acetic anhydride giving the observed acylated indazole.

3.7 Conclusions and Future Work

It has been demonstrated that kinetically stable nitrosamides can be used to synthesize a diverse group of functionalized aromatic compounds in high yields. This work also clearly demonstrates the role that dielectric constant plays in these reactions, as well as when exceptions to these effects are present as was observed in a number of the reactions involving nitriles. This

work has also expanded upon the understanding of the role acetate species that is generated during the decomposition of these nitrosamide systems and how the inhibition of these acetate species can be obtained under acidic conditions, allowing for other mechanistic pathways to occur, and yielding alternative products in high yields as was the case with the reaction of these nitrosamide systems with sulfonic acids.

While the work presented here demonstrates that efficient solvolysis of nitrosamides can be achieved to produce desirable products in high yields, a number of issues remain that must be addressed in order to make this nitrosamide methodology readily practical for advanced synthetic applications. As shown, nitrosamide solvolysis is generally only practically efficient when the substrate has a high dielectric constant and is used as a solvent, limiting this methodology. A method of performing these reactions in a stoichiometric, or near stoichiometric, fashion must be developed if this goal is to be realized. Based on the presented work it seems the area in which efforts should be focused is in finding an inert solvent system with a high dielectric constant which won't add to aromatic ring while still allowing homolysis of the nitrosamide to occur. Such a solvent system would effectively allow for any nucleophilic substrate to readily react with the carbocation formed by the decomposition of the nitrosamide, even at stoichiometric ratios. It is possible that these conditions can be met through the use of long chain ethers saturated with lithium salts. Ethers are often employed as solvents due to their chemical inertness. In the case of ethers such as dimethoxyethane these ethers are also capable of readily solubilizing lithium salts by chelating the lithium cations. As demonstrated in this work, the addition of lithium salts has a profound impact on nitrosamide reactivity, allowing solvolysis to occur in low dielectric constant solvents. It is proposed that salt saturated ether solutions would be the ideal medium for performing

stoichiometric reactions between nitrosamides and a desired substrate, allowing for efficient reactivity, as well as efficient work up.

These stable nitrosamides present a number of other opportunities for the field of synthetic organic chemistry. Given the stabilized nature of the nitrosamide functionality in these systems it seems evident that these systems would be ideal for exploring new areas of nitroso metal chemistry. Nitrosamine metal complexes are known, and their chemistry has been generally explored with many of these nitrosamide metal complexes displaying unique and potentially useful reaction behavior (Figure 119).[106]

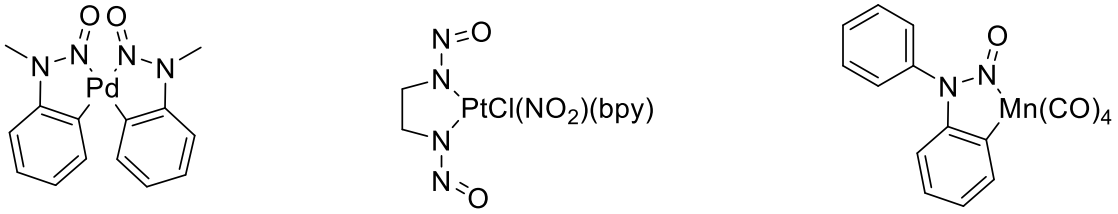

Figure 119 : Examples of known nitrosamine metal complexes.[106]

On the other hand, nitrosamide and especially N-aromatic nitrosamide metal complexes are sparsely known.[107] Those that are known have been found to be relatively stable as is the case with the reported rhenium N-nitrosocarbamate complexes reported by Bohle and co-workers (Figure 120).[107] It stands to reason that the kinetically stabilized nitrosamides developed in this work would be able to readily engage reactions with metals, potentially opening up new areas in NO chemistry and catalysis.[107]

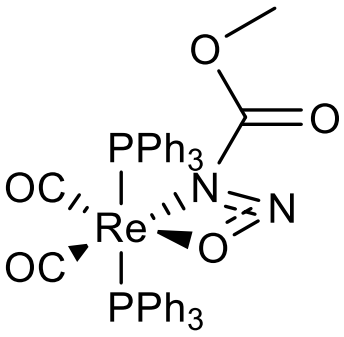

Figure 120: Recent example of a nitrosocarbamate metal complex.[107]

In continuing to explore the synthetic potential of these nitrosamide systems it is evident that more chemical systems must be explored in order to determine if nitroamides can play a significant role in the synthesis of complex molecules, especially in regard to using nitrosamides to accomplish late stage transformations in complex molecular systems. Diazonium salts have been demonstrated to be able to affect late stage transformations in complex molecules, as was demonstrated by Evans and co-workers in the total synthesis of Teicoplanin Aglycon. While impressive, the reaction to install a single chloride only proceeded with a 56% yield.[23] Based on the improved reactivity of nitrosamides relative to their diazonium counterparts, it is speculated that nitrosamides could be far more efficient at affecting such late stage transformations. Work has already been carried out within this area of interest by using nitrosamides to synthesize functionalized paracyclophanes, which will be presented in Chapter 4.

3.8 Experimental Section

General Methods:

Unless otherwise noted, all starting materials and reagents were obtained from commercial suppliers and used without further purification. All solvents were used as obtained unless noted. All reactions were performed in dried glassware under open atmosphere with magnetic stirring unless otherwise noted. Chromatography: TLC was performed using silicagel 60 F_{254} sheets from Merck and visualized under UV light. Chromatography was performed on 150 mesh neutral aluminum oxide from Sigma Aldrich. Analytical Instrumentation: IR spectra were recorded on a Thermo Scientific Nicolet 6700 FTIR spectrometer with peaks reported in cm^1. NMR spectra were recorded on a Varian VNMRS 300, 400, and 500 MHz NMR spectrometers. Chemical shifts are expressed in ppm relative to solvent signals. NMR spectra were processed using Mnova (www.mestrelab.com/software/mnova-nmr). Nomenclature: IUPAC nomenclature was used to name each compound. Compounds reported in the literature that lack spectral data are marked with an (*). Compounds not reported in the literature are marked with an (**). Coupling constants are reported for compounds not reported in the literature.

General Procedure for the Solvolysis of N-Aromatic Nitrosamides in water

The desired nitrosamide (0.2-0.3 mmol) was dissolved in 5 mL of acetone. The solution was then added to a flask containing 30 mL of water. The mixture was stirred magnetically while being heated to 80 °C. The temperature was maintained for 2 hrs. Over the course of the reaction the reaction transitioned from bright yellow to clear, which indicated that the reaction was finished. In situations where the mixture turned red or orange during heating the desired product was obtained in low yields or was not obtained at all. The mixture was allowed to cool to room

temperature and was extracted with 2-3x with dichloromethane. The organic fraction was dried over magnesium sulfate, then dried under reduced pressure to give the phenol as a clear or yellow liquid. The resulting crude products were then analyzed by ^{1}H-NMR. Further purification was then carried out if needed by column chromatography using a neutral alumina solid phase. Dichloromethane was employed as the mobile phase. In cases where dichloromethane gave poor separation a 50/50 mixture of hexanes and ethyl acetate was used as the mobile phase. Percent yields were based on isolated yields of the reactions. In the case of reactions that required purification percent yield was based off the isolated yield after purification. Purity was gauged by the ^{1}H-NMR spectra of the products. Products were determined to be sufficiently pure if only the desired product and residual NMR solvent peaks were observed in the ^{1}H-NMR spectrum of the product.

2,6-dimethylphenol (15a)

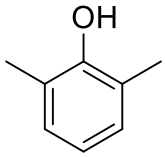

^{1}H-NMR (300 MHz, Chloroform-*d*): δ 2.24 (s, 6H, ArMe), 4.66 (bs, 1H, ArOH), 6.75 (t, 1H, ArH), 6.99 (d, 2H, ArH).

Yield: 98%

Anderson, K. W.; Ikawa, T.; Tundel, R. E.; Buchwald, S, L. The Selective Reaction of Aryl Halides with KOH: Synthesis of Phenols, Aromatic Ethers, and Benzofurans. *J. Am. Chem. Soc.* **2006**, *128*, 10694-10695.[74]

2,6-diethylphenol (16a)

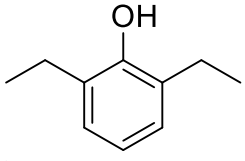

^{1}H-NMR (300 MHz, Chloroform-*d*): δ 1.23 (t, 6H, CH_3), 2.64 (q, 4H, $ArCH_2$), 4.68 (bs, 1H, ArOH), 6.84 (t, 1H, ArH), 7.01 (d, 2H, ArH).

>98%

Ieda, N.; Nakagawa, H.; Horinouchi, T.; Peng, T.; Yang, D.; Tsumoto, H.; Suzuki, T.; Fukuharad, K.; Miyata, N. Peroxynitrite generation from a NO-releasing nitrobenzene derivative in response to photoirradiation. *Chem. Commun*. **2011**, *47*, 6449–6451.[108]

Duroquinone (17a)

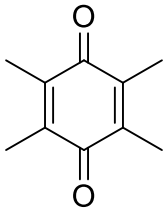

^{1}H-NMR (500 MHz, Chloroform-*d*): δ 2.02 (s, 12H, $ArCH_3$)

IR: 1637 cm^{-1}

Melting point: 110 °C

Yield: 90%

Miyamura, H.; Shiramizu, M.; Matsubara, R.; Kobayashi, S. Aerobic Oxidation of Hydroquinone Derivatives Catalyzed by Polymer-Incarcerated Platinum Catalyst. *Angew. Chem. Int. Ed*. **2008**, *47*, 8093–8095.[109]

2,5-dimethylphenol (18a)

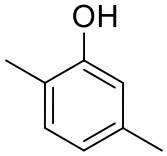

^{1}H-NMR (300 MHz, Chloroform-*d*): δ 2.19 (s, 3H, ArMe), 2.27 (s, 3H, ArMe), 6.61 (s, 1H, ArH), 6.67 (d, 1H, ArH), 7.03 (d, 1H, ArH).

Yield: 93%

Paul, R.; Ali, M. A.; Punniyamurthy, T. Copper-Catalyzed Hydroxylation of Aryl Halides with Tetrabutylammonium Hydroxide: Synthesis of Substituted Phenols and Alkyl Aryl Ethers. *Synthesis*, **2010**, *24*, 4268–4272.[110]

2-(*tert*-butyl)phenol (19a)

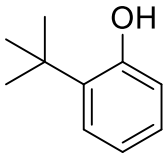

^{1}H-NMR (300 MHz, Chloroform-*d*): δ 1.41 (s, 9H, $(CH_3)_3C$), 4.90 (bs, 1H, ArOH), 6.66 (d, 1H, ArH), 6.85 (t, 1H, ArH), 7.07 (t, 1H, ArH), 7.27 (d, 1H, ArH).

Yield: 68%

Kamitori, Y.; Hojo, M.; Masuda, R.; Izumi, T.; Tsukamoto, S. Silica Gel as an Effective Catalyst for the Alkylation of Phenols and Some Heterocyclic Aromatic Compounds. *J. Org. Chem*. **1984**, *49*, 4161-4165.[111]

General Procedure for the Solvolysis of N-Aromatic Nitrosamides in Alcohols

The desired nitrosamide (0.2-0.3 mmol) was dissolved in 5 mL of the desired alcohol. The solution was then added to a flask containing 30 mL of the desired alcohol. The mixture was stirred magnetically while being heated to 70 °C. The temperature was maintained for 2 hrs. Over the course of the reaction the reaction transitioned from bright yellow to clear, which indicated that the reaction was finished. In situations where the mixture turned red or orange during heating the desired product was obtained in low yields or was not obtained at all. The mixture was allowed to cool to room temperature and was dried under reduced pressure to give the aryl ether as a light-yellow oil. The resulting crude products were then analyzed by ^{1}H-NMR. Further purification of the aryl ether was then carried out if needed by vacuum distillation or by column chromatography using a neutral alumina solid phase. Dichloromethane was employed as the mobile phase. In cases where dichloromethane gave poor separation a 50/50 mixture of hexanes and ethyl acetate was used as the mobile phase. Percent yields were based on isolated yields of the reactions. In the case of reactions that required purification percent yield was based off the isolated yield after purification. Purity was gauged by the ^{1}H-NMR spectra of the products. Products were determined

to be sufficiently pure if only the desired product and residual NMR solvent peaks were observed in the ^{1}H-NMR spectrum of the product.

2-methoxy-1,3-dimethylbenzene (15b)

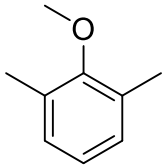

^{1}H-NMR (400 MHz, Chloroform-d) δ 7.01 (d, 2H, ArH), 6.92 (dd, 1H, ArH), 3.73 (s, 3H, OMe), 2.29 (s, 6H, ArMe).

Yield: 83%

Routasalo, T.; Helaja, J.; Kavakka, J.; Koskinen, A. M. P. Development of Bis(2-picolyl)amine–Zinc Chelates for Imidazole Receptors. Eur. J. Org. Chem. **2008**, 3190–3199.[112]

2-ethoxy-1,3-dimethylbenzene (15c)

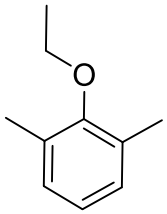

^{1}H-NMR (300 MHz, Chloroform-d) δ 7.01 (d, 2H, ArH), 6.91 (dd, 1H, ArH), 3.85 (q, 2H, OCH_2), 2.28 (s, 6H, ArMe), 1.44 (t, 3H, CH_3).

Yield: 92%

Torraca, K. E.; Huang, X.; Parrish, C. A.; Buchwald, S. L. An Efficient Intermolecular Palladium-Catalyzed Synthesis of Aryl Ethers. J. Am. Chem. Soc. **2001**, *123*, 10770–10771.[113]

2-isopropoxy-1,3-dimethylbenzene (15d)

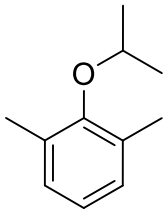

^{1}H-NMR (300 MHz, Chloroform-d) δ 7.0 (m, 2H, ArH), 6.89 (dd, 1H, ArH), 4.18 (hept, J = 6.1Hz, 1H, ArCH), 2.27 (s, 6H, ArMe), 1.29 (dd, J = 6.2 Hz, 6H, $CH(CH_3)_2$).

Yield: 85%

Miller, B.; McLaughlin, M. P.; Marhevka, V. C. Meta substitution in electrophilic benzylations of 2,6-dimethylphenol and alkyl 2,6-dimethylphenyl ethers: product distributions and mechanism. *J. Org. Chem.* **1982**, *47*, 710-719.[114]

1,3-dimethyl-2-propoxybenzene (15e)

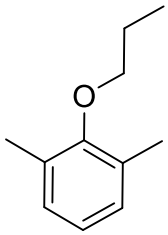

^{1}H-NMR (300 MHz, Chloroform-d) δ 6.99 (d, 2H, ArH), 6.89 (dd, 1H, ArH), 3.71 (t, 2H, OCH_2), 2.27 (s, 6H, ArMe), 1.81 (m, 2H, CH_2), 1.06 (t, 3H, CH_3).

Yield: 78%

Miller, B.; McLaughlin, M. P.; Marhevka, V. C. Meta substitution in electrophilic benzylations of 2,6-dimethylphenol and alkyl 2,6-dimethylphenyl ethers: product distributions and mechanism. *J. Org. Chem.* **1982**, *47*, 710-719.[114]

2-butoxy-1,3-dimethylbenzene (15f)

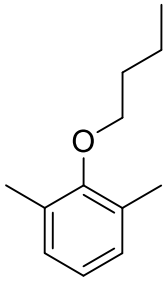

^{1}H-NMR (300 MHz, Chloroform-d) δ 7.30 – 6.73 (m, 3H, ArH), 3.82 (t, J = 7.6 Hz, 3H,OCH_2), 2.27 (s, 6H, ArMe), 1.82 (p, J = 7.7 Hz, 2H, CH_2), 1.64 – 1.36 (m, 2H, CH_2), 1.04 (t, J = 6.6 Hz, 3H, CH_3).

Yield: 75%

Torraca, K. E.; Huang, X.; Parrish, C. A.; Buchwald, S. L. An Efficient Intermolecular Palladium-Catalyzed Synthesis of Aryl Ethers. J. Am. Chem. Soc. **2001**, *123*, 10770–10771.[113]

1,3-diethyl-2-methoxybenzene (16b)

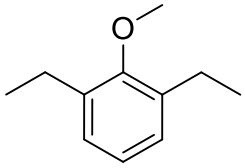

^{1}H-NMR (300 MHz, Chloroform-d) δ 7.09 (d, 1H, ArH), 6.96 (d, 2H, ArH), 3.71 (s, 3H, OMe), 2.65 (q, 4H, $ArCH_2$), 1.21 (t, 6H, CH_3).

Yield: 92%

Bates, R. B.; Siahaan, T. J.; Suvannachut, K.; Vasey, S. K.; Yager, K. M. Preparation and reactions of trianions from the dimethylphenols. *J. Org. Chem*. **1987**, *52*, 4605-4608.[115]

2-ethoxy-1,3-diethylbenzene (16c)

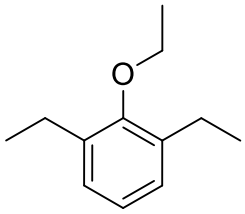

^{1}H-NMR (300 MHz, Chloroform-d) δ 7.11 – 6.98 (m, 3H, ArH), 3.85 (q, 2H, OCH_2), 2.69 (q, 4H, $ArCH_2$), 1.53 (t, 3H), 1.36 (t, 6H).

Yield: 92%

Bates, R. B.; Siahaan, T. J.; Suvannachut, K. A new rearrangement of alkoxybenzyl anions. J. Org. Chem. **1990**, *554*, 1328-1334.[116]

1,3-diethyl-2-isopropoxybenzene (16d)**

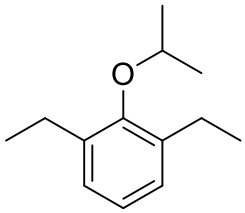

1H-NMR (300 MHz, Chloroform-d) δ 7.18 – 6.98 (m, 3H), 4.05 (hept, J = 5.7 Hz, 1H), 2.59 (q, J = 6.6, 4H), 1.36 (t, J = 5.7 Hz, 6H), 1.19 (d, J = 6.7 Hz, 6H).

Yield: 90%

1,3-diethyl-2-propoxybenzene (16e)**

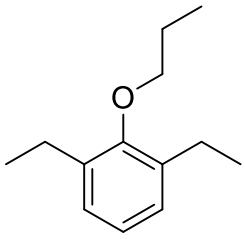

^{1}H-NMR (300 MHz, Chloroform-d) δ 7.17-6.95 (m, 3H, ArH), 3.74 (t, J=6.6Hz, 2H, OCH_2), 2.69 (q, J=7.6 Hz, 4H, $ArCH_2$), 1.85 (dtd, J=7.4, 6.5 Hz, 2H, CH_2), 1.25 (t, J=7.6 Hz, 6H, CH_3), 1.09 (t, J=7.4 Hz, 3H, CH_3).
Yield: 87%

2-butoxy-1,3-diethylbenzene (16f)**

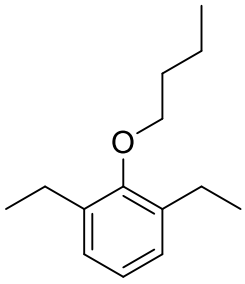

^{1}H-NMR (300 MHz, Chloroform-*d*) δ 7.14 (t, 1H, ArH), 7.05 (m, 2H, ArH), 3.76 (t, J=6.4Hz, 2H, OCH_2), 2.67 (q, *J* = 7.5Hz, 4H, $ArCH_2$), 1.80 (pent, J=7.7Hz, 2H, CH_2), 1.55 (sxt, J=7.6Hz, 2H, CH_2), 1.23 (t, J=7.3Hz, 6H, CH_3), 1.00 (t, *J* = 7.5 Hz, 3H, CH_3).

Yield: 77%

1,4-dimethoxy-2,3,5,6-tetramethylbenzene (17b)

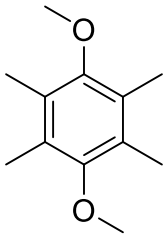

^{1}H-NMR (300 MHz, Chloroform-*d*) δ 3.65 (s, 6H, OCH_3), 2.22 (s, 12H, ArMe).

Yield: 90%

Fuchs, M.; Simeo, Y.; Ueberbacher, B. T.; Mautner, B.; Netscher, T.; Faber, K. Enantiocomplementary Chemoenzymatic Asymmetric Synthesis of (R)- and(S)-Chromanemethanol. *Eur. J. Org. Chem*. **2009**, 833–840.[117]

1,4-diethoxy-2,3,5,6-tetramethylbenzene (17c)

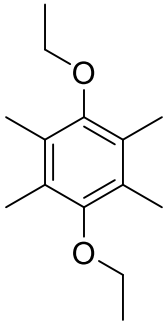

^{1}H-NMR (300 MHz, Chloroform-d) δ 3.70 (q, 4H, OCH3), 2.14 (s, 12H, ArMe), 1.40 (t, 6H, CH_3).

Yield: 90%

Rathore, R.; Kochi, J. K. Isolation of Novel Radical Cations from Hydroquinone Ethers. Conformational Transition of the Methoxy Group upon Electron Transfer. J. *Org. Chem*. **1995**, *60*, 4399-4411.[118]

1,4-diisopropoxy-2,3,5,6-tetramethylbenzene (17d)**

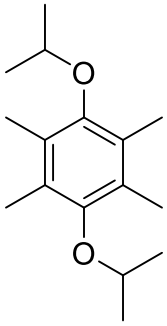

^{1}H-NMR (300 MHz, Chloroform-*d*) δ 4.01 (hept, *J* = 6.0Hz, 2H, OCH), 2.13 (s, 12H, ArMe), 1.25 (d, *J* = 6.2Hz, 12H, $CH(CH_3)_2$).

Yield: 78%

1,2,4,5-tetramethyl-3,6-dipropoxybenzene (17e)

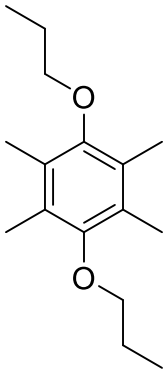

^{1}H-NMR (300 MHz, Chloroform-*d*) δ 3.61 (t, 4H, OCH_2), 2.15 (s, 12H, ArMe), 1.84 (sxt, 4H, CH_2), 1.06 (t, 6H, CH_3).

Yield: 87%

Róhrich, J.; Müllen, K. A Donor-Type Cyclophane with a Strongly Bent Tetrathiafulvalene Unit. *J. Org. Chem*. **1992**, *57*, 2374-2379.[119]

2-methoxy-1,4-dimethylbenzene (18b)

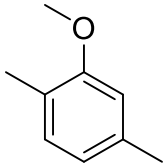

1H-NMR (300 MHz, Chloroform-d) δ 7.01 (d, 1H, ArH), 6.67 (d, 2H, ArH), 3.82 (s, 3H, OCH_3), 2.33 (s, 3H, ArMe), 2.18 (s, 3H, ArMe).

Yield: 93%

Alonso, F.; Barba, I.; Yus, M. Reactivity of 3,6-dimethoxy-3,6-dimethylcyclohexa-1,4-diene: nuclear versus benzylic nucleophilic substitution. *Tetrahedron*. **1990**, *46*, 2069-2080.[120]

2-ethoxy-1,4-dimethylbenzene (18c)

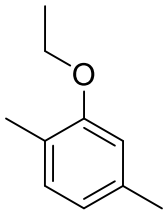

^{1}H-NMR (300 MHz, Chloroform-d) δ 7.02 (d, 1H, ArH), 6.65 (d, 2H, ArH), 4.02 (q, 2H, OCH_2), 2.31 (s, 3H, ArMe), 2.18 (s, 3H, ArMe), 1.42 (t, 3H, CH_3).

Yield: 90%
Alonso, F.; Barba, I.; Yus, M. Reactivity of 3,6-dimethoxy-3,6-dimethylcyclohexa-1,4-diene: nuclear versus benzylic nucleophilic substitution. *Tetrahedron*. **1990**, *46*, 2069-2080.[120]

2-isopropoxy-1,4-dimethylbenzene (18d)

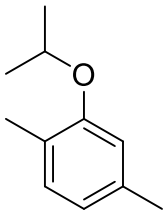

^{1}H-NMR (300 MHz, Chloroform-d) δ 6.82 (d, 3H, ArH), 4.49 (h, 1H, OCH), 2.23 (s, 3H, ArMe), 2.16 (s, 3H, ArMe), 1.32 (d, 6H, MeCH).

Yield: 48%

Alonso, F.; Barba, I.; Yus, M. Reactivity of 3,6-dimethoxy-3,6-dimethylcyclohexa-1,4-diene: nuclear versus benzylic nucleophilic substitution. *Tetrahedron*. **1990**, *46*, 2069-2080.[120]

1,4-dimethyl-2-propoxybenzene (18e)*

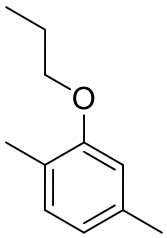

^{1}H-NMR (300 MHz, Chloroform-d) δ 7.02 (t, 1H, ArH), 6.93 (m, 2H, ArH), 3.71 (t, 2H, OCH_2), 2.29 (s, 3H, ArMe), 2.27 (s, 3H, ArMe), 1.91 – 1.78 (m, 2H), 1.25 (t, 3H, CH_3).

Yield: 54%

Stalmach, U.; Detert, H. Synthesis and Electronic Spectra of Substituted p-Distyrylbenzenes for the Use in Light-Emitting Diodes. *J. Prakt. Chem*. **2000**, 342, 10-16.

1-(*tert*-butyl)-2-methoxybenzene (19b)

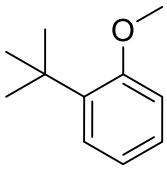

1H-NMR (300 MHz, Chloroform-d) δ 7.28 (dd, 1H, ArH), 7.19 (dt, 1H, ArH), 6.90 (t, 2H, ArH) 3.84 (s, 3H, OMe), 1.38 (s, 9H, $C(CH_3)_3$).

Yield: 90%

Kamitori, Y.; Hojo, M.; Masuda, R.; Izumi, T.; Tsukamoto, S. Silica Gel as an Effective Catalyst for the Alkylation of Phenols and Some Heterocyclic Aromatic Compounds. *J. Org. Chem*. **1984**, *49*, 4161-4165.[111]

1-(*tert*-butyl)-2-ethoxybenzene (19c)**

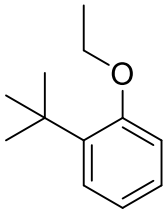

^{1}H-NMR (300 MHz, Chloroform-*d*) δ 7.28 (dd, J=7.7Hz, 1.7Hz 1H, ArH), 7.17 (td, J=7.3Hz, 1.8Hz, 1H, ArH), 6.87 (td, J=8.2Hz, 1.5Hz, 2H, ArH), 4.06 (q, *J* = 7.0 Hz, 2H, OCH_2), 1.47 (t, *J* = 6.9 Hz, 3H, CH_3), 1.39 (s, 9H, $C(CH_3)_3$).

Yield: 90%

1-(*tert*-butyl)-2-propoxybenzene (19e)**

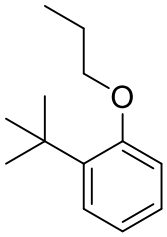

^{1}H-NMR (300 MHz, Chloroform-*d*) δ 7.28 (dd, *J*=7.7Hz, 2Hz 1H, ArH), 7.16 (td, *J*=7.7Hz, 1.7Hz, 1H, ArH), 6.88 (t, *J*=7.7, 1.2Hz, 2H, ArH), 3.95 (t, *J* = 6.4 Hz, 2H, OCH_2), 1.89 (sxt, *J*=7.4Hz, 2H, CH_2), 1.40 (s, 9H, $C(CH_3)_3$), 1.10 (t, J=7.4Hz, 3H, CH_3).

Yield: 75%

2-methoxybenzoic acid (20a)

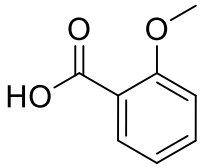

^{1}H-NMR (300 MHz, Chloroform-d) δ 8.04 (dd, 1H), 7.55 (dd, 2H), 7.44 (t,1H), 7.07 (t, 1H, ArH), 3.92 (s, 3H, OMe).

Yield: 93%

Kalinowska, M.; S´wisłocka, R.; Lewandowski, W. The spectroscopic (FT-IR, FT-Raman, UV and 1H, 13C NMR) and theoretical studies of alkali metal o-methoxybenzoates. *Journal of Molecular Structure*. **2006**, *792–793*, 130–138.[121]

2-ethoxybenzoic acid (20b)

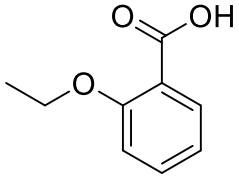

^{1}H-NMR (300 MHz, Chloroform-d) δ 8.19 (dd, 1H, ArH), 8.05 (dd, 1H, ArH), 7.80 (td, 1H, ArH), 7.43 (t, 1H, ArH), 4.38 (q, 2H, OCH2), 1.39 (t, 3H, CH3).

Yield: 95%

Perkins, M. V.; Kitching, W.; Drew, R. A.; Moore, C. J.; Konig, W. A. Chemistry of Fruit Flies: Composition of the Male Rectal Gland Secretions of some Species of South-East Asian Dacinae. Re-examination of Dacus cucurbitae (Melon Fly). *J. Chem. Soc., Perkin Trans.* **1990**, *1,* 1111-1117.[122]

General Procedure for the Solvolysis of N-Aromatic Nitrosamides In the Presence of Lithium Salts

A flask was charged with 0.185 g (4.36 mmol) of lithium chloride (lithium perchlorate was also used in the same manner) followed by 30 mL of *tert*-butanol (0.0145 M). The resulting mixture was then heated to reflux for 10 minutes or until all of the lithium chloride had dissolved, at which point the solution was allowed to cool to room temperature. The desired nitrosamide (0.2-

0.3 mmol) was dissolved in 5mL of *tert*-butanol. The solution was then added to a flask containing the *tert*-butanol lithium chloride mixture. The mixture was stirred magnetically while being heated to 80 °C. The temperature was maintained for 2 hrs. Over the course of the reaction the mixture transitioned from bright yellow to clear, which indicated that the reaction was finished. The mixture was allowed to cool to room temperature and was dried under reduced pressure to give a solid mixture of lithium chloride and the aryl ether. The crude mixture was dissolved in water and extracted with dichloromethane 2-3x. The organic layer was dried over magnesium sulfate, then dried under reduced pressure to give the *tert*-butyl ether as a yellow oil. The resulting crude products were then analyzed by ^{1}H-NMR. Further purification of the aryl ether was then carried out by column chromatography using a neutral alumina solid phase. Dichloromethane was employed as the mobile phase. In cases where dichloromethane gave poor separation a 50/50 mixture of hexanes and ethyl acetate was used as the mobile phase. Percent yields were based on isolated yields of the reactions. In the case of reactions that required purification percent yield was based off the isolated yield after purification. Purity was gauged by the ^{1}H-NMR spectra of the products. Products were determined to be sufficiently pure if only the desired product and residual NMR solvent peaks were observed in the ^{1}H-NMR spectrum of the product.

2-(*tert*-butoxy)-1,3-dimethylbenzene (21)

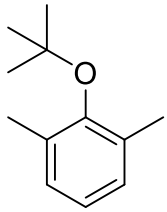

^{1}H-NMR (300 MHz, Chloroform-d) δ 6.98 (d, 2H, ArH), 6.88 (t, 1H, ArH), 2.29 (s, 6H, ArMe), 1.37 (s, 9H, $C(CH_3)_3$).

Yield: 93%

Lindstedt, E.; Stridfeldt, E.; Olofsson, B. Mild Synthesis of Sterically Congested Alkyl Aryl Ethers. *Org. Lett*. **2016**, *18*, 4234-4237.[93]

2-(*tert*-butoxy)-1,3-diethylbenzene (22)**

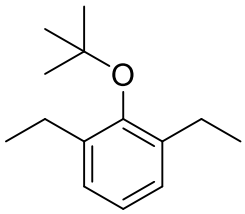

^{1}H-NMR (300 MHz, Chloroform-d) δ 7.02 – 6.96 (m, 3H, ArH), 2.71 (q, J=7.6Hz 4H, $ArCH_2$), 1.34 (s, 9H, $C(CH_3)_3$), 1.18 (t, J=7.6Hz, 6H, CH_3).

Yield: 89%

General Procedure for the Solvolysis of N-Aromatic Nitrosamides In the Presence of Sulfonic Acids

The desired nitrosamide (0.2-0.3 mmol) was dissolved in 5 mL of of *tert*-butanol. The solution was then added to a flask containing 30 mL *tert*-butanol. The mixture was stirred magnetically while 1 mL of methane sulfonic acid was added to the mixture (0.428 M sulfonic acid). The mixture was heated to 80 °C. The temperature was maintained for 2 hrs. Over the course of the reaction the mixture transitioned from bright yellow to clear, which indicated that the reaction was finished. In situations where the mixture turned red or orange during heating the desired product was obtained in low yields or was not obtained at all. The mixture was allowed to cool to room temperature and was concentrated under reduced pressure to give a yellow oil. The oil was dissolved in dichloromethane and washed three times with 10% sodium bicarbonate solution. The organic layer was dried over magnesium sulfate and dried under reduced pressure to give the desired aryl mesylate as a white crystalline solid. The resulting crude products were then analyzed by ^{1}H-NMR. If needed, further purification of the was carried out by column chromatography using a neutral alumina solid phase. Dichloromethane was employed as the mobile phase. In cases where dichloromethane gave poor separation a 50/50 mixture of hexanes and ethyl acetate was used as the mobile phase. Percent yields were based on isolated yields of the

reactions. In the case of reactions that required purification percent yield was based off the isolated yield after purification. Purity was gauged by the ^{1}H-NMR spectra of the products. Products were determined to be sufficiently pure if only the desired product and residual NMR solvent peaks were observed in the ^{1}H-NMR spectrum of the product.

2,6-dimethylphenyl methanesulfonate (24)

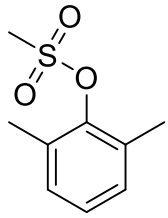

^{1}H-NMR (300 MHz, Chloroform-d) δ 7.09 (s, 3H, ArH), 3.29 (s, 3H, S-Me), 2.39 (s, 6H, ArMe).

Yield: >98%

Leowanawat, P.; Zhang, N.; Resmerita, A. M.; Rosen, B. M.; Percec, V. Ni(COD)2/PCy3 Catalyzed Cross-Coupling of Aryl and Heteroaryl Neopentylglycolboronates with Aryl and Heteroaryl Mesylates and Sulfamates in THF at Room Temperature. *J. Org. Chem.* **2011**, *76*, 9946-9955.[95]

2,5-dimethylphenyl methanesulfonate (25)

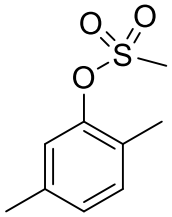

^{1}H-NMR (300 MHz, Chloroform-d) δ 7.14 (d, 1H, ArH), 7.10 (s, 1H, ArH), 7.02 (m, 1H, ArH), 3.18 (s, 3H, S-CH_3), 2.33 (s, 3H, ArMe), 2.31 (s, 3H, ArMe).

Yield: 82%

Alsabeh, P. G.; Stradiotto, M. Addressing Challenges in Palladium-Catalyzed Cross-Couplings of Aryl Mesylates: Monoarylation of Ketones and Primary Alkyl Amines. *Angew. Chem. Int. Ed.* **2013**, *52*, 7242 –7246.[123]

2,6-dimethylphenyl 4-methylbenzenesulfonate (26)

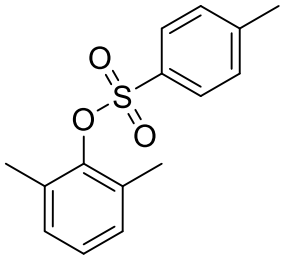

^{1}H-NMR (400 MHz, Chloroform-d) δ 7.90 – 7.79 (m, 2H, ArH), 7.41 – 7.31 (m, 2H, ArH), 7.05 – 7.01 (m, 3H, ArH), 2.47 (s, 3H, ArMe), 2.21 (s, 6H, ArMe).

Agrawal, T.; Cook, S. P. Iron-Catalyzed Cross-Coupling Reactions of Alkyl Grignards with Aryl Sulfamates and Tosylates. *Org. Lett*. **2013**, *15*, 96-99.[100]

General Procedure for the Solvolysis of N-Aromatic Nitrosamides In Nitriles

The desired nitrosamide (0.2-0.3 mmol) was dissolved in 5mL of the desired nitrile. The solution was then added to a flask containing 30 mL of the desired nitrile. The mixture was stirred magnetically while being heated to 70 °C. The temperature was maintained for 2 hrs. Over the course of the reaction the mixture transitioned from bright yellow to clear, which indicated that the reaction was finished. In situations where the mixture turned red or orange during heating the desired product was obtained in good to moderate yields or was not obtained at all. The mixture was allowed to cool to room temperature and was dried under reduced pressure to give the desired imide as a solid. The resulting crude products were then analyzed by ^{1}H-NMR. If needed, further purification of the was carried out by column chromatography using a neutral alumina solid phase. Dichloromethane was employed as the mobile phase. In cases where dichloromethane gave poor separation a 50/50 mixture of hexanes and ethyl acetate was used as the mobile phase. Percent yields were based on isolated yields of the reactions. In the case of reactions that required purification percent yield was based off the isolated yield after purification. Purity was gauged by the ^{1}H-NMR spectra of the products. Products were determined to be sufficiently pure if only the

desired product and residual NMR solvent peaks were observed in the ^{1}H-NMR spectrum of the product.

N-acetyl-N-(2,6-dimethylphenyl)acetamide (27a)

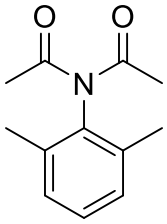

^{1}H-NMR (300 MHz, Chloroform-*d*) δ 7.13 (m, 3H, ArH), 2.22 (s, 6H, O=CCH_3), 2.11 (s, 6H, ArMe).

Yield: 94%

Ayyangar, N. J.; Srinivasan, K. V. Effect of substituents in the formation of diacetanilides. *Can. J. Chem*. **1984**, *62*, 1292-1296.[124]

N-acetyl-N-(2,6-dimethylphenyl)acrylamide (27b)

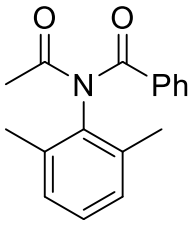

^{1}H-NMR (400 MHz, Chloroform-*d*) δ 7.60 (d, 2H, ArH), 7.45 (d, 1H, ArH), 7.35 (t, 2H, ArH), 7.13 (m, 3H, ArH), 2.25 (s, 6H, ArMe), 2.24 (s, 3H, O=CCH_3).[125]

Yield: 68%

Wang, F.; Wei, T. Q.; Xu, P.; Wang, S. Y.; Ji, S. J. Mn(III)-mediated radical cascade reaction of boronic acids with isocyanides: Synthesis of diimide derivatives. *Chinese Chemical Letters*. **2019**, *30*, 379-382.

N-acetyl-N-(2,6-dimethylphenyl)acrylamide (27c)**

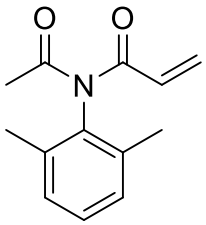

^{1}H-NMR (400 MHz, Chloroform-*d*) δ 7.14 (m, 3H, ArH), 6.48 (dd, *J* = 16.7, 1.7 Hz, 1H, CH), 6.17 (dd, *J* = 16.7, 10.3 Hz, 1H, CH), 5.66 (dd, *J* = 10.3, 1.7 Hz, 1H, CH), 2.49 (s, 3H, O=CCH_3), 2.11 (s, 6H, ArMe).

Yield: 89%

N-acetyl-N-(2,5-dimethylphenyl)acetamide (28a)*

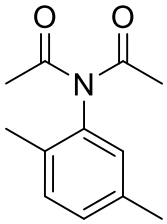

^{1}H-NMR (300 MHz, Chloroform-d) δ 7.18 (t, 2H, ArH), 6.88 (s, 1H, ArH), 2.33 (s, 3H, ArMe), 2.27 (s, 6H, O=CCH$_3$), 2.10 (s, 3H, ArMe).

Yield: 94%

Abbas, S. A.; Hickinbottom, W. J. Molecular rearrangements. Part VII. NN-diacylanilines. J. *Chem. Soc. C*, **1966**, 1305-1306.[126]

N-acetyl-N-(2,5-dimethylphenyl)benzamide (28b)**

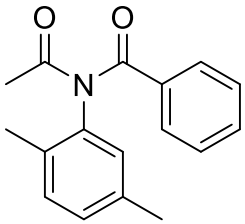

^{1}H-NMR (300 MHz, Chloroform-*d*) δ 7.83 (m, 1H, ArH), 7.54 (m, 5H, ArH), 7.06 (d, *J*=7.5Hz, 1H, ArH), 6.89 (d, *J*=7.5Hz, 1H, ArH), 2.31 (s, 3H, ArMe), 2.21 (s, 3H O=CCH$_3$,), 2.20 (s, 3H, ArMe).

Yield: 64%

N-acetyl-N-(2,5-dimethylphenyl)acrylamide (28c)**

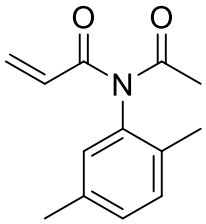

^{1}H-NMR (300 MHz, Chloroform-d) δ 7.18 (t, 2H, ArH), 6.88 (s, 1H, ArH), 6.46 (dd, J=16.8Hz, 1.8Hz, 1H, CH), 6.23 (dd, J = 16.8, 10.2 Hz, 1H, CH), 5.73 – 5.56 (dd, J=10.2Hz, 1.8Hz, 1H, CH), 2.47 (s, 3H, O=CCH$_3$), 2.32 (s, 3H, ArMe), 2.08 (s, 3H, ArMe).

Yield: 86%

N-acetyl-N-(2,6-diethylphenyl)acetamide (29)

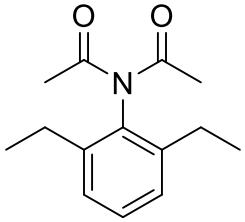

^{1}H-NMR (300 MHz, Chloroform-*d*) δ) 7.21 (dq, 2H, ArH), 7.17 – 7.06 (m, 1H, ArH) 2.55 – 2.38 (q, 4H, $ArCH_2$), 2.25 (s, 6H, $O=CCH_3$), 1.20 (t, 6H, CH_3).

Yield: 94%

Ayyangar, N. J.; Srinivasan, K. V. Effect of substituents in the formation of diacetanilides. Can. J. Chem. 1984, 62, 1292-1296.[124]

N-acetyl-N-(2,6-dimethylphenyl)butyramide (Characterized as a mixture) (30)**

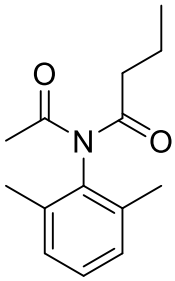

^{1}H-NMR (300 MHz, Chloroform-*d*) δ 7.14 – 7.06 (m, 3H, ArH), 2.44 – 2.35 (t, 2H, $O=CCH_2$), 2.32 (s, 3H, $O=CCH_3$), 2.12 (s, 6H, ArMe), 1.65 (h, J = 7.3 Hz, 2H, CH_2), 0.91 (t, J = 7.4 Hz, 3H, CH_3).

N-acetyl-N-(2-(*tert*-butyl)phenyl)propionamide (31)

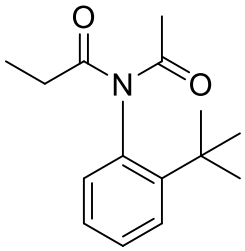

^{1}H-NMR (500 MHz, Benzene-*d*) δ: 7.28 (dd, 1H). 7.04 (ddd, 1H), 6.91 (ddd, 1H), 6.53 (dd, 1H), 2.34 (q, 2H), 2.20 (s, 3H), 1.19 (s, 9H), 1.02 (t, 3H).

Kondo, K.; Iida, T.; Fujita, H.; Suzuki, T.; Yamaguchi, K.; Murakami, Y. A Chiral Axis due to an Acyclic Imide–Ar Bond: A Study of Steric Effects of Acyl Groups on Racemization, *Tetrahedron*. **2000**, *56*, 8883-8891.[127]

Procedure for the Solvolysis of N-(2,6-dimethylphenyl)-N-nitrosoacetamide (1a) in Nitrobenzene

A flask was charged with 30 mL of nitrobenzene, followed by 0.0453 g (0.236mmol) of N-(2,6-dimethylphenyl)-N-nitrosoacetamide pre-dissolved in 5 mL of nitrobenzene, giving a homogenous solution. The reaction solution was heated to 80 °C. Upon reaching 80 °C the reaction was run for two hours, during which the reaction was followed by color change. Over the course of the reaction the reaction solution transitioned from yellow to a deep red color. Upon seeing full consumption of the N-aromatic Nitrosamide the reaction solution was concentrated under reduced pressure, giving the nitrone as a blood red crystalline solid. The resulting crude products were analyzed by ^{1}H-NMR. Further purification was then carried out by recrystallization from diethyl ether. Purity was gauged by the ^{1}H-NMR spectra of the products. Products were determined to be sufficiently pure if only the desired product and residual NMR solvent peaks were observed in the ^{1}H-NMR spectrum of the product.

3,5-dimethyl-4-oxo-N-phenylcyclohexa-2,5-dien-1-imine oxide (32)

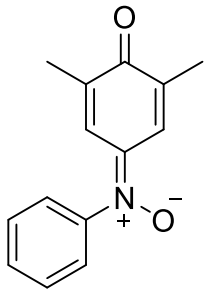

^{1}H NMR (500 MHz, Chloroform-d) δ 7.90 (dq, J=2.9, 1.4 Hz, 1H), 7.61-7.51 (m, 3H), 7.51-7.44 (m, 2H), 6.90 (dq, J= 2.8, 1.4 Hz, 1H), 2.16 (d, J=1.4 Hz, 3H), 1.96 (d, J=1.4 Hz, 3H).

^{13}C NMR (126 MHz, Chloroform-*d*) δ 186.46, 145.44, 143.13, 140.86, 134.93, 130.83, 129.44, 125.88, 124.90, 124.61, 16.83, 16.81.

Shift (ppm) multiplicity, coupling (Hz) DEPT	Proton	2D spectra shows correlation to protons at δ (ppm)		
		COSY	HSQC	HMBC
16.8(1)	1.96	6.9	1.96	6.9
16.8(3)	2.16	7.9	2.16	7.9
124.6	6.9	7.9	7.47	7.47, 7.57
124.9	7.47	-	7.9	6.9,
125.8	7.56	-	6.9	1.96, 7.90
129.4	7.57	-	7.56	2.16, 7.57
130.8	7.9	6.9	7.57	7.47
134.9	-		-	1.96
140.8	-		-	2.16
143.1	-		-	1.96, 2.16
145.4	-		-	7.47, 7.56
186.4	-		-	1.96, 2.16, 6.90, 7.9

IR: 1685 cm^{-1}, 1535 cm^{-1}

Yield: 85%

Damavandy, J.A.; Jones, R.A.Y. Cycloaddition reactions of quinoneimine N-oxides and of fluorenoneimine N-oxide: exocyclic nitrones conjugated with electron-withdrawing rings. *J. Chem. Soc., Perkin Trans. 1*. **1981**, 712-17.[102]

General Procedure for the Synthesis of Indazoles

The desired nitrosamide (methyl or ethyl groups must be present at the *ortho* position to the nitrosamide group) (0.2-0.3 mmol) was dissolved in 5 mL of benzene (toluene and carbon tetrachloride will provide the same results) and transferred to a round bottom flask containing 30 mL of benzene. The mixture was stirred magnetically while being heated to 80 °C. The temperature was maintained for 2 hrs. Over the course of the reaction the reaction transitioned from bright yellow to clear, which indicated that the reaction was finished. In situations where the mixture turned red or orange during heating the desired product was still obtained in good to excellent yields. The mixture was allowed to cool to room temperature and was dried under reduced pressure to give the desired indazole as a snow white solid. The resulting products were analyzed by 1H-NMR. In all cases the indazole was the only product and no purification steps were required. Purity

was gauged by the ^{1}H-NMR spectra of the products. Products were determined to be sufficiently pure if only the desired product and residual NMR solvent peaks were observed in the ^{1}H-NMR spectrum of the product.

7-methyl-1H-indazole (33)

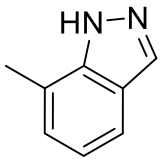

^{1}H NMR (300 MHz, Chloroform-*d*) δ 10.79 (bs, 1H, NH), 8.18 (s, 2H, N=CH), 7.63 (dd, 1H, ArH), 7.19 (dt, 1H, ArH), 7.11 (t, 1H, ArH), 2.64 (s, 3H, ArMe).
Yield: >98%

Giroud, M.; Ivkovic, J.; Martignoni, M.; Fleuti, M.; Trapp, N.; Haap, W.; Kuglstatter, A.; Benz, J.; Kuhn, B.; Schirmeister, T.; Diederich, F. Inhibition of the Cysteine Protease Human Cathepsin L by Triazine Nitriles: Amide···Heteroarene π-Stacking Interactions and Chalcogen Bonding in the S3 Pocket. *ChemMedChem*. **2017**, *12*, 257-270.[103]

6-methyl-1H-indazole (34)

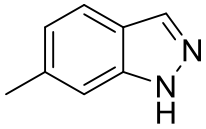

^{1}H-NMR (300 MHz, Chloroform-*d*): δ 2.49 (s, 3 H, CH3), 7.01 (d, 1 H, ArH)), 7.28 (s, 1 H, ArH), 7.64 (d, 1 H, ArH), 8.04 (s, 1 H, N=CH), 10.27 ppm (bs, 1 H, NH).

Yield: 96%

Giroud, M.; Ivkovic, J.; Martignoni, M.; Fleuti, M.; Trapp, N.; Haap, W.; Kuglstatter, A.; Benz, J.; Kuhn, B.; Schirmeister, T.; Diederich, F. Inhibition of the Cysteine Protease Human Cathepsin L by Triazine Nitriles: Amide···Heteroarene π-Stacking Interactions and Chalcogen Bonding in the S3 Pocket. *ChemMedChem*. **2017**, *12*, 257-270.[103]

7-ethyl-3-methyl-1H-indazole (35)**

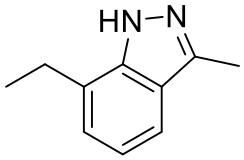

^{1}H-NMR (300 MHz, Chloroform-*d*) δ 7.53 (dd, 1H, ArH), 7.22 – 7.03 (m, J= 2H, ArH), 2.89 (q, *J*=7.7Hz, 2H, $ArCH_2$), 2.59 (s, 3H, $N=CCH_3$), 1.38 (t, *J*=7.6Hz, 3H, Me).

Yield: >98%

Chapter 4: The Application of N-Aromatic Nitrosamide Chemistry to the Functionalization of Cyclophanes

The synthesis of functionalized [2.2]paracyclophanes and their larger derivatives are targets of interest due to their unique physical properties that are brought about from the close proximity of the aromatic rings. Many cyclophane material applications have been realized ranging from using cyclophanes for energy storage and energy transport to using cyclophanes as key parts in molecular machines. The diversity of these systems has been limited by the difficulty associated synthesizing many of these systems. While there are a number of ways to access [2.2]paracyclophane systems these syntheses can become quickly complicated in cases when a desired functionality is needed. Such functionalities must generally be installed before the formation of the cyclophane which can result in decreased yields of the desired cyclophane system depending on the nature of the functional group or groups. Post-functionalization of the cyclophane is also possible but post-functionalization methods generally suffer from poor selectivity, as well as low yields, giving small amounts of isomer mixtures. For many applications this proves to be too inefficient to be useful.

In the case of larger paracyclophane systems, these issues are further compounded by the fact that forming larger ring systems is fairly difficult and generally gives very low yields of the desired product. Such problems are immediately apparent in the synthesis of [2.2.2.2]paracyclophane from *para*-di(bromomethyl)benzene. Generally, this synthesis is accomplished through the use of a Wurtz coupling which employs the use of sodium metal, or the use of a transition metal catalyst is required. In both cases the desired cyclophane is obtained in yields below 10% with the Wurtz coupling method giving a 9% yield and the catalyst method giving a yield of 2.7% (Figure 121).[128,129] Given the low yields of these products, any attempts to

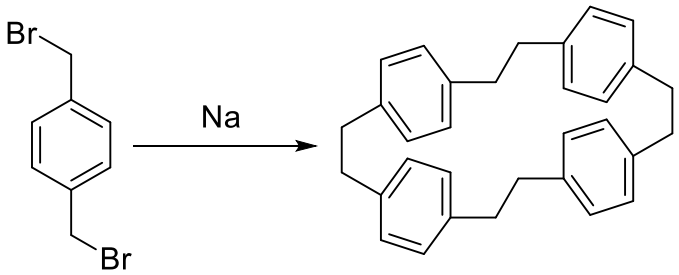

Figure 121: Fomation of [2.2.2.2]paracyclophane using Wurtz compling methods.[128,129]

post-functionalize these systems to make them suitable for chemical or material applications would be an energy intensive and highly inefficient task, to say the least.

In order to overcome the issues of inefficient cyclophane synthesis and inefficient post-functionalization, it is apparent that finding functionalized aromatic systems that naturally give specific cyclophane structures is the most promising route to making functionalized cyclophanes in yields high enough to make chemical or material applications feasible. Work by Morvant and Glatzhofer demonstrated that this was an achievable goal when they were able to successfully synthesize cyclophanes (36) and (37) (Figure 122).[38] Morvant reported a yield of 17.4% for cyclophane (36) and a yield of 14.5% for cyclophane (37). Compared to the yields usually observed for such reactions this is a significant achievement. More importantly, both cyclophanes were readily isolated and purified by simple extraction methods.[38]

(37)

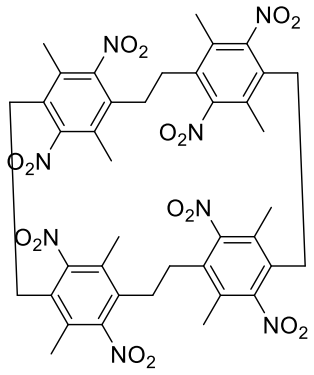

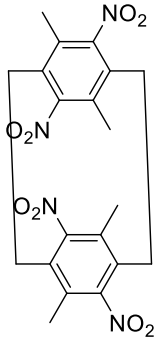

(36)

Figure 122: Nitro cyclophanes synthesized by Morvant.

The improved yields of these nitrocyclophane systems allows for the potential synthesis and characterization of various functionalized cyclophane systems. The chemical reactivity of aryl nitro groups is well known and provides a useful way of making aryl amines, which can be used to access a number of different functional groups. Beyond the presence of transformable functional groups and high yields of these cyclophanes relative to other systems, the unique steric environment of these cyclophanes makes them promising synthetic starting points for accessing other functionalized cyclophane systems by way of N-aromatic nitrosamide decomposition/solvolysis. As previously demonstrated, N-aromatic nitrosamides can be stabilized by the introduction of steric bulk at positions *ortho* to the nitrosamide functionality. Work by Glatzhofer has demonstrated that [2.2]paracyclophane scaffolds are capable of tolerating nitrosation conditions well, suggesting that the use of N-aromatic nitrosamides may be an ideal way of performing post-functionalization reactions on cyclophane scaffolds (Figure 123).[18] In

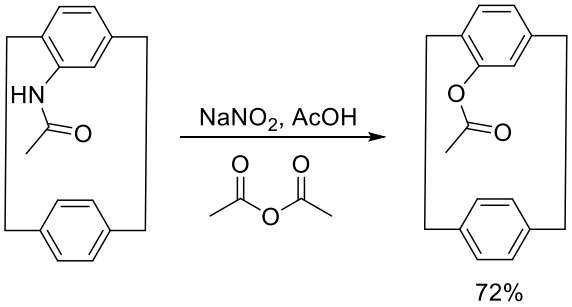

Figure 123: Example of the use of N-aromatic nitrosamides to affect late stage functionalization in cyclophane scaffolds.

cyclophanes (36) and (37) the presence of the methyl groups and cyclophane bridge heads that are both *ortho* to the nitro groups in these cyclophane systems make them potential substrates for the formation of kinetically stable N-aromatic nitrosamides, possibly allowing for the isolation of these nitroso derivatives, which can then be decomposed in a wide variety of solvents and allowing for the synthesis of a diverse array of functionalized cyclophanes.[18]

It was anticipated that reduction of these nitrosamides under acylating conditions would give the corresponding amide cyclophanes which will be able to react with $AcOH/NaNO_2$ to give kinetically stable N-aromatic nitrosamide cyclophanes. It was thought that these nitrosamide cyclophanes would possibly behave in a manner similar to their small molecule counterparts, and that by heating in a variety of solvents, a number of different functional groups could be accessed in high yield. It was further proposed that hydrolysis of these nitrosamide cyclophanes followed by spontaneous oxidation by air would allow for the formation of the corresponding cyclophane quinones in one synthetic step, eliminating the need for a subsequent oxidation reaction, the precedence for such behavior being derived from the autooxidation of hydroduroqunione.

4.1 Synthesis of *Anti*-5,8,13,16-tetramethyl-4,7,12,15-tetranitro[2.2]paracyclophane and *Anti*-5,8,13,16,21,24,29,32-octamethyl-4,7,12,15,20,23,28,31-octanitro[2.2.2.2]-paracyclophane

In order to begin these investigations, the synthesis of cyclophanes (36) and (37) was carried out using the procedure developed by Morvant (Figure 124). The required Hoffman salt was prepared

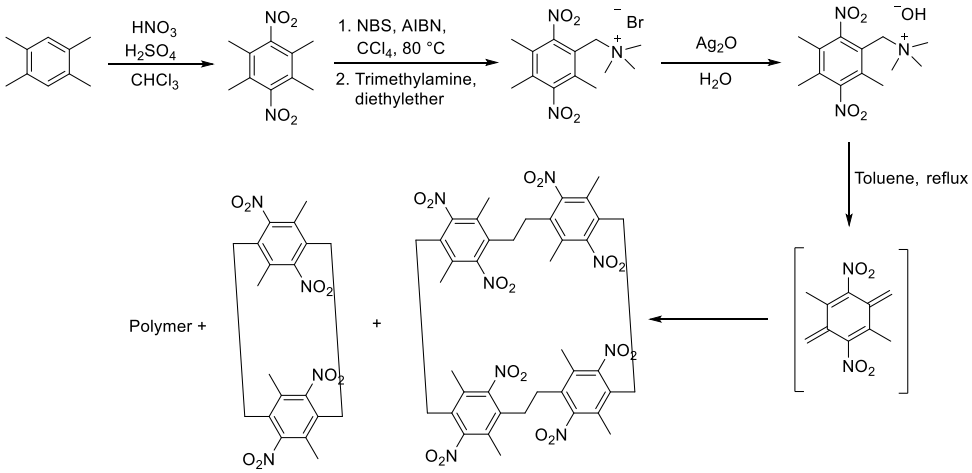

Figure 124: Synthesis of cyclophanes (36) and (37).

from the radical bromination of dinitrodurene followed by displacement with trimethylamine gas to give the trimethylammonium bromide salt, 5.00 grams of the salt was dissolved in 50 mL of water and treated with silver oxide to afford the hydroxide salt in solution. This solution was filtered and used directly by heating together with 400 mL of toluene and 60 mg of phenothiazine. Removal of water with a Dean-Stark trap gave the resulting cyclophanes, polymer, and alcohol side product. Separation and purification of the mixture gave 210 mg of cyclophane (37) and 854 mg of cyclophane (36). The improved methods reported in this work make the nitrocyclophane systems first synthesized by Morvant attractive synthetic starting points for the synthesis of other functionalized cyclophanes.

4.2. Screening Reduction Conditions for Polynitrocyclophanes

In order to explore the potential synthetic utility of nitrosamide chemistry on these cyclophane systems, proper reduction and acylating conditions were required in order to obtain the cyclophane amides. Generally, the reduction of aryl nitro groups to amines can be readily achieved using a number of methods, with catalytic hydrogenation being one of the most mild and successful methods for accomplishing this task. Previous work with dinitrodurene showed that standard catalytic hydrogenation methods were ineffective due to the steric bulk surrounding the nitro groups. As dinitrodurene is the monomeric repeat unit for both nitrocyclophanes, it was used as an analog to screen various reductive conditions in order to determine what reaction conditions would be most effective on the polynitro systems. As catalytic hydrogenation appeared to be the most desirable route to achieve the reduction of these aryl nitro groups a number of hydrogen transfer conditions were explored. It was hypothesized that the steric bulk of the methyl groups was increasing the energy needed for hydrogenation to occur and as such, a transfer hydrogenation

method that could be readily heated with no risk of fire or explosion was needed. It was quickly identified that a combination of palladium on carbon with ammonium formate in ethanol/acetic acid could readily and selectively reduce both nitro groups of dinitrodurene. Mono-reduction could be achieved by controlling the addition of the ammonium formate as well as the heat. Addition of excess ammonium formate and heating the reaction to reflux solvent gave the diamine after 2 hours. Concentrating the reaction mixture and adding acetic anhydride to the concentrate successfully gave the diamide (38) repeatably in over 80% yield (Figure 125). Attempts to carry out the reaction in acetic anhydride with acetic acid were met with failure as little to no conversion was observed.

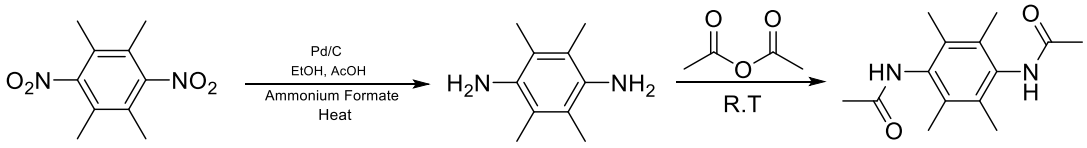

Figure 125: Reduction of dinitrodurene followed by acylation to give the diamide derivative.

Carrying these reaction conditions over to the cyclophane systems were met with failure for both cyclophane systems. While partial reduction could be achieved for both systems, attempting to obtain complete reduction seemingly resulted in hydrogenolysis of the bridges for both cyclophane systems. This was not surprising in the case of cyclophane (36), as it has been shown that palladium and platinum can ring open [2.2]paracyclophane systems due to their high strain energy. In the case of cyclophane (37), this result was surprising given that the strain energy of the system was expected to be much smaller when compared to the [2.2]paracyclophane system.

The reduction of dinitrodurene by tin chloride has been previously reported in the literature in which the reduction yields the ammonium tin salt which can be directly converted to duroquinone using iron chloride, making this method an attractive route to the cyclophane quinone systems. The reduction of dinitrodurene was carried out by suspending the dinitrodurene in a mixture of acetic acid and hydrochloric acid. An excess of tin chloride was added to the clear

solution which was heated to 90 °C for 1 hour. Upon cooling a white precipitate readily formed which was collected by filtration and dried. NMR analysis, along with solubility tests in water showed that the precipitate was the durene diammonium salt. A portion of the salt was covered in acetic anhydride and treated with 1 drop of triethyl amine. Upon addition of the triethyl amine the salt rapidly dissolved in the acetic anhydride. Concentrating the mixture under reduced pressure followed by washing with water gave amide (39). The remaining portion of the salt was dissolved in water and added to an aqueous solution of iron chloride. This rapidly gave a yellow precipitate which was collected by filtration and dried to give duroquinone in over 80 % yield (Figure 126).

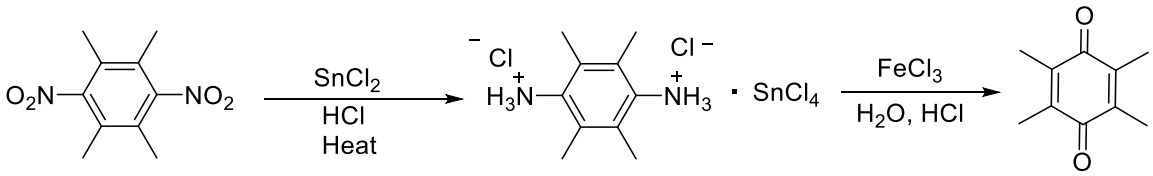

Figure 126: Reduction of dinitro durene followed by oxidation with $FeCl_3$ to give duroquinone.

Applying these same reaction conditions to both cyclophane systems successfully gave the ammonium salts of both cyclophane systems (Figure 127) which were characterized by ^{1}H-NMR.

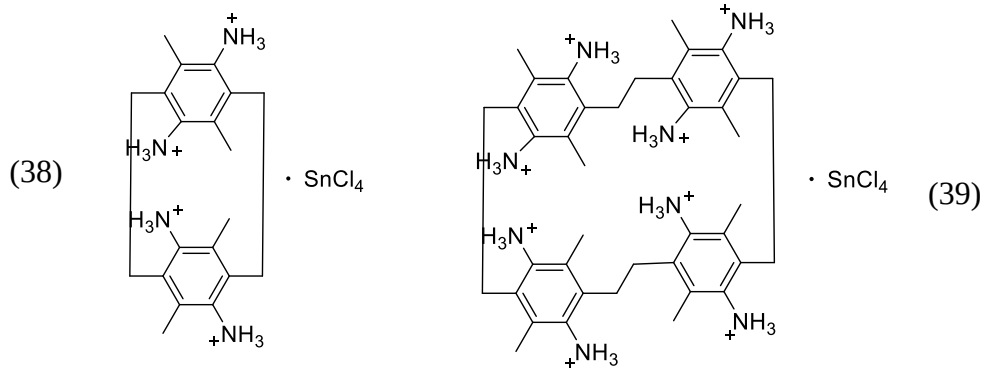

Figure 127: Corresponding cyclophane ammonium tin salts.

Yields for this reaction were found to be inconsistent and isolation of the cyclophane products was found to be extremely difficult if precipitation did not occur in an efficient manner. The best yields for these reactions was only about 50%, ruling this reaction out as an effective way of accessing the cyclophane amides. The reaction between the cyclophane ammonium salts and iron chloride deviated greatly from the behavior observed for the ammonium durene system. Rather than

obtaining the desired quinone, which was expected to precipitate out of the aqueous solution as an orange or yellow solid, a deep green solution formed instead (Figure 128). All attempts to extract

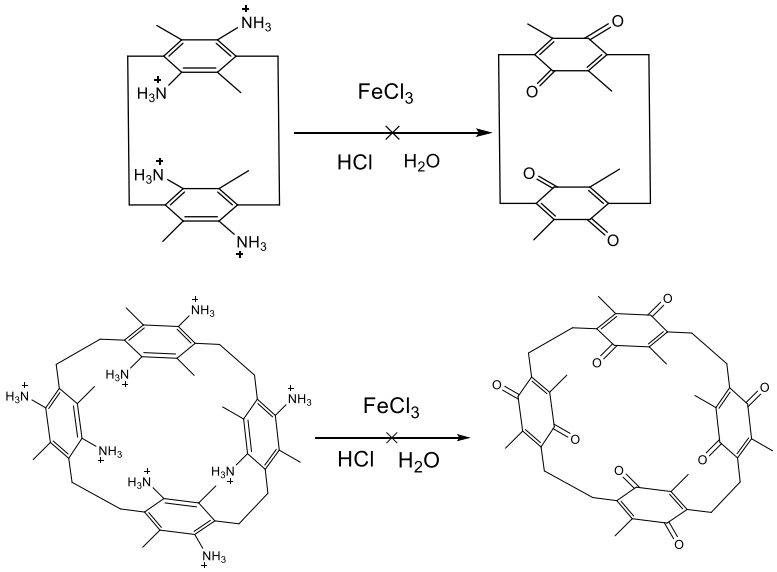

Figure 128: Attempted oxidations of the cyclophane ammonium salts with iron trichloride.

the colored species out of solution with non-polar solvents were met with failure. Extraction with a mixture of methanol and dichloromethane gave a deep blue extract which, when dried, was found to be insoluble in all common non-polar organic solvents but readily soluble in polar solvents such as methanol and water. All attempts at NMR analysis failed, leading to the conclusion that the colored species in question was paramagnetic. While disappointing, these results are in line with what was reported by Morvant, who had encountered the same issues when attempting the same type of reaction. These results make the need for an alternative way to access phenol and quinone moieties necessary.

It was determined that a method that could quickly and selectively reduce the nitro groups of the cyclophanes in the presence of acetic anhydride was needed, as the amines could be readily converted into their corresponding amides upon their formation. The use of zinc in a mixture of acetic acid and acetic anhydride had already proven useful in the formation of amide (40).

Applying these reaction conditions to the cyclophane systems was successful and repeatable giving yields of the cyclophane amides in about 75% (Figure 129). For both cyclophane systems the

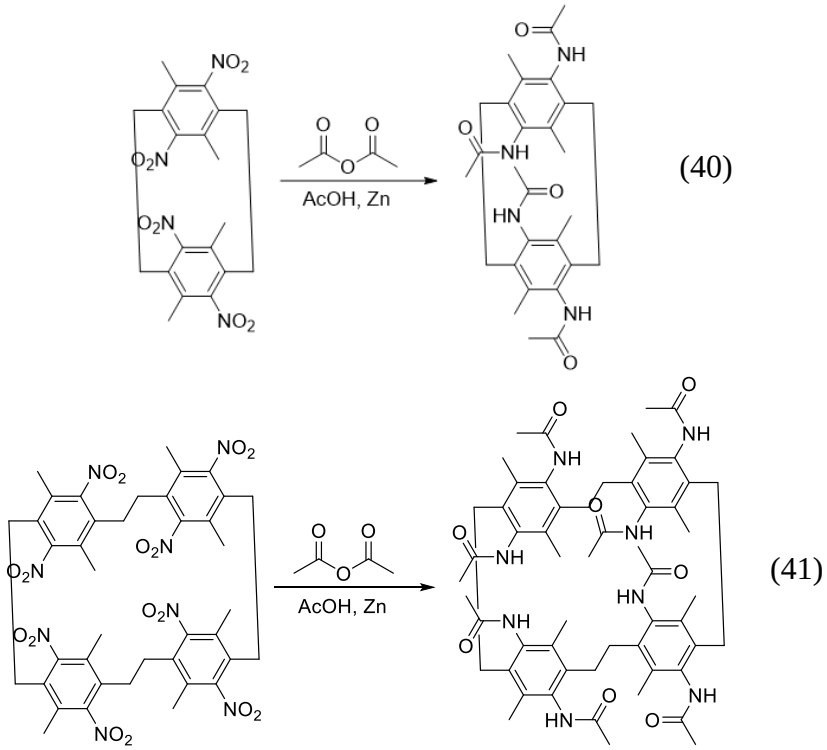

Figure 129: Synthesis of amide cyclophanes from their starting nitro cyclophanes.

reduction was carried out by dissolving the cyclophane in 15 mL of acetic anhydride and 10 ml of acetic acid. The solution was vigorously stirred, and zinc powder was gradually added over a period of 30 minutes. Upon initial addition the reaction mixture was observed to turn yellow and then deep green, and addition of zinc was continued until the reaction mixture became fully transparent and remained so regardless of the presence of air. It is important to note that addition of the full amount of zinc at the start of the reaction would result in the reaction failing to go to completion and would require further addition of zinc powder, resulting in the use of a large excess. Adding small portions of zinc powder over the 30-minute period resulted in the need of only a slight excess of the zinc. Reactions were worked up by filtration, followed by concentration under reduced pressure which gave a light brown solid for both amide cyclophane systems.

Trituration of the crude cyclophane (40) with chloroform was sufficient to remove any organic impurities from the reaction product. The remaining solid consisted of a mixture of cyclophane (40) and zinc acetate. The mixture was extracted with acetonitrile, filtered, then concentrated under reduced pressure to give cyclophane (40) as a tan solid. ^{1}H-NMR analysis of cyclophane (40) was obtained in deuterated methanol (Figure 130). Examination of the ^{1}H-NMR

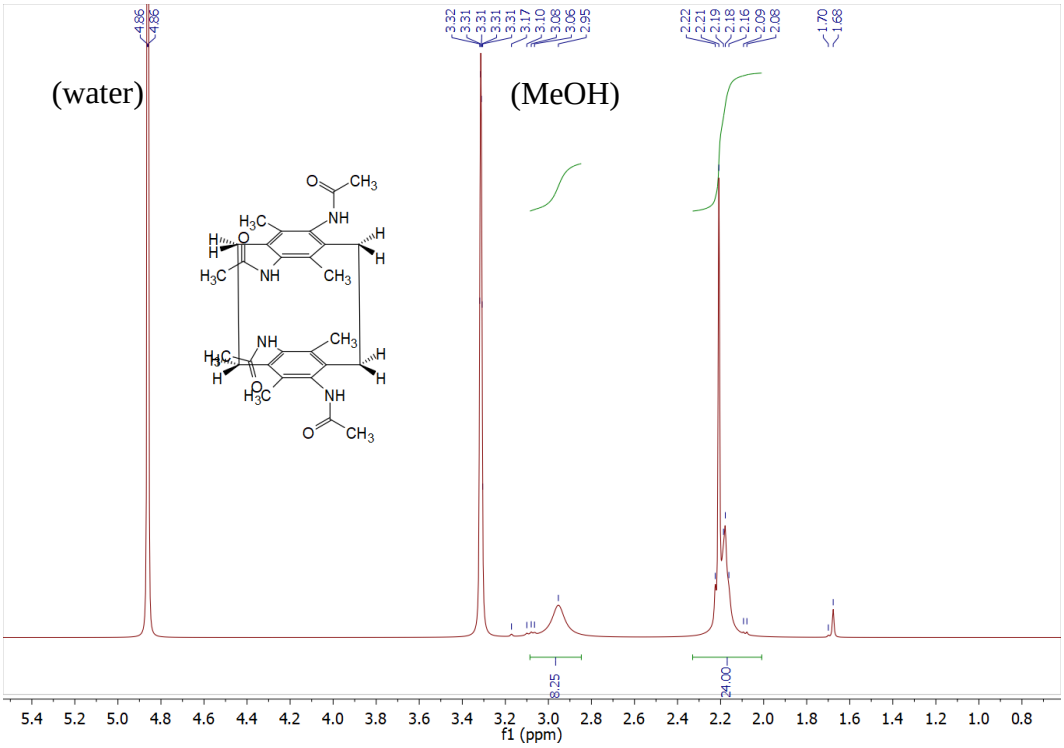

Figure 130: ^{1}H-NMR spectrum of cyclophane (40) at 25 °C.

spectrum of cyclophane (40) showed that significant line broadening was occurring in regard to the methylene bridge protons and the methyl group protons of the ring indicating that molecule was dynamic at room temperature. Variable temperature NMR experiments showed that heating the sample to 100 °C in DMSO had no effect on the spectrum. Cooling the sample to -40 °C in methanol resulted in the resolution of the broad peaks into partially resolved signals. Fine structure splitting was also observed for the methylene bridge protons, indicating that they had now become diastereotopic (Figure 131). This was supported by variable temperature HSQC experiments which

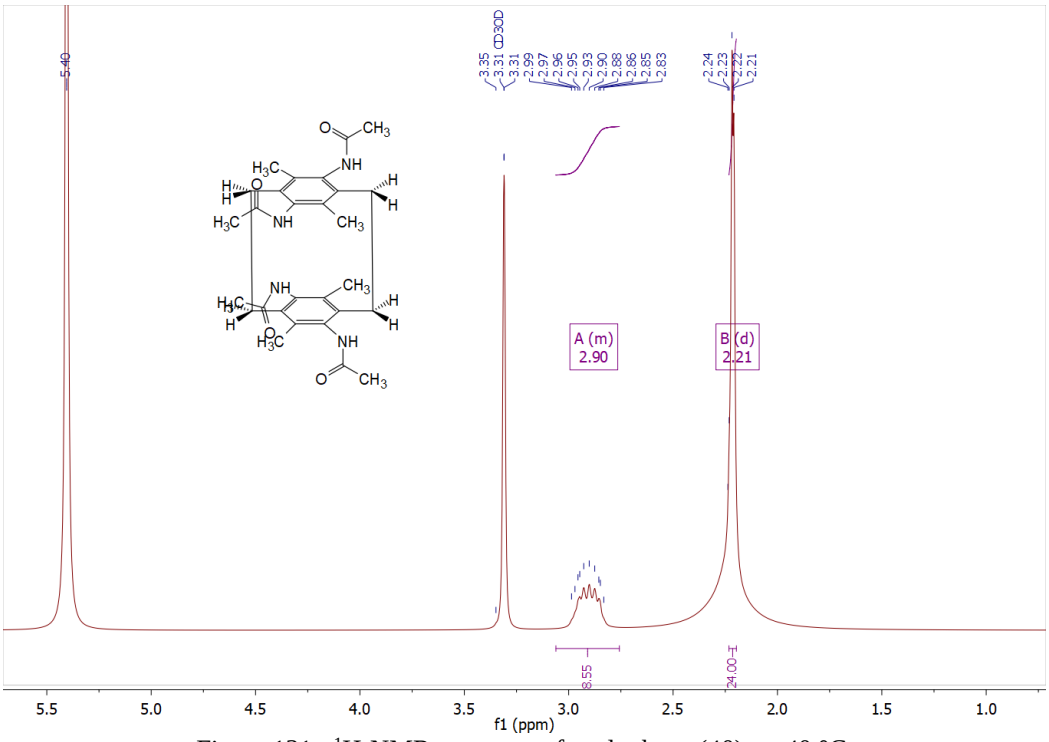

Figure 131 : ^{1}H-NMR spectrum of cyclophane (40) at -40 °C.

showed only one correlation for the methylene bridge protons at room temperature. When cooled to -40 °C HSQC experiments showed two different correlations of the methylene bridge protons to the same carbon. The results of these variable temperature NMR experiments suggest that at room temperature cyclophane (40) is in a dynamic equilibrium between two different conformations, resulting in the observed line broadening (Figure 132). This motion most likely

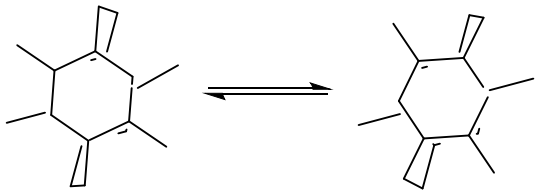

Figure 132: Generalized model for the proposed structural dynamic equilibrium of cyclophane (40). The amides and double bonds of the structure are omitted for clarity.

comes about from a twisting motion about the cyclophane bridges. Cooling the sample stops the motion about the bridge heads resulting in the methylene bridge protons becoming diastereotopic. Rotation about the aryl and amide methyl groups in not hindered and as such a singlet is observed for both groups. COSY, HSQC, and HMBC NMR experiments at -40 °C allowed for the structural

assignment of cyclophane (40), while IR analysis confirmed the presence of the amide functional groups (Figure 133). Purification of cyclophane (41) was carried

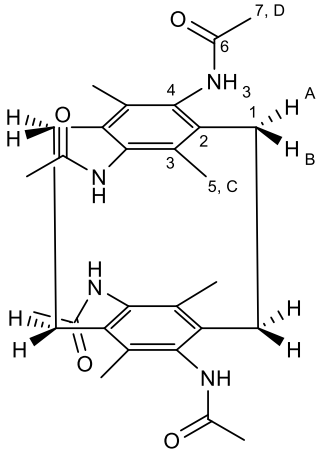

^{1}H δ (ppm)	^{13}C δ (ppm)	
A: 2.95	1: 28.10	5: 14.13
B: 2.95	2: 128.47	6: 169.41
C: 2.17	3: 132.14	7: 21.40
D: 2.20	4: 134.95	

IR: 3250 cm^{-1}, 1648 cm^{-1}

Figure 133: NMR assignments and selected IR signals of cyclophane (40).

out by trituration of the crude reaction product with chloroform, followed by extraction with acetonitrile. The resulting solution was filtered, concentrated under reduced pressure, and recrystallized from a mixture of 1 mL of DMSO and 3 ml of water, which gave the pure cyclophane (41) as a white crystalline solid. Analysis of the ^{1}H-NMR of cyclophane (41) was obtained in deuterated methanol (Figure 134). COSY, HSQC, and HMBC NMR experiments,

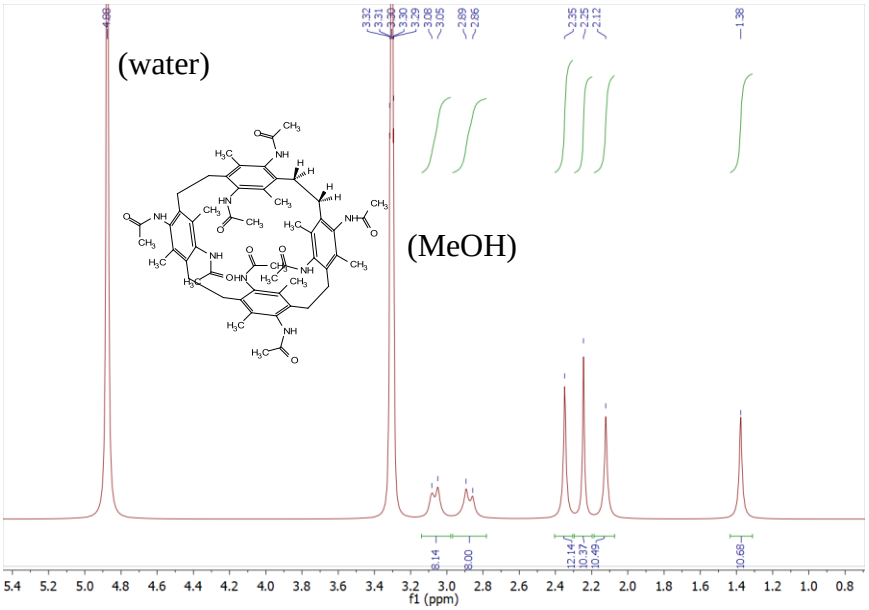

Figure 134: ^{1}H-NMR spectrum of cyclophane (41).

allowed for the structural assignment of cyclophane (41), while IR analysis confirmed the presence of the amide functional groups (Figure 135). The observed chemical shifts for the amide groups

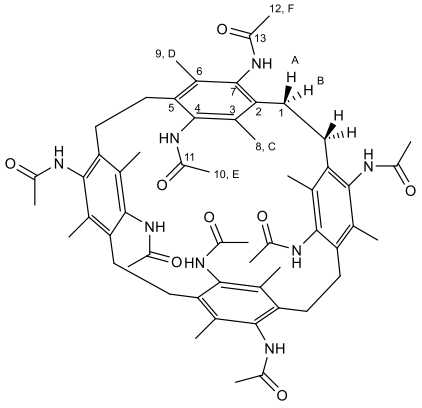

^{1}H δ (ppm)	^{13}C δ (ppm)	
A: 2.86	1: 27.69	7: 134.28
B: 3.08	2: 133.63	8: 15.12
C: 1.38	3: 135.47	9: 13.53
D: 2.35	4: 139.38	10: 22.32
E: 2.12	6: 125.67	11: 171.54
F: 2.25		12: 21.15

IR: 3250 cm^{-1}, 1648 cm^{-1}

Figure 135: NMR assignments and selected IR signals of cyclophane (41).

and aryl methyl groups were normal with the exception of the singlet observed at 1.38 ppm which is indicative of a large shielding effect. The magnitude by which aromatic shielding could influence proton chemical shift was determined though the synthesis of two methylated naphthalenophanes (Figure 136). The structures of the two cyclophanes were determined by NMR

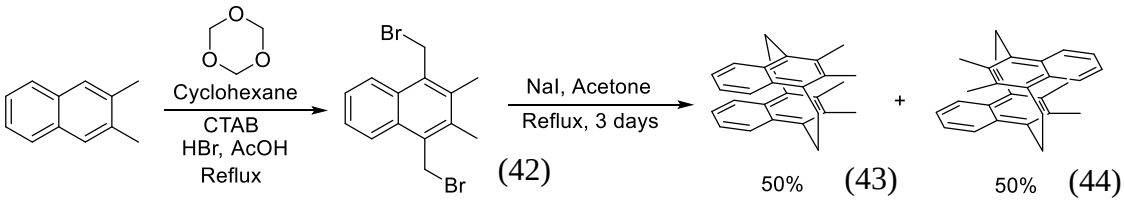

Figure 136: Synthesis of *Syn*- and *Anti*-[2.2]tetramethylnaphthalenophanes.

analysis and single crystal x-ray diffraction (Appendix A, pgs 221-222). The *syn*-naphthalenophane (43) showed a singlet at 2.3 ppm which corresponded to the protons of the methyl groups while the *anti*-naphthaleneophane (44) showed a singlet at 1.6 ppm which corresponded to the methyl groups. The difference between these chemical shifts gives a 0.7 ppm difference between shielded and non-shielded protons. The distance from the methyl group to the ring in cyclophane (44) was measured to be 2.69 Å. Relating this difference back to the octa-amide system showed that a difference of 0.7 ppm would in fact place the singlet at 1.37 at 2.07 ppm

which is well in range of what is observed for the chemical shifts of the other three singlets, suggesting that the observed chemical shift is in fact due to shielding effects caused by the aromatic rings. Measurement of the inner methyl groups to the closest shielding aromatic ring gave a distance of 2.63 ppm. Based on these comparisons, it seems that the constructed model of cyclophane (44) is fairly representative of what its behavior is in solution. Examination of the possible three-dimensional conformations of the macrocycle led to the development of a structure that readily results in 4 methyl groups in the shielding zone of the aromatic rings in a similar fashion to what was observed for the *anti*-[2.2]tetramethylnaphthaleneophane (Figure 137).

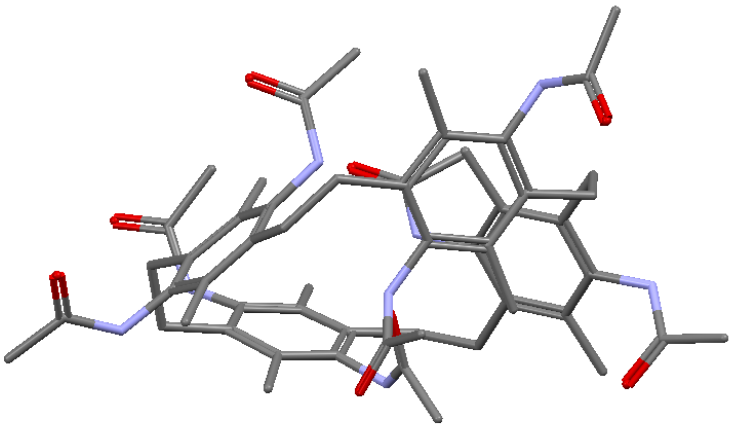

Figure 137: Proposed structural model of cyclophane (41).

The 3D structure of cyclophane (41) was further probed through the use of rotating frame rotating-frame Overhauser effect spectroscopy (ROSY NMR) which allows for the detection of through space proton-proton coupling (Figure 138). Selective excitation of the shielded methyl

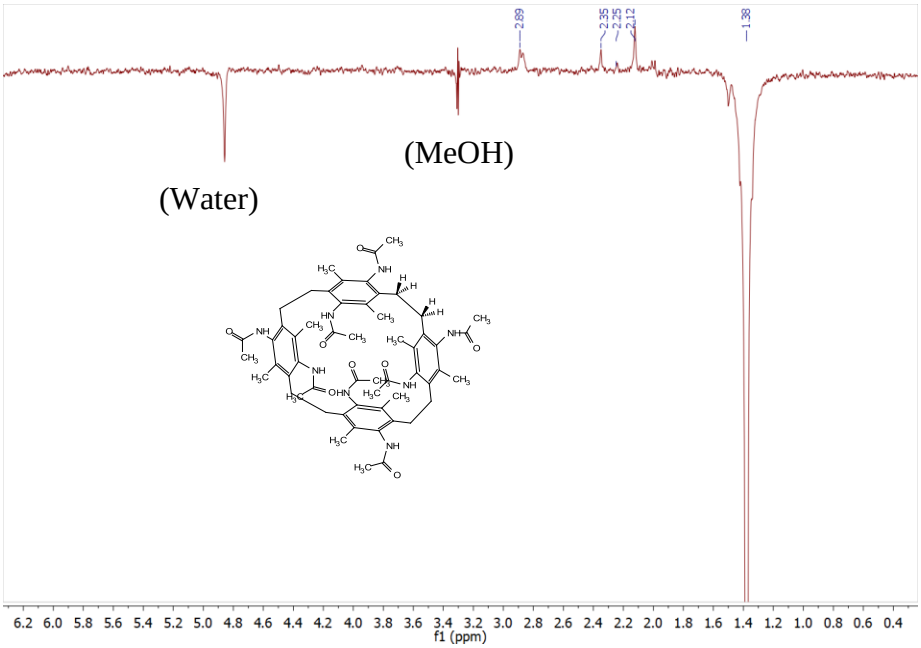

Figure 138: 1-D ROSY spectrum of cyclophane (44) with selective excitation occurring at the methyl peak at 1.38 ppm.

groups at 1.38 ppm showed through space couplings to the bridge protons at 2.89 ppm as well as the “outer” aryl methyl groups at 2.35 ppm and the “inner” amide methyl groups at 2.12 ppm. A weak coupling to the “outer” amide methyl groups at 2.25 ppm was also observed. Variable temperature NMR experiments showed that cooling cyclophane (41) in methanol to -40 °C had no effect on the NMR spectrum. Heating cyclophane (41) in DMSO to 100 °C resulted in the coalescence of the bridge protons into a single broad peak, but no coalescence or change in chemical shifts were seen for the methyl groups of the aromatic rings or the methyl groups of the amides. This is an important finding as it suggests that even at elevated temperatures the two sets of the aryl methyl groups and two sets of the amide methyl groups are tucked within the pocket of the [2.2.2.2] cyclophane. These results also suggest that the cyclophane (41) is in fact a fairly rigid structure even at elevated temperatures.

Relative to what is known for other [2.2.2.2]paracyclophane structures the effect of the methyl groups and amides on the [2.2.2.2]paracyclophane structure is pronounced. In the case of

[2.2.2.2]paracyclophane the lack of functionalization results in a large degree of dynamic behavior. NMR studies of [2.2.2.2]paracyclophane performed by Tabushi and co-workers, show that at room temperature the bridge protons of the structure exist as a single broad peak.[128,129] Cooling the sample to -111 °C results in peak separation with the formation of two doublets located at 3 ppm and 2.5 ppm in an identical fashion to what is observed for the [2.2.2.2]octaamide system. This observed behavior was attributed to the [2.2.2.2]paracyclophane adopting an all-face state in which one of the bridge protons experiences a greater degree of shielding relative to the other, giving similar behavior to what is observed for cyclophane (41) at room temperature (Figure 139).[128,129]

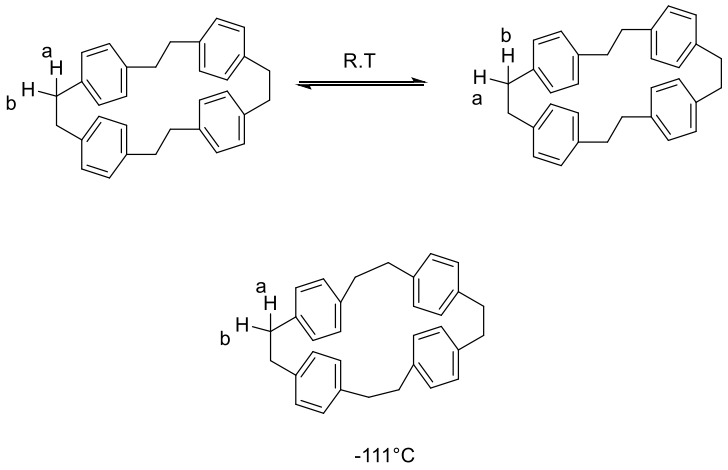

Figure 139: Geometric models of [2.2.2.2]paracyclophane proposed by Tabushi and co-workers in order to explain the large difference in NMR behavior at room temperature vs. the NMR behavior at -111°C.[128,129]

The work reported by Tabushi and co-workers supports the supposition that cyclophane (41) is in a locked conformation at room temperature due to the large degree of steric bulk, resulting in the observed separation of the bridge protons which only coalesce upon heating.[128,129] It is important to note that the model proposed by Tabushi and co-workers places the [2.2.2.2]paracyclophane in a rectangular shape with two sets of the bridges being in a gauche conformation while two other sets are in an *anti*-conformation. This structural behavior was observed by Morvant and co-workers in the octanitro [2.2.2.2]paracylophane system, (Figure 140), which assumed a so called rectangular conformation at room temperature resulting in four different

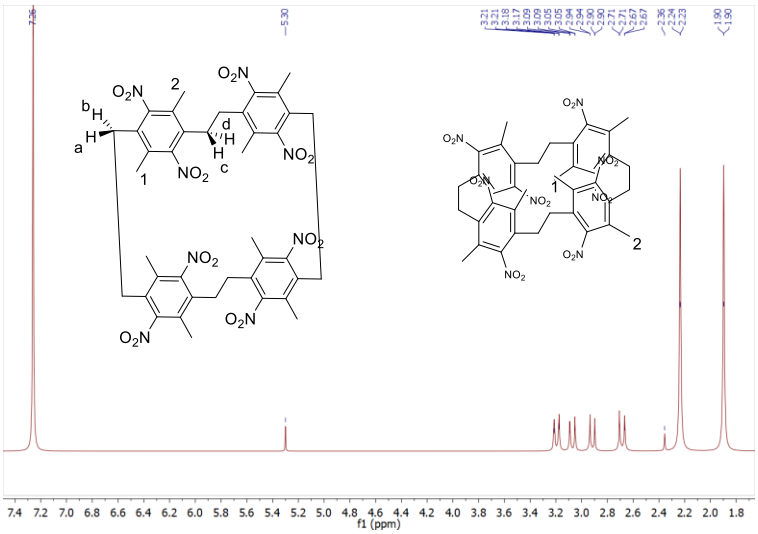

Figure 140: Different perspectives of the [2.2.2.2] octanitro system, demonstrating the rectangular shape it adopts in solution at room temperature, resulting in different chemical and magnetic environments.[38]

signals for the bridge protons the gauche-bridge protons and *anti*-bridge protons would all be experiencing different magnetic and chemical environments as well as two sets of methyl group signals.[37] These different environments are due to the fact that the resulting rectangular structure results in one so called inner methyl group and one outer methyl group. Upon heating Morvant and co-workers observed partial coalescence at 66 °C, with full coalescence being observed at 80 °C with the methyl group signals merging into a single peak. The bridge signals merge into a single peak, indicating that despite the presence of the methyl groups the [2.2.2.2]octanitro paracylophane system is capable of full dynamic movement at elevated temperatures, which is a stark contrast to cyclophane (41) which only showed bridge coalescence upon heating with no changes in the signals of the methyl groups, suggesting that while the adopted structure of cyclophane (41) is due to steric influences the adopted structure of cyclophane (37) is due to other influences besides sterics.[38] Further work by Tabushi and co-workers demonstrated that in solution [2.2.2.2]paracylophane systems monosubstituted with electron withdrawing groups all assume the rectangular geometry observed by Morvant, suggesting that the adopted geometry is due to dipole π interactions between the aromatic rings and the electron poor nitro groups.[129] Interestingly, the

crystal structure of cyclophane (37) obtained by Morvant showed that in the solid state at low temperatures cyclophane (37) adopts an all gauche geometry, strongly resembling the proposed model of cyclophane (41) with one set of the methyl groups in the shielding zone of the aromatic ring (Figure 141).[38,129]

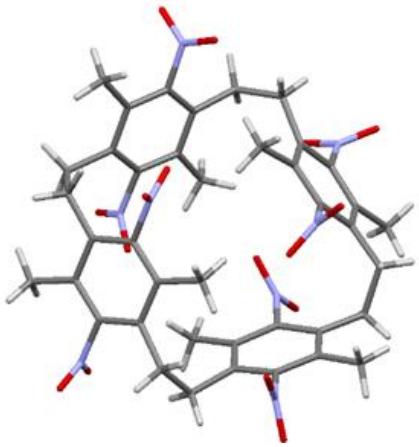

Figure 141 : Crystal structure of cyclophane (37) obtained by Morvant.[38]

These results strongly support the supposition that cyclophane (41) adopts an all gauche conformation at room temperature, in a similar fashion to what is observed in the crystal structure of the [2.2.2.2]octanitro system, resulting in strong shielding effects for one set of the methyl groups and a moderate shielding effects of one set of the amides. Given this information it is seemingly the case that the amide groups of the [2.2.2.2]octaamide system could be more sterically hindered than the amides of the [2.2]tetraamide cyclophane system, the exact opposite of what was expected for these systems at first glance. The degree to which these factors impact the nitrosation of these systems will be discussed in section 4.3.

4.3 Nitrosation of *Anti*-5,8,13,16-tetramethyl-4,7,12,15-tetraamido[2.2]paracyclophane and *Anti*-5,8,13,16,21,24,29,32-octamethyl-4,7,12,15,20,23,28,31-octaamido[2.2.2.2]-paracyclophane and Attempted Rearrangements.

Nitrosation of both cyclophane systems was carried out using the same methodology used for the small molecule systems. In the case of cyclophane (40) the cyclophane was dissolved in a 2:1 ratio of acetic anhydride to acetic acid. The resulting solution was cooled to 0 °C using an ice bath, after which 16 equivalents of $NaNO_2$ were added to the stirring reaction mixture. The clear solution instantly turned yellow and evolved a yellow gas. The reaction solution gradually turned blue and then transitioned to yellow. The reaction was allowed to run at a sustained 10 °C for 16 hours, and reaction workup gave a yellow/ orange solid which demonstrated significant solubility in dichloromethane. IR analysis of the compound showed peaks indicative of nitrosation at 1738 cm^{-1}, 1575 cm^{-1}, and 1520 cm^{-1}. Most importantly IR analysis demonstrated that the free NH of the amide at 3250 cm^{-1} was completely gone indicating that successful nitrosation had occurred. Heating the presumed nitrosolated cyclophane (40) in acetic anhydride for 4 hours at 80 °C gave an orange/red material upon reaction workup. ^{1}H-NMR of the crude material showed a complex mixture of products. New cyclophane bridges were observed in the crude spectra which were assumed to be part of the ester cyclophane. Repeated column chromatography of the crude material using acetonitrile as the mobile phase gave 6 mg of cyclophane (45) with minor impurities giving a yield of 18% (Figure 142). Repeating the reaction gave similar yields and, in some cases, failed to give the desired compound at all, instead yielding a mixture of decomposition products, ^{1}H-NMR analysis of the [2.2]ester cyclophane was obtained in deuterated chloroform (Figure 143).

COSY, HSQC, and HMBC NMR experiments allowed for the structural assignment of cyclophane (45), while IR analysis confirmed the presence of the ester functional groups (Figure 144).

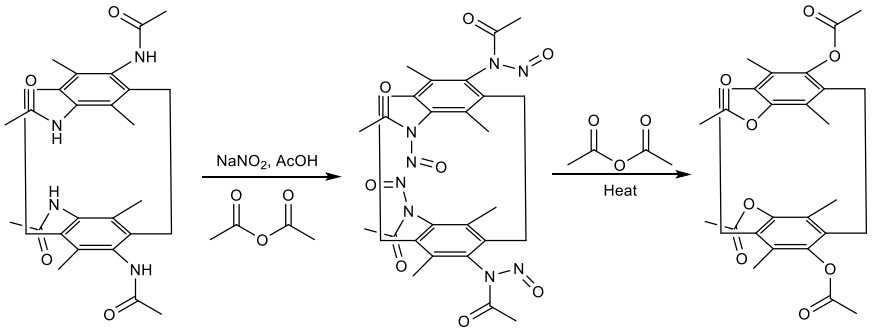

Figure 142: Nitrosation of cyclophane (45) followed by rearrangement in acetic anhydride.

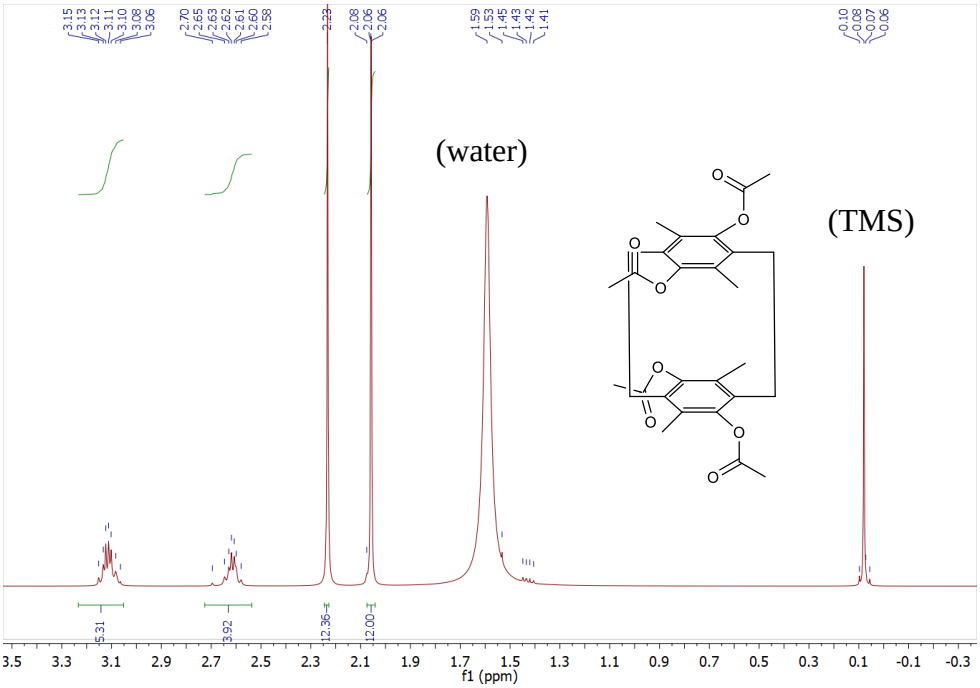

Figure 143: ^{1}H-NMR of cyclophane (45).

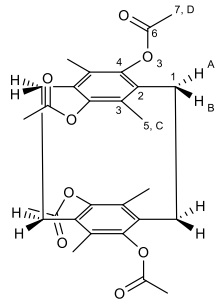

^{1}H δ (ppm)	^{13}C δ (ppm)	
A: 2.62	1: 26.99	5: 14.71
B: 3.11	2: 137.16	6: 182.09
C: 2.06	3: 142.92	7: 25.54
D: 2.23	4: 152.27	
IR: 1748 cm^{-1}		

Figure 144: NMR assignments and selected IR signals of cyclophane (45).

Cyclophane (41) was nitrosolated using the same procedure used for cyclophane (40). Heating the assumed nitrosolated octaamido cyclophane in acetic anhydride resulted in the formation of a red/orange solid upon workup by evaporation. ^{1}H-NMR analysis of the crude material gave poorly resolved spectra that were consistent with a large number of degradation products. All attempts to purify the material to improve the quality of the NMR spectra were met with no success suggesting that decomposition of the cyclophane was occurring (Figure 145). In

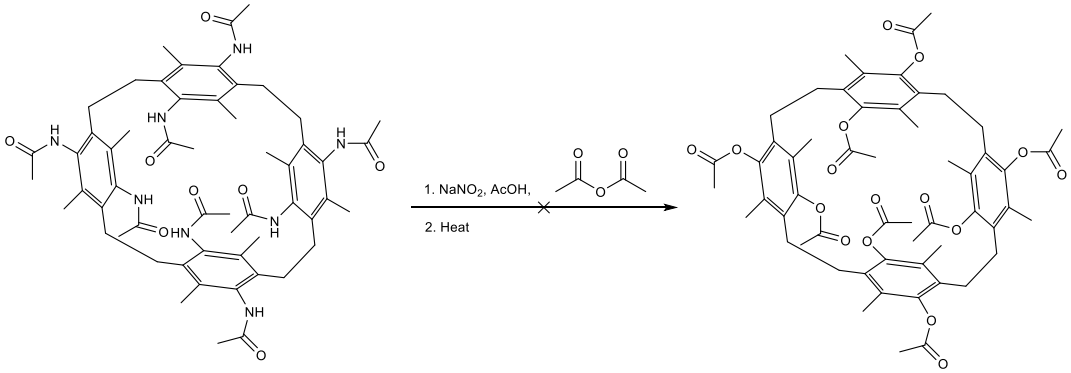

Figure 145: Attempted nitrosation and rearrangement of cyclophane (41).

the case of cyclophane (41) it was proposed that the poor reactivity of these rearrangements was due to the large degree of steric crowding caused by the steric bulk of the methyl groups of the amides and aromatic rings as well as the fact that two sets of the amides were tilted into the center of the macrocycle, these steric factors make the nitrosation of these amides difficult to impossible. The results of the variable temperature NMR studies suggest that heating the reaction will not improve the nitrosation process as two sets of the amides remain towards the inside of macrocycle even at 100 °C.

In an attempt to further improve the yield of cyclophane (45) other milder nitrosolating agents were explored. Isobutyl nitrite was used as the nitrosolating agent in the reaction. Nitrosation of cyclophane (40) was carried out in acetic anhydride using 5 equivalents of isobutyl nitrite. Addition of the isobutyl nitrite resulted in the reaction solution turning a deep emerald green color. The reaction was allowed to stir for 3 hours before being worked up by evaporation. ^{1}H-NMR analysis showed that the reaction provided the same NMR spectra obtained from the usage of $NaNO_2$. Heating the isolated nitrosolated cyclophane (40) in acetic anhydride gave the same crude reaction mixture that was observed from using $NaNO_2$ showing no improvements in the yield of the ester cyclophane suggesting the main factor that hinders the formation of the desired ester is the rearrangement of the nitrosamides. It was proposed that carrying out the nitrosation and heating of each amide individually could possibly improve the yields of these reactions as well as their downstream behavior. The reaction between *anti*-5,8,13,16-tetramethyl-4,7,12,15-tetraamido[2.2]paracyclophane and isobutyl nitrite was carried out in acetic anhydride in an iterative process. ^{1}H-NMR analysis of the crude product showed it to be a complex mixture of products, seemingly demonstrating that an iterative approach to these cyclophane scaffolds was ineffective.

In an attempt to access both hydroquinone/quinone cyclophane systems directly using nitrosamide chemistry cyclophane (40) was nitrosolated, isolated, then dissolved in 5 mL of acetone. The acetone solution was then added to a round bottom flask containing 20 mL of water. The reaction was heated at 80 °C for 2 hours. A tan solid was observed to gradually form and crash out of solution during the course of the reaction. The reaction was filtered, then extracted with dichloromethane. The organic extract was dried and concentrated under reduced pressure. IR and NMR analysis showed of that none of the desired quinone or hydroquinone was observed, instead

a complex mixture of products was obtained. Attempts to dissolve the tan precipitates in common organic solvents were also met with failure, suggesting that the resulting material might be polymeric.

Based on the results obtained from the observed nitrosamide reactions the sensitivity of the polyamide cyclophane systems under nitrosolating conditions seems to present a major barrier to achieving the desired transformations in a desired manner. The fact that both iterative nitrosation and nitrosation isolation methods failed to give the desired products in good yield was attributed to the large amount of reactive amide groups that must rearrange in a controlled manner in order to access the desired product.

4.4 Conclusions and Future Work

This work has demonstrated that nitrosamide chemistry is not simply limited to simple small molecules but can be extended to poly aromatic systems as well, allowing for the late stage installation of useful functionalities within these molecules. In the case of the cyclophane systems examined in this work, a number of challenges were encountered in regard to their nitrosation and subsequent rearrangement. In both cyclophane systems it seems that the steric environment that is induced by close proximity of the aromatic rings coupled with large number of methyl groups in these systems makes the rearrangement of the nitrosamide fairly difficult to achieve for these systems. The successful nitrosation and rearrangement and these systems is seemingly further complicated by the fact that attempting to get such a large number of nitrosamide functionalities to rearrange and eliminate on the same molecule seemingly results in the degradation of these cyclophane systems and the generation of a number of undesired products. This fact is seemingly confirmed by the results obtained from the treatment of cyclophane (40) with $NaNO_2$ in acetic acid

and acid anhydride which resulted in a new cyclophane product that was found to the desired cyclophane (45). While similar attempts to access the *anti*-5,8,13,16,21,24,29,32-octamethyl-4,7,12,15,20,23,28,31-octaacetoxy[2.2.2.2]paracyclophane resulted in complex product mixtures that could not be resolved.

It is also possible that the $NaNO_2$ reagent is in some way responsible for the cyclophane degradation as cyclophane NO_x complexes are known and have been demonstrated to result in side reactions (Figure 146).[130] Such side reactions could be readily occurring during the nitrosation

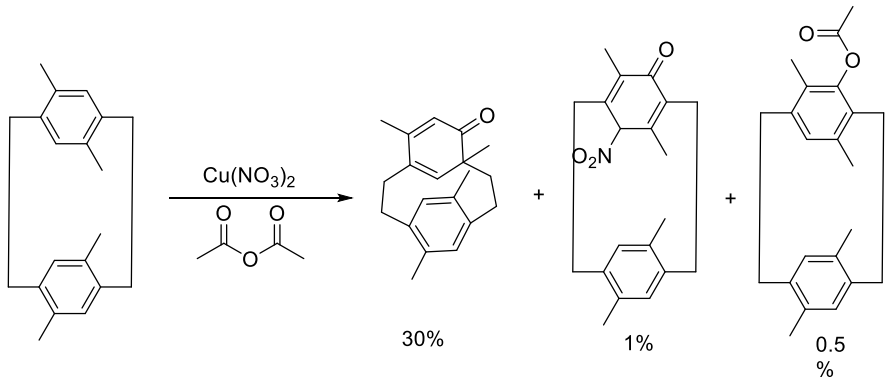

Figure 146: Oxidation products formed from the nitration of terta methyl substituted [2.2]paracyclophanes.[130]

of the cyclophane systems presented this work. Given the unique structure and extreme steric environment around the cyclophane systems studied in this work it seems that other complex aromatic systems should be explored in order to further evaluate the effectiveness of N-aromatic nitrosamides at installing functional groups in complex molecular architectures. It has already been established that cyclophane systems can respond well to nitrosation conditions and that the extreme degradation behavior observed in this work is most likely due to the complexity of the substrates rather than the nitrosation methodology itself.[130,131] In order to evaluate the extent to which cyclophane structure impacts the efficiency of nitrosation a series of nitro cyclophanes with varying degrees of steric bulk should be tested in order to determine at what point the amount of steric bulk begins to drastically inhibit the efficiency of the nitrosation reaction.

Overall, this work has demonstrated that nitrosation methodology can be extended to poly aromatic systems, but that in the case of sterically compressed molecules multi nitrosation elimination reactions can be exceedingly difficult to achieve in an efficient manner. These results are important as knowing that such limitations exist will help in the development of other cyclophane syntheses in which nitrosamide rearrangements can be used for late stage functionalization of key functional groups. It is also important to note that all other attempts at accessing the desired cyclophane phenols/quinones were met with failure for both cyclophane systems, while the nitrosamide approach was actually capable giving the desired [2.2]ester cyclophane, all be it in low yield. These results suggest that these scaffolds in particular are overly delicate, and the fact that that the developed nitrosamide chemistry was capable of giving the desired [2.2]ester cyclophane at all is reason enough to continue the pursuit of this chemistry.

4.5 Experimental

General Methods:

Unless otherwise noted, all starting materials and reagents were obtained from commercial suppliers and used without further purification. All solvents were used as obtained unless noted. All reactions were performed in dried glassware under open atmosphere with magnetic stirring unless otherwise noted. Chromatography: TLC was performed on silicagel 60 F_{254} sheets from Merck and visualized under UV light. Chromatography was performed on 150 mesh neutral aluminum oxide from Sigma Aldrich. Analytical Instrumentation: IR spectra were recorded on a Thermo Scientific Nicolet 6700 FTIR spectrometer with peaks reported in cm^1. NMR spectra were recorded on a Varian VNMRS 300, 400, and 500 MHz NMR spectrometers. Chemical shifts are expressed in ppm relative to solvent signals. NMR spectra were processed using Mnova (www.mestrelab.com/software/mnova-nmr).X-ray crystallography analysis was carried out at the University of Oklahoma using a Bruker APEX ccd area detector (1) and graphite-monochromated Mo Ka radiation (l = 0.71073 Å) source. Crystal structures were visualized using CCDC Mercury software (http://www.ccdc.cam.ac.uk/products/mercury/). Nomenclature: IUPAC nomenclature was used to name each compound. Compounds reported in the literature that lack spectral data are marked with an (*). Compounds not reported in the literature are marked with an (**). Coupling constants are reported for compounds not reported in the literature. Reported COSY correlations refer to J-3 proton-proton couplings, HSQC correlations refer to ^{13}C-^{1}H J-1 couplings, HMBC correlations refer to ^{13}C-^{1}H J-2 and J-3 couplings.

Procedure for the Synthesis of Nitrocyclophanes:

The synthesis of nitrocyclophanes (36) and (37) was performed using the methodology developed by Morvant. NMR analysis of both compounds provided ^{1}H-NMR spectral data that

was a match to the ^{1}H-NMR spectral data reported by Morvant. Morvant, M. C., "Synthesis, properties, and applications of polynitro- and polyamino(2.2)paracyclophanes". Ph.D. Dissertation, University of Oklahoma, Norman, OK, 1996.

***Anti*-5,8,13,16-tetramethyl-4,7,12,15-tetranitro[2.2]paracyclophane (36)**

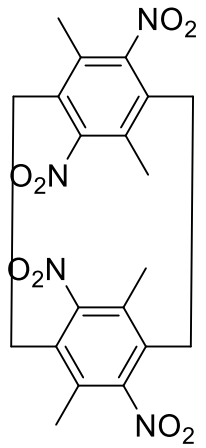

^{1}H NMR (300 MHz, Chloroform-*d*) δ 3.74 (m, 4H, CH_2Ar), 3.16 (m, 4H, CH_2Ar), 2.31 (s, 12H, ArMe).

***Anti*-5,8,13,16,21,24,29,32-octamethyl-4,7,12,15,20,23,28,31-octanitro[2.2.2.2]paracyclophane (37)**

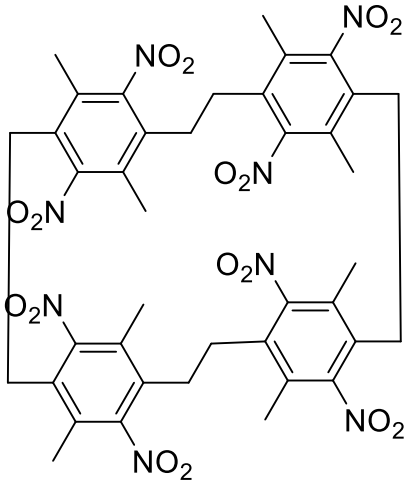

^{1}H NMR (300 MHz, Chloroform-*d*) δ 3.19 (d, 4H, CH_2Ar), 3.07 (d, 4H, CH_2Ar), 2.92 (d, 4H, CH_2Ar), 2.68 (d, 4H, CH_2Ar), 2.23 (s, 12H, ArMe), (1.90, 12H, ArMe).

General Procedure for the synthesis of aryl ammonium salts

A round bottom flask was charged with 0.080 g (0.357 mmol) of dinitrodurene followed by 10 mL of concentrated HCl and 2-3 ml of acetic acid, which resulted in a fine suspension of the nitro aromatic in the acid solution. The reaction mixture was then stirred magnetically while 1.61 g (7.14 mmol) $SnCl_2.2H_2O$ was added to the stirring mixture (10 equivalents per nitro group). Upon complete addition the reaction was then stirred until all of the $SnCl_2.2H_2O$ had fully dissolved. The reaction was then heated at 90 °C for 1 hour. Allowing the reaction to cool to room temperature resulted in the formation of a white precipitate, upon cooling the reaction in an ice bath further precipitation occurred. The white precipitate was then filtered off and washed 4 times with diethyl ether, and then was allowed to dry over vacuum which gave a fluffy white powder which was found to be the corresponding aryl ammonium salt. Yields for the durene ammonium salt were typically 68% while yields for the cyclophane salts were typically between 50 and 40%. Yields were based on the weight of the salt relative to the weight of starting material used in the reaction).

Anti*-5,8,13,16-tetramethyl-4,7,12,15-tetraammonium[2.2]paracyclophane (38)*

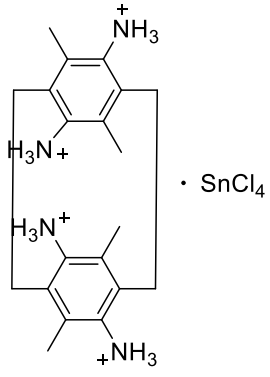

^{1}H NMR (300 MHz, Methanol-d_4) δ 3.45 – 3.33 (m, J = 8.1, 5.2 Hz, 4H), 3.18 (m, J = 8.1, 5.2 Hz, 4H), 2.21 (s, 12H).

Anti*-5,8,13,16,21,24,29,32-octamethyl-4,7,12,15,20,23,28,31-octaammonium[2.2.2.2]paracyclophane (39)*

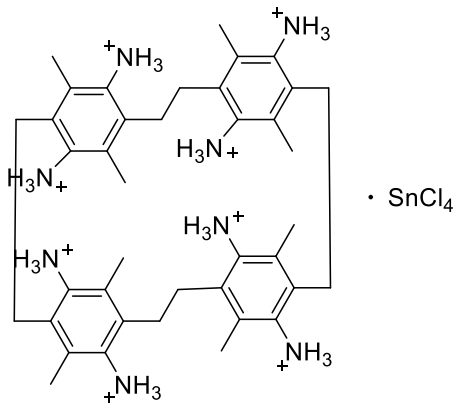

^{1}H NMR (300 MHz, Methanol-d_4) δ 3.15 (m, 8H), 2.85 (m, 8H), 1.61 (s, 12H), 1.49 (s, 12H).

Procedure for the Synthesis of N,N'-(2,3,5,6-tetramethyl-1,4-phenylene)diacetamide (3)

In a round bottom flask dinitrodurene (0.255 g) (1.1 mmol) was dissolved in a mixture of acetic anhydride (15 mL) and acetic acid (5 mL). The mixture was stirred magnetically at room temperature and 6 equiv of zinc powder (0.447 g) (6.8 mmol) was added, in small portions, to the flask over a period of 30 minutes. As the reaction started the color of the mixture changed from clear to a deep yellow and eventually to an emerald green. After the initial zinc addition was completed excess zinc was added over the period of another 30 minutes until the reaction went clear again. The progress of the reaction was also monitored by thin layer chromatography using silica gel plates as the stationary phase and dichloromethane as the mobile phase. The reaction was deemed complete when only one immobile spot was observed. The mixture was filtered through a fine glass frit to remove the left-over zinc powder. The clear solution was dried under reduced pressure to give a solid mixture of zinc acetate (confirmed by IR and melting point) and the desired product. The product was extracted from the mixture with acetonitrile. Removal of the acetonitrile under reduced pressure gave the desired product as a white solid. The resulting product was analyzed by ^{1}H-NMR. Purity was gauged by the ^{1}H-NMR spectra of the products. Products were determined to be sufficiently pure if only the desired product and residual NMR solvent peaks were observed in the ^{1}H-NMR spectrum of the product.

N,N'-(2,3,5,6-tetramethyl-1,4-phenylene)diacetamide (3)

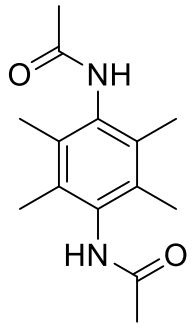

^{1}H NMR (300 MHz, DMSO-d_6) δ 2.02 (s, 6H), 1.99 (s, 12H).

IR: 3250 cm^{-1}, 1648 cm^{-1}

Procedure for the Synthesis of *Anti*-5,8,13,16-tetramethyl-4,7,12,15-tetraamido[2.2]paracyclophane (40)

In a round bottom flask cyclophane (36) (0.125 g) (0.28 mmol) was dissolved in a mixture of acetic anhydride (20 mL) and acetic acid (5 mL). The mixture was stirred magnetically at room temperature and 12 equiv of zinc powder (0.221 g) (3.4 mmol) was added, in small portions, to the flask over a period of 30 minutes. As the reaction started the color of the mixture changed from clear to a deep yellow and eventually to an emerald green. After the initial zinc addition was completed excess zinc was added over the period of another 30 minutes until the reaction went clear again. Upon returning to a clear or faint yellow color the mixture was stirred for 2 hours to ensure that the reaction had reached completion. The mixture was filtered through a fine glass frit to remove the left-over zinc powder. The clear solution was dried under reduced pressure to give a solid mixture of zinc acetate (confirmed by IR and melting point) and the desired product. The product was extracted from the mixture with acetonitrile. Removal of the acetonitrile under reduced pressure gave the desired product as a tan solid. The resulting product was analyzed using 1-D and 2-D NMR experiments as well as by FTIR. Purity was gauged by the ^{1}H-NMR spectra of

the products. Products were determined to be sufficiently pure if only the desired product and residual NMR solvent peaks were observed in the ^{1}H-NMR spectrum of the product.

Anti*-5,8,13,16-tetramethyl-4,7,12,15-tetraamido[2.2]paracyclophane (40)*

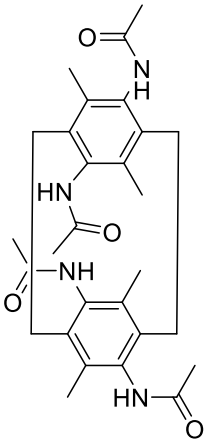

^{1}H NMR (400 MHz, MeOH-*d*) δ 2.92 (m, 8H, CH_2Ar), 2.20 (s, 12H, Me-C=O), 2.17 (s, 12H, ArMe).

^{13}C NMR (500 MHz, MeOH- *d*) δ 14.13 (ArMe), 21.40 (Me-C=O), 28.10 (CH_2Ar), 128.47, 132.14, 134.95, 169.41 (C=O).

Shift (ppm) multiplicity, coupling (Hz) DEPT phase	2D spectra shows correlation to protons at δ (ppm)	
	HMQC	HMBC
14.1	2.17	-
21.4	2.2	-
28.1	2.92	-
128.4	-	2.17, 2.92
132.1	-	2.17, 2.92
134.9	-	2.17, 2.92
169.4	-	2.2

IR: 3252.08 cm^{-1} (N-H), 2928.87 cm^{-1}, 2160.54 cm^{-1}, 1979.69 cm^{-1}, 1644.40 cm^{-1} (N-C=O).

Yield: 77%

Procedure for the Synthesis of *Anti*-5,8,13,16,21,24,29,32-octamethyl-4,7,12,15,20,23,28,31-octaamido[2.2.2.2]paracyclophane (41)

In a round bottom flask cyclophane (37) (0.150 g) (0.17 mmol) was gently warmed in a mixture of acetic anhydride (20 mL) and acetic acid (5 mL) until all of the cyclophane had dissolved. The mixture was allowed to cool to room temperature and then stirred magnetically. Zinc powder (24 eqiv) (0.265 g) (4.1 mmol) was added, in small portions, to the flask over a period of 30 minutes. As the reaction started the color of the mixture changed from clear to a deep yellow and eventually to an emerald green. After the initial zinc addition was completed excess zinc was added over the period of another 30 minutes until the reaction went clear again. Upon returning to a clear or faint yellow color the mixture was stirred for 2 hours to ensure that the reaction had reached completion. The mixture was filtered through a fine glass frit to remove the left-over zinc powder. The clear or faint yellow solution was dried under reduced pressure to give a solid mixture of zinc acetate (confirmed by IR and melting point) and the desired product. The product was extracted from the mixture with acetonitrile. Removal of the acetonitrile under reduced pressure gave the desired product as a tan solid. The resulting crude product was analyzed using 1-D and 2-D NMR experiments as well as by FTIR. Purity was gauged by the ^{1}H-NMR spectra of the products. Products were determined to be sufficiently pure if only the desired product and residual NMR solvent peaks were observed in the ^{1}H-NMR spectrum of the product. In almost all cases the product had to be purified by room temperature recrystallization from a mixture of DMSO (1 mL) and water (3 mL). Crystals were collected by decanting off the mother liquor, the remining crystals were then washed with dichloromethane and dried under reduced pressure.

Anti*-5,8,13,16,21,24,29,32-octamethyl-4,7,12,15,20,23,28,31-octaamido[2.2.2.2]paracyclophane (41)*

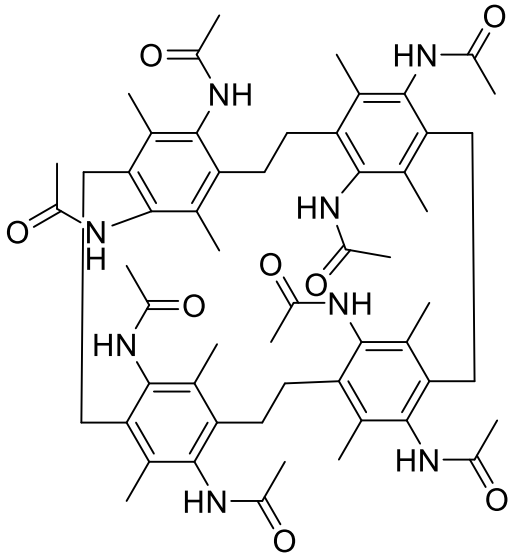

^{1}H NMR (300 MHz, Methanol-*d*) δ 3.07 (d, *J* = 10.1 Hz, 8H, CH_2Ar), 2.88 (d, *J* = 10.7 Hz, 8H, CH_2Ar), 2.35 (s, 12H), 2.25 (s, 12H), 2.12 (s, 12H), 1.38 (s, 12H).

^{13}C NMR (500 MHz, MeOH- *d*) δ 13.53, 15.12, 21.15, 22.32, 27.69, 125.67, 134.28, 139.48, 171.30, 171.54.

Shift (ppm) multiplicity, coupling (Hz) DEPT	Proton	2D spectra shows correlation to protons at δ (ppm)		
		COSY	HSQC	HMBC
13.5	3.07	2.88	2.35	-
15.1	2.88	3.07	1.38	-
21.1	2.35	-	2.25	-
22.3	2.25	-	2.12	-
27.6	2.12	-	3.07, 2.88	-
125.6	1.38	-	-	1.38
133.63	-	-	-	-
134.2	-	-	-	1.38
135.4	-	-	-	2.35
139.4	-	-	-	1.38
171.3	-	-	-	2.25
171.5	-	-	-	2.12

1D ROSY Correlations (excitation of protons at 1.38) (500 MHz, MeOH- *d4*) δ (1.38, 2.12), (1.38, 2.35), (1.38, 2.88).

IR: 3265.60 cm^{-1} (N-H), 2937.27 cm^{-1}, 1724.64 cm^{-1} (weak), 1659.86 cm^{-1} (N-C=O)

Yield: 62%

Procedure for the Bromomethylation of Dimethylnaphthalene

A two necked round bottom flask fitted with a reflux condenser was charged with 2.00 g (12.8 mmol) of the desired methylated benzene, 2.1 equivalents of paraformaldehyde (0.769 g) (25.6 mmol), cetyltrimethylammonium bromide (CTAB) (0.035 g) (0.096 mmol), cyclohexane (20 mL), acetic acid (10 mL), and phosphoric acid (0.5 mL). The reaction mixture was stirred vigorously (magnetic) and 10 mL of 48% hydrobromic acid was added using a dropping funnel attached to a side arm of the flask. The mixture was heated to 80 °C for 24 hours. The reaction mixture was cooled using an ice bath to give a large amount of white solid. The reaction mixture was diluted with 20 mL of water and filtered off over vacuum to give a large amount of while fluffy solid, which was washed with water 3 times followed by washing with 5% aqueous sodium bicarbonate. The wet solid was then allowed to dry over vacuum to give the final product as a free moving white powder which could be used immediately or recrystallized from chloroform if further purification was needed. Reaction yields always ranged between 86-98%.

1,4-bis(bromomethyl)-2,3-dimethylnaphthalene (42)**

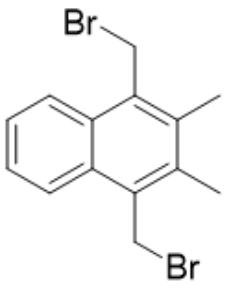

^{1}H-NMR (300 MHz, Chloroform-*d*) δ 8.29 – 7.89 (dd, 6.6, 3.3 Hz, 2H, ArH), 7.60 (dd, *J* = 6.6, 3.3 Hz, 2H, ArH), 5.02 (s, 2H, CH_2Br), 2.52 (s, 3H, ArMe).

Yield: 98%

Procedure for the Synthesis of *Syn*- and *Anti*-[2.2]tetramethylnaphthaleneophane

A round bottom flask was charged with 10 g (66 mmol) of sodium iodide and 325 mL of acetone. The reaction mixture was then fitted to a Soxhlet extractor containing 2.5 g (7.3 mmol) of 1,4-bis(bromomethyl)-2,3-dimethylnaphthalene. The reaction mixture was stirred magnetically and heated to reflux such that the acetone readily collected in the basin of the Soxhlet extractor, resulting in the slow extraction of 1,4-bis(bromomethyl)-2,3-dimethylnaphthalene into the reaction mixture. Reaction progress was monitored visually by color change. As the reaction progressed the mixture became a dark purple-red. This color change was also accompanied by the precipitation of a white solid which was assumed to be sodium bromide. The reaction was allowed to run for a total of three days at which point the reaction was allowed to cool to room temperature. The reaction mixture was then diluted with 100 mL of water followed by the addition of 10 g of sodium thiosulfate. Upon addition of the sodium thiosulfate the reaction was stirred vigorously resulting in the color of the reaction mixture transitioning from a deep red to transparent with a large amount of snow-white precipitate which was determined to be the desired cyclophanes. The reaction mixture was gently filtered off over vacuum to give a clean mixture of the two cyclophane isomers as a white crystalline powder. The powder was washed vigorously with aqueous sodium thiosulfate to ensure that all traces of iodine and iodide had been removed. The dried cyclophane mixture was then stored in a freezer until needed. Yields of the cyclophane mixture ranged between 65-80 %. X-ray diffraction quality crystals were obtained by separation of the two isomers by fractional crystallization in chloroform. Once separated, X-ray quality crystals of the *anti*-isomer were obtained from slow growth in chloroform, while X-ray quality crystals of the *syn*-isomer were obtained from co-crystallization with the anti-isomer. Pure anti could also be obtained by heating the cyclophane mixture to 280 °C in tetraglyme resulting in the isomerization of the *syn*

isomer to the *anti*. Workup from tetraglyme was performed by simply diluting the solution with 3 times its volume with water resulting in the precipitation of the desired cyclophane which was then obtained by filtration.

Syn*-[2.2] tetramethylnaphthaleneophane (43)*

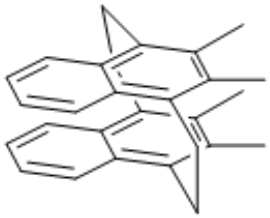

^{1}H NMR (300 MHz, Chloroform-*d*) δ 7.44 – 7.35 (dd, 4H, ArH), 6.83 – 6.70 (dd, 4H, ArH), 3.84 – 3.74 (m, 4H, CH_2Ar), 3.58 – 3.48 (m, 4H, CH_2Ar), 2.28 (s, 12H, ArMe).

Yield: 50%

Anti*-[2.2] tetramethylnaphthaleneophane (44)*

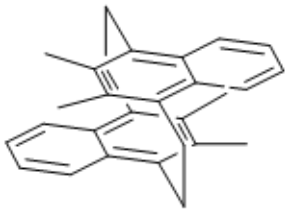

^{1}H NMR (300 MHz, Chloroform-*d*) δ 7.86 (dd, *J* = 6.3, 3.3 Hz, 4H, ArH), 7.24 – 7.18 (dd, *J* = 6.3, 3.3 Hz ,4H, ArH), 3.83 – 3.62 (m, 4H, CH_2Ar), 3.58 – 3.39 (m, 4H, CH_2Ar), 1.61 (s, 12H, ArMe).

Yield: 50%

Procedure for the nitrosolation and rearrangement of *Anti*-5,8,13,16-tetramethyl-4,7,12,15-tetraamido[2.2]paracyclophane

A flask was charged with 0.050 g (0.101 mmol) of *Anti*-5,8,13,16-tetramethyl-4,7,12,15-tetraamido[2.2]paracyclophane followed by 6 mL of acetic acid and 12 mL of acetic anhydride. The reaction solution was then cooled to 0 °C and was charged with three equivalents of $NaNO_2$ per amide group (0.0840 g) (1.22 mmol). Upon addition of the $NaNO_2$ the reaction flask was quickly stoppered. The reaction solution turned a bright blue color which was followed by the

evolution of a brown/yellow gas. Within 15 minutes all of the gas had been consumed resulting in the blue solution transitioning to a dark yellow which gradually turned a darker red. The reaction mixture was then allowed to stir at 0 °C for one hour, followed by stirring at room temperature for 1 hour. Reaction workup was carried out by pouring the reaction mixture into a vacuum flask, which was then fitted with a glass funnel. A gentle vacuum was then pulled, pulling air over the reaction solution, which allowed for the quick evaporation of the acetic acid/acetic anhydride solvent mixture at room temperature. Evaporation yielded a yellow/white solid mixture of what was assumed to be sodium acetate and the N-aromatic nitrosamide. The solid mixture was then extracted with dichloromethane which readily dissolved the N-aromatic nitrosamides without dissolving the assumed sodium acetate. The resulting heterogenous mixture was then passed through a cotton plug to give a deep red solution which upon drying yielded a red oil which upon washing with a 1:1 mixture of ethyl acetate and hexanes gave an off white/tan solid. Heating the dried material in 100% acetic anhydride for 2 hrs at 80 °C gave a light-yellow solution which was concentrated under reduced pressure to give a light orange solid. Repeated column chromatography of the material on neutral alumina with acetonitrile as the mobile phase gave the *Anti*-5,8,13,16-tetramethyl-4,7,12,15-tetraacetoxy[2.2]paracyclophane as a semi pure compound.

Anti*-5,8,13,16-tetramethyl-4,7,12,15-tetraacetoxy[2.2]paracyclophane (45)*

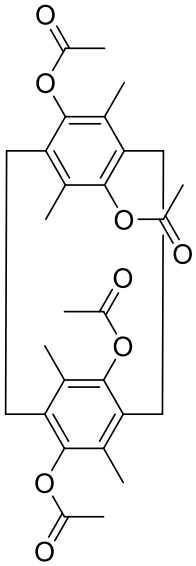

^{1}H NMR (500 MHz, Chloroform-*d*) δ 3.19 – 3.03 (m, 4H, CH_2Ar), 2.69 – 2.53 (m, 4H, CH_2Ar), 2.23 (s, 12H, Me-C=O), 2.06 (s, 12H, ArMe).

^{13}C NMR (500 MHz, Chloroform-*d*) δ 14.71, 25.54, 26.99 (CH_2Ar), 137.16, 142.92, 152.27, 182.09.

Shift (ppm) multiplicity, coupling (Hz) DEPT	Proton	2D spectra shows correlation to protons at δ (ppm)		
		COSY	HSQC	HMBC
14.7	2.06	-	2.03	-
25.5	2.23	-	2.23	-
26.9	2.61	3.12	3.12, 2.61	-
137.1	3.12	2.61	-	2.03, 2.62, 3.12
142.9	-		-	2.03, 2.62, 3.12
152.2	-		-	2.03, 2.62, 3.12
182	-		-	2.23

IR: 2937.27 cm^{-1}, 1748 cm^{-1} (O-C=O)

Yield: 18%

Chapter 5: Fabrication of Inorganic Organic Hybrids

Organic–inorganic hybrids are promising materials due to their strong performance properties and ease of fabrication, with their light emission/adsorption and electron conductivity properties being one of the main areas of interest. Most commercial semiconducting light adsorption/emission devices rely on fully inorganic materials. In the case of photovoltaic devices, it is semi-conductive silicon that is responsible for the generation of a photo current in the presence of light by nature of its small band gap. In the case of light emitting diodes or LED's it is a number of different mixed inorganic compounds that are responsible for the emission of visible light with aluminum gallium nitride and zinc selenide being common materials.[132,133,134] In all cases light production arises from the wide bandgaps of these materials resulting in light being produced when an electron moves from the conduction band to the valence band.[133] In both cases the production of these inorganic materials requires the use of high temperatures to produce large ingots of the semiconducting material which must then be further processed into semiconducting wafers in a clean room facility resulting in a process that is both highly energy intensive as well time consuming.[59] In direct contrast to this are organic and organic–inorganic hybrid semiconductors which are readily formed through solution-based methods at moderate temperatures. Active devices can be made from these materials using low temperature solution-based methods which upon proper deposition yield a functional layer.[59]

The light emission properties of hybrid organic−inorganic materials are strongly dependent on their structural dimensionality, with 3D inorganic materials showing Wannier excitons which show small exciton binding energies (typically below 50 meV) and large distances between the excited electron and the corresponding hole (typically 100 Å).[59,133,134] Conversely, low-dimensional hybrid halides demonstrate much stronger charge localization and exciton binding

energies of 500 meV or greater, values that are comparable to those of bound Frenkel excitons in organic materials with radiuses of 10 Å (Figure 147).[59,136] Such high exciton binding energies

(A) Frenkel exciton (B) Wannier exciton

Figure 147: Diagram A shows a generalized example of a Frenkel exciton in which tight binding of the electron and hole are maintained. Diagram B shows a generalized example of a Wannier excition in which small binding energy on the electron and hole result in a large separation of the two species in the solid material.[59,136]

can accordingly result in stable excitons and excitonic emission due to charge recombination.[135,136,137] Therefore low-dimensional organic−inorganic hybrid halides are promising candidates for the development of light emitting materials.[59,136]

5.1 Fabrication of Hybrid Organic−Inorganic Halides of Group 12 Metals

A number of organic inorganic hybrid materials with desirable optical and electronic properties are known for group 3 metals through group 11 metals. Group 12 metal-based hybrid halides show a remarkable structural flexibility in their tunable dimensionality and tolerance of various organic cations. While hybrid materials containing group 12 metals have been previously reported the optical and electronic properties of the hybrid halides of group 12 metals remain largely unexplored.[104] In order to probe the behavior and potential applications of group 12 metal hybrids the previously reported organic trimethyl(2,3,4,5,6-pentamethylbenzyl)ammonium (denoted as (R)) bromide and iodide was used to prepare 0-D hybrid (R)-M-X halides, where M = Zn or Cd, and X = Br or I. This work has since been published in the journal ACS Omega.[61]

Trimethyl(2,3,4,5,6-pentamethylbenzyl)ammonium bromide was prepared from pentamethyl benzene by bromomethylation followed by treatment with trimethylamine gas (Figure 148).[61]

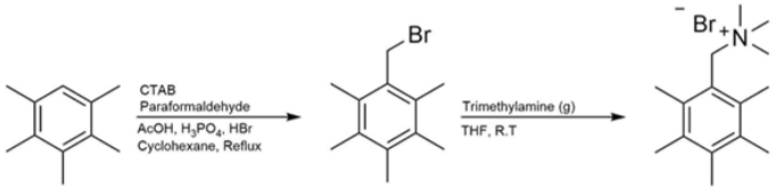

(46)

Figure 148: Synthesis of trimethyl(2,3,4,5,6-pentamethylbenzyl)ammonium bromide.

Trimethyl(2,3,4,5,6-pentamethylbenzyl)ammonium iodide was prepared from pentamethyl benzene by bromomethylation followed by treatment with excess dimethylamine (2.5 equivalents) in diethyl ether. The reaction was quenched after a 24-hour period by the addition of magnesium sulfate to the reaction solution. The reaction mixture was then filtered and dried under reduced pressure to give the desired amine. The resulting dimethyl(2,3,4,5,6-pentamethylbenzyl)amine was then methylated with methyl iodide in THF to give the desired trimethyl(2,3,4,5,6-pentamethylbenzyl)ammonium iodide, both products were characterized by ^{1}H-NMR as well as by their melting point (Figure 149).[61] Crystals of inorganic organic hybrids and their

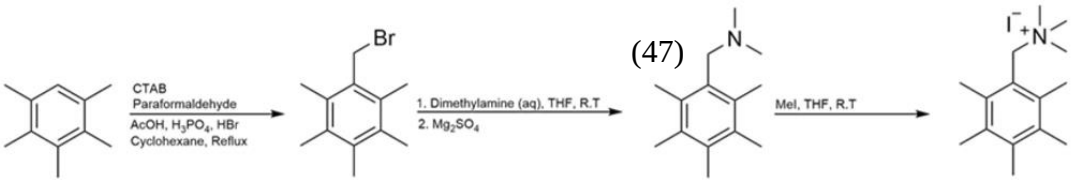

(48)

Figure 149: Synthesis of trimethyl(2,3,4,5,6-pentamethylbenzyl)ammonium iodide.

characterization were carried out by Rachel Roccanova, while low temperature measurements and DFT calculations of the materials were carried out by the other respective authors. Crystals of (R)$ZnBr_3$(DMSO) were made by separately solvating (R)X (X =Br) in 2 mL of DMSO and ZnX_2 in 1 mL of methanol and then mixing the stoichiometric 1:1 molar ratio solutions together. The solution was then heated to 65 ℃ which gradually yielded crystals as evaporation occurred (Figure 150). Attempts to form the zinc iodide analogs all resulted in decomposition products. Crystals of

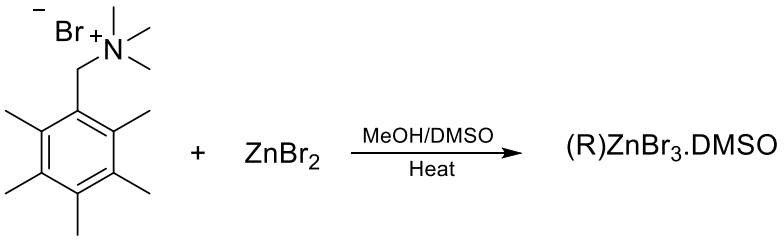

Figure 150: Reaction of trimethyl(2,3,4,5,6-pentamethylbenzyl)ammonium bromide with zinc bromide to form the corresponding zinc hybrid.

$(R)_2CdBr_4$·DMSO were made by a stoichiometric reaction with 2:1 molar ratio of (R)Br/$CdBr_3$ at 65 °C which gradually gave colorless block crystals (Figure 151). Crystals of (R)CdI_3(DMSO)

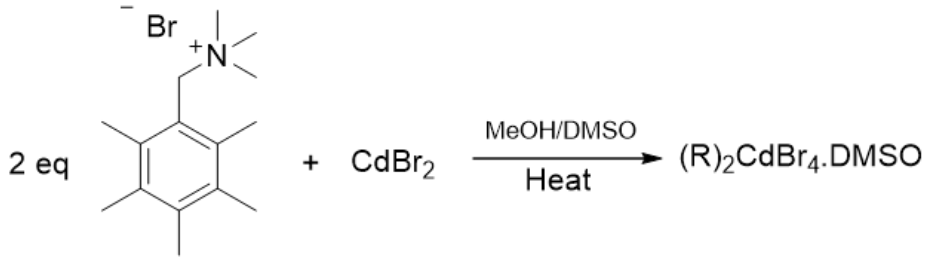

Figure 151: Reaction of trimethyl(2,3,4,5,6-pentamethylbenzyl)ammonium bromide with cadmium bromide to form the corresponding cadmium hybrid.

crystals were made through slow evaporation of their stoichiometric solutions as light-yellow blocks over a 3-week crystallization period. Single crystals were obtained using low-temperature solution reactions (Figure 152). X-ray crystallography showed all compounds formed 0-D crystal

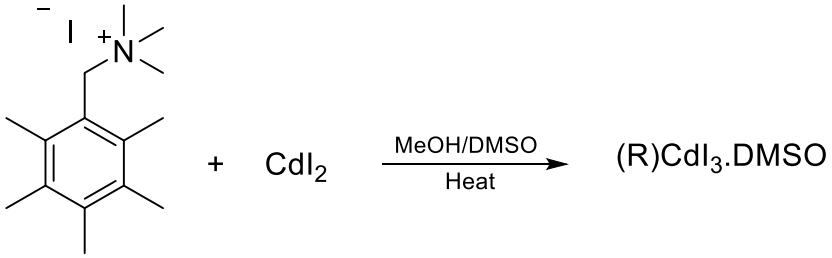

Figure 152: Reaction of trimethyl(2,3,4,5,6-pentamethylbenzyl)ammonium iodide with cadmium iodide to form the corresponding cadmium hybrid.

structures featuring alternating layers of organic cations and inorganic anions that are based on tetrahedral coordination around the metal cations, while powder x-ray diffraction showed that all formed compounds contained no impurities.[61] The crystal structure of (R)$ZnBr_3$(DMSO) showed that the DMSO had been incorporated into the hybrid structure with DMSO forming a direct

coordination to the metal through the oxygen of the DMSO (Figure 153). Direct DMSO

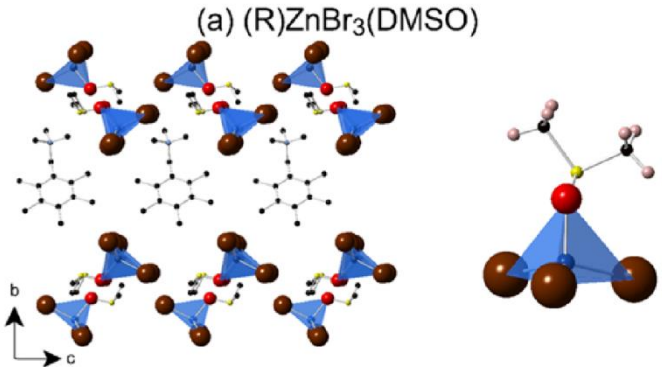

Figure 153: Crystal structure of (R)$ZnBr_3$(DMSO).

coordination was also observed in the crystal structure of (R)CdI_3(DMSO) In the case of (R)$_2CdBr_4$· DMSO, DMSO was incorporated into the crystal structure as well, but showed no direct coordination to the metal due to the tetrahedral coordination of the halides (Figure 154).

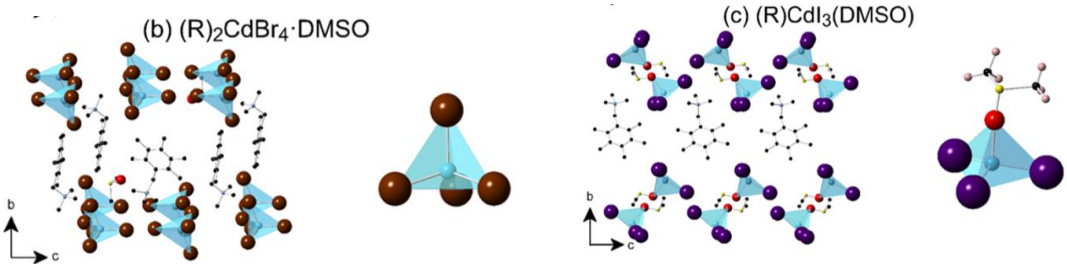

Figure 154: Crystal structures of (R)$_2CdBr_4$DMSO and (R)CdI_3(DMSO).

Stability studies of the formed compounds were carried out by allowing the compounds to sit under ambient conditions for a period of one month. Periodic powder x-ray diffraction spectra were collected on the compounds and showed that all compounds were air stable for several days with (R)$ZnBr_3$(DMSO) and (R)$_2CdBr_4$·DMSO being more robust than (R)CdI_3(DMSO) which showed significant losses to crystallinity over a period of two weeks.[61]

5.2 Optical Properties of (R)$ZnBr_3$(DMSO), (R)2$CdBr_4$·DMSO, and (R)CdI_3(DMSO)

The light emission properties of the fabricated metal organic hybrids were carried out through optical absorption, photoluminescence, and photoluminescence excitation studies. Optical absorption spectra show a sharp absorption at ~290 nm, accompanied by a shoulder at 315, 320, and 360 nm for (R)$ZnBr_3$(DMSO), (R)2$CdBr_4$·DMSO, and (R)CdI_3(DMSO), these absorptions were attributed to the organic cation. PLE spectra show the presence of a sharp peak at 386, 399, and 445 nm for (R)$ZnBr_3$(DMSO), (R)2$CdBr_4$·DMSO, and (R)CdI_3(DMSO) which was assigned to the excitonic absorption. All three compounds exhibited broadband emission spectra with full width at half maximum (FWHM) values ranging from 162 nm for (R)CdI_3(DMSO) to 188 nm for (R)$ZnBr_3$(DMSO) (Figure 155).[61]

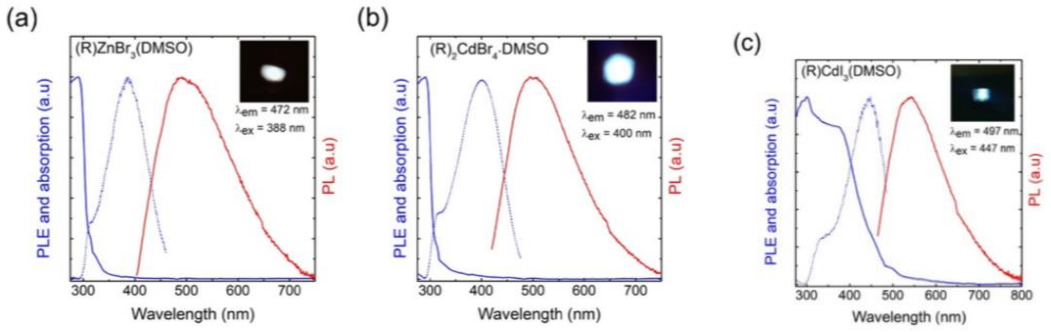

Figure 155: PL and PLE spectra of (R)$ZnBr_3$(DMSO), (R)2$CdBr_4$·DMSO, and (R)CdI_3(DMSO).

In the case of (R) $ZnBr_3$(DMSO) bright broadband white light emission was observed while blue light emission was observed for (R)2$CdBr_4$·DMSO and in the case of (R)CdI_3(DMSO) green light emission was observed. Photoluminescence Quantum Yield (PLQY) measurements showed that that (R)$ZnBr_3$(DMSO) had a PLQY of 3.07% while (R)2$CdBr_4$·DMSO had a PLQY of 0.32 % and (R)CdI_3(DMSO) had a PLQY of 0.27%. PLQY measurements of the organic cations themselves showed that the trimethyl(2,3,4,5,6-pentamethylbenzyl)ammonium bromide had a PLQY of 2.44% while the iodide had a PLQY of 0.42% demonstrating that the presence of zinc

bromide enhances the PLQY of the organic cation while the presence of cadmium bromide or iodide actually hinders the PLQY of the organic cation (Table 15).[61] These results also suggest that the observed light emission in the three different hybrids originates from the organic cation itself. This hypothesis was further supported by the fact that the photoluminescence behavior of

Table 15: Optical data for (R)$ZnBr_3$(DMSO), (R)2$CdBr_4$·DMSO, and (R)CdI_3(DMSO).

Hybrid	PLQY%	PLE_{max}(nm)	PL_{max}(nm)	Stokes shift (nm)
(R)$ZnBr_3$(DMSO)	3.07	386	491	105
$(R)_2CdBr_4$(DMSO)	0.32	399	501	102
(R)CdI_3(DMSO)	0.27	445	515	70
(R)Br	2.44	378	462	84
(R)I	0.42	416	514	98

(R)$ZnBr_3$(DMSO) and (R)2$CdBr_4$·DMSO was found to be temperature dependent. At room temperature the PL spectra of both hybrids shows only one broad band. Upon cooling the PL spectra of both hybrids shows additional peaks which resolve into sharp bands below 200 K (Figure 156).[104] The lack of any low temperature phase transitions for either hybrid along with the

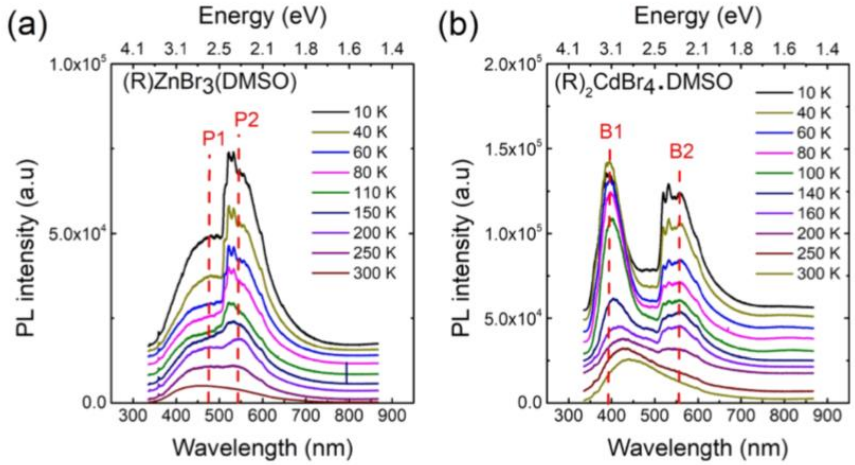

Figure 156: Low temperature PL spectra for (R)$ZnBr_3$(DMSO) and (R)2$CdBr_4$·DMSO.

fact that the observed low temperature behavior is quite similar for both hybrids supports the hypothesis that the observed emission is due to the organic cation. A number of different

phenomena could be responsible for the observed low temperature PL behavior such as exciton-phonon coupling. Photoluminescence lifetime measurements were also obtained for the hybrids and showed relatively short excitation lifetimes with (R)$ZnBr_3$(DMSO) giving lifetime measurements of 13 ns, while (R)$2CdBr_4$·DMSO and (R)CdI_3(DMSO) had lifetimes of 21.1 ns and 9.0 ns respectively.[61]

5.3 Electronic Structure Calculations

In order to further elucidate the role of the organic cation in the light emission behavior of the fabricated hybrids band structure calculations were performed in order to determine if and how the electronic structure of the organic cation was interacting with the electronic structure of the metal halides. In the case of (R)$ZnBr_3$(DMSO) band structure calculations showed that both the valence band maximum (VBM) and the conduction band minimum (CBM) consisted of the bonding and anti-bonding orbitals of the organic cation pi system. DFT calculations carried out using the PBE0 hybrid functional calculation demonstrated that the (R)$ZnBr_3$(DMSO) hybrid had a bandgap of 3.82 eV with the wavefunctions of the electron and hole are highly localized on the organic cation (Figure 157).[61,137,138]

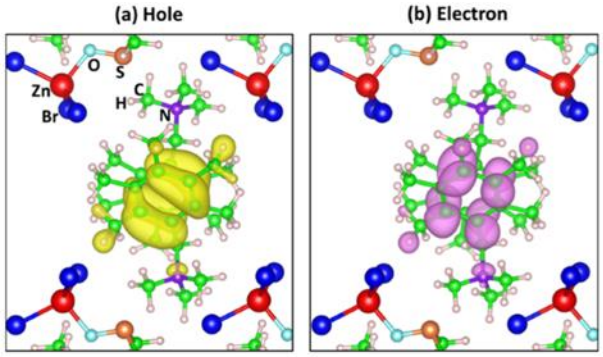

Figure 157: Results of DFT calculations demonstrating the localization of electrons and holes on the organic cation in the (R)$ZnBr_3$(DMSO) hybrid.

In the case of (R)2$CdBr_4$·DMSO and (R)CdI_3(DMSO) DFT calculations showed that the hybrid materials had a bandgaps of 3.61 eV and 3.39 eV respectively with the VBM of the hybrid structures consisting of the bonding orbitals of the organic cation pi system while the CBM of the hybrid structures consisted of the S orbitals of the metal halide. These results offer a potential explanation as to why PLQY enhancement was observed in the (R)$ZnBr_3$(DMSO) hybrid while PLQY diminishments where observed in the cadmium hybrids. The electronic structure of the (R)$ZnBr_3$(DMSO) hybrid is such that the orbitals of the zinc bromide do not participate in the formation of the conduction band leading to a high degree of exciton localization which is what gives rise to the observed PLQY.[61] In the case of the cadmium hybrids the participation of the cadmium S orbitals in the conduction band could serve to decrease exciton localization which in turn results in a lower probability of emissive electron hole recombination, which would explain the diminished PLQYS observed for the cadmium hybrids. This proposed explanation is supported by the band structure diagrams of the three hybrid materials. In the case of the zinc hybrid the band structure diagram shows that the VBM and CBM are significantly flat with negligible indirect bandgap character (Figure 158).[61,139,140] Based on the negligible indirect bandgap character in

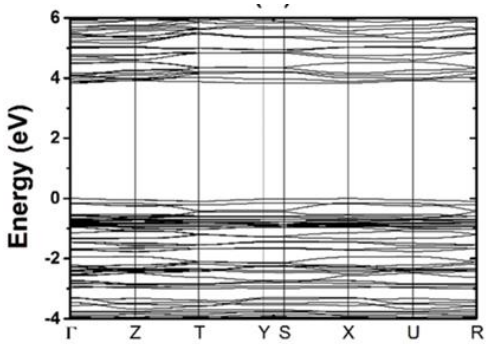

Figure 158: Band structure of (R)$ZnBr_3$(DMSO).[61]

the band structure it is likely that excitation can occur in a fashion that is similar to the processes seen for direct bandgap structures. In the case of the cadmium hybrid structures the indirect bandgap character of the band structures is more pronounced (Figure 159).[104] In band structures containing indirect bandgap character excitation and emissive recombination become more difficult due to the fact that phonon interactions are needed in order to allow the excited electron to move from the VBM to the CBM and vice versa. In the case of an excitation process a phonon

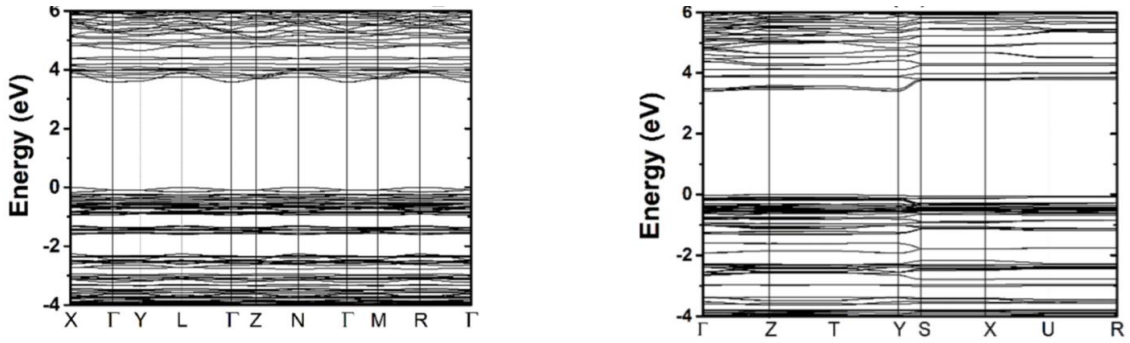

Figure 159: Band structures of $(R)_2CdBr_4$·DMSO and (R)CdI_3(DMSO).[61]

must be absorbed to allow for the transition from the VBM to the CBM, while in the case of an emission process a phonon must be emitted to allow the electron to fall from the CBM back to the VBM. A generalized example of these processes is outlined in Figure (160).[139,140,141] These phonon

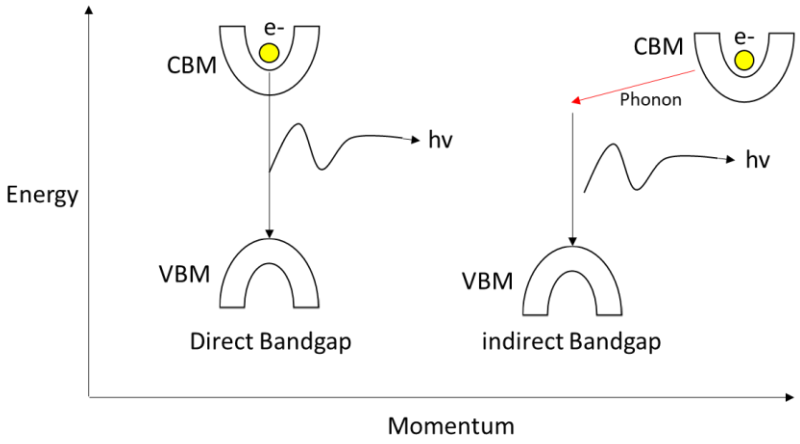

Figure 160: Generalized processes for emissive recombination in direct and indirect semiconductors. In the direct semiconductor the excited electron is able to fall from the CBM to the VBM by direct emission of light. In the

indirect semiconductor the excited electron must first emit a phonon, followed by the emission of light in order to fall from the CBM to the VBM.[139]

processes typically result in longer lived excitons which can diffuse or decay through non radiative processes which in turn results in less light emission. It is for these reasons that the majority of commercial LED's and other light emitting materials are made from direct band gap materials.

5.4 Fabrication of Iron Based Hybrid Organic−Inorganic Halides

In order to better understand the effect that organic cation bulk had on the light emission properties of 0-D organic-inorganic hybrids a series of methylated benzene organic cations were synthesized and used to prepare a series of iron based organic-inorganic hybrids. By varying the steric bulk of the organic cation while keeping the metal salt constant it was proposed that the effects of organic cation steric bulk and ionization energy on the bandgap and PLQY of the hybrid material could be readily determined. Iron was chosen as a prime target due to its low electron affinity, making it similar in electron donating behavior to zinc, and its low cost and low environmental toxicity relative to other metals such as lead. It was also hypothesized that the transition metal nature of iron would allow for the metal to participate in the excitation and emission process allowing for potentially stronger and possibly tunable light emission.

The organic cations used in the fabrication of these iron hybrids were trimethyl benzyl ammonium bromide salts with the methylation of the benzyl group ranging from the previously used trimethyl(2,3,4,5,6-pentamethylbenzyl)ammonium bromide all the way to the trimethyl-1-phenylmethylammonium bromide (Figure 161). All ammonium salts were prepared in the same

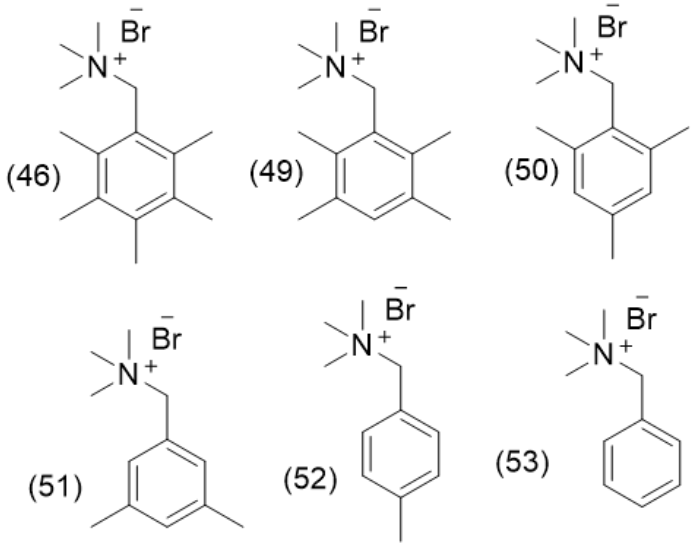

Figure 161: Synthesized ammonium salts used in the production of iron bromide organic hybrids.

manner as the initial trimethyl(2,3,4,5,6-pentamethylbenzyl)ammonium bromide. Compound (51) was prepared by radical bromination followed by treatment with trimethyl amine (Figure 162).

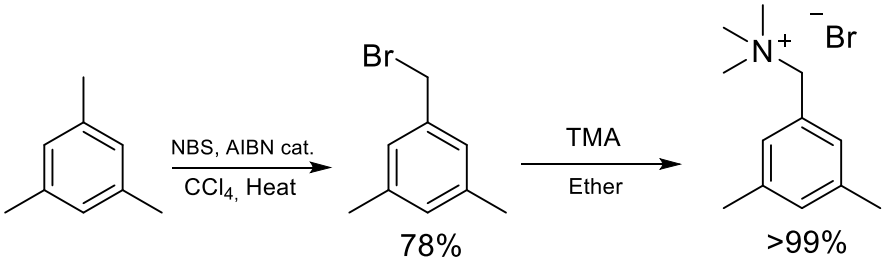

Figure 162: Synthesis of 1-(3,5-dimethylphenyl)-N,N,N-trimethylmethanammonium bromide (4).

Compounds (52) and (53) were prepared from their commercially available benzyl bromides by treatment with trimethyl amine gas.

Initial attempts at preparing the desired iron hybrids using the DMSO/MeOH solvent system that was used to prepare the zinc and cadmium hybrids reported earlier were met with failure due to the fact that in the presence of iron and DMSO all of the corresponding organic cations underwent elimination of the trimethyl amine group. These issues were resolved by simply using straight methanol as the solvent system which resulted in no degradation of the organic cations. Crystals of the desired iron hybrids were obtained over the period of a few days by slowly

heating 1:1 stoichiometric solutions of iron tri bromide with the corresponding organic cation to evaporation at 65 °C. Crystals were formed for all organic-inorganic hybrids, with the exception of N,N,N-trimethyl-1-phenylmethylammonium bromide (6) which proved be too hygroscopic and unstable to result in crystal formation (Figure 163). X-ray crystallography showed all compounds formed 0-D crystal structures featuring alternating layers of organic cations and inorganic anions.

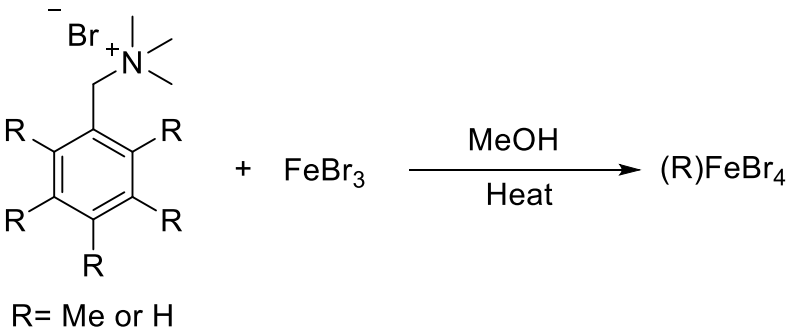

Figure 163: General synthesis of Iron based organic inorganic hybrids.

The crystal structures of the hybrids, made from compounds 1, 2, 3, and 5 all showed structures featuring alternating layers of pi stacked organic cations and inorganic anions that are based on tetrahedral coordination around metal cations with normal bond lengths and bond angles for both the organic and metal halide portions of the hybrid structures. These single crystal structures in conjunction with powder x-ray diffraction spectra demonstrated that targeted compounds were successfully fabricated (Figures 164-167).

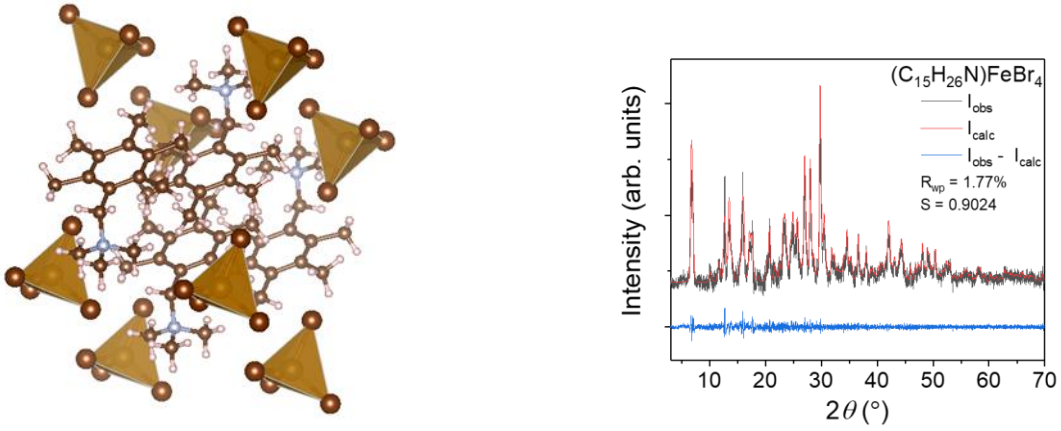

Figure 164: Single crystal structure and powder x-ray data for the pentamethylammonium iron bromide hybrid.

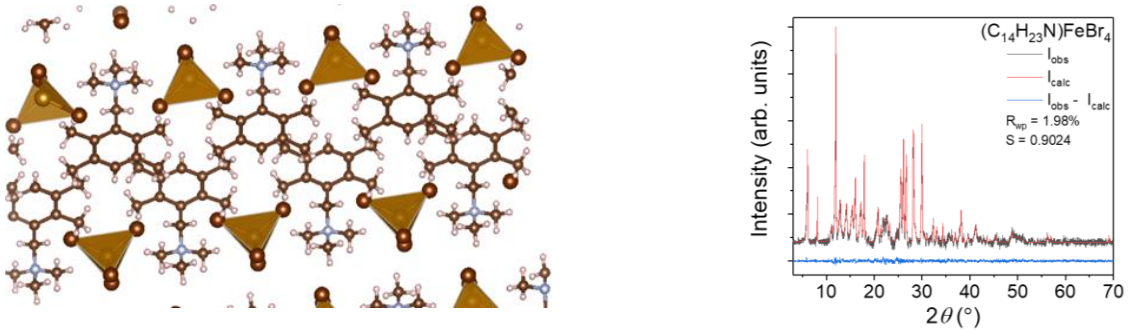

Figure 165: Single crystal structure and powder x-ray data for the tetramethylammonium iron bromide hybrid.

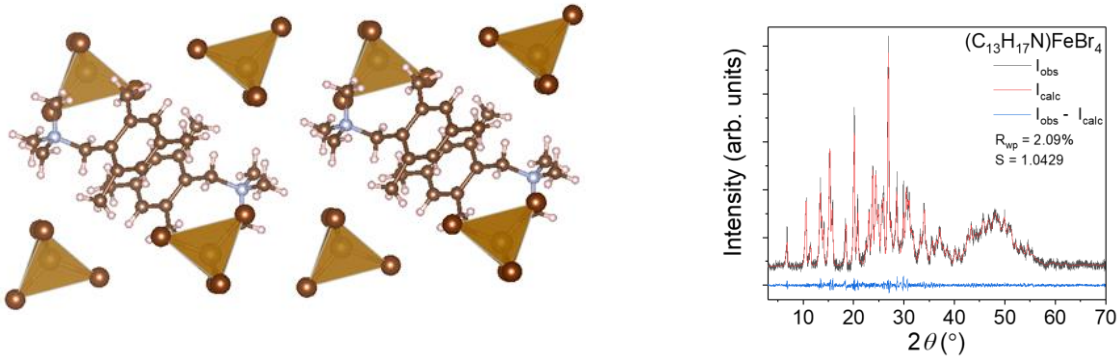

Figure 166: Single crystal structure and powder x-ray data for the trimethylammonium iron bromide hybrid.

Figure 167: Single crystal structure and powder x-ray data for the monomethylammonium iron bromide hybrid.

In the case of the iron bromide hybrid made from compound 4 single crystal data showed that the structure of the hybrid material consisted of alternating layers of pi stacked organic cations and bridging metal halides in which a single bromide was shared between two iron centers which

presents an unusual structure resulting in distortions of the iron tetrahedra (Figure 168). Powder XRD analysis of the hybrid material showed impurities within the material. The presence of impurities suggests that a redox event or disproportionation occurred which is what led to the formation of the bridged iron halides.

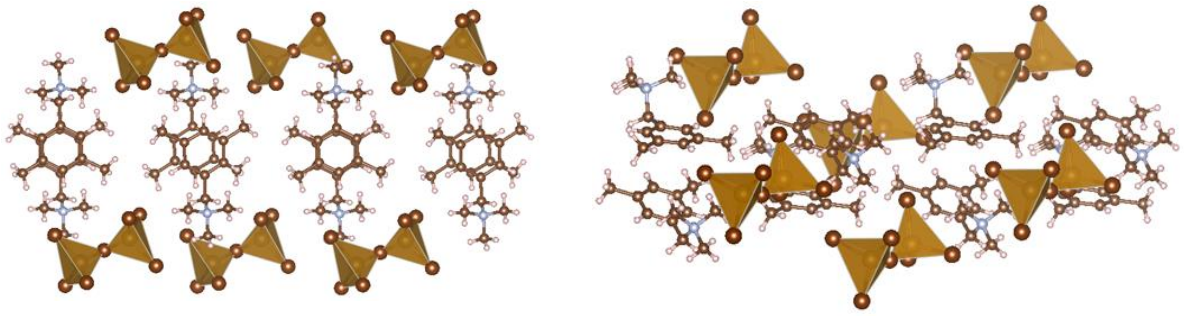

Figure 168: Single crystal structure of the dimethylammonium iron bromide hybrid, demonstrating the bridging metal halides.

5.5 Optical Properties of Iron Based Hybrid Organic-Inorganic Halides

Upon successful fabrication and structural characterization of the desired hybrid materials optical measurements were attempted on all of the fabricated hybrids. The light emission properties of the fabricated metal organic hybrids were carried out through photoluminescence, and photoluminescence excitation studies. The optical bandgaps of the different hybrids were measured using diffuse reflectance spectroscopy. Photoluminescence, and photoluminescence excitation studies of the iron-trimethyl(2,3,4,5,6-pentamethylbenzyl)ammonium bromide hybrid demonstrated that the material emitted bluish-yellow light with PL and PLE measurements showing an excitation wavelength of 326 nm and an emission wavelength of 397 nm and a PLQY of 5.32% which shows a marked improvement relative to the zinc hybrid that was previously discussed (Figure 169).[61] In going from the pentamethyl system to the lower methylated systems a significant drop in PLQY was observed. Iron- trimethyl(2,3,5,6-tetramethylbenzyl)ammonium

bromide was found to be a blue light emitter. PL and PLE measurements showed an excitation wavelength of 334 nm and a strong emission wavelength at 394 followed by a weaker emission at

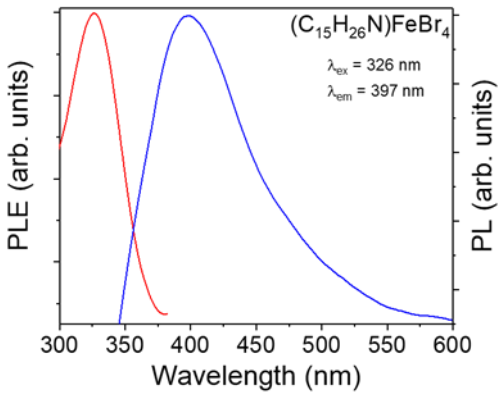

Figure 169: PL and PLE spectra and for the pentamethyl iron bromide hybrid.

571 nm and a PLQY of 1.42% (Figure 170). The large emission peak at 394 nm was attributed

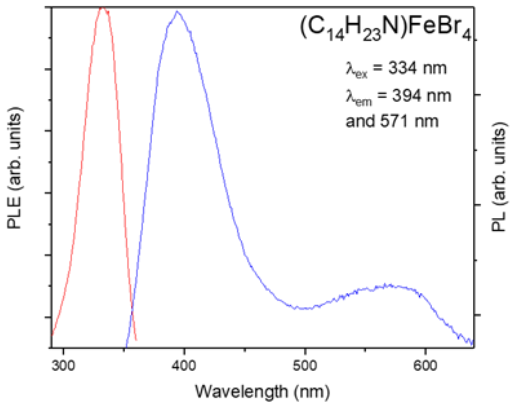

Figure 170: PL and PLE spectra for the tetramethyl iron bromide hybrid.

to normal exciton recombination while the smaller emission peak at 571 nm was attributed to the self-trapping of excitons. Self-trapping of excitons occurs when excitons interact strongly with the crystal lattice through phonon interactions resulting in exciton moving to a lower energy level without immediate recombination. The exciton can that recombine to give emission at a lower wavelength or undergo reexcitation (Figure 171).[139,140] PL and PLE measurements of iron-trimethyl(2,4,6-trimethylbenzyl)ammonium bromide demonstrated that the hybrid was also a blue

light emitter with an excitation wavelength of 326 nm and a emission wavelength at 400 nm and a PLQY of 1.81 % which shows a small increase relative to the PLQY of the iron- trimethyl(2,3,5,6-

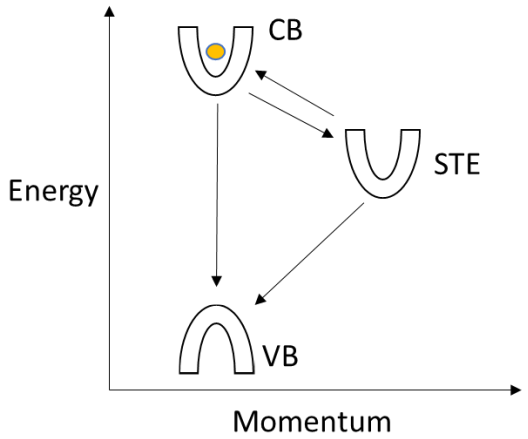

Figure 171: Generalized process by which a formed exciton can become self-trapped by phonon interactions. A excited electron in the conduction band (CB) and recombine with the hole in the valence band (VB) or can interact with the crystal lattice through phonon interactions resulting in the electron moving to a lower energy state that is not aligned with the valence band containing the electron hole preventing recombination in a similar manner to what is observed for indirect bandgap systems (Figure 160). The self-trapped exciton (STE) can then undergo recombination through further lattice interactions resulting in emission or can undergo excitation to a higher energy level.[139,140]

tetramethylbenzyl)ammonium bromide hybrid (Figure 172). PL and PLE measurements of the

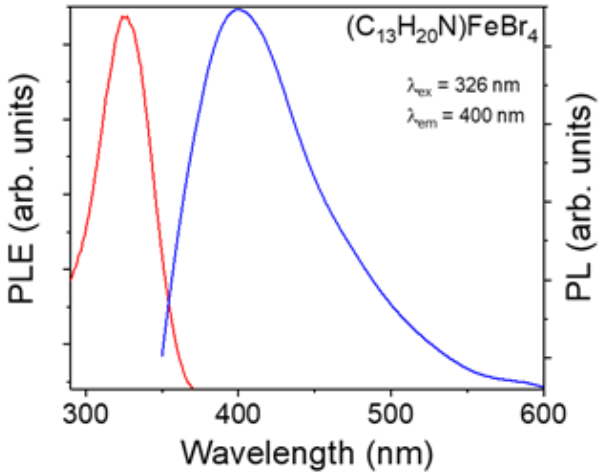

Figure 172: PL and PLE for the trimethyl iron bromide hybrid.

iron hybrid of compound 4 demonstrated that the compound emitted blue light with an excitation wavelength of 325 nm and an emission wavelength at 425 nm (Figure 173). PL and PLE measurements of the iron hybrid of compound 5 demonstrated that the compound emitted blue

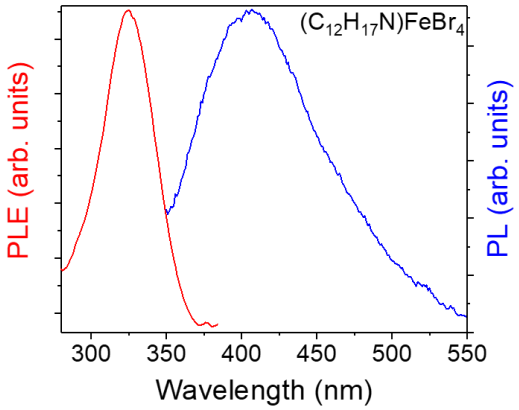

Figure 173: PL and PLE spectra for the dimethyl iron bromide hybrid (0.46 % PLQY).

light with an excitation wavelength of 380 nm with two shoulder peaks and an emission wavelengths at 430 nm and 460 nm (Figure 174). Working under the assumption that the organic

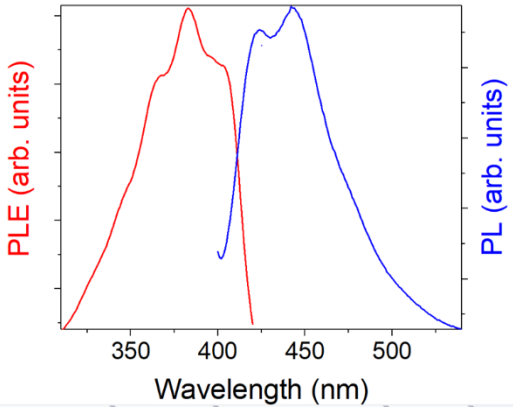

Figure 174: PL and PLE spectra for the monomethyl iron bromide hybrid. (0.47% PLQY).

cations were acting as luminescent centers in these hybrid materials, in a similar fashion to what was observed for the previously discussed (R)$ZnBr_3$(DMSO) hybrid, PLQY measurements were obtained for the free organic salts giving PLQY values of 2.44%, 0.08%, and 0.62%, 0.46%, and

0.47% for the pentamethyl, tetramethyl, and trimethyl, dimethyl, and mono methyl salts respectively. The PLQY trend observed in the iron hybrids follows the same trend observed in the PLQY's of the free organic salts with the pentamethyl bromide giving the highest PLQY value followed by a significant drop for the tetramethyl bromide, which is followed by a small increase for the trimethyl bromide, suggesting that the organic cations are the luminescent centers in these hybrids as well. It is important to note that in all cases the presence of iron bromide resulted in significant improvements in the PLQY values relative to the free salts.

In order to determine if the steric bulk or ionization potentials of the organic cations had any impact of the electronic properties of the hybrid materials diffuse reflectance measurements were performed to determine the optical bandgap of the hybrid materials. Diffuse reflectance measurements of the compounds showed that the optical bandgap of the hybrids decreased as steric bulk decreased with the optical bandgap values being 2.17 eV, 2.00 eV, and 1.98 eV, 1.97 eV, and 1.85 eV respectively (Figure 175). These results suggest that steric bulk plays a dominant role

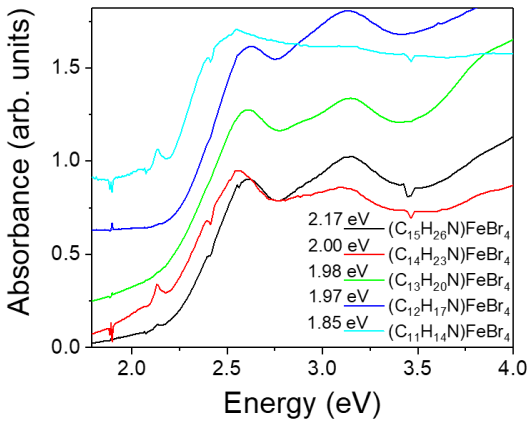

Figure 175: Diffuse reflectance spectra of the organic cation iron bromide hybrids.

in determining the electronic structure of the resulting organic inorganic hybrids. Diffuse reflectance measurements demonstrated that as the steric bulk of the organic cation decreases so does the bandgap of the hybrid material with the largest changes in the optical bandgap being

observed for the trimethyl, dimethyl and mono methyl benzene hybrids. This decrease in bandgap is seemingly due to the reduction in the space between the metal halides which is reflected in the crystal structures of the fabricated hybrids. The light emission behavior of the resulting hybrids is less straight forward as neither steric factors nor ionization potential values seem to trend well with the corresponding light emission behavior.

Importantly, what does seem to be an excellent predictor for the performance of these 0-D organic inorganic hybrid materials is the PLQY behavior of the free organic cations. As these species are relatively isolated both physically and electronically within the metal hybrid the majority of the light emission properties of the hybrid are due to the organic cation and as such, the development of organic-inorganic hybrids using organic cations with high PLQY performance is seemingly a promising way of readily improving and tuning the light emission behavior of these organic cations potentially paving the way more efficient light emitting materials.

5.6 Conclusions and Future Work

It has been demonstrated that functional light emitting 0-D organic inorganic hybrids can be fabricated using readily synthesizable bulky organic cations. It has also been shown that interactions between the metal halides and the organic cations do occur despite the large steric bulk of the organic cations. These interactions can serve to enhance or diminish light emission properties of these hybrids relative to the light emission properties of the free organic cations. Examples of improvements in light emission properties were observed in the reported zinc pentamethyl hybrid and as well as in all of the iron hybrids with the iron pentamethyl hybrid showing the greatest improvement in light emission as exhibited by its 5.32% PLQY value. The improvement in light emission for these systems is attributed to the fact that the electronic structure

of the light emitting organic cations is separated from the electronic structure of the metal halides due to the steric bulk of the cation as well as by differences in energy levels resulting in highly localized excitations which then quickly recombine to give off light.

This hypothesis is supported by the fact that interactions between the electronic structure of the organic cation and the electronic structure of the metal halide were observed for both pentamethyl cadmium hybrids, both of which suffered from reduced PLQY values relative to the free organic cation. This work also demonstrates that the color of the light emitted by these hybrid systems in potentially tunable by varying the metal halide, as was seen in the light emission of the pentamethyl zinc hybrid vs the pentamethyl iron hybrid. In the case of the zinc hybrid white light emission was observed while in the case of the iron hybrid yellow light emission was observed. This work lays a solid foundation for the design and fabrication of 0-D organic inorganic light emitting hybrid materials through the use of light emitting bulky organic cations, but a great deal of future work is needed in order to realize 0-D light emitting materials that will be competitive with commercially available light emitting devices.

Immediate future work should focus on understanding the interactions between organic cations and the metal halides present in the hybrid structure. While this work has readily demonstrated that improvements in light emission can be obtained by combining light emitting organic cations with metal halides the mechanism behind this improvement is still not well understood.[142] Determining how the presence of metal halides improves the light emission properties of organic cations will directly lead to the development of higher performing light emission materials.[142] This work demonstrates that the fabrication of 0-D organic inorganic hybrids is a promising method for the development of light emitting materials for LED or scintillator applications. Further enhancements in these materials can be realized by using emissive

organic cations with intrinsically high PLQY behavior in conjunction with metal halides that also exhibit strong emission properties. The presence of the metal halide could serve to improve the light emission behavior of the organic cation as demonstrated in this work while also acting as an emitter in its own right. The ability to match metal halides and organic cations that emit different colors can allow for the fabrication of inorganic organic hybrids that demonstrate strong color mixing leading to tunable light emitting materials.

5.7: Experimental Methods

General Methods:

Unless otherwise noted, all starting materials and reagents were obtained from commercial suppliers and used without further purification. All solvents were used as obtained unless noted. NMR spectra were recorded on a Varian VNMRS 300, 400, and 500 MHz NMR spectrometers. Chemical shifts are expressed in ppm relative to solvent signals. NMR spectra were processed using Mnova (www.mestrelab.com/software/mnova-nmr). The preparation and characterization of the reported organic inorganic hybrids was carried out by Rachel Roccanova using the methods reported in chapter 5. Photoluminescence measurements were carried out on a Horiba Fluorolog spectrofluorometer while diffuse reflectance measurements were carried out on a Lambda 750 Uv-vis spectrometer. Single crystal and powder x-ray diffraction data was collected using Bruker Apex CCD diffractometer with a graphite monochromated Mo Kα (λ = 0.71073 Å) radiation and a Rigaku MiniFlex600 system equipped with a D/teX detector using a Ni-filtered Cu Kα radiation source. Crystal structures were visualized using ccdc Mercury software (http://www.ccdc.cam.ac.uk/products/mercury/). Temperature dependence PL spectra were measured on single-crystal samples using a double monochromator U1000 equipped with a photomultiplier. Calculations were performed by Mao-Hua Du based on DFT implemented in the VASP code. The interaction between ions and electrons was described by the projector augmented wave method. The kinetic energy cutoff of 400 eV for the plane-wave basis was used for all calculations. Electronic band structures and DOSs were calculated using the Perdew−Burke−Ernzerhof (PBE) exchange-correlation functional, whereas excitons were treated by using the more advanced hybrid PBE0 functional, which has 25% nonlocal Fock exchange. Previous PBE0 calculations have provided accurate results on exciton properties in hybrid

organic−inorganic halide perovskites. The relevant data for sections 5.1, 5.2, and 5.3 can be found in the publication: Saparov, B.; Roccanova, R.; Houck, M.; Yangui, A.; Han, D.; Shi, H.; Wu, Y.; Glatzhofer, D. T.; Powell, D. R.; Chen, S.; Fourati, H.; Lusson, A.; Boukheddaden, K.; Du, M. Broadband Emission in Hybrid Organic–Inorganic Halides of Group 12 Metals. *ACS Omega*. **2018**, *3*, 18791–18802. Compounds reported in the literature that lack spectral data are marked with an (*). Compounds not reported in the literature are marked with an (**). Coupling constants are reported for compounds not reported in the literature. Crystal structures are located in Appendix A.

Synthesis of N,N-dimethyl-1-(2,3,4,5,6-pentamethylphenyl)methylamine

A 100 mL round bottom flask was charged with 1.00 g of 1-(bromomethyl)-2,3,4,5,6-pentamethylbenzene (4 mmol) and THF (50 mL). Dimethylamine was introduced by adding 1.41 g of a 40 wt% aqueous solution (0.564 g dimethylamine, 12.5 mmol) dropwise and the reaction flask was stoppered. The solution was stirred magnetically for 24 hours, the reaction was quenched by the addition of solid Mg_2SO_4. The Mg_2SO_4 was removed by vacuum filtration, the filtrate was concentrated under reduced pressure for 24 hours to give product N,N,2,3,4,5,6-heptamethyl-benzylamine in 86 % yield a white crystalline solid.

N,N-dimethyl-1-(2,3,4,5,6-pentamethylphenyl)methylamine (47)

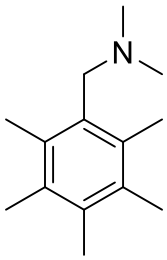

^{1}H-NMR (CDCl3, δ, ppm): 2.24 (s, 6H, CH3), 2.26 (s, 3H, CH3), 2.28 (s, 6H, N-CH3), 2.33 (s, 6H, CH3), 3.49 (s, 2H, CH2-N).

Yield: 86%

Saparov, B.; Roccanova, R.; Houck, M.; Yangui, A.; Han, D.; Shi, H.; Wu, Y.; Glatzhofer, D. T.; Powell, D. R.; Chen, S.; Fourati, H.; Lusson, A.; Boukheddaden, K.; Du, M. Broadband Emission in Hybrid Organic–Inorganic Halides of Group 12 Metals. *ACS Omega*. **2018**, *3*, 18791–18802.[61]

Synthesis of trimethyl(2,3,4,5,6-pentamethylbenzyl)ammonium iodide

A 100 mL round bottom flask was charged with 1.0 g of N,N-dimethyl-1-(2,3,4,5,6-pentamethylphenyl)methylamine (4.0 mmol) and THF (20 mL). Methyl iodide (1.4 g, 9.8 mmol) were added dropwise to the solution. The flask was stoppered, and the solution was stirred magnetically for 24 hours. Within the first 3 hours most of the product precipitated as a white solid. Solvent and excess methyl iodide were removed under reduced pressure to give product trimethyl (2,3,4,5,6-pentamethylbenzyl) ammonium iodide in 98% yield as a white polycrystalline solid.

Trimethyl(2,3,4,5,6-pentamethylbenzyl)ammonium iodide (48)

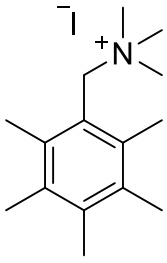

^{1}H NMR (CDCl3, δ, ppm): 2.25 (s, 6H, CH3), 2.29 (s, 3H, CH3), 2.44 (s, 6H, CH3), 3.34 (s, 9H, NCH3), 5.00 (s, 2H, CH2-N).

Yield: >98%

Saparov, B.; Roccanova, R.; Houck, M.; Yangui, A.; Han, D.; Shi, H.; Wu, Y.; Glatzhofer, D. T.; Powell, D. R.; Chen, S.; Fourati, H.; Lusson, A.; Boukheddaden, K.; Du, M. Broadband Emission in Hybrid Organic–Inorganic Halides of Group 12 Metals. *ACS Omega*. **2018**, *3*, 18791–18802.[61]

General Procedure for the bromomethylation of methylated benzenes

A three necked round bottom flask fitted with a reflux condenser was charged with 2.0 grams of the desired methylated benzene, 1.2 equivalents of paraformaldehyde, cetyltrimethylammonium bromide (CTAB) (0.035 g) (0.096 mmol), cyclohexane (20 mL), acetic acid (10 mL), and phosphoric acid (0.5 mL). The reaction mixture was stirred vigorously

(magnetic) and 10 mL of 48% hydrobromic acid was added using a dropping funnel attached to a side arm of the flask. The mixture was heated to 80 °C for 24 hours. The reaction mixture was cooled using an ice bath, diluted with 20 mL of water, transferred to an Erlenmeyer flask, and extracted three times with dichloromethane using a separatory funnel. The combined organic layers were dried over magnesium sulfate, which was removed by vacuum filtration, and the filtrate was concentrated under reduced pressure to give the bromomethylated product as either a solid or a viscous oil.

Procedure for the radical bromination of mesitylene

A round bottom flask was charged with 5.0 g (42 mmol) of mesitylene followed by followed by 100 mL of CCl_4. The solution was stirred magnetically while 7.4 g (42 mmol) of NBS was added to the stirring solution, followed by 0.0682 g (0.415 mmol) (cat. Amount) of recrystallized AIBN. The reaction was then heated at reflux for 6 hours or until succinimide was observed to float to the top of the reaction mixture indicating that all of the NBS had been converted into succinimide. Upon complete consumption of the NBS the reaction mixture was allowed to cool to room temperature before being filtered through a glass frit removing the succinimide and giving a clear solution of CCl_4. The solution was then concentrated under vacuum to the desired benzyl bromide. Characterization of the reaction mixture was performed using ^{1}H-NMR spectroscopy.

General Procedure for the synthesis of methylated benzene ammonium bromide salts

A round bottom flask was charged with 5.0 g of the desired benzyl bromide and diethyl ether (100 mL). The reaction flask was sealed with a rubber septum and an excess of trimethylamine gas was introduced into the reaction flask through a cannula needle. The reaction mixture was stirred magnetically overnight at room temperature. The white solid that formed was

collected by gentle vacuum filtration and dried under reduced pressure. In the case of hygroscopic ammonium salts the salts were dried under reduced pressure and stored under vacuum to prevent the introduction of water from the atmosphere.

Trimethyl(2,3,4,5,6-pentamethylbenzyl)ammonium bromide (46)

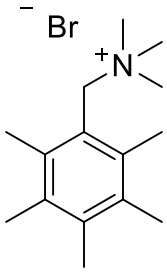

^{1}H-NMR (CDCl3, δ, ppm): 2.24 (s, 6H, CH3), 2.28 (s, 3H, CH3), 2.45 (s, 6H, CH3), 3.37 (s, 9H, N-CH3), 5.04 (s, 2H, CH2-N).

Yield: >98%

Saparov, B.; Roccanova, R.; Houck, M.; Yangui, A.; Han, D.; Shi, H.; Wu, Y.; Glatzhofer, D. T.; Powell, D. R.; Chen, S.; Fourati, H.; Lusson, A.; Boukheddaden, K.; Du, M. Broadband Emission in Hybrid Organic–Inorganic Halides of Group 12 Metals. *ACS Omega*. **2018**, *3*, 18791–18802.[61]

Trimethyl(2,3,5,6-tetramethylbenzyl)ammonium bromide (49)

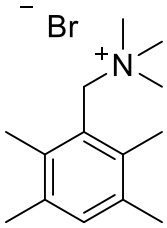

^{1}H NMR (300 MHz, Chloroform-*d*) δ 6.67 (s, 1H, ArH), 4.73 (s, 2H, $ArCH_2$), 3.29 (s, 9H, $N(CH_3)_3$), 2.31 (s, 6H, ArMe), 2.28 (s, 6H, ArMe).

Yield: >98%

Watanabe, H.; Jones, F. N.; Hauser, C. R. Formation of Cyclopropyl Ring by Action of Sodium Amide on *exo*-Methyleneammonim Ions Obtained from Rearrangement of Certain 2,6-Dimethylbenzyltrimethylammonium Ions. *J. Org. Chem.* **1969**, *34*, 2393-2397.[143]

Trimethyl(2,4,6-trimethylbenzyl)ammonium bromide (50)

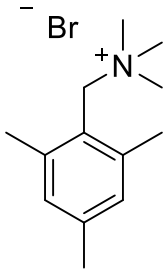

^{1}H NMR (300 MHz, Chloroform-*d*) δ 6.99 (s, 2H, ArH), 4.90 (s, 2H, CH_2Br), 3.45 (s, 9H, $N(CH_3)_3$), 2.53 (s, 6H, ArMe), 2.30 (s, 3H, ArMe).

Yield: >98%

Liu, X. Y.; Zhu, H. B.; Shen, Y. J.; Jiang, J.; Tu, T. Efficient N -heterocyclic carbene nickel pincer complexes catalyzed cross coupling of benzylic ammonium salts with boronic acids. *Chinese Chemical Letters*. **2017**, *28*, 350–353.[144]

Trimethyl(3,5-dimethylbenzyl)ammonium bromide (51)

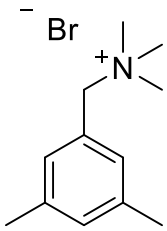

^{1}H NMR (300 MHz, Chloroform-*d*) δ 7.14 (d, 3H, ArH), 4.86 (s, 2H, CH_2-N), 3.41 (s, 9H, $N(CH_3)_3$), 2.32 (s, 6H, ArMe).

Yield: >98%

Li, J.; Zheng, Z.; Xiao, T.; Xu, P. F.; Wei, H. Nickel-Catalyzed Directed Benzylation of Ortho C−H Bonds in Aromatic Amides through C−H/C−N Cleavage. *Asian Journal of Organic Chemistry*. **2017**, *7*, 133–136.[145]

trimethyl(4-methylbenzyl)ammonium bromide (52)

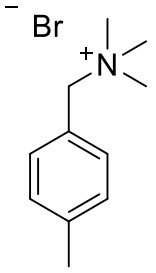

^{1}H NMR (300 MHz MeOH-*d*): δ 7.53 (d, 2H, ArH), 7.34 (d, 2H, ArH), 4.64 (s, 2H, CH_2-N), 3.14–3.17 (s, 9H, $N(CH_3)_3$), 2.39 (s, 3H, ArMe).

Yield: >98%

Li, J.; Zheng, Z.; Xiao, T.; Xu, P. F.; Wei, H. Nickel-Catalyzed Directed Benzylation of Ortho C−H Bonds in Aromatic Amides through C−H/C−N Cleavage. *Asian Journal of Organic Chemistry*. **2017**, *7*, 133–136.[145]

References

1. Roy, R. R., Jr. Conversion of aromatic amines and N-aromatic amides to O-aromatic esters, biphenyls, aromatic halides and energetic materials via nitrosamide intermediates. Ph.D. Dissertation, University of Oklahoma, Norman, OK, 2002.

2. Bamberger E., Ber., 1897, 30, 366.

3. Grieve W. S. M.; Hey D. H. The Rate of Decomposition of some p-Substituted Nitrosoacetanilides in Benzene. *J. Chem. Soc*. **1935**, *1797*, 689-691.

4. Robertson, A. K. Bidentate Reactive Intermediates. Ph.D. Dissertation, University of Edinburgh, **1971**.

5. Hey, D. H.; Webb, J. S.; Williams, G. H. Acylarylnitrosamines. Part VI. The rearrangement, decomposition, and deacylation of acylarylnitrosamines. *J. Chem. Soc*. **1952**, 4657-4665

6. Huisgen, R. Nitroso-acyl-amine und Diazo-ester II Acylwanderung und Acylablösung bei Nitroso-acyl-aniliden. *Justus Liebigs Annalen der Chemie*. **1951**, *573*, 163-181.

7. Huisgen, R.; Reinertshofer, J.; Nitroso-acyl-amine und Diazo-ester VII. Nitroso-caprolactam und seine Reaktionen. *Justus Liebigs Annalen der Chemie*. **1952**, *575*, 174-197.

8. De Tar, D. F. The Mechanism of the Reaction of N-Nitrosoacetanilide with Methanol. *J. Am. Chem. Soc*. **1951**, *73* (4), 1446–1449.

9. Huisgen, R.; Nakaten, H. Nitroso-acyl-amine und Diazo-ester IX Die Jacobsonsche Indazolsynthese und die Konfiguration der Diazo-ester. *Justus Liebigs Annalen der Chemie*. **1954**, *586*, 84-109.

10. Miles, P.; Suschitzky, H. Reactions of acylarylnitrosamines-II. *Tetrahedron.* **1962**, *18*, 1369-1376.

11. Rüchardt, C.; Freudenberg, B. Der thermische zerfall von nitroso-acylarylaminen. *Tetrahedron Lett*., **1964**, 3623-3628.

12. Binsch, G.; Rüchardt, C. Electron Spin Resonance Study of the Phenyldiazotate Free Radical, the Key Intermediate in Phenylations with Aromatic Diazo Compounds. *J. Am. Chem. Soc*. **1966**, *88*, 173–174.

13. Suschitzky H. Aromatic Fluorine as a Chemical Label for Detecting Reaction Mechanism. *Angew. Chem. internat. Edit*. **1967**, *6*, 596-607.

14.Chalfront G. R.; Hey, D. H.; Liang, K. Y.; Perkins, M. J. The effect of additives on the thermal decomposition of benzoyl peroxide in benzene. *Chem. Commun*. (London), **1967**, 367-369.

15. Cadogan, J. G.; Paton, R. M.; Thomson, C. New evidence on the mechanism of the decomposition of N-nitrosoacetanilide in solution: detection of a new radical. *J. Chem. Soc. D*. **1969**, 614-615.

16. Cadogan, J. G.; Paton, R. M.; Thomson, C. Acylarylnitrosamines. Part 111. Decomposition of 2,5-Di-(N-nitroso- acetamido)-l,4-di-t-butylbenzene and Related Compounds. *J. Chem. Soc. B.* **1971**, 583-595.

17. Cadogan, J. G.; Paton, R. M.; Thomson, C. New evidence on the mechanism of the decomposition of acetylarylnitrosamines in diethyl ether. *J. Chem. Soc. D,* **1970**, 229-229.

18. Glatzhofer, D. T.; Roy, R. R.; Cossey, K. N. Conversion of N-aromatic amides to O-aromatic esters. *Org. Lett*. **2002**, *4*, 2349–2352.

19. Hicks, C.; Duffy, B.; Hargaden, G. Synthesis and Modification of Octafluoro[2.2]Paracyclophane (Parylene AF4). *Organic Chemistry Frontiers*, **2014**, *1*, 716-725.

20. Dolbier, W. R.; Zhai, Y.; Wheelus, W.; Battiste, M. A.; Ghiviriga, I.; Bartberger, M. D. Remarkable Efficiency of the Aryne Chemistry of (Dehydro)octafluoro[2.2]paracyclophane When Using the Cadogan Method. *J. Org. Chem.* **2007**, *72*, 550-558.

21. Kürti, László, and Barbara Czakó. 2005. Strategic applications of named reactions in organic synthesis: background and detailed mechanisms. Amsterdam: Elsevier Academic Press.

22. Carey, Francis A., and Richard J. Sundberg. 2007. Advanced organic chemistry. Part B, Part B. New York, NY: Springer.

23. Evans, D. A.; Katz, J. L.; Peterson, G. S.; Hintermann, T. Total Synthesis of Teicoplanin Aglycon. *J. Am. Chem. Soc.* **2001**, *123*, 12411-12413.

24. Murray, C. D., Mechanisitic Studies Into the Reaction of Diazonium and Related Compounds. Ph.D. Dissertation, University of Edinburgh, 1974.

25. Shriver, J. A.; Flaherty, D. P.; Herr, C. C. Aryl Ethers from Arenediazonium Tetrafluoroborate Salts: from Neat Reactions to Solvent-mediated Effects. *Journal of the Iowa Academy of Science*. **2009**, *116*, 1-4.

26. Barclay, R. L.; Dust, J. M. Sterically hindered aromatic compounds. XI. Spectral and product studies of the decomposition of N-nitrosoacetanilides. *Can. J. Chem*. **1982**, *60*, 607.

27. Joergensen, K. A.; Ghattas, A. B.; Lawesson, S. O. Studies on organophosphorus compounds. XLV. Thiation of some sterically hindered N-nitrosamides. *Bulletin de la Societe Chimique de France*. **1984**, *204*, 5-6.

28. Anh, N. V.; Williams, R. M. Bis-semiquinone (bi-radical) formation by photoinduced proton coupled electron transfer in covalently linked catechol–quinone systems: Aviram's hemiquinones revisited. *Photochem. Photobiol. Sci*. **2012**, *11*, 957–961.

29. Philip M. Keehn, Stuart M. Rosenfeld,. “Cyclophanes Volume II”.1983, New York, Academic Press.

30. Collins, M. S.; Carnes, M. E.; Nell, B. P.; Zakharov, L. N.; Johnson, D. W. A facile route to old and new cyclophanes via self-assembly and capture. *Nat. Commun*. **2016**, *7*, 1-7.

31. Pellegrin, M. Contribution à l'étude de la réaction de Fittig. Recl. *Trav. Chim. Pays-Bas.* **1899**, *18*, 457–465.

32. Cram, D. J.; Steinberg, H.; Macro Rings. I. Preparation and spectra of the paracyclophanes. *J. Am. Chem. Soc.* **1951**, 73, 5691–5704.

33. Hopf, H. Acetylenic cyclophanes: emerging carbon-rich compounds for molecular construction and practical applications. *Tetrahedron*. **2008**, *64*, 11504–11516.

34. Rolf Gleiter, Henning Hopf., "Modern Cyclophane Chemistry". 2004, Wiley.

35. Kotha, S.; Shirbhate, M. E.; Waghule, G. T. Selected synthetic strategies to cyclophanes. *Beilstein J. Org. Chem*. **2015**, *11*, 1274–1331.

36. Longone, D. T., Simanyi, L. H., Paracyclophanes. III. Octamethyl[2.2]paracyclophane. A Highly Strained Cyclophane. *J. Org. Chem*. **1964**, *29*, 3245-3249.

37. Braun, C.; Brase, S.; Schafer, L. L. Planar-Chiral [2.2]Paracyclophane-Based Amides as Proligands for Titanium- and Zirconium-Catalyzed Hydroamination. *Eur. J. Org. Chem*. **2017**, 1760–1764.

38. Morvant, M. C., "Synthesis, properties, and applications of polynitro- and polyamino(2.2)paracyclophanes". Ph.D. Dissertation, University of Oklahoma, Norman, OK, 1996.

39. Tsuji, Y.; Yoshizawa, K. Current Rectification through π–π Stacking in Multilayered Donor–Acceptor Cyclophanes. *J. Phys. Chem. C*. **2012**, *116*, 26625−26635.

40. Beijun, C.; Kaifer, A. E. Cathodic Voltammetric Behavior of Pillar[5]quinone in Nonaqueous Media. Symmetry Effects on the Electron Uptake Sequence. *J. Am. Chem. Soc*. **2015**, *137*, 9788−979.

41. Marshak, M. P.; Lin, K.; Chen, Q.; Gerhardt, M. R.; Tong, L.; Kim, S. B.; Eisenach, L.; Valle, A. W.; Hardee, D.; Gordon, R. G.; Aziz, M. J. *Science*. **2015**, *349*, 1529-1532.

42. Rebafka, W.; Staab, H. A. An "Intramolecular Quinhydrone". *Angew. Chem. internat. Edit*. **1973**, 12, 776-777.

43. Staab, H. A.; Herz, C. P. Stereoisomeric Quinhydrones of the [2.2](1,4)Naphthalenophane Series. *Angew. Chem. Int. Ed. Engl*. **1977**, 16, 392-393.

44. Staab, H. A.; Volker, S. [2.2.2.2](1,2,4,5)Cyclophane Quinhydrone-A Donor-Acceptor Cyclophane with an Extremely Short Transannular Distance. *Angew. Chem. int. Ed. Engl*. **1978**, *17*, 756-757.

45. Taniguchi, H.; Morita, Y.; Agawa, T.; Nomura, E. Syntheses and NMR behavior of calix[4]quinone and calix[4]hydroquinone. *J. Org. Chem*. **1992**, *57*, 3662-367.

46. Neugebauer, F. A.; Staab, H. A.; Valenzuela, J.; Wartini, A. R. [2.2]Paracyclophane-4,7,12,15-tetrone, [2.2](1,4)Naphthalenophane-4,7,14,17-tetrone, and 1,4,8,11-Pentacenetetrone Radical Anions-A Comparative ESR Study. *Eur. J. Org. Chem*. **1998**, 221-227.

47. Ogoshi, T.; Demachi, K.; Masaki, K.; Yamagishi, T. Diastereoselective synthesis of meso-pillar[6]arenes by bridging between hydroquinone units in an alternating up-and-down manner. *J. Org. Chem*. **2011**, *76*, 328–331.

48. Norcross, B. E.; Becker, D.; Cukier, R. I.; Schultz, R. M. Paracyclophane phenols and derivatives. I. Synthesis and pKA values of 4-hydroxy- and 4-amino[2.2]paracyclophane. *J. Org. Chem*, **1967**, *32*, 220-222.

49. Xin, D.; Ma, Y.; He, F. Synthesis of new planar chiral [2.2]paracyclophane Schiff base ligands and their application in the asymmetric Henry reaction. *Tetrahedron: Asymmetry*, **2010**, *21*, 333-338.

50. Chen, J.; Zhu, Z.; Hong, M.; Guo, D.; Shi, J.; Tao, Z.; Chen, J. All-Solid-State Lithium Organic Battery with Composite Polymer Electrolyte and Pillar[5]quinone Cathode. *J. Am. Chem. Soc*. **2014**, *136*, 16461−16464.

51. Lukas Schmidt-Mende, Jonas Weickert., "Organic and Hybrid Solar Cells: An Introduction". 2016, Walter de Gruyter GmbH.

52. BCC Research., A History of Perovskite Solar Cells. BCC Research, 2018, http://blog.bccresearch.com/a-history-of-perovskite-solar-cells.

53. Weber, D. $CH_3NH_3PbX_3$, a Pb(II)-System with Cubic Perovskite Structure. *Zeitschrift für Naturforschung B*. **2014**, *33*, 1443–1445.

54. Mitzi, D. B.; Field, C. A.; Harrison, W. T. A.; Guloy, A. M. Conducting tin halides with a layered organic-based perovskite structure. *Nature*. **1994**, *369*, 467-469.

55. Miyasaka, T.; Kojima, A.; Teshima, K.; Shirai, Y. Organometal Halide Perovskites as Visible-Light Sensitizers for Photovoltaic Cells. *J. Am. Chem. Soc*., **2009**, *131*, 6050–6051.

56. Snaith, H. J.; Li, W.; Zhang, W.; Reenen, S. V.; Sutton, R. J.; Fan, J.; Haghighirad, A. A; Johnston, M. B.; Wang, L. Enhanced UV-light stability of planar heterojunction perovskite solar cells with caesium bromide interface modification. *Energy Environ. Sci*., **2016**, *9*, 490-498.

57. Jeangros, Q.; Sahli, F.; Werner, J.; Kamino, B. A.; Brauninger, M.; Monnard, R.; Paviet-Salomon, B.; Barraud, L.; Ding, L.; Diaz Leon, J. J.; Sacchetto, D.; Cattaneo, G.; Despeisse, M.; Boccard, M.; Nicolay, S.; Niesen, B.; Ballif, C. Fully textured monolithic perovskite/silicon tandem solar cells with 25.2% power conversion efficiency. *Nature Materials*. **2018**, *17*, 820–826.

58. Friend, R. H.; Zhao, B.; Bai, S.; Kim, V.; Lamboll, R.; Shivanna, R.; Auras, F.; Richter, J. M.; Yang, L.; Dai, L.; Alsari, M.; She, X.; Laing, L.; Zhang, J.; Lilliu, S.; Gao, P.; Snaith, H. J.; Wang, J.; Greenham, N. C.; Di, D. High-efficiency perovskite–polymer bulk heterostructure light-emitting diodes. *Nature Photonics*. **2018**, *12*, 783–789.

59. Saparov, B.; Mitzi, D. B. Organic–Inorganic Perovskites: Structural Versatility for Functional Materials Design. *Chem. Rev*. **2016**, *116*, 4558–4596.

60. Ma, B.; Zhou, C.; Lin, H.; Tian, Y.; Yuan, Z.; Clark, R.; Chen, B.; Van de Burgt, L.; Wang, J. C.; Zhou, Y.; Hanson, K.; Meisner, Q. J.; Neu, J.; Besara, T.; Lambers, E.; Djurovich, P. Luminescent zero-dimensional organic metal halide hybrids with near-unity quantum efficiency. *Chem. Sci*., **2018**, *9*, 586-593.

61. Saparov, B.; Roccanova, R.; Houck, M.; Yangui, A.; Han, D.; Shi, H.; Wu, Y.; Glatzhofer, D. T.; Powell, D. R.; Chen, S.; Fourati, H.; Lusson, A.; Boukheddaden, K.; Du, M. Broadband Emission in Hybrid Organic–Inorganic Halides of Group 12 Metals. *ACS Omega*. **2018**, *3*, 18791–18802.

62. Kubiak, C. P., Stires, J. C., McLaurin, E. Infrared spectroscopic determination of the degree of charge transfer in complexes of TCNE with methyl-substituted benzenes. *J., Chem. Commun*. **2005**, 3532-3534.

63. Chakraborty, D.; Das, R. Silver Triflate Catalyzed Acetylation of Alcohols, Thiols, Phenols, and Amines. *Synthesis*. **2011**, *10*, 1621-1625.

64. Nef, J. U. XXXVI.-Carboxyl-derivatives of benzoquinone. *J. Chem. Soc., Trans*. **1888**, *53*, 428-459.

65. Matsumura, G.; Yamagughi, K. Structure of N-aryl-N-nitrosoureas. *Acta Cryst*. **1992**, *48*, 1051-1054.

66. Sueyoshi, S.; Tanno, M. Studies on the Conformation of 1-Aryl-1-nitrosoureas and Related Compounds. *Chem. Pharm. Bull*. **1987**, *35*, 1353-1359.

67. Xi, Zhiwen.; Hao, Wenyan.; Wang, Pingping.; Cai, Mingzhong. Ruthenium(III) Chloride Catalyzed Acylation of Alcohols, Phenols, and Thiols in Room Temperature Ionic Liquids. *Molecules*. **2009**,*14*, 3528-3537.

68. Abiko, A.; Inoue, T.; Masamune, S. Mechanism of the Double Aldol Reaction: The First Spectroscopic Characterization of a Carbon-Bound Boron Enolate Derived from Carboxylic Esters. *J. Am. Chem. Soc*. **2002**, *124*, 10759–10764.

69. Pradal, A.; Toullec, P. Y.; Michelet, V. Gold-Catalyzed Oxidative Acyloxylation of Arenes. *Org. Lett*. **2011**, *13*, 6086–6089.

70. Sartori, G.; Casnati, G.; Bigi, F. Ortho-coordinated acylation of phenol systems. *J. Org. Chem*. **1990**, *55*, 4371-4377.

71. Chandrasekhar, S.; Kumar, H. V. The reaction of aspirin with base. *Tetrahedron Letters*. **2011**, **52**, 3561-3564.

72. Ohtaka, J.; Sakamoto, T.; Kikugawa, Y. A one-pot procedure for trifluoroacetylation of arylamines using trifluoroacetic acid as a trifluoroacetylating reagent. *Tetrahedron Letters*. **2009**, *50*, 1681-1683.

73. Anslyn, Eric V.,Dougherty, Dennis A.,Modern Physical Organic Chemistry. Sausalito, CA : University Science, 2006.

74. Anderson, K. W.; Ikawa, T.; Tundel, R. E.; Buchwald, S. L. The Selective Reaction of Aryl Halides with KOH: Synthesis of Phenols, Aromatic Ethers, and Benzofurans. *J. Am. Chem. Soc*. **2006**, 128, 10694-10695.

75. Koskinen, A.; Routasalo, T.; Helaja, J.; Kavakka, J. Development of Bis(2-picolyl)amine–Zinc Chelates for Imidazole Receptors. *Eur. J. Org. Chem*. **2008**, 3190–3199.

76. Du, S.; Li, Z.; Tian, Z.; Xu, L. Synthesis, Antifungal Activity and QSAR of Novel Pyrazole Amides as Succinate Dehydrogenase Inhibitors. *Heterocycles*. **2018**, 96, 74-85.

77. Rüchardt, C.; Hassmann, V. Eine Vereinfachung der Jacobsonschen Indazol-Synthese. *Synthesis*. **1972**, 375-376.

78. Powell, E.; P.; Lee, Y. H.; Partch, R.; Dennis, D.; Morey, T.; Varshney, M. Pi-Pi complexation of bupivacaine and analogues with aromatic receptors: implications for overdose remediation. *International Journal of Nanomedicine*. **2007**, *2*, 449-459.

79. Mohan, R.; Kalla, N.; Lim, J.; Bae, J.; Kim, I. Sulfated choline ionic liquid catalyzed acetamide synthesis by grindstone method. *Tetrahedron Letters*. **2017**, *58*, 1595-1599.

80.Shilpa, G.; Basavalinganadoddy, T. ^{1}H and ^{13}C NMR spectral studies on N-(j,k-dichlorophenyl)- and N-(j,k-dimethylphenyl)acetamides and substituted acetamides. *Zeitschrift fuer Naturforschung, A: Physical Sciences*. **2007**, *62*, 84-90.

81.Neumann, J. J.; Rakshit, S.; Droege, T.; Glorius, F. Palladium-Catalyzed Amidation of Unactivated C(sp3)-H Bonds: from Anilines to Indolines. *Angew. Chem. Int. Ed*. **2009**, *48*, 6892 –6895.

82.Giri, R.; Lam, J. K.; Yu, J. Q. Synthetic Applications of Pd(II)-Catalyzed C-H Carboxylation and Mechanistic Insights: Expedient Routes to Anthranilic Acids, Oxazolinones, and Quinazolinones. *J. Am. Chem. Soc*. **2010**, *132*, 686-693.

83.Abdelhamid, A. O.; Mohamed, G. S.; .Reaction with hydrazonoyl halides XXIII [1]: Synthesis and reactions of C-coumarinoyl-N-arylformohydrazonoyl bromides. *Heteroatom Chemistry*, **1999**, *10*, 355-362.

84.Cook, A. K.; Emmert, M.H.; Sanford, M. S. Steric Control of Site Selectivity in the Pd-Catalyzed C–H Acetoxylation of Simple Arenes. *Org. Lett*. **2013**, *15*, 5428-5431.

85.Penhoat, M.; Bohn, P.; Dupas, G.; Papamicaël, C.; Marsais, F.; Levacher, V. New development of Meyers' methodology: stereoselective preparation of an axially chiral 5,7-fused bicyclic lactam related to circumdatins/benzomalvins and asperlicins. *Tetrahedron: Asymmetry*, **2006**, *17*, 281-286.

86. Lambooy, J. P. An Improved Method for the Hydrolysis of Diazonium Salts. *J. Am. Chem. Soc*., **1950**, *72*, 5327–5328.

87. Ogawa, A.; Taniguchi, T.; Imoto, M.; Takeda, M,; Nakai, T.; Mihara, M.; Iwai, T.; Ito, T.; Mizuno, T.; Nomoto, A. Hydrolysis of Diazonium Salts Using a Two-Phase System (CPME and Water). *Heteroatom Chemistry*. **2015**, *26*.

88. Bogdal, D. Microwave-assisted Organic Synthesis. *Tetrahedron Organic Chemistry Series*. **2005**, *25*, 47-190.

89. Smith, L. I. Duroquinone. *Org. Synth*. **1930**, *10*, 40.

90. Korzeniowski, Stephen, Reactivity and Reactions of Aryldiazonium Ions in Nonpolar Media. Ph.D Dissertation, Pennsylavania State University, 1978.

91. Cadogan, J. I. G.; Cook, J.; Harger, M. J. P.; Hibbert, P. G.; Sharp, J. T. Acylarylnitrosamines. Part 11. The Formation of Arynes in the Anomalous Decompositions of *o*-*t*-Butyl-and 2,5-*Di*-*t*-butyl-N-nitrosoacet-anilide. *J. Chem. Soc. B*, **1971**, 595-601.

92. Manege, L.C.; Ueda, T.; Hojo, M.; Fujio, M. Concentrated salt effects on the rates of solvolyses involving carbocations as reaction intermediates in acetone–water mixed solvents. *J. Chem. Soc., Perkin Trans*. **1998**, *2*, 1961-1966.

93. Olofsson, B.; Lindstedt, E.; Stridfeldt, E. Mild Synthesis of Sterically Congested Alkyl Aryl Ethers. *Org. Lett*. **2016**, *18*, 4234–4237.

94. Filimonov, V.D.; Trusova, M.; Postnikov, P.; Krasnokutskaya, E.A.; Lee, Y.M.; Hwang, H.Y.; Kim, H.; Chi, K. Unusually Stable, Versatile, and Pure Arenediazonium Tosylates: Their Preparation, Structures, and Synthetic Applicability. *Org. Lett*. **2008**, *10*, 3961–3964.

95. Percec, V.; Leowanawat, P.; Zhang, Na.; Resmerita, A.; Rosen, B.M. Ni(COD)2/PCy3 Catalyzed Cross-Coupling of Aryl and Heteroaryl Neopentylglycolboronates with Aryl and Heteroaryl Mesylates and Sulfamates in THF at Room Temperature. J. *Org. Chem*. **2011**, 76, 9946–9955.

96. Yoneda, N.; Fukuhara, T.; Mizokami, T.; Suzuki, A. A Facile Preparation of Aryl Triflates. Decomposition of Arenediazonium Tetrafluoroborate Salts in Trifluoromethanesulfonic Acid. *Chemistry letters*. **1991**, *20*, 459-460.

97. Barbero, M.; Cadamuroa, S.; Dughera, S. Copper-free Sandmeyer cyanation of arenediazonium o-benzenedisulfonimides. *Org. Biomol. Chem*. **2016**, *14*, 1437-1441.

98. Patrick, T.B.; Willaredt, R.P.; DeGonia, D.J. Synthesis of biaryls from aryltriazenes. *J. Org. Chem*., **1985**, *50*, 2232–2235.

99. Lei, X.; Jalla, A.; Abou Shama, M.; Stafford, J.; Cao, B. Chromatography-Free and Eco-Friendly Synthesis of Aryl Tosylates and Mesylates. *Synthesis.* **2015**, *47*, 2578-2585.

100. Cook, S.P.; Agrawal, T. Iron-Catalyzed Cross-Coupling Reactions of Alkyl Grignards with Aryl Sulfamates and Tosylates. *Org. Lett*. **2013**, *15*, 96–99.

101. Kikukawa, K.; Kono, K.; Wada, F.; Matsuda, T. Reaction of Arenediazonium Salts with Nitriles in the Presence of Sodium Carboxylates. A Convenient Synthesis of Unsymmetrical N-Aryl Acyclic Imides. *Bulletin of the Chemical Society of Japan*, **1982**, *55*, 3671-3672.

102. Damavandy, J.A.; Jones, R.A.Y. Cycloaddition reactions of quinoneimine N-oxides and of fluorenoneimine N-oxide: exocyclic nitrones conjugated with electron-withdrawing rings. *J. Chem. Soc., Perkin Trans. 1*. **1981**, 712-17.

103. Giroud, M.; Ivkovic, J.; Martignoni, M.; Fleuti, M.; Trapp, N.; Haap, W.; Kuglstatter, A.; Benz, J.; Kuhn, B.; Schirmeister, T.; Diederich, F. Inhibition of the Cysteine Protease Human Cathepsin L by Triazine Nitriles: Amide···Heteroarene π-Stacking Interactions and Chalcogen Bonding in the S3 Pocket. *ChemMedChem*. **2017**, *12*, 257-270.

104. Ruechardt, C.; Hassmann, V. Aromatic diazonium salts. X. A one-pot procedure for the Jacobson synthesis of indazole. *Liebigs Annalen der Chemie*. **1980**, *6*, 908-927.

105. Bartsch, R.A.; Yang, I. Phase transfer catalyzed synthesis of indazoles from *o*-alkylbenzenediazonium tetrafluoroborates. *Journal of Heterocyclic Chemistry*. **1984**, *21*, 1063.

106. Lee, J.; Chen, L.; West, A. H.; Richter-Addo, G.B. Interactions of Organic Nitroso Compounds with Metals. *Chem. Rev*. **2002**, *102*, 1019–1066.

107. Bohle, D.S.; Chua, Z.; Perepichka, I.; Rosadiuk, K. Lewis acid stabilization and activation of primary N-nitrosamides. *RSC Adv*. **2017**, *7*, 8205-8219.

108.Ieda, N.; Nakagawa, H.; Horinouchi, T.; Peng, T.; Yang, D.; Tsumoto, H.; Suzuki, T.; Fukuharad, K.; Miyata, N. Peroxynitrite generation from a NO-releasing nitrobenzene derivative in response to photoirradiation. *Chem. Commun*. **2011**, *47*, 6449–6451.

109.Miyamura, H.; Shiramizu, M.; Matsubara, R.; Kobayashi, S. Aerobic Oxidation of Hydroquinone Derivatives Catalyzed by Polymer-Incarcerated Platinum Catalyst. *Angew. Chem. Int. Ed*. **2008**, *47*, 8093–8095.

110.Paul, R.; Ali, M. A.; Punniyamurthy, T. Copper-Catalyzed Hydroxylation of Aryl Halides with Tetrabutylammonium Hydroxide: Synthesis of Substituted Phenols and Alkyl Aryl Ethers. *Synthesis*, **2010**, *24*, 4268–4272.

111.Kamitori, Y.; Hojo, M.; Masuda, R.; Izumi, T.; Tsukamoto, S. Silica Gel as an Effective Catalyst for the Alkylation of Phenols and Some Heterocyclic Aromatic Compounds. *J. Org. Chem*. **1984**, *49*, 4161-4165.

112.Routasalo, T.; Helaja, J.; Kavakka, J.; Koskinen, A. M. P. Development of Bis(2-picolyl)amine–Zinc Chelates for Imidazole Receptors. Eur. J. Org. Chem. **2008**, 3190–3199.

113.Torraca, K. E.; Huang, X.; Parrish, C. A.; Buchwald, S. L. An Efficient Intermolecular Palladium-Catalyzed Synthesis of Aryl Ethers. J. Am. Chem. Soc. **2001**, *123*, 10770–10771.

114.Miller, B.; McLaughlin, M. P.; Marhevka, V. C. Meta substitution in electrophilic benzylations of 2,6-dimethylphenol and alkyl 2,6-dimethylphenyl ethers: product distributions and mechanism. *J. Org. Chem*. **1982**, *47*, 710-719.

115.Bates, R. B.; Siahaan, T. J.; Suvannachut, K.; Vasey, S. K.; Yager, K. M. Preparation and reactions of trianions from the dimethylphenols. *J. Org. Chem*. **1987**, *52*, 4605-4608.

116. Bates, R. B.; Siahaan, T. J.; Suvannachut, K. A new rearrangement of alkoxybenzyl anions. J. Org. Chem. **1990**, *554*, 1328-1334.

117.Fuchs, M.; Simeo, Y.; Ueberbacher, B. T.; Mautner, B.; Netscher, T.; Faber, K. Enantiocomplementary Chemoenzymatic Asymmetric Synthesis of (R)- and(S)-Chromanemethanol. *Eur. J. Org. Chem*. **2009**, 833–840.

118. Rathore, R.; Kochi, J. K. Isolation of Novel Radical Cations from Hydroquinone Ethers. Conformational Transition of the Methoxy Group upon Electron Transfer. J. *Org. Chem*. **1995**, *60*, 4399-4411.

119. Róhrich, J.; Müllen, K. A Donor-Type Cyclophane with a Strongly Bent Tetrathiafulvalene Unit. *J. Org. Chem*. **1992**, *57*, 2374-2379.

120. Alonso, F.; Barba, I.; Yus, M. Reactivity of 3,6-dimethoxy-3,6-dimethylcyclohexa-1,4-diene: nuclear versus benzylic nucleophilic substitution. *Tetrahedron*. **1990**, *46*, 2069-2080.

121. Kalinowska, M.; S´wisłocka, R.; Lewandowski, W. The spectroscopic (FT-IR, FT-Raman, UV and 1H, 13C NMR) and theoretical studies of alkali metal o-methoxybenzoates. *Journal of Molecular Structure*. **2006**, *792–793*, 130–138.

122. Perkins, M. V.; Kitching, W.; Drew, R. A.; Moore, C. J.; Konig, W. A. Chemistry of Fruit Flies: Composition of the Male Rectal Gland Secretions of some Species of South-East Asian Dacinae. Re-examination of Dacus cucurbitae (Melon Fly). *J. Chem. Soc., Perkin Trans.* **1990**, *1*, 1111-1117.

123.Alsabeh, P. G.; Stradiotto, M. Addressing Challenges in Palladium-Catalyzed Cross-Couplings of Aryl Mesylates: Monoarylation of Ketones and Primary Alkyl Amines. *Angew. Chem. Int. Ed.* **2013**, *52*, 7242 –7246.

124.Ayyangar, N. J.; Srinivasan, K. V. Effect of substituents in the formation of diacetanilides. *Can. J. Chem*. **1984**, *62*, 1292-1296.

125.Wang, F.; Wei, T. Q.; Xu, P.; Wang, S. Y.; Ji, S. J. Mn(III)-mediated radical cascade reaction of boronic acids with isocyanides: Synthesis of diimide derivatives. *Chinese Chemical Letters*. **2019**, *30*, 379-382.

126.Abbas, S. A.; Hickinbottom, W. J. Molecular rearrangements. Part VII. NN-diacylanilines. J. *Chem. Soc. C*, **1966**, 1305-1306.

127.Kondo, K.; Iida, T.; Fujita, H.; Suzuki, T.; Yamaguchi, K.; Murakami, Y. A Chiral Axis due to an Acyclic Imide–Ar Bond: A Study of Steric Effects of Acyl Groups on Racemization, *Tetrahedron*. **2000**, *56*, 8883-8891.

128. Tabushi, I.; Yamada, H.; Kuroda, Y. Preparations and properties of higher [2n]paracyclophanes, cyclic oligomers of p-xylylene. *J. Org. Chem*. **1975**, 40, 1946-1949.

129. Tabushi, I.; Yamada, H. Temperature dependent chemical shift change in 4-substituted(2.2.2.2)paracyclophanes. *Tetrahedron*. 1977, *33*, 1101-1104.

130. Horita, H.; Sakata, Y.; Misumi, S. Layered compounds. XXX. Unusual reaction of methyl substituted [2.2]paracyclophanes with cupric nitrate in acetic anhydride. *Tetrahedron Letters*, **1976**, *18*, 1509-1512

131. Duan, Jian-Xin., Chemistry of 1,1,2,2,9,9,10,10-octafluoro-[2,2]-paracyclophane: Its synthesis and reactions, Ph.D dissertation, 2001, University of Florida.

132. Mitzi, D. B. Synthesis, structure, and properties of organic inorganic perovskites and related materials. *Prog. Inorg. Chem*. **2007**, *48*,1−121.

133. Braunstein, R. Radiative Transitions in Semiconductors. *Phys. Rev*. **1892**, *99*, 1892-1893.

134. Zheludev, N. The life and times of the LED: a 100-year history. The life and times of the LED-a 100-year history. *Nature Photonics*. **2007**, *1*, 189–192.

135. Davydov, A.S. Absorption Spectra of Crystals at Low Temperatures. *Ukr. J. Phys*. **1948**. 53, 210-218.

136. Frenkel, J. On the Transformation of light into Heat in Solids. I. *Phys. Rev*. **1931**, *37*, 17-44.

137. Liang, W. Y. Excitons. *Phys. Educ*. **1970**, 5, 226–228.

138. Furukawa, M.; Mizuno, K.; Matsui, A.; Tamai, N.; Yamazaiu, I. Branching of Exciton Relaxation to the Free and Self-Trapped Exciton States. *Chemical Physics*. **1989**, *138*, 423-432.

139. J.I. Pankove, Optical Processes in Semiconductors. Dover, 1971.

140. Mahan, Gerald. Condensed Matter in a Nutshell. Princeton: Princeton University Press, 2010.

141. Jensen, H.W.; Marschner, S.R.; Levoy, M.; Hanrahan, P. A practical model for subsurface light transport. *Computer graphics and interactive techniques*. **2001**, 511-518.

142. Cortecchia, D.; Yin, J.; Petrozza, A.; Soci, C. White light emission in low-dimensional perovskites. *J. Mater. Chem. C*. **2019**, *7*, 4956-4969.

143. Watanabe, H.; Jones, F. N.; Hauser, C. R. Formation of Cyclopropyl Ring by Action of Sodium Amide on *exo*-Methyleneammonim Ions Obtained from Rearrangement of Certain 2,6-Dimethylbenzyltrimethylammonium Ions. *J. Org. Chem.* **1969**, *34*, 2393-2397.

144. Liu, X. Y.; Zhu, H. B.; Shen, Y. J.; Jiang, J.; Tu, T. Efficient N -heterocyclic carbene nickel pincer complexes catalyzed cross coupling of benzylic ammonium salts with boronic acids. *Chinese Chemical Letters*. **2017**, *28*, 350–353.

145. Li, J.; Zheng, Z.; Xiao, T.; Xu, P. F.; Wei, H. Nickel-Catalyzed Directed Benzylation of Ortho C−H Bonds in Aromatic Amides through C−H/C−N Cleavage. *Asian Journal of Organic Chemistry*. **2017**, *7*, 133–136.

Appendix A: Crystallographic Data

Crystal structure of N,N'-(2,3,5,6-tetramethyl-1,4-phenylene)bis(N-nitrosoacetamide) (1a) (complexed with acetonitrile).

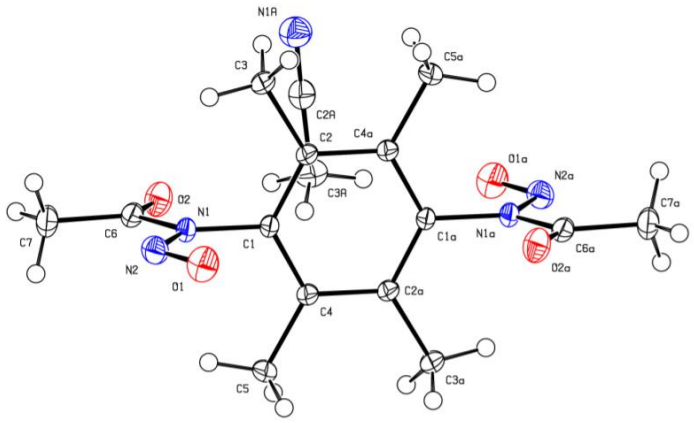

Bond precision: C-C = 0.0020 A Wavelength=0.71073

Cell: a=7.5205(6) b=8.5303(7) c=8.7316(7)
alpha=76.4377(12) beta=68.2055(12) gamma=87.3206(13)
Temperature: 100 K

	Calculated	Reported
Volume	505.10(7)	505.10(7)
Space group	P -1	P -1
Hall group	-P 1	-P 1
Moiety formula	C14 H18 N4 O4, 2(C2 H3 N)	?
Sum formula	C18 H24 N6 O4	C18 H24 N6 O4
Mr	388.43	388.43
Dx,g cm-3	1.277	1.277
Z	1	1
Mu (mm-1)	0.093	0.093
F000	206.0	206.0
F000'	206.09	
h,k,lmax	10,11,12	10,11,12
Nref	2830	2824
Tmin,Tmax	0.959,0.982	0.715,0.746
Tmin'	0.958	

Correction method= # Reported T Limits: Tmin=0.715 Tmax=0.746
AbsCorr = MULTI-SCAN

Data completeness= 0.998 Theta(max)= 29.582

R(reflections)= 0.0517(2622) wR2(reflections)= 0.1700(2824)

S = 0.999 Npar= 127

Full data set can be found at University of Oklahoma Reciprocal Net (Sample number: 18015)

Crystal structure of *Syn*-[2.2]tetramethylnaphthalenophane

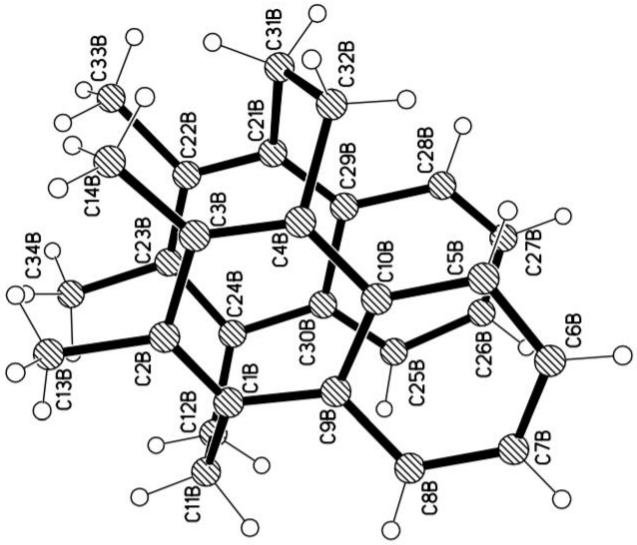

```
Bond precision:  C1- C = 0.0133 A        Wavelength=0.71073

Cell:            a=8.7711(8)     b=8.5053(8)         c=18.6314(16)
                 alpha=90        beta=95.374(2)      gamma=90
Temperature:     100 K

                 Calculated                  Reported
Volume           1383.8(2)                   1383.8(2)
Space group      P c                         P c
Hall group       P -2yc                      P -2yc
Moiety formula   C28 H28, 2(C H Cl3)         C28 H28, 2(C H Cl3)
Sum formula      C30 H30 Cl6                 C30 H30 Cl6
Mr               603.24                      603.24
Dx,g cm-3        1.448                       1.448
Z                2                           2
Mu (mm-1)        0.641                       0.641
F000             624.0                       624.0
F000'            625.94
h,k,lmax         10,10,23                    10,10,23
Nref             5482[ 2746]                 5437
Tmin,Tmax        0.836,0.880                 0.841,0.883
Tmin'            0.836

Correction method= # Reported T Limits: Tmin=0.841 Tmax=0.883
AbsCorr = MULTI-SCAN

Data completeness= 1.98/0.99       Theta(max)= 26.069

R(reflections)= 0.0674( 3759)      wR2(reflections)= 0.2109( 5437)

S = 1.157                  Npar= 412
```

Full data set can be found at University of Oklahoma Reciprocal Net (Sample number: 16012)

Crystal structure of *Anti*-[2.2]tetramethylnaphthalenophane

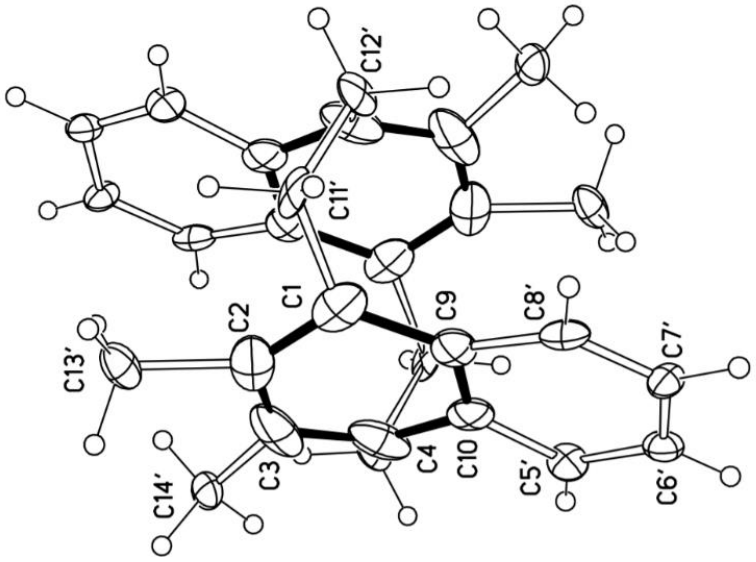

Bond precision: C-C = 0.0083 A Wavelength=0.71073

Cell: a=8.554(4) b=8.900(4) c=9.088(4)
alpha=81.203(7) beta=83.238(7) gamma=84.219(6)
Temperature: 100 K

	Calculated	Reported
Volume	676.6(5)	676.6(5)
Space group	P -1	P -1
Hall group	-P 1	-P 1
Moiety formula	C28 H28, 2(C H Cl3)	C28 H28, 2(C H Cl3)
Sum formula	C30 H30 Cl6	C30 H30 Cl6
Mr	603.24	603.24
Dx,g cm-3	1.480	1.481
Z	1	1
Mu (mm-1)	0.655	0.655
F000	312.0	312.0
F000'	312.97	
h,k,lmax	10,11,11	10,10,11
Nref	2678	6994
Tmin,Tmax	0.815,0.877	0.744,0.880
Tmin'	0.730	

Correction method= # Reported T Limits: Tmin=0.744 Tmax=0.880
AbsCorr = MULTI-SCAN

Data completeness= 2.612 Theta(max)= 26.076

R(reflections)= 0.0739(5219) wR2(reflections)= 0.2331(6994)

S = 1.039 Npar= 238

Full data set can be found at University of Oklahoma Reciprocal Net (Sample number: 15152)

Crystal structure of $(C_{15}H_{26}N)FeBr_4$

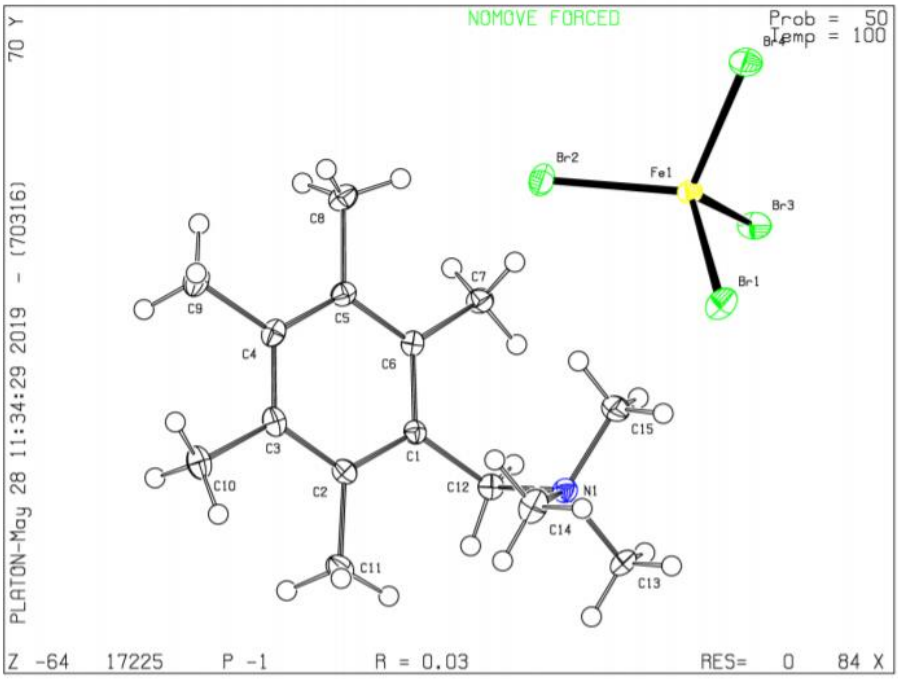

Bond precision: C-C = 0.0034 A Wavelength=0.71073

Cell: a=7.683(4) b=8.957(5) c=15.686(9)
alpha=76.146(9) beta=87.099(9) gamma=86.407(9)
Temperature: 100 K

	Calculated	Reported
Volume	1045.3(10)	1045.3(10)
Space group	P -1	P -1
Hall group	-P 1	-P 1
Moiety formula	C15 H26 N, Br4 Fe	Fe Br4; C15 H26 N
Sum formula	C15 H26 Br4 Fe N	C15 H26 Br4 Fe N
Mr	595.82	595.86
Dx,g cm-3	1.893	1.893
Z	2	2
Mu (mm-1)	8.361	8.361
F000	578.0	578.0
F000'	576.77	
h,k,lmax	11,13,22	11,13,22
Nref	6854	6484
Tmin,Tmax	0.297,0.637	0.400,0.660
Tmin'	0.101	

Correction method= # Reported T Limits: Tmin=0.400 Tmax=0.660
AbsCorr = MULTI-SCAN

Data completeness= 0.946 Theta(max)= 31.330

R(reflections)= 0.0293(5205) wR2(reflections)= 0.0688(6484)

S = 1.001 Npar= 198

Full data set can be found at University of Oklahoma Reciprocal Net (Sample number: 17225)

Crystal structure of $(C_{14}H_{23}N)FeBr_4$

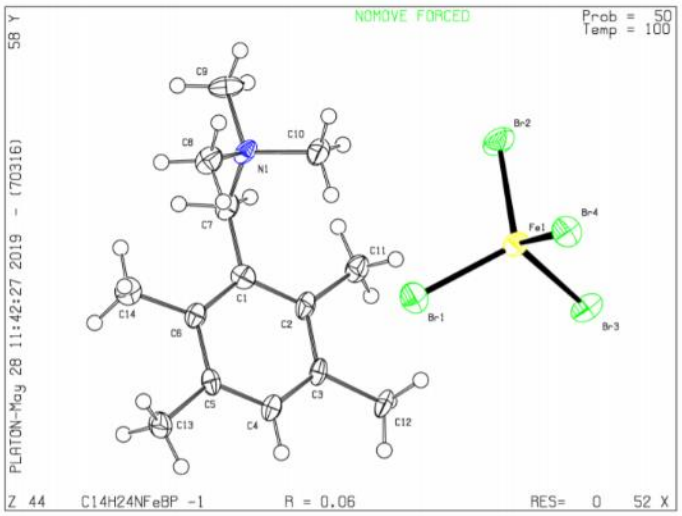

Bond precision: C-C = 0.0119 A Wavelength=0.71073

Cell: a=7.919(3) b=8.560(3) c=15.173(5)
alpha=99.563(7) beta=92.399(7) gamma=90.532(8)
Temperature: 100 K

	Calculated	Reported
Volume	1013.2(6)	1013.2(6)
Space group	P -1	P -1
Hall group	-P 1	-P 1
Moiety formula	C14 H24 N, Br4 Fe	?
Sum formula	C14 H24 Br4 Fe N	C14 H25 Br4 Fe N
Mr	581.79	582.84
Dx,g cm-3	1.907	1.910
Z	2	2
Mu (mm-1)	8.623	8.623
F000	562.0	564.0
F000'	560.78	
h,k,lmax	9,10,18	9,10,18
Nref	3853	3815
Tmin,Tmax	0.389,0.586	0.310,0.620
Tmin'	0.190	

Correction method= # Reported T Limits: Tmin=0.310 Tmax=0.620
AbsCorr = MULTI-SCAN

Data completeness= 0.990 Theta(max)= 25.680

R(reflections)= 0.0567(3322) wR2(reflections)= 0.1774(3815)

S = 1.006 Npar= 188

Full data set can be found at University of Oklahoma Reciprocal Net (Sample number: C14H24FeB)

Crystal structure of $(C_{13}H_{20}N)FeBr_4$

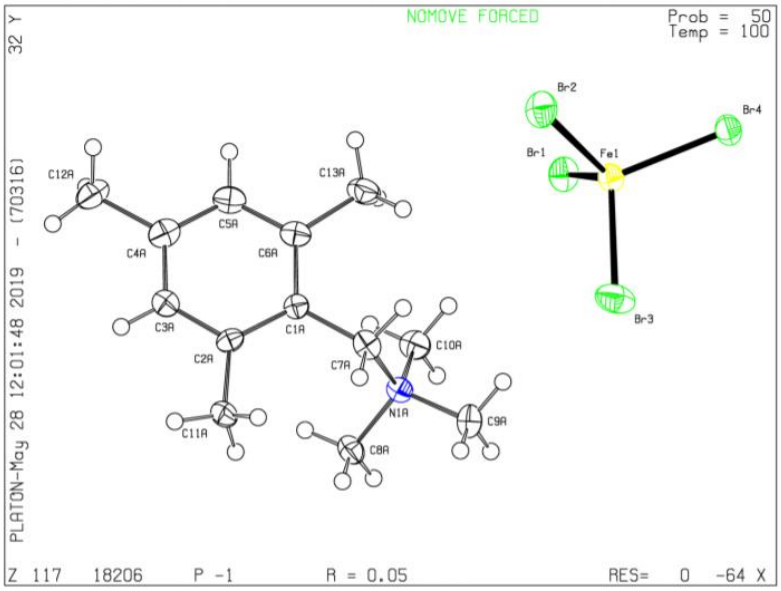


```
Bond precision:  C-C = 0.0072 A          Wavelength=0.71073

Cell:          a=8.5400(16)      b=8.6208(17)      c=13.463(3)
               alpha=99.536(5)   beta=99.835(5)    gamma=95.525(5)
Temperature:   100 K

                Calculated                Reported
Volume          955.2(3)                  955.2(3)
Space group     P -1                      P -1
Hall group      -P 1                      -P 1
Moiety formula  C13 H22 N, Br4 Fe         Fe Br4; C13 H22 N
Sum formula     C13 H22 Br4 Fe N          C13 H22 Br4 Fe N
Mr              567.77                    567.80
Dx,g cm-3       1.974                     1.974
Z               2                         2
Mu (mm-1)       9.144                     9.145
F000            546.0                     546.0
F000'           544.78
h,k,lmax        12,13,20                  12,13,20
Nref            6909                      6890
Tmin,Tmax       0.138,0.455               0.233,0.408
Tmin'           0.053

Correction method= # Reported T Limits: Tmin=0.233 Tmax=0.408
AbsCorr = MULTI-SCAN

Data completeness= 0.997          Theta(max)= 32.515

R(reflections)= 0.0510( 3490)     wR2(reflections)= 0.1343( 6890)

S = 1.012                 Npar= 178
```

Full data set can be found at University of Oklahoma Reciprocal Net (Sample number: 18206)

Crystal structure of $(C_{12}H_{17}N)FeBr_4$

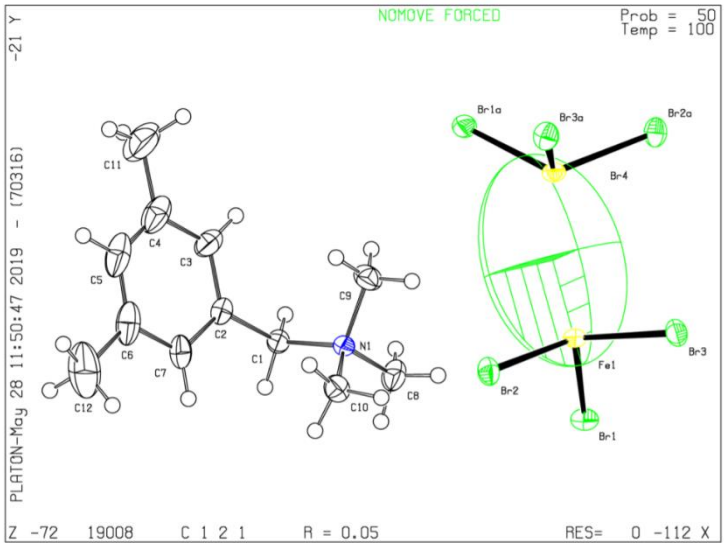

Bond precision: C-C = 0.0140 A Wavelength=0.71073

Cell: a=17.0112(5) b=8.2785(2) c=12.8041(4)
alpha=90 beta=105.4687(11) gamma=90

Temperature: 100 K

	Calculated	Reported
Volume	1737.85(9)	1737.85(9)
Space group	C 2	C 1 2 1
Hall group	C 2y	C 2y
Moiety formula	2(C12 H20 N), Br7 Fe2	?
Sum formula	C24 H40 Br7 Fe2 N2	C12 H20 Br3.50 Fe N
Mr	1027.58	513.82
Dx,g cm-3	1.964	1.964
Z	2	4
Mu (mm-1)	8.898	8.898
F000	990.0	990.0
F000'	988.04	
h,k,lmax	26,13,20	26,13,20
Nref	7199[3807]	7176
Tmin,Tmax	0.468,0.546	0.270,0.580
Tmin'	0.173	

Correction method= # Reported T Limits: Tmin=0.270 Tmax=0.580
AbsCorr = ?

Data completeness= 1.88/1.00 Theta(max)= 34.240

R(reflections)= 0.0457(5983) wR2(reflections)= 0.1308(7176)

S = 1.064 Npar= 164

Full data set can be found at University of Oklahoma Reciprocal Net (Sample number: 19008)

Crystal structure of $(C_{11}H_{14}N)FeBr_4$

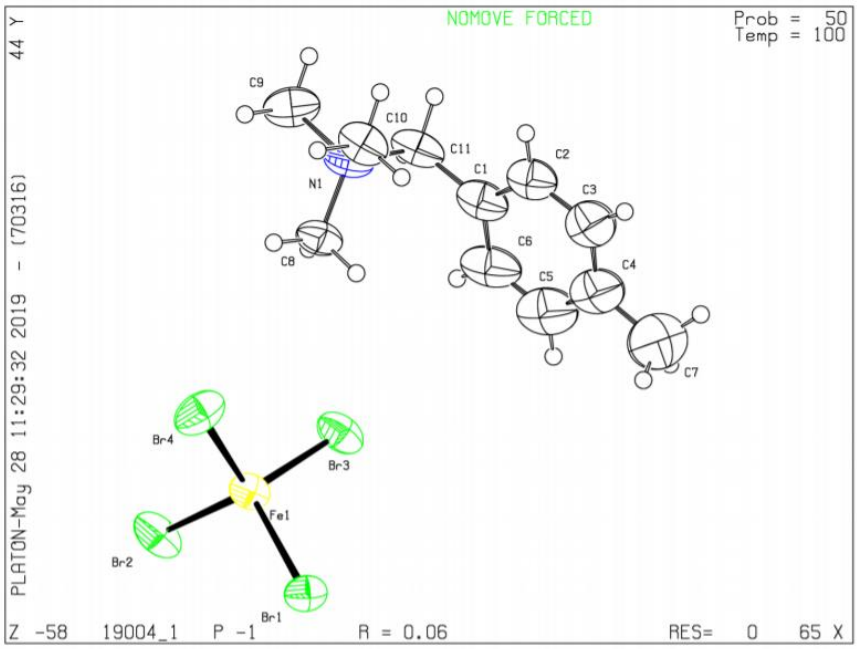

Bond precision: C-C = 0.0185 A Wavelength=0.71073

Cell: a=7.5804(11) b=8.8075(12) c=13.1536(19)
alpha=84.621(5) beta=84.368(5) gamma=87.694(4)
Temperature: 100 K

	Calculated	Reported
Volume	869.7(2)	869.7(2)
Space group	P -1	P -1
Hall group	-P 1	-P 1
Moiety formula	C11 H18 N, Br4 Fe	Fe Br4; (C11 H18 N)
Sum formula	C11 H18 Br4 Fe N	C11 H18 Br4 Fe N
Mr	539.71	539.75
Dx,g cm-3	2.061	2.061
Z	2	2
Mu (mm-1)	10.037	10.038
F000	514.0	514.0
F000'	512.80	
h,k,lmax	9,10,15	9,10,15
Nref	3187	3186
Tmin,Tmax	0.462,0.537	0.360,0.570
Tmin'	0.294	

Correction method= # Reported T Limits: Tmin=0.360 Tmax=0.570
AbsCorr = MULTI-SCAN

Data completeness= 1.000 Theta(max)= 25.350

R(reflections)= 0.0582(2352) wR2(reflections)= 0.1641(3186)

S = 1.031 Npar= 159

Full data set can be found at University of Oklahoma Reciprocal Net (Sample number: 19004_1)